Operating characteristics of a Transparent Cathode Discharge

Thesis submitted in accordance with the requirements of the
University of Liverpool for the degree of Doctor in Philosophy

by

Thomas Hardiment

October 2017

Acknowledgements

Sincere thanks are extended to all those who have provided me with opportunities and encouragement over the course of my studies. In particular, I would like to thank my partner Catriona Baillie, for her support during this time, and also Prof. Jaap Vandenberg, for his kind donation of power supplies. Most of all, I am grateful to Dr. Mark Bowden, for his patience and good advice in supervising this project.

This work is dedicated to my family.

Operating characteristics of a Transparent Cathode Discharge

Thomas Hardiment

Abstract

A Transparent Cathode Discharge has been studied, with the aim of identifying operating regimes in which ions and neutrals are reactive species. The device consists of a cylindrical, powered cathode grid, that has generally been operated within a grounded anode grid, held concentric with the cathode. The principal mode structure evident across the operating pressure range is found to represent discharges sustained respectively by the activity of electrons at higher pressures, and ionic and neutral species at lower pressures. This is ascertained by analysis of the optical emission from the plasma, showing processes of excitation to be caused by these species. The discharge occurring at higher pressures, of tens to hundreds mTorr, has been characterised as an electron-driven 'cathode-confined' mode, that is shown to be sustained in part by the so-called 'hollow cathode effect'. The discharge occurring at lower pressures, of units to tens mTorr, is characterised as an 'anode-focussed ion beam' mode, composed of radially-convergent ion beams. These are found to be formed with a focussing effect caused by potential surfaces associated with the apertures of the anode grid, distinguishing this mode from the 'star' mode described elsewhere in IEC research. Doppler-shifted light from these low-pressure discharges provides direct evidence for the presence of energetic ions and neutrals. Quasi-spherical space charge objects are observed to appear within the cathode, during operation at moderately low pressures of units to tens mTorr, and cathode currents of tens of mA. These are found to resemble configurations characterised in the wider literature as consisting of a spherical double layer, surrounding a localised concentration of relatively positive space charge, and having a potential difference close to the ionisation potential of the parent gas species. Larger space charge objects, termed 'fireballs', are observed to appear at a narrower range of conditions, and to show some analogous characteristics to these. Analysis of distributions of current and optical emission indicate the fireball objects to have a more complex internal structure, containing several regions of distinct potential. The current and emission structure of these objects shows periodic evolution, on timescales of tens μs, that is associated with the physical transport of the core of the object along the axis of the cathode. The occasional decoupling, and different current-voltage progressions, of axial and radial electron currents indicate the outer part of the potential structure to follow separate dynamics to those of the core region. The relative absence of fluctuations in ion current to the cathode indicates the core region to be referenced negative with respect to this outer structure, meaning that the overall potential profile of the object appears to constitute a 'double well' structure. The physical dependences shown by the different operating modes upon the geometry of the electrode arrangement have been identified, so that the type and stability of plasma produced may be engineered by informed design of discharge apparatus. These principles have been verified in the limited testing of both a planar grid configuration, and a multiple-element cathode configuration. These might be expected to be favourable for creating additionally-stable ion- and neutral-driven plasmas, and for higher-power operation in a convergent geometry, respectively.

Table of Contents

List of equations

Equation (1): $$p = N\,k_B T \quad \rightarrow \quad N = \frac{p}{k_B T}$$

Equation (2): $$I_k = I_i \times (1 + \gamma_{SE})$$

Equation (3): $$I_k = I_i \times (1 + \gamma_{SE}) = I_e \times (1 + \gamma_{SE})$$

Equation (4): $$\lambda_{mfp} = \frac{1}{N\,\sigma}$$

Equation (5): $$\varepsilon_H = \frac{1}{2} m_H \left(\frac{\Delta\lambda\, c}{\lambda} \right)^2$$

Equation (6): $$D = \lambda_i \times \sqrt{m_e / m_i}\ .$$

Equation (7): $$t_{iz} = \frac{1}{N\,\sigma_i\, v_e}$$

Nomenclature

N	= number density	ε_{iz}	= ionisation energy
p	= pressure	t_{iz}	= ionisation time
k_B	= the Boltzmann constant	m_H	= hydrogen mass
n	= principal quantum number	m_i	= ion mass
I_k	= metered cathode current	m_e	= electron mass
I_i	= ion current	v_e	= electron velocity
I_e	= primary electron current	Φ	= potential
I_{SE}	= secondary electron current	Φ_{DL}	= double layer potential
γ_{SE}	= secondary electron yield	D	= diameter of ADLO
λ_{mfp}	= mean free path	ε_H	= hydrogen energy
λ_i	= mean free path for ionisation	T	= temperature
σ	= cross section	V	= voltage
σ_i	= cross section for ionisation	R	= resistance
d	= distance between electrodes	r	= radius
ε	= kinetic energy	c	= speed of light
λ	= wavelength	$\Delta\lambda$	= Doppler shift

Chapter 1
Introduction and Literature Review

1.1 Introduction to research

This thesis describes the experimental investigation of a type of plasma known as a Transparent Cathode Discharge (TCD), that has previously been studied in the field of Inertial Electrostatic Confinement (IEC) for fusion applications. This work constitutes the preliminary phase of a research project that aims to assess the utility of this type of discharge as a process plasma source.

Plasma is sometimes described as the fourth state of matter. If solid, liquid and gas phases are thought of in terms of an incremental particle energy overcoming cohesive forces within a substance, then plasma is a state that may result when particle energies are sufficiently great for a degree of ionisation to be maintained.

Most of the observable matter in the universe exists as a plasma, the properties of which may vary considerably. Stars are composed of hot, very dense plasma, consisting of matter that is fully ionised; much of interstellar space is filled with a more tenuous plasma, of significantly lesser density and degree of ionisation. A broadly similar degree of variation occurs in naturally-occurring terrestrial plasmas, such as those found in lightning and the ionosphere.

Plasma was created artificially as the necessary confluence of vacuum and high voltage technology occurred in the second half of the nineteenth century. The work of instrument makers such as Geissler, and experimentalists including Crookes and Roentgen enabled the observation of X-rays and cathode rays, leading to Thompson's discovery of the electron, and the subsequent perforation of the cathode led to Goldstein's observation of anode rays, similarly instrumental in the discovery of the proton.

Plasmas are currently used in a wide range of industrial and medical processes, which exploit their capacities for electro-chemical reactivity and mechanical erosion and/or deposition. Properties such as temperature, species composition and density may make different plasmas more or less suitable for particular applications. The vast majority of these, and indeed laboratory plasmas in general, are sustained by the activity of energetic electrons, and it is this that ultimately determines the reactive profile of the resulting plasma.

The TCD is distinct in having significantly-active populations of ionic and neutral species. In such a plasma, the energetic ions and neutrals may transfer energy to background particles more effectively than electrons might, by virtue of their similar mass. This will in turn affect characteristics such as gas heating and molecular fragmentation, and so the resulting plasma might be expected to contain a quite different mix of reactive species.

Significant differences in chemistry and temperature could cause a TCD plasma to have a quite different reactive profile from those of existing process sources. This could result in novel applications, or constitute improvements over current technologies, and it is these possibilities that motivate this research.

This initial part of the research project involves the operation of a TCD device in simple atomic gases, across a relatively wide range of operating conditions. Principal objectives are the understanding of physical processes at work within the discharge, and the dependences these show upon both conditions and the physical form of the device.

The rest of this chapter provides the background necessary to understand the research presented later in the thesis. The next section is a brief overview of some basics of plasma processes relevant to TCDs, which is followed by an overview of IEC devices and a review of research literature in this field. The final section briefly outlines the structure of the rest of the thesis.

1.2 Background to discharge plasmas

This section aims to convey some of the physical properties that influence the generation and maintaining of a plasma. Many aspects of plasma behaviour are neglected, but a brief description is made of some important processes and dependences upon conditions which contribute to plasma properties.

In the plasma state, the behaviour of a substance is largely determined by the populations of excited and charged particles. This means plasma may be heated and contained by electric and magnetic fields, and may exert a considerable reactive pressure. For a discharge to be self-sustaining, the processes causing generation of charged particles must be balanced by those by which they are lost. This state of affairs is determined by the dynamics of motion of charged particles, and by the collisions that these experience with the gas in which the discharge occurs. These properties also determine the reactive profile of the plasma, and the conditions that are required for it to exist. Some of the factors that influence these are considered briefly in the following.

Plasmas are generally obtained under controlled conditions by the application of an electric field of sufficient strength to cause 'breakdown' of a substance. This term refers to a sequence of events that cause the substance, usually a gas, to become ionised and so able to carry an electric current.

Breakdown generally occurs against a background of random ionisations caused by cosmic rays, which cause a low level of charged particles to be present. For these to result in breakdown, they must become sufficiently energised in the applied electric field to then create further ionisations, before being lost to recombination with other particles or a volume boundary, such as the containing vessel wall. Should this occur, populations of charged particles become significantly more abundant, and an

equilibrium state is reached, in which the rate at which charged particles are produced is balanced with that at which they are lost.

In the situation where this occurs in a DC field between two electrodes, the emission of secondary electrons from the cathode, mainly caused by the incident ion flux, also plays an important role in the creation of charge carriers. For a discharge to sustain, electron free paths must be both long enough to pick up sufficient energy to cause further ionisation, and also short enough so that one electron emitted from the cathode will result in a sufficient ion flux at the cathode surface for a fresh electron to be emitted. These factors are formulated as the Townsend breakdown criteria [1, Ch. 10], with two Townsend coefficients, α and γ, describing the rate of ionisation per unit length within the gas, and the rate of secondary electron emission from the cathode per incident ion, respectively.

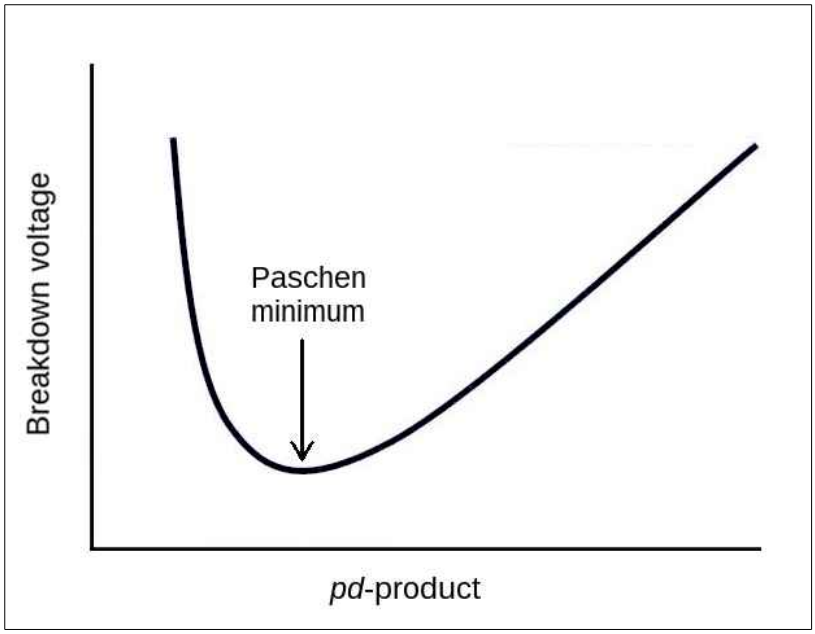

Fig. 1. Form of the Paschen curve, showing dependence of breakdown voltage upon pd product

These mechanisms are reflected in Paschen's Law, which states that a minimum electric field is required for breakdown at a certain value of the product of pressure, *p*, and electrode separation, *d*, (the *pd* product). When breakdown voltage is plotted against *pd*, a characteristic curve is obtained that shows this minimum (Fig. 1). For a given electrode spacing and voltage, increasing the pressure above this ideal value reduces the energy picked up between more frequent collisions, and so a stronger electric field is required to compensate; this causes the increase in breakdown voltage seen in the right-hand branch of the Paschen curve. Conversely, a reduction in pressure reduces the number of collisions per emitted electron. In order to compensate for this reduction, a stronger electric field acts to maintain the ionisation yield by increasing the energy of ions impacting the cathode, and so the secondary electron yield. The breakdown voltage therefore also increases on the left-hand branch of the curve.

From this description, the importance of collisions occurring between charged particles and the background gas is apparent. Whilst collisions clearly constitute an important mechanism of charged particle creation, they also cause processes such as molecular dissociation and electronic excitation of the background gas. Excitation occurs when atomically-bound electrons are given additional energy in a collision that is not sufficient for them to be released. This energy is largely released in the form of photons, which may go on to react with further background particles, or be released from the volume. Such emission at visible wavelengths causes the luminescence that is a typical characteristic of a plasma.

Energy imparted to particles in collisions, and the energised states that may result, also enable various chemical reactions to occur between particles. The collisional dynamics therefore play a large part in determining both the reactive profile of a plasma, and also the magnitude of the electric field required for it to be sustained. As described above, the nature of collisional processes are strongly influenced by the pressure at which a discharge occurs, since this determines the density of the background gas matrix and so affects both the frequency of collisions and the degree of energy gained by particles from the electric field between collisions. Pressure is therefore an important factor in defining the properties of a plasma. The degree of charge generation resulting from ionising collisions also affects the magnitude of current that may be drawn through a plasma. Voltage-current characteristics in a discharge follow a consistent evolution with levels of current; a diagram of the different regimes is given in [1, p.310], reproduced in Fig. 2.

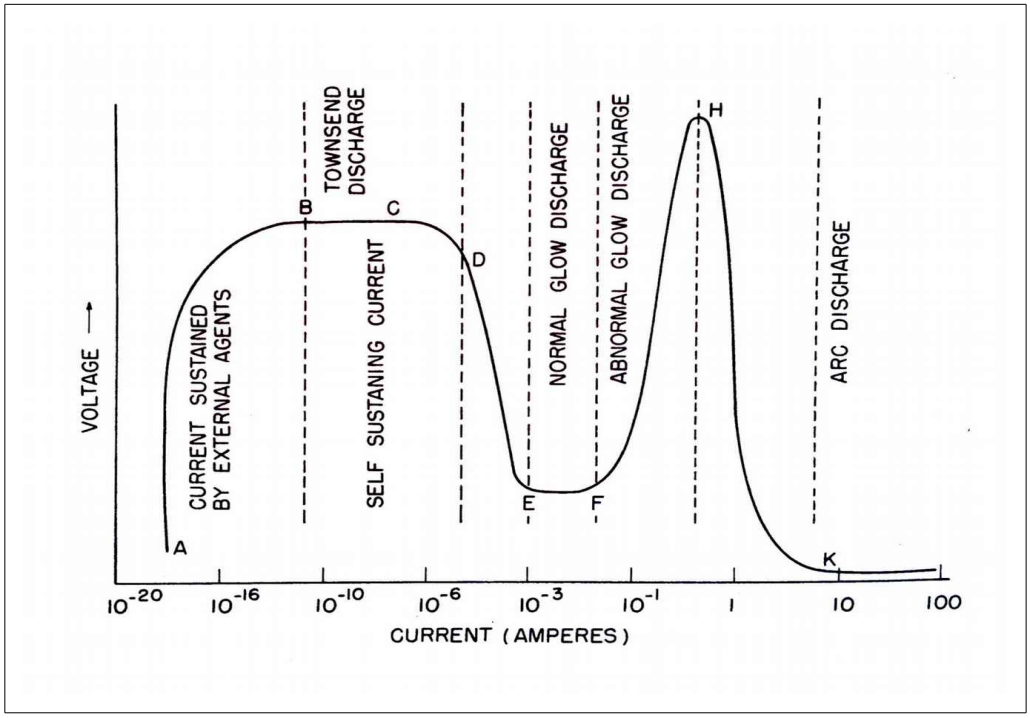

Fig. 2. Discharge current-voltage regimes. Reproduced from [1]

At conditions on the low-*pd* side of the Paschen minimum, and with the increasing of *pd* to just above the breakdown value, the discharge initially encounters a regime that exhibits a negative differential resistance; increasing current provides more charge carriers, lowering the effective resistance and reducing the voltage across the discharge. With increasing levels of current, the current-voltage relation quickly flattens through a 'normal glow' region where the current increases rapidly for a tiny increase in voltage, until the density of electrons at the cathode is sufficient for those newly-emitted to be shielded from the anode potential, causing them to accumulate in front of the cathode. Electron current is then drawn from this reservoir of space charge, and operation is said to be 'space charge-limited'. In this 'abnormal glow' regime of operation, the current-voltage relation is determined by the dynamics of space charge-limited flow. In the collision-less regime, this is proportional to the three-halves power of the anode voltage (the Child-Langmuir law), and has a coefficient known as the perveance, which is determined by physical characteristics of the set-up such as the geometry and size of the electrodes and volume.

The plasma state is distinguished from that of the boundary regions that generally surround plasmas, across which charged particles are lost from the volume, and which are known as sheaths. The distinction between sheath and plasma regions was first made by Langmuir in [2], in which plasma is described in terms of being a region in which a sufficient degree of ionisation occurs for ions and electrons to accumulate, with their losses to the containing vessel determined by their respective densities and velocities.

The dynamics of a collection of charged particles are considerably influenced by the fact that ions and electrons have very different mass. This means an electron will travel much faster than an ion with a similar energy, as described by classical equations of motion; kinetic energy is related to velocity by $\varepsilon = \frac{1}{2} m v^2$, in which ε refers to energy, m refers to mass and v to velocity. This may be re-arranged to describe velocity, as $v = \sqrt{2\varepsilon/m}$. From these it may be appreciated that for electrons and ions having the same energy, their respective velocities will be related by $\sqrt{m_e/m_i}$, in which the subscripts '*e*' and '*i*' refer to electrons and ions respectively, and for which typical values of are of the order 10^{-3}. The greater flux of electrons at the boundary that typically results causes the potential of the plasma to become positive with respect to its surrounds. This acts to limit electron losses and also to increase ion losses, and so the plasma potential adjusts to keep these equal, and so preserve quasi-neutrality.

1.3 Background to Inertial Electrostatic Confinement

Prior to a review of the published literature concerning TCD operation, the historical background of Inertial Electrostatic Confinement (IEC) research, and general device configuration are first outlined, to provide context for the reference works described.

1.3.1 Overview of IEC research

The field of IEC originated in the 1950s and '60s as an approach to creating fusion plasmas [3-5]. The original objective in IEC work was the electrostatic confinement and acceleration of ions, by and within a negative space charge of electrons. The creation was proposed of a complex space charge configuration termed a 'poissor' [6], composed of concentric shells of opposing charge. This was to constitute a potential structure consisting of nested potential wells of alternating polarity, as illustrated in Fig. 3. The effect of such a structure would be to cause ions to be accelerated through a central zone of high density and reactivity, achieving inertial confinement by electrostatic forces.

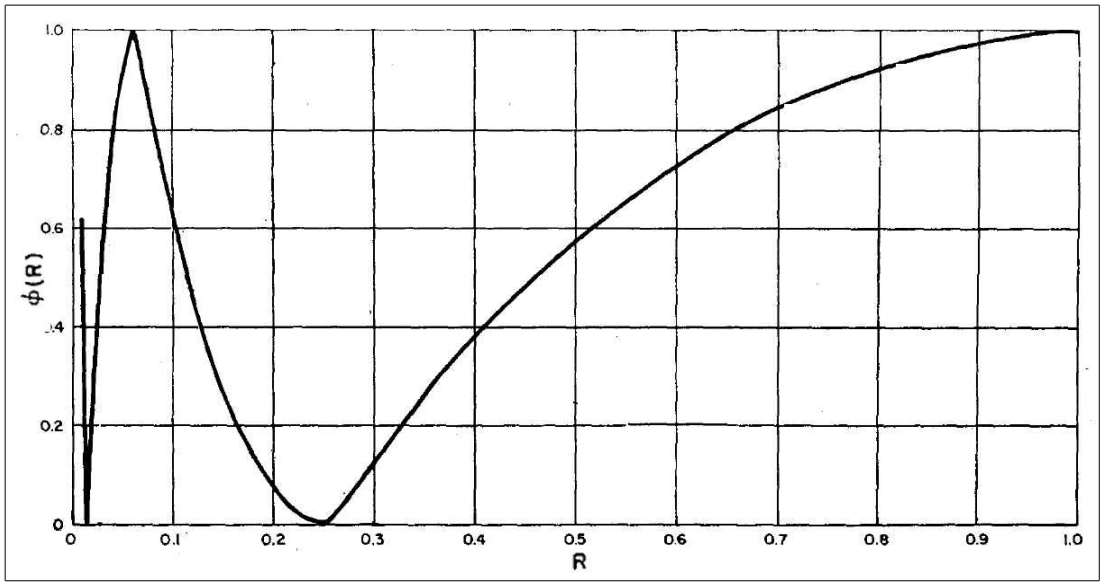

Fig. 3. Nested potential wells in 'poissor' object. Reproduced from [7]

Research continued through the 1970s, but the repetition of encouraging early results [7] and direct measurement of poissor structures proved elusive. Despite a narrowing in the breadth of fusion research, a low level of IEC research oriented toward high-gain operation continued into the 1990s with the pursuit of grid-less approaches by R. W. Bussard and others in the Polywell™ [8] and Periodically Oscillating Plasma Sphere (POPS) [9] programmes. An overview of the development of some of this work is given in [10], noting the considerable contributions made by researchers in the USSR.

At the same time, work carried out in part by G. H. Miley reported interesting physics seen at higher-pressure conditions. This served to expand the scope of the field, with the readily-achievable fusion reactivity in the glow discharge regime and device simplicity making it attractive for non-power fusion applications. The revival in IEC research has been accompanied by an awareness fostered on internet sites, particularly www.fusor.net, which enabled and encouraged enthusiasts to build their own working fusion reactor, and in doing so helped to make tabletop IEC reactors the subject of high school projects and science fairs. This accessibility of fusion conditions has led to development for applications utilising fusion products such as

neutron and proton sources, and a neutron source based on the principle is considered to be the first commercial application of a fusing plasma [11]. Interest has also been shown in application as a spacecraft thruster [12], [13], and proof-of-principle as a proton source for medical isotope production has been demonstrated [14].

A large proportion of the published literature concerns device optimisation for fusion, whether for power generation or other purposes. Some of this work concentrates on establishing theoretical limits of efficacy for power generation, in an attempt to ascertain analytically whether the potential can exist for reaching break-even [15], [16], [17], whilst some focusses on new configurations and topologies to attempt to overcome perceived shortcomings in this regard [8], [9], [18]. A considerable body of work however concerns experimental measurement and observation, often in conjunction with a simple model, aimed towards the better understanding of operation in simple configurations operating at higher-pressure conditions. These describe different 'modes' of operation, identified by Miley et al., and principally referred to as 'jet' and 'star' configurations [12], [19], [20], [21], [22], [23]. Much literature concentrates on these phenomena, and their implications for charge flow focussing and confinement. Another continuing topic of research interest has been the formation of poissor-type spatially-oscillating potential structures within the cathode, due to space charge accumulation and trajectory intersection e.g. [22], [24], [25]. The focus on fusion applications has meant comparatively few experiments have been performed within gases other than hydrogen or deuterium.

1.3.2 Overview of IEC devices

An IEC device utilises grid electrodes in operation at low pressures, in which path lengths are significant fractions of the device dimension. This has been most commonly implemented in a spherical geometry.

Both spherical and cylindrical configurations have been described, with electrode configurations used in early IEC work having a central mesh grid variously as cathode or anode. In more recent work, a relatively open grid cathode has generally been used, as in [26], and the term TCD refers to a discharge obtained in this configuration.

In some cases this has been surrounded by differently-biased or floating outer electrodes e.g. [27], [28], often to assist operation at pressures below those required to sustain a glow discharge. To this end, devices have also featured electron emitters, electron guns and ion guns [7], [9], [27], [28], [29]. Meyer provides a succinct characterisation of these different classes of device in [30], and Miley and Murali give a comprehensive overview of the development of IEC devices and the understanding of their operation in [31]. The majority of experiments at higher pressures have featured a central, spherical cathode, which in the most simple configuration uses the grounded chamber wall as the anode, as shown in Fig. 4. Basic principles of operation in this simple arrangement are briefly outlined below.

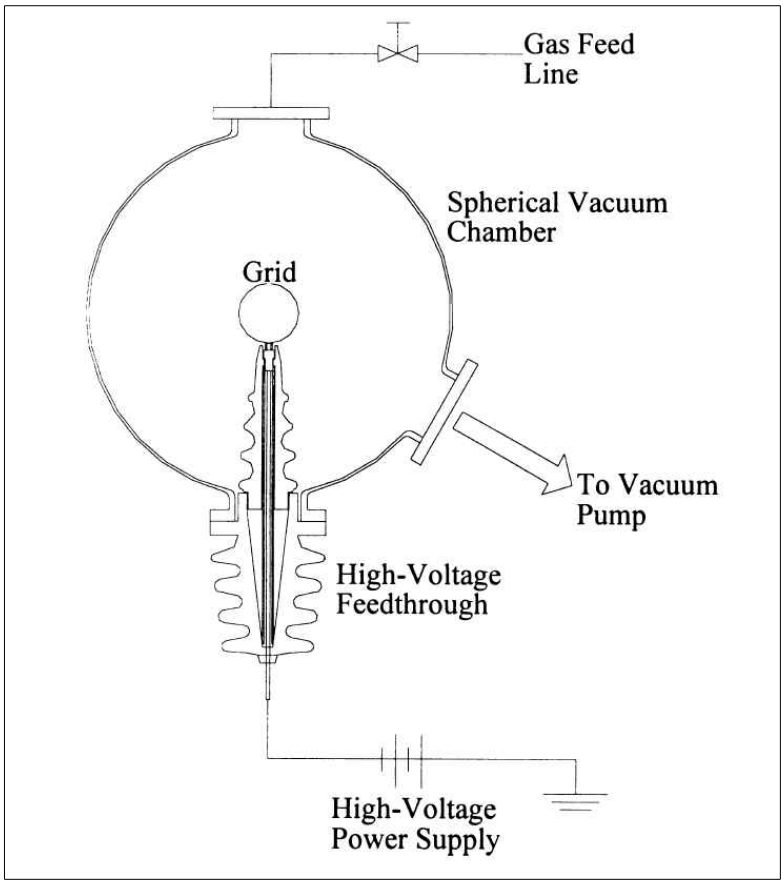

Fig. 4. Schematic of simple TCD device. Reproduced from [11]

Potentials applied to the cathode are typically units to tens of kilovolts, creating a strong electric field in the region surrounding the cathode. Fig. 5 shows a simplified schematic of this type of IEC device, that illustrates the effect this has upon charged particles created by ionisation within the inter-electrode region. These are accelerated by the electric field, causing electrons to flow outwards to the walls and those positive ions which pass through the cathode apertures to converge within the central region.

At pressures low enough for mean-free paths to be appreciable fractions of the inter-electrode distance, ions may be accelerated to keV energies. The importance of charge-exchange reactions in hydrogen has been noted as causing the transfer of much of this energy to neutrals, creating an outwardly-directed energetic neutral flux [32]. The high-energy ion and neutral populations, and long path lengths afforded by the grid construction of the cathode, cause the discharge that may be obtained in this apparatus to differ considerably from those that occur between planar electrodes.

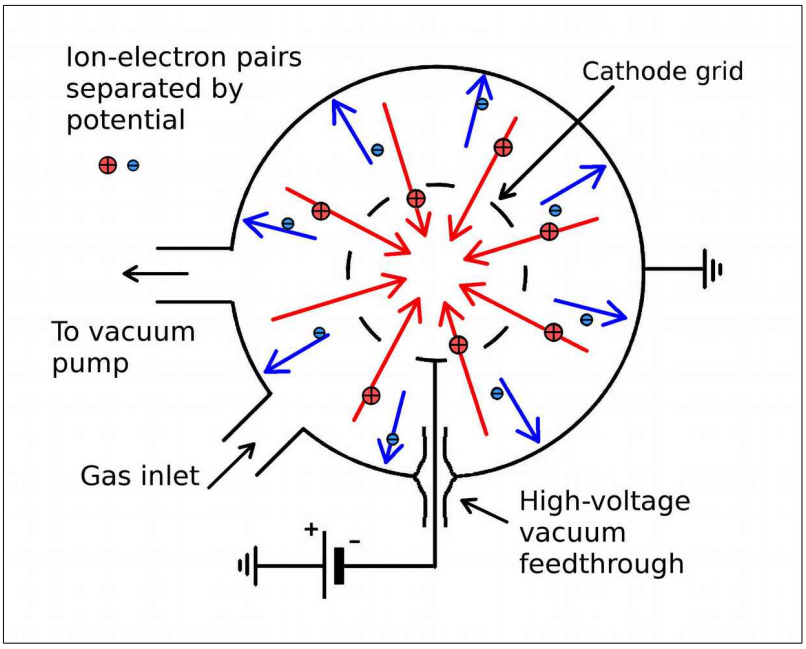

Fig. 5. Simplified schematic of TCD operation

1.4 Background to TCD operation and literature review

In the following section, the published literature on IEC research is reviewed. Some of this work has concentrated upon operation at conditions of pressure considerably lower than those at which a glow discharge may sustain. This is in the interest of maximising the energy and lifetime of ions for fusion, by minimising the energy lost in collisions with the background gas. This study however concerns the operation of a TCD as a self-sustained glow discharge, in which collisions are required for the discharge to ignite and sustain, and so it is the research conducted at conditions of higher pressure that is more relevant to this study.

Some of this work has concentrated upon aspects of the operating conditions at which breakdown occurs, which may be described in terms of known electric field and background particle density distributions. Other work focusses upon properties of the discharge once established. At these conditions, the accumulation of populations of charged particles creates self-induced electric fields, which add to those produced by the electrodes. This self-affecting dynamic may cause plasma to display complex non-linear behaviour and to form structures in the form of plumes, filaments and layers. The processes contributing to ignition will continue to sustain the discharge, but within a less well-defined environment.

This distinction provides a useful means of arranging material relating to this study, and so in the following discussion of TCD operating principles, areas relevant to the ignition of the discharge are initially treated, turning subsequently to the behaviour of the plasma that results. Topics addressed first include electric field distributions, electrode transparency, secondary electron production and breakdown voltages, before moving on to charge flow, mode structure and space charge objects.

1.4.1 Breakdown conditions

The physical processes involved in the initial electrical breakdown of a gas are understood to be due to separation of charge in an applied electric field following background ionisation events, leading to further electron impact ionisation and liberation of more electrons in the volume between the electrodes. For breakdown in a DC field, emission of secondary electrons from the cathode caused mainly by the ion flux incident upon the electrode, also plays an essential role in the creation of charge carriers.

It was mentioned previously that the average path length between collisions is important for determining the energy particles acquire in the electric field. The dimensions of the volume are also important, since these determine the number of collisions that may occur as a particle travels between the electrodes. The increase in effective dimension associated with grid electrodes means that discharges produced using these may have a somewhat different dependence upon pressure, but the same processes enable the discharge to ignite and sustain.

This section of the review will look at the published literature concerning the background electric field in a TCD device, the breakdown voltage-*pd* relation, the concept of effective grid transparency and mechanisms of electron emission.

1.4.1.1 Electric field distribution

In the absence of a plasma, the electric field between concentric electrodes will follow a $1/r^2$ or $1/r$ distribution for spherical and cylindrical cases respectively, according to flux conservation and radial orientation of field lines. The effect of grid electrodes is to cause some local departure from these distributions, associated with the periodic arrangement of grid-wires and apertures. The form of TCD devices described in the literature mostly consists of a largely-transparent central grid electrode, surrounded by either a relatively finer-meshed anode or simply centred within a spherical chamber that serves as anode; in either case the outer electrode being a much closer approximation to a spherical surface than the inner.

The nature of the perturbations to the vacuum potential distribution caused by a grid electrode is described by several researchers. Examples of these, produced by the cathode grid in an IEC device, are mapped by Gu and Miley [24], who show a plot of contours within and in the near vicinity of the cathode (see Fig. 6), and Taniuchi et al. [33], who show how this form varies with different aperture size. Further examples of equipotential plots may be found in Ohnishi and Osawa's work [34], and also in that of Kurt and Arslan [35], [36].

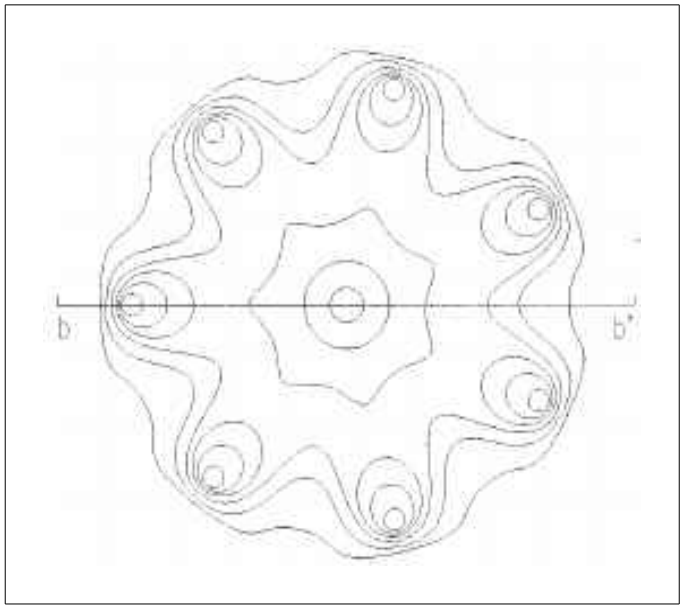

Fig. 6. Equipotential lines around cathode grid wires. Reproduced from ref. [24]

1.4.1.2 Breakdown voltage-pressure relations

Miley and co-workers record breakdown voltages for a variety of *pd*, using hydrogen and deuterium fills [21]. It is commented that the relation is similar to that seen in more conventional discharges with solid electrodes, but with notably different striking voltage for the same values of *pd*; this is seen in *pd*-breakdown voltage relations for various grid cathode discharges in both gases. In this work, *d* is defined to be the dimension between the cathode radius and the chamber wall.

The relations measured are noted to resemble the Paschen curves seen in planar electrode discharges, but at a third or so of the *pd* product value, showing that breakdown may occur at significantly lower pressure for a given voltage when using a transparent cathode. The data for different species and different grid diameters (H_2 and D_2; 3.7 cm, 7.5 cm and 15 cm) is analysed, and the breakdown voltage found to be a function of the ion mass over the square of the *pd* product, with grid diameter having little apparent influence. A plot of the breakdown data compared with calculated Paschen curves is reproduced as Fig. 7.

In [37], Dobson and Hrbud also provide breakdown voltages for H_2 and D_2 that broadly agree with those of Miley; these results do however show some dependence on grid diameter, with a lower voltage required for the same *pd* when using a larger grid.

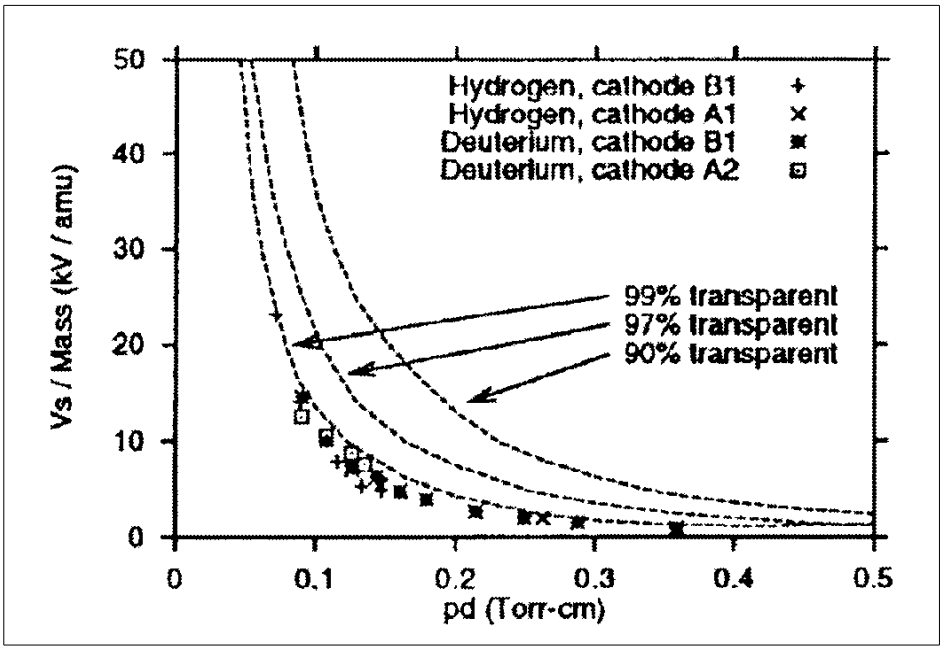

Fig. 7. Striking voltages and calculated Paschen curves, reproduced from [21]

1.4.1.3 Effective grid transparency

Miley et al. [21] infer that the lower voltage required to strike a low-pressure discharge using a transparent cathode may be attributed to an increase in the path length that is multiplied with the Townsend α -coefficient, due to an ion's ability to pass through the cathode apertures; the theory depends upon an 'effective' rather than a purely geometric grid transparency. This concept is tested by constructing two initially identical test spherical shell cathodes, each having two holes cut out; one with the two holes cut diametrically opposite to each other, and the other having them cut at 90° apart. The breakdown voltage-pressure relations for these electrodes show that whilst their geometric transparency is equal, the one with holes at 90° to each other exhibits similar characteristics to a solid electrode, whereas the other has a curve closer to those of the transparent grids. This supports the hypothesis that it is the effective transparency, i.e. the transparency to ions on a radial path passing through the cathode, that differentiates the TCD from planar discharges in this respect. Monte Carlo modelling of the discharge for different effective grid transparencies is carried out, and the best fit to experimental Paschen curves (for ~90 % geometrically transparent grids) is for an effective transparency as high as 99 %. This is seen as further evidence to support the concept of effective transparency as applied to analysis of TCDs.

Dobson and Hrbud also address the issue of effective grid transparency in the setting up of parameters for a model in [37]. They formulate a measure of how the effective grid transparency differs from the geometric in terms of a parameter for grid absorption efficiency, that has a value less than unity when the effective transparency exceeds the geometric. They comment that Miley's findings correspond to an

absorption efficiency of around 0.1, which differs significantly from an assessment by Dolan which gives typical values of around 1.35.

Dolan's approach, given in [10], formulates an effective grid transparency as a function of (and always a fraction of), the geometric transparency. The rationale for this is that ions passing too close to the grid wires will be deflected, so that a region of the aperture bordering the grid wires will be effectively non-transparent. The formulation is limited in that it is only a function of the geometric transparency, and so takes no account of the grid topology; identical results would be arrived at in cases having the same geometric transparency but in which a different fraction of aperture area is located within a given distance from a grid wire.

There is rationale behind these assessments, and it is reasonable to expect that both mechanisms will affect the effective transparency in a real situation. The fit to Paschen data provided by Miley et al. in [21] provides important experimental corroboration however, suggesting that the recirculation effect outweighs the grid wire deflections, at least with the grid topologies used in their experiment.

1.4.1.4 Secondary electron emission

Murali, Santarius and Kulcinski examine the electron emission mechanisms in a TCD device in [38]. Their rationale for the study is that ion current contributes to fusion, and electron current to loss, and so minimising electron emission from the grid will help to maximise efficiency. They note that previous work on scaling fusion reactivity with (ion) current has ignored this distinction, which may explain why fusion yields have not fulfilled expectations.

Electron emission processes examined are secondary emission from the grid, as well as thermionic, photo- and field-emission. Thermionic and field emission are shown to be largely avoidable, but both secondary electron emission from the cathode and wall bremsstrahlung emission are noted to be relevant, and to be non-linear with power. The secondary electron emission effect was investigated using W25%Re and Re single-loop grids; the Re grid was found to give a 27 % improvement in neutron production rate, attributed to a lower secondary electron emission coefficient for Re. Grid heating was reduced at conditions of similar power but higher voltage and lower current. Higher secondary electron emission at higher incident ion energy is shown to be the case for a variety of species impacting Mo, and the importance of this in formulating an ion recirculation current equation is observed; they also note the secondary electron emission coefficient's variation with ion species present should be accounted for, as any heavier impurity ions will have a higher secondary electron emission coefficient. For efficiency, the authors recommend an aluminium wall lining to reduce photo-emission, and polishing spot-welds to avoid field-emission at high voltages.

1.4.2 Discharge operation

With the presence of a discharge, the additional influence of charged particles must also be considered, which may modify the background potential and locally screen more distant features.

Two references suggest that the degree to which this occurs may not be overly significant, at least in parts of the chamber volume. Dobson and Hrbud [37] comment that over their operating pressure range of 0.2 Pa to 6 Pa (1.5 mTorr to 45 mTorr), the electron density outside of the cathode is sufficiently low for the plasma to be considered as confined to the cathode interior. Their experimental and modelled results imply an ionisation fraction of the order of 10^{-4}, indicating the vast majority of particles in the chamber to be neutrals. Discussing their modelling of a TC device, Emmert and Santarius [39] note that the particle densities in a glow discharge of this kind are low enough to leave the background potential largely unaltered by space charge.

Not all accounts however describe an emission distribution limited to the cathode interior. Patterns of emission are frequently described to include plumes and beams which pass through electrode apertures radially, and these are often described as defining features of modes of operation. In this section, the literature concerning these modes is reviewed, along with that describing current-voltage relations, collisional processes and virtual electrodes.

1.4.2.1 Current-voltage relations

Current-voltage characteristics are recorded in the examination of IEC discharge characteristics by Miley et al. in [21], and are reproduced in Fig. 8. Over the 5 mTorr -15 mTorr pressure range used, the breakdown voltage is found to be approximately the same as the subsequent operating voltage, with the current-voltage relation in the flat portion of the normal glow discharge regime shown in Fig. 2, with a small increase in voltage causing a large increase in current. The voltages are units to tens of kilovolts, and the currents units to tens of milliamps. Further examples of current-voltage and pressure data from a TCD are given in [40].

1.4.2.2 Mode structure; jet and star modes

The unique nature of IEC discharges gives rise to some characteristic features. As mentioned in the introduction, two distinctive discharge modes are associated with higher-pressure operation, that are most commonly referred to as the 'star' and 'jet' modes. These are described in [19], along with a third, as the 'star', 'halo' and central spot' modes; no further mention is found of the central spot mode, and the halo mode appears to be referred to thereafter as the 'jet' mode. Both the star and jet modes involve visibly luminous features passing radially through grid apertures, with the star mode having spoke-type structures emanating from all or most apertures, and the

jet mode having one or more formations variously described as resembling a beam or a plume (see Fig. 9).

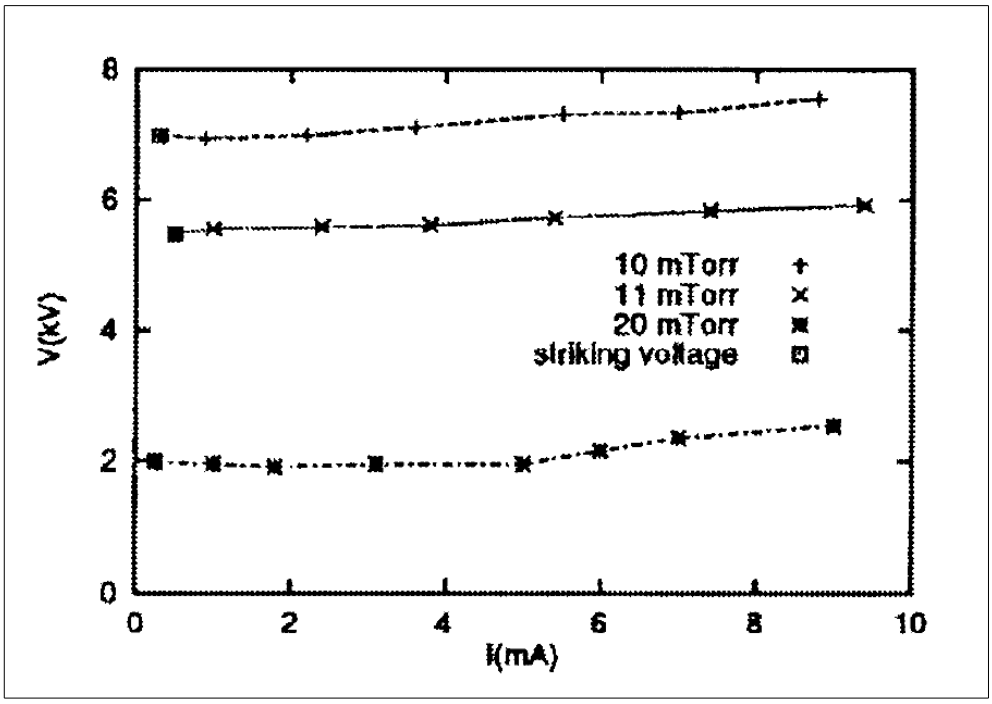

Fig. 8. Current-voltage relations presented in [21]

In [21], Miley et al. note that the star mode occurs at *pd* of below ~0.5 Torr-cm in hydrogen and deuterium discharges. Furthering the discussion of effective grid transparency outlined above, they explore the possibility that the formation of spokes or 'ion microchannels' of the star mode may increase the effective transparency of the grid, as ions preferentially pass through the grid apertures. The formation of these microchannels is attributed to an electrostatic lensing effect caused by the deviations from a spherical potential distribution in the vicinity of the grid apertures (Fig. 6). They observe that the curvature of these surfaces will have a defocussing effect for incoming ions as they approach the grid, and so serve to remove those less well-aligned with the microchannel path. For ions and electrons exiting the cathode however, the potential surfaces will have a focussing effect. For a re-circulating ion current, this would tend to keep the ions in a suitable radial location during deceleration, to be re-accelerated back through the aperture. It is concluded that these selection and focussing mechanisms are likely to be causing the formation of microchannels.

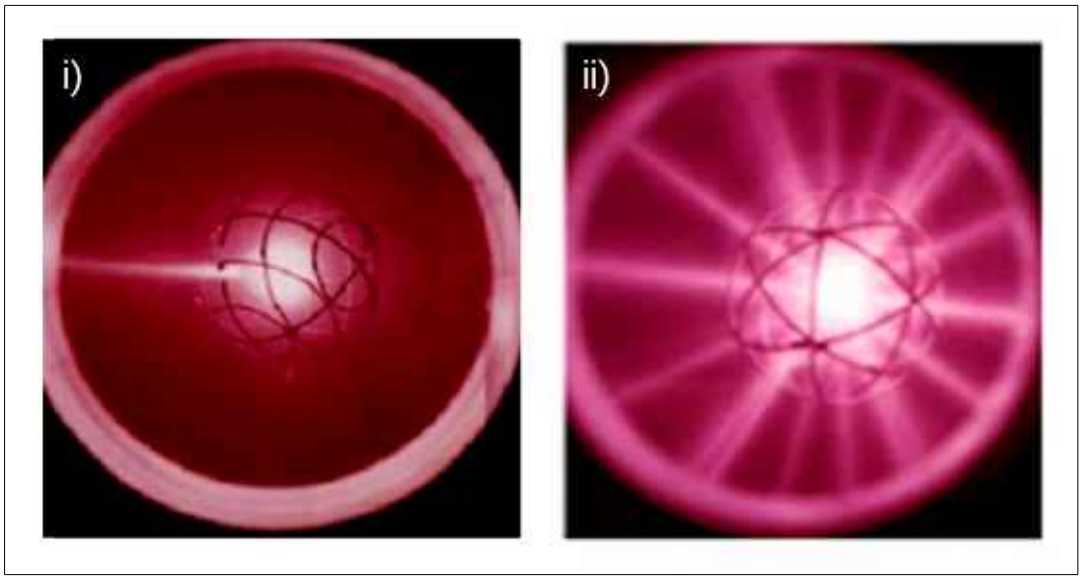

Fig. 9. Photographs of i) jet and ii) star mode discharges. Reproduced from ref. [12]

The role played by these mechanisms in microchannel formation is supported by ion trajectory simulations showing longer lifetimes for ions on microchannel trajectories, reproduced as Fig. 10. It is also observed that ions created from ion impact ionisation would be preferentially born on these paths. This would act as further selection, helping to create higher particle densities along microchannel paths. The microchannelling phenomenon may therefore increase the effective grid transparency, but the net contribution made to any recirculating ion current is not clearly established. In fact, it is suggested in [41] that at the relatively-high pressures used in Miley's experiments, most ions will be expected to charge exchange with background gas particles on the first pass through the grid, and so any re-circulation will be negligible.

Other researchers have also investigated the concept of effective cathode transparency. Neutron production rates are recorded for cathodes with geometric transparencies of 80 % to 90 % by Taniuchi et al. [33], who find that over this range an increased fusion rate is achieved with a *less* geometrically-transparent cathode. This is attributed to enhanced microchannel focussing as the cathode field becomes more spherical, suggesting that the defocussing effect may be significant and so providing further insight into effective grid transparency. This is corroborated by Thorson et al. [41], whose observations of core spreading at low pressures are attributed to grid effects, with a reduction in wire spacing achieving a better focus.

The jet mode is given less treatment. In the brief description of the 'halo' mode given in [19], this is described as being accompanied by an electron jet, and to require the enlargement of one of the grid apertures for its formation. It is noted to occur at slightly higher pressures than the star mode, and to display around twice the fusion reactivity, at conditions of somewhat higher pressure and lower voltage. The jet is described as evolving from an electron beam to a plume with increasing pressure in [23]. In [19] the jet is also described as being composed of electrons, although in [12] this is described as being a space-charge neutralised plasma beam.

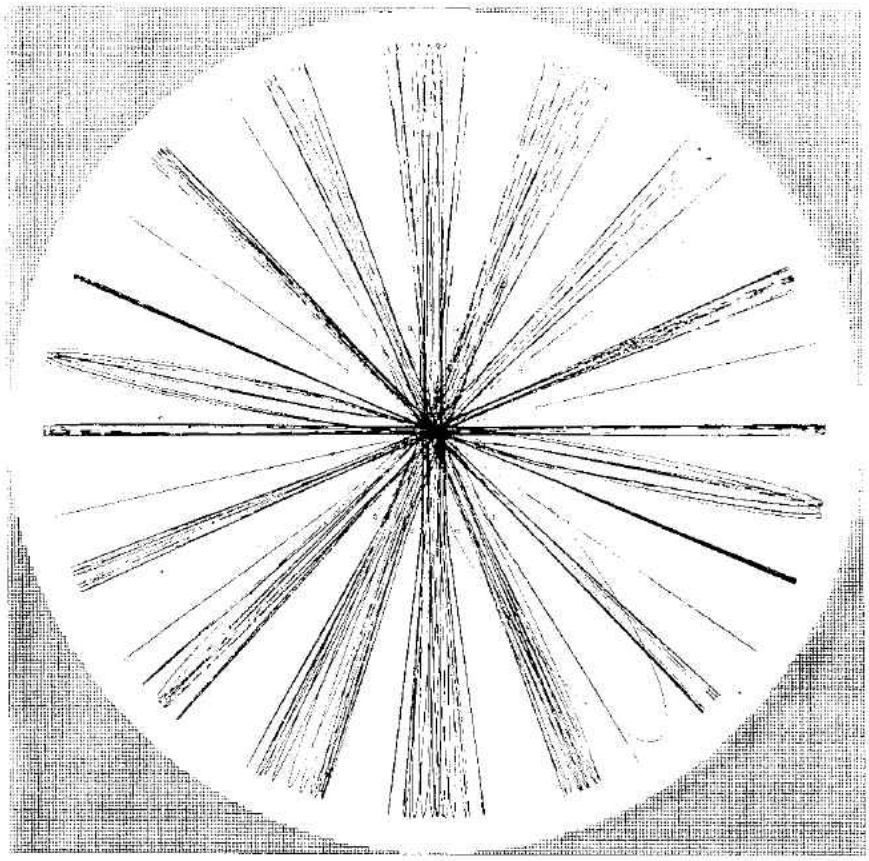

~~Fig. 9.~~ SIMION calculation of ion paths in the IEC. The trajectory "bundles" resemble microchannels while a dense plasma "core" is formed by intercepting trajectories at the center of the sphere (the shaded outer region defines the chamber wall).

Fig. 10. Modelled ion trajectories, reproduced from [21]

The spoke-like formations described by Miley et al. as the 'star' mode have also been described by other authors. In [20], Meyer et al. report ion density profiles and floating potential measurements made with Langmuir probes, in regions both with and without microchannels. These show microchannels to be neutral at a narrow range of perveance around 4 $mA \cdot kV^{-3/2}$, which is also observed to be the approximate value of perveance at which the star mode transitions to the jet mode. Ion densities are shown to be several times greater than electron densities at perveances either side of this range, with an order of magnitude difference at values below ~2 $mA \cdot kV^{-3/2}$. They also show that the heterogeneous structure of the star mode persists into the jet mode regime, despite a single jet generally being visible over much of the range. Much material is common to this work and [22]. An observation made in [22] concerning the star mode is that spokes were present at most but not all of the cathode apertures. The grid structure used in these experiments is described as consisting of highly transparent inner and outer grids, with each having a different form.

In another star mode experiment, Murali et al. [42] report that during cathode displacement, the hotspots caused by microchannel flux upon an intermediate spherical mesh electrode were observed to move coincidentally with the cathode being rotated, whilst retaining their particular shape. This is further evidence for a direct association between microchannel features and the cathode grid apertures.

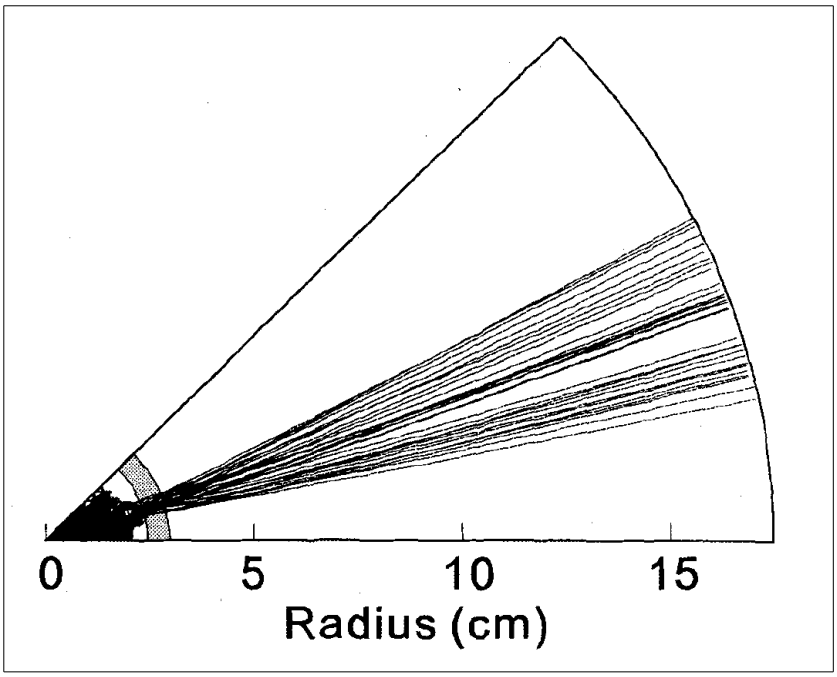

Fig. 11. Modelled electron trajectories, out-streaming from cathode centre. Reproduced from [43].

There are grounds for making an association between the radial beams of the star mode and the dynamics of electrons born by ionisation within the cathode. Ohnishi and co-workers [43] observe that in a collisional regime, such electrons will be plentiful, and must be able to exit the cathode in order to travel to the wall. It is therefore theorised that these will accumulate in sufficient numbers to counter the positive space charge introduced by injected ions, and so cause the potential within the cathode to be maintained at a level sufficiently negative for them to be able to escape through the cathode apertures. The authors develop a particle-in-cell modelling code that simulates steady-state conditions, and find that this is indeed projected to occur. The solution indicates electrons to be transported from the cathode apertures in a narrow, beam-like spread of radial trajectories; resembling a star mode beam; a plot of these trajectories is reproduced as Fig. 11. Ions in the system are indicated to follow paths that pass much closer to the cathode grid, but still to recirculate through the apertures to a considerable degree.

1.4.2.3 Collisional processes

Various diagnostics and observations are reported concerning the species composition, and the nature of particle flow and collisional processes in TCD devices.

In [44], Boris and Emmert investigate the ion species composition of the source region outside their anode grid using an ion acoustic wave diagnostic, comparing the results with formulated rate equations and demonstrating the variety of interactions and species that may occur with a deuterium fill. This work is built upon further in [39] and [45] in which Emmert and Santarius develop a model of ion-neutral interactions for atomic and molecular species. The presence of negative ions in TCD plasmas has been confirmed by Boris et al.in [46], who detected deuterium anions due to both thermal electron attachment near the cathode and also charge-transfer interactions in the inter-electrode region.

Dobson and Hrbud's study [37] was noted to indicate the vast majority of particles in the chamber to be neutrals. The significance of this relatively abundant background neutral population in determining the predominant interactions within the discharge is noted by many researchers. In [41] Thorson finds no evidence for a centralised fusion source in an IEC, concluding that reactivity with background neutrals dominates. In [47] Boris, Kulcinski et al. report measuring fusion ion energies with FIDO (Fusion Ion DOppler shift, imparted by fusion products). The results show most interaction to be occurring with low-energy molecular reactions, and that most fusion occurs in collisions with background neutrals.

In [20] Meyer notes the variation in recognised importance of the fusion reactivity contribution made by fast neutrals with background neutrals, considered by some to be the principle fusion mechanism whilst completely neglected by others. Miley et al. [21] also comment that charge-exchanged fast neutrals significantly augment ion flow. This picture is added to in [32], in which Khachan describes the IEC glow discharge in terms of being an effective neutral beam source, using Doppler-shift spectroscopy to detect ions picking up energy before charge-exchange takes place to create the radially outward-directed fast neutral flux.

Murali et al. [48] use a fine 'chord-wire' stretched across the path of ion flux to infer the flow rate by heating effects. Khachan and Samarian [49] use the observed drift of dust particles dropped through the centre of a two-loop cylindrical cathode to diagnose an ion flow directed outwardly from the cathode centre. Forces and charge accumulation are evaluated; no force other than ion drag can account for the motion. It is noted that the negligible electrostatic drift may also indicate a space charge accumulation at the centre of the cathode. Doppler-shift spectroscopy in [32] also indicates an ion flow moving outwardly from the cathode, which is explained in terms of a positive charge accumulation, or 'virtual anode' existing at the centre of the cathode. Further work concerning the formation of such virtual electrodes are described in the following section.

1.4.2.4 Virtual electrodes and space charge objects

Evidence for the poissor formations originally pursued in IEC research was presented in Hirsch's 1967 paper [7]. In this work, a numerical solution of Poisson's equation for mono-energetic ion and electron distributions is shown to indicate multiple nested potential wells, caused by space charge distributions within the cathode (illustrated in Fig. 3). The paper also records an exceptionally high neutron production rate for an IEC device of 10^{10} neutrons per second, which was achieved using six orthogonal ion guns at very low pressure, and is estimated to be consistent with a core ion density of between 10^{18} m^{-3} and 10^{20} m^{-3}. Bremsstrahlung collimation results show a double peak of emission within the core region, agreeing with the interpretation of multiple potential well formation causing high densities of trapped ions. Much work has subsequently been directed towards the investigation of virtual electrode formation, both theoretical and experimental.

While Hirsch's model assumed highly idealised particle distributions, subsequent work using finite angular momentum spreads has indicated that in practice, the multiplicity of such potential wells is likely to be limited to a 'double well', signifying a negative well contained within a positive virtual anode, as illustrated in Fig. 12. References [25], [37], [50] and [51] all detail theoretical modelling that has predicted the existence of double potential well structures; [51] also provides a recent review of research on this topic. Tzonev et al. [52] found that a large spread in ion angular momentum was not necessarily an obstacle to double well formation, and in [53] Momota and Miley find the focussing of the secondary particle, (i.e. the electrons) to be critical for the depth of the second (negative) well produced. Dynamic analysis of the injection of positive space charge into a cylinder performed by Hockney [54] indicated that stable double wells may form over a range of injected current levels and distributions. None of these models considers all of the collisional processes occurring at conditions having a significant background pressure of neutrals. Very little modelling has been done in a collisional regime, but that reported by Ohnishi et al. [50] predicts the transitory existence of double and even triple wells. A comprehensive review is included in [30], describing the modelling done by many workers, including some of those mentioned above, in a variety of configurations. In this paper, results from earlier calculations made by Langmuir and Blodgett, Lavrent'ov, Swanson, Dolan, and Hirsch are reproduced.

Experimental researchers have struggled to reproduce the results reported by Hirsch. Direct measurement of poissor structures is made difficult by the perturbing effect of probes, and so a variety of indirect approaches have been utilised. The results of some experiments do appear to show evidence for double well structures, although many of these are subject to significant uncertainties.

Dobson and Hrbud [37] present a theoretical model having a double well solution, which agrees with electron density measurements made using microwave interferometry, that show eccentric minima within the cathode region during operation at higher pressures of between 15 mTorr and 30 mTorr in argon and deuterium.

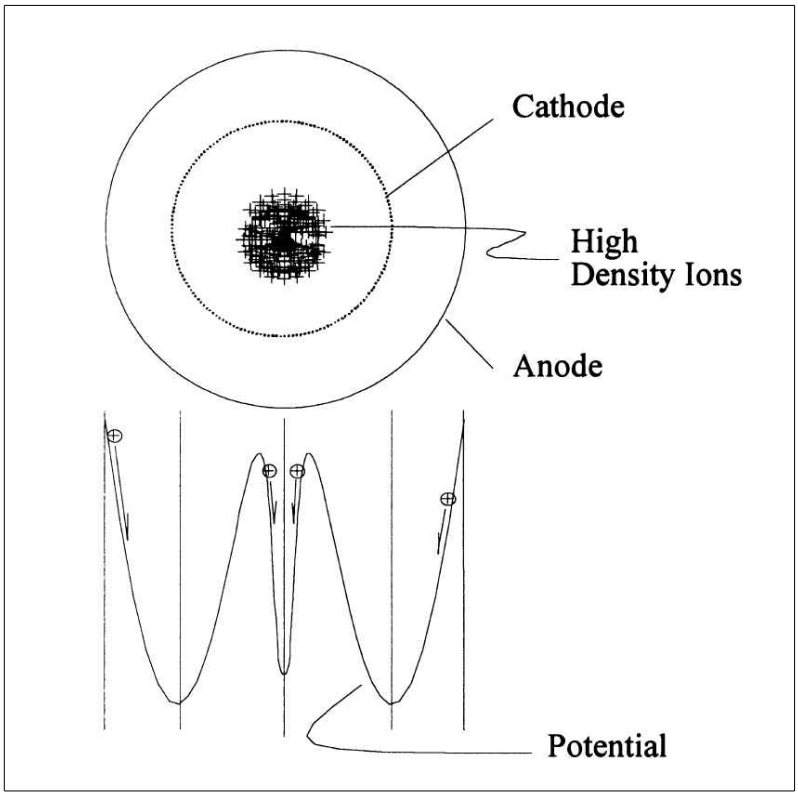

Fig. 12. Illustration of double potential well profile (reproduced from [11]).

Swanson et al. [55] investigate potential structure in an IEC device having a mesh anode, using the deflection and degree of focussing of an electron beam that is directed across the core region. They find evidence that the injection of electrons into this anode in vacuum conditions causes a negative potential well to develop, that has a parabolic profile. With background gas admitted into the chamber at pressures of the order 10^{-5} Torr, this potential profile is found to develop a centralised region of positive potential, so forming a multiple potential well structure within the anode.

In [24], Gu and Miley report a double peak in fusion proton counts from a TCD core region, obtained by performing an Abel inversion of counts from D-D fusion taken over angles across the cathode. This is taken to be definitive evidence of the existence of double potential well structures, but doubt is cast on this certainty by the work by Matsuura et al. [56] who show that a radial profile of the neutron production rate may be calculated using a weakly collisional model. In this model, the potential is solved and in turn ion velocity, and the neutron production rate assessed from this. Crucially, the work shows that a double peak in reactivity may be possible without the need for a double well. Meyer et al. also comment in [25] that the findings of Gu and Miley regarding the depth of the well detected do not match their theoretical analysis.

Use of a laser-induced fluorescence technique is reported to show a double potential well with a depth of several hundred volts in a 30 mTorr helium discharge by Yoshikawa et al. in [57]. This technique uses a laser to excite a particular electronic state of helium, which subsequently emits light having a degree of polarisation sensitive to the local electric field.

In the description of the previously-mentioned 'halo' mode [19], it is stated that this structure is believed to represent a double potential well, that results from the formation of a virtual cathode. The reference given for this statement is an M.S. Thesis written by Gu at the University of Illinois, but it has not been possible to follow up this reference further, as the thesis is not listed in the University of Illinois library catalogue.

The existence of a positive virtual anode at the core of spherical devices is however widely reported. In ref. [20] Meyer et al. report the detection of a virtual anode via floating potential measurements at perveances over ~6 $mA \cdot kV^{-3/2}$ (with a deep example seen at a higher perveance of ~23 $mA \cdot kV^{-3/2}$). Khachan et al. [58], [32] use Doppler-shift spectroscopy and Langmuir probe data to establish ion energies and potential, showing the existence of a virtual anode in a two-loop cylindrical cathode.

With the exception of Swanson's work, all of the experiments described above have been conducted at pressures of units mTorr to tens mTorr, which constitute collisional conditions. In [27], Langmuir probe measurements are reported to show a large positive potential within the centre of a grid cathode, during operation at conditions of significantly lower pressure (reproduced as Fig. 13).

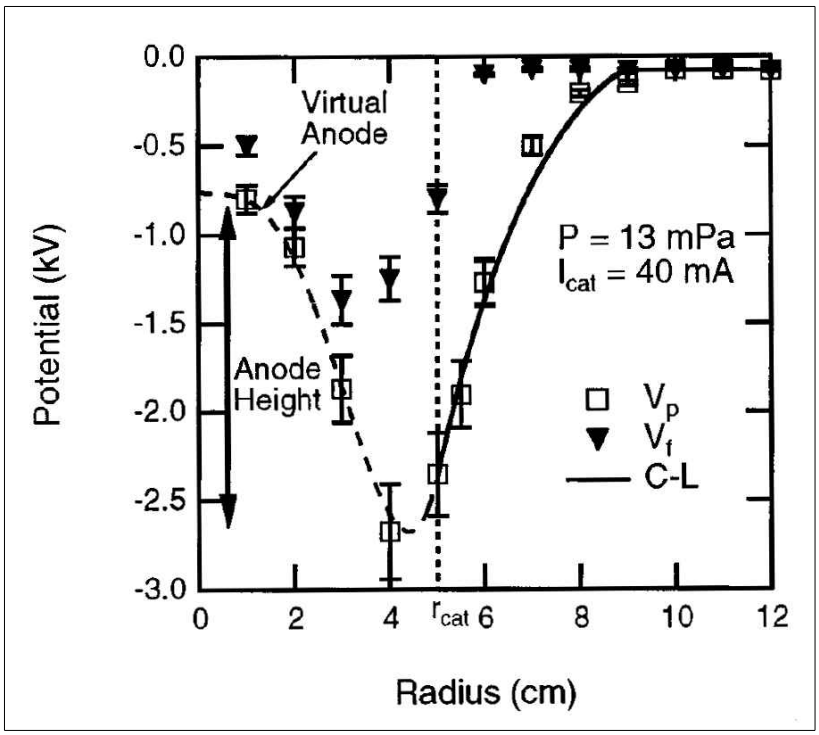

Fig. 13. Plasma and floating potential measurements showing virtual anode at centre of IEC device. Reproduced from [27].

1.4.2.5 IEC fusion

Fusion reactions result in the release of energetic reaction products, such as neutrons, protons etc, with the emitted species depending upon the fuel used. This makes fusing IEC discharge plasmas suitable for non-power applications that utilise these fusion products, as outlined in Section 1.3.1. Fusion power remains a concern for IEC research however, and in [31] Miley and Murali discuss the fusion performance of IEC systems, and how they compare with more widely-researched approaches such as laser Inertial Confinement Fusion (ICF) and Tokamaks.

It is noted that any successful fusion power system must satisfy the Lawson Criterion, after [59], in which $n\tau$, the product of density, n, and confinement time, τ, must exceed a threshold value, at a certain ion temperature, T_i; these determined by factors such as the fuel used and the ion energy distribution. In contrast to approaches in which fusion products may heat the plasma sufficiently to enable 'ignition', IEC systems are described in [31] as 'wet wood burners', in which a fraction of the fusion power must be fed back in to maintain the reaction. The inefficiency associated with this characteristic is noted to increase the value of $n\tau$ required for power production. Achieving high T_i is relatively easy in IEC devices, since ions may be accelerated to energies corresponding to the majority of the applied potential; the possibility of obtaining a beam-like, non-Maxwellian ion energy distribution further enhances the scope for IEC systems in this respect. These properties make IEC technology capable of fusing aneutronic fuels, which is in contrast to many other approaches. Use of such fuels however requires significantly greater values of $n\tau$, and it is in this respect that conditions in simple IEC devices fall short; whilst fusion rates useful for some non-power applications are readily obtained, the energy gain, Q, for these reactors is typically between 10^{-7} and 10^{-9}.

The principal loss route in simple IEC systems comes from a relatively poor degree of ion confinement, as ions are projected to make only around 10 passes through the core before impacting the cathode. Research directed towards improving the efficiency of IEC devices aims to address this issue, either by improving ion focussing with additional grids e.g. [17], or by utilising alternative approaches to developing a space charge potential well for ion acceleration [8]. It is for this reason that there is such an interest in the possible formation of double potential wells in IEC plasmas. The POPS scheme [9] aims to not only confine ions within a negative potential well, but also to cause them to undergo coherent, harmonic oscillations. Successful application of such approaches is envisaged to enable orders of magnitude improvements in ion confinement, but other significant inefficiencies are noted to remain. These include the tendency for Coulomb interactions to cause the beam-like ion energy distribution to relax to a Maxwellian on a shorter time-scale than that for fusion to occur [16], and also energy losses via radiative Bremsstrahlung that increase with electron temperature [15]. It is observed in [31] that these issues make net power output challenging, but that there is no apparent 'show-stopper'.

An example of the formulation of the Lawson criterion for an IEC plasma, in which ions undergo POPS-type oscillations within a cylindrical, virtual cathode, may be found in [60]. Assuming a potential well-depth of 100 kV and a radius of 0.8 cm, the

criterion is calculated to be satisfied for a discharge pulse of around 3 ms, during which time the ion population would converge some 10^5 times. The analysis refers to the experimental investigation of nanosecond vacuum micro-discharges [61], in which virtual cathode well-depths of 10's kV, and periodic neutron yields corresponding to ion oscillation frequencies of 10's MHz have been recorded. Interestingly, the gain of such systems is shown to scale inversely with square of radius, in marked contrast to Tokamak-based approaches.

1.4.3 Summary

In summary, the IEC literature contains a small but substantial body of work describing the operating characteristics of TCDs, almost exclusively in a spherical geometry. Because of the fusion interest of this research, many of the details concern neutron production rates, although some measurements of current-voltage relations and breakdown voltage-pressure relations are also reported.

The literature broadly agrees on a picture of a convergent ion flow, with several different investigations finding this to result in the formation of a region of positive space charge within the cathode, known as a virtual anode. The idea of recirculating ion beams seems unlikely to apply generally to operation at glow discharge pressures, which is characterised rather in terms of a significant degree of interaction with background neutrals occurring throughout the chamber, with charge exchange indicated to a principal reaction.

The spherical TCD device is described as operating in characteristic modes, although these are quite poorly-defined, with the exception of the star mode. Regarding the others, which are variously called halo, jet, and central spot modes, there is scant mention of these except for the jet mode, and a degree of confusion surrounds the operating characteristics of all of these.

The star mode is characterised by the presence of organisational features of the discharge, referred to as ion microchannels. These appear as spoke-like lines of bright emission that follow radial chords through the cathode apertures, and are clearly shown to be associated with the location of these. The discrete nature of the grid is understood to cause distortion in the vacuum potential distribution, which is taken to indicate that the microchannel features are caused by electrostatic lensing. This lensing effect is noted to be focussing for particles leaving the cathode, and defocussing for those entering it.

The additional path length afforded to particles passing through the cathode apertures is convincingly associated with observed breakdown parameters, indicating that particles do follow these trajectories. It is also shown that organised structures such as radial beams may result from various selection mechanisms that may be associated with these (de)focussing potential surfaces.

The interaction of particle flows with the grid apertures is considered in terms of an effective grid transparency. Considerable variation is evident in the different

assessments made of this, which may indicate either an enhancement over the geometrical transparency, or a diminishing, with reasonable arguments made for either position.

Some evidence exists for the formation of double potential wells, but generally at higher pressure than those of Hirsch's experiments. What effect these may have on the characteristics of the discharge is unclear.

This concludes the review of IEC literature. Before moving on to describe the experimental work undertaken, the structure of the rest of the thesis is briefly outlined in the following section.

1.5 Thesis overview

In the next chapter, the experimental apparatus and equipment used to make observations of the discharge are described. The experimental observations are then recorded in a series of subsequent chapters.

In Chapter 3, the first set of observations provides an account of the mode structure that is found to characterise operation across a wide range of conditions of pressure and voltage. Measurements and analysis are directed towards the understanding of the nature of processes instrumental in the sustaining of the discharge in these modes, in order to make clear distinctions between them.

These principal modes are studied further in Chapters 4 and 5, in which measurements provide further details of electrical characteristics and distributions of emission, and some of the physical dependences shown upon the geometry of the electrodes are investigated. The material included in these chapters is broadly separated according to mode, but the scope of some of this is relevant more generally.

Chapters 6 and 7 are concerned with a variety of space charge-related features that generally occur at operating conditions of relatively high current. Some of these resemble modes mentioned in the literature, and an effort is made to characterise them in an effort to shed further light upon the different types of IEC plasma. This is done by again considering both the physical processes sustaining the objects and the dependences shown upon the physical nature of the apparatus.

In Chapter 8, some of the insights gained into the operation of the discharge are applied to the devising of different electrode geometries, that may be more or less suitable for different applications. Two such formats are detailed, and results are described of brief, proof-of-principle experimental testing.

Further material is included in two appendices. In the first of these, the elements of the thesis that are intended for publication are outlined. The second contains a short set of considerations regarding the analysis of photographs of optical emission distributions.

Chapter 2
Experimental methods

This chapter contains an account of the apparatus and equipment used for the making of experimental observations. It is divided into sections, describing first the experimental apparatus, and then the diagnostic approach and equipment used.

2.1 Experimental set-up

This section A schematic of the experimental set-up is shown in Fig. 14.

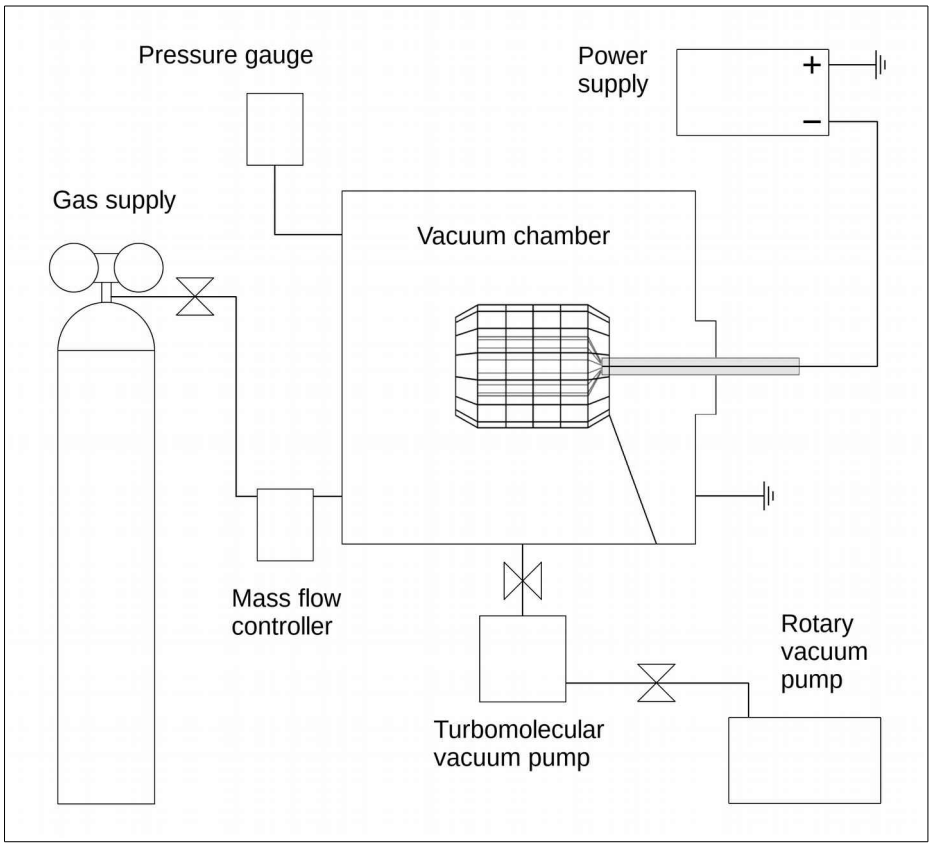

Fig. 14 Diagram showing principal elements of the experimental rig.

2.1.1 Vacuum system

The experiment is contained within a cube-shaped TrinosLine vacuum chamber with 30 cm sides. Five of the sides are stainless steel, and the top is acrylic. The chamber is equipped with circular ports located at the centre points of sides of the chamber. These are arranged in pairs of two different sizes, so that ports on opposing sides are of the same diameter. The diameters of these are 10 cm and 4 cm.

Two additional 4-cm ports are located off-centre, and opposite each other, and one further located in the centre of the chamber floor.

The chamber ports are used for connection of vacuum pumps, gas and electrical feed-through components and vacuum monitoring equipment. A viewport window is also generally fitted to one of the two larger ports.

The port in the chamber floor is used for attachment of the vacuum pumps. There are two of these, which are used for attaining different vacuum levels, with operation generally involving the simultaneous operation of both. The majority of the gas inside the chamber is evacuated using an Edwards RV3 rotary vane pump. This provides a level of vacuum sufficient for the operation of a Leybold Turbovac50, which is a small turbo-molecular pump. The operation of these pumps provides a base pressure of around 10^{-5} Torr in the chamber.

Small quantities of gas may be admitted into the chamber, with the flow of this regulated by mass flow controllers. Two MKS GE50A series units are connected, with maximum flow rates of 20 sccm and 100 sccm respectively. They are operated by means of an MKS 647C control unit.

Pressure is monitored by two types of gauge; these are a Pfeiffer CMR375 capacitance manometer suitable for monitoring pressures smaller than around 90 mTorr, and a Pfeiffer PCR260 dual pirani gauge used at higher pressures. The gauges are connected to a Pfeiffer TPG Dual gauge control unit. The capacitance gauge is generally used where possible, since the output of this is considered more reliable at low pressures, and requires no correction for gas species.

Two processes that may occur during operation of the plasma affect the use of the viewport windows; these are sputtering and X-ray generation. Sputtering is a process in which the flux of particles upon surfaces within the chamber causes material to be ejected into the volume. This material is then deposited again, which is a problem when sputtered electrode material is deposited upon glass windows, since they become obscured. Sputtering is found to be particularly significant during operation in heavier gases, and at lower pressures. At operating conditions of high current in argon, the optical transmission of viewport glasses may become largely compromised in tens of minutes of operation. For this reason, glass shields are installed so as to cover the inside face of the acrylic chamber lid and the larger viewport. For operation at conditions where deposition upon port glasses is extreme, this may be mitigated to some extent by the use of shutters, since the reduced conductance constricts the flow of sputtered material.

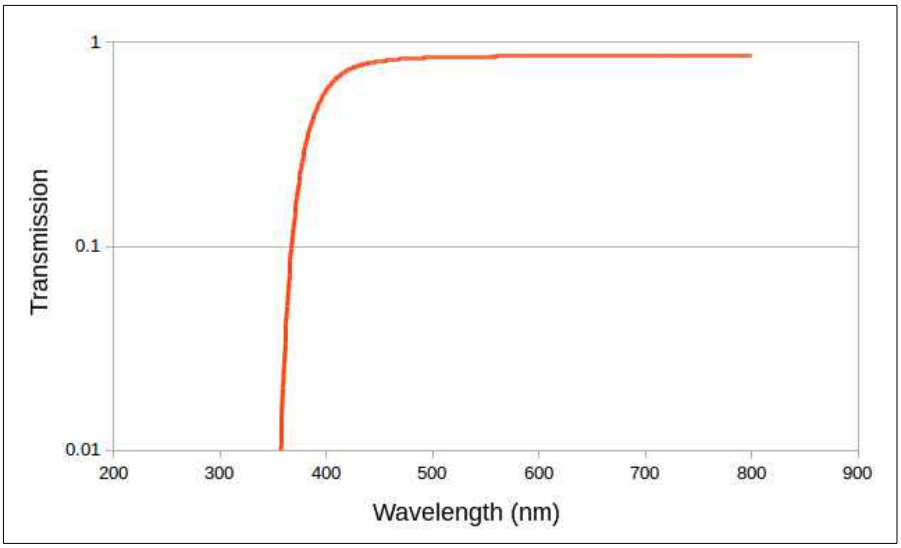

Fig. 15. Spectral transmission of X-ray glass fitted to viewport

X-rays are generated when high-velocity particles impact surfaces. The chamber walls are 10 mm thick stainless steel which provides adequate shielding for this, but the operation of this plasma source at low pressures is found to cause a considerable amount of ionising radiation to be detected at the window and the acrylic lid. For this reason, the viewport window is made from high lead-content glass, and a sheet of similar material is additionally installed beneath the lid. The transmission of this glass also attenuates frequencies in the near UV, as illustrated by the manufacturer's transmission profile (Fig. 15).

2.1.2 Electrodes

The chamber contains two cylindrical, coaxially-aligned grid electrodes, with the cathode positioned inside the anode. Both electrodes have fourteen apertures around the circumference, and are made from 1.6 mm diameter stainless steel. The cathode is 10 cm long, and has half the radius of the anode. The anode has an additional row of apertures at each end, terminating at a ring of some 80 % of the main radius giving it a barrel-shaped form. Fig. 16. shows a sketch of the electrodes. The high-voltage feed-through serves as the cathode support, whilst the anode grid is supported by a simple stainless steel stand, electrically isolated from the chamber. The cathode has a radial geometric transparency of ~0.82, and the anode ~0.88; these are calculated for the portion of the electrodes corresponding to the central four rows of apertures.

The cathode feed-through is constructed from a Pfeiffer porcelain feed-through rated to 30 kV, which is modified using a double-walled alumina assembly to which the cathode grid is fixed. The design of this was found to be necessary to avoid continual arcing that appears to result from charge accumulating upon the surface of the outer alumina tube.

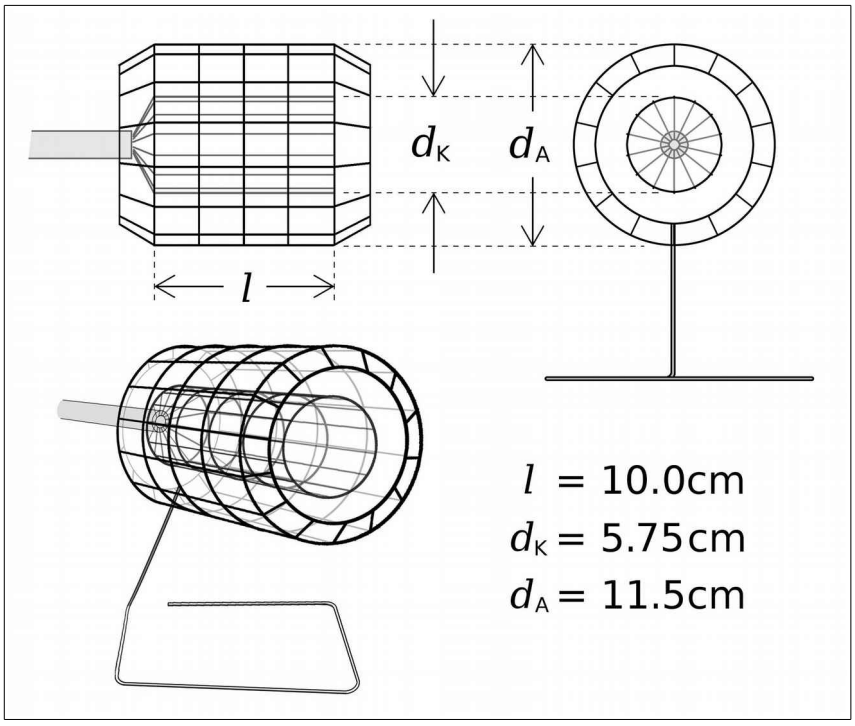

Fig. 16. The form and dimensions of the electrodes and their means of support

2.1.3 Power supplies

The cathode is driven by one of two available Glassman WX series power supplies, one capable of sourcing 35 mA at voltages up to 30 kV, and the other 100 mA up to 10 kV. In practice, the voltage has often been limited by the feed-through arrangement to around 20 kV.

These power supplies operate in either a constant-current or a constant-voltage mode. Limiting values for levels of voltage and current are programmable, with the operating mode automatically selected by whichever of these limits the output. Generally high dI/dV is found to make operation more stable in the current-limited mode, with voltage controllable by varying the gas flow.

2.2 Diagnostics

The TCD is a plasma for which operating conditions may vary significantly in terms of pressure and voltage. At different conditions the plasma takes very distinct forms, some of which are strongly anisotropic in spatial distribution. These may contain relatively small structural elements, and some resemble beam-like flows of particles.

Much analysis and interpretation of Langmuir probe characteristics assume a Maxwellian distribution of particle energies, and are subject to error should the real distributions depart from these conditions (see e.g. [62]). High operating voltages, and the likelihood of non-Maxwellian energy distributions amongst charged particle

populations, therefore make the implementation and interpretation of Langmuir probes problematic. The insertion of probes may also perturb space charge configurations, and so for these reasons this diagnostic approach has not been developed for the project.

The techniques that have been used for the making of experimental observations have been essentially limited to the measurement of electrical parameters and optical emission, and therefore have been non-invasive. The experimental approach has been to characterise the discharge in terms of these properties, before then making strategic alterations to the electrode arrangement in order to explore the physical dependences shown upon these.

Additional equipment was introduced, and in some cases fabricated, throughout the course of study, and diagnostic capabilities evolved continually until the end of experimental work. Some of these were therefore not available for large parts of the project, and time constraints allowed some to be used only once. The following description of equipment used is sub-divided into parts treating the monitoring of electrical and optical characteristics.

2.2.1 Electrical measurements

2.2.1.1 ADC system

This system is used to record various electrical signals generated during operation of the plasma. These include the analogue monitoring signals for cathode voltage and current generated by the power supplies, and also an analogue signal generated by the pressure gauge controller. Current flowing to the anode grid is converted to a voltage developed across a small resistance to ground, and a similar arrangement is used for the currents incident at collectors located elsewhere in the chamber; these are described in more detail later on in this section.

The ADC function on an Arduino microcontroller is used to digitise these voltages, which may then be logged on a PC. These signals are buffered, and in some cases inverted and/or attenuated on a shield, so as to present positive signals of between 0V and a reference voltage to the microcontroller. The ADC is 10-bit, and so the resolution of measurements made using this system is around 0.1 % of full scale. The maximum time resolution allowed for by the speed of the microcontroller is found to be around 4 ms.

The signal paths introduce some non-linearity to the transfer functions, which is found to principally affect the monitoring of the signals from the power supply and pressure gauge controller, which operate on scales of between 0 V and 10 V. In order to account for these, the transfer functions of the system were measured using variable test voltages measured on the bench, and an appropriate correction is applied to values recorded using this system.

2.2.1.2 Current collectors

At different times, different arrangements were used for sampling axial and radial current flows within the chamber. Unless specifically stated, the measurements described in the following chapters were made using collectors with dimensions as described below. These arrangements are illustrated in Fig. 17.

Axial collector:

Since the axial line of the electrode arrangement usually terminated in a chamber port, a KF40 blanking plate was generally used as this collector. A seal was adapted so as to enable the blank to remain electrically isolated from the chamber when the clamp was removed; once under vacuum, the ambient pressure external to the chamber was sufficient to maintain the integrity of the joint without the clamp. The diameter of the port was around 4 cm; this, in a wall of dimension 30 cm x 30 cm constitutes an areal fraction of around 1.4 %.

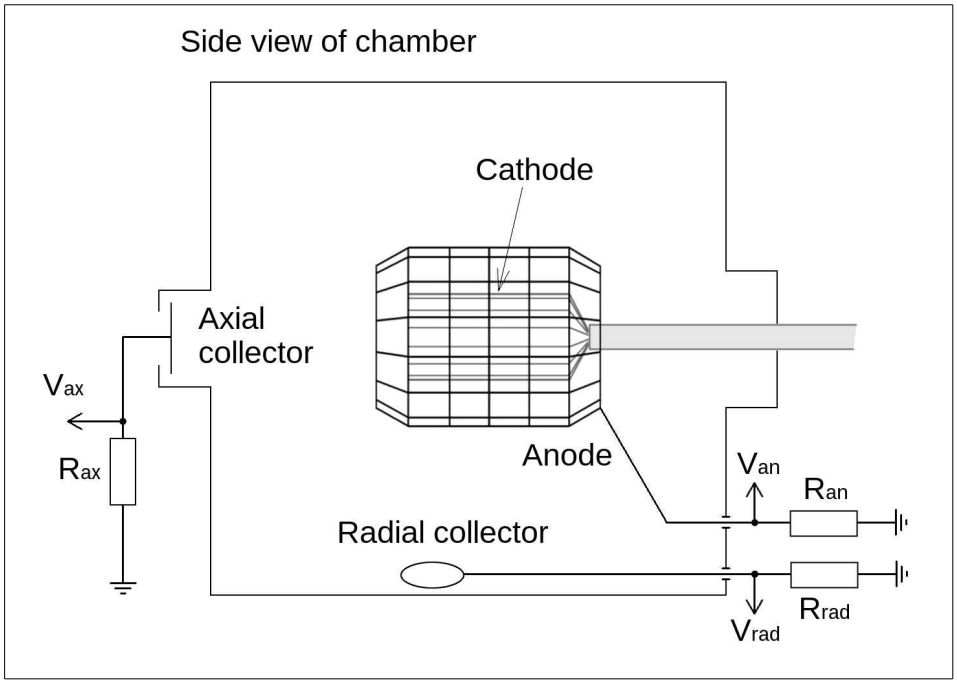

Fig. 17. The arrangements for measuring anode current, and radially- and axially-directed currents within the chamber

Radial collector:

This was a circular, stainless steel disc, of around 3.5 cm diameter, held close to the floor of the chamber, at an angle normal to a radial chord passing through the axis of the electrode assembly. The surface of this collector is around 12 cm from the axis. This means its area is around 1 % of that of a corresponding cylindrical surface, co-axial with the electrodes, that extends for an axial length roughly equivalent to that of the anode.

2.2.1.3 Cathode current sensor

A means of directly measuring cathode current was contrived, which needed to be able to float to high voltages with respect to ground. This was accomplished by means of a battery-powered circuit attached to the cathode feed-through, that created an optical signal that was the analogue of cathode current.

The circuit operated as a voltage-controlled current source. By sensing the voltage dropped across a small resistance in series with the cathode, a current was supplied to an LED which was proportional to cathode current. The brightness of the LED was therefore also proportional to cathode current, and this could then be measured via an optic fibre and the photodiode detector described below.

This equipment was not routinely available, and where measurements were made using this device it is indicated as such in the textual description.

2.2.1.4 Oscilloscopes

Oscilloscopes were mostly used to monitor the time-varying behaviour of electrical signals generated from the current collectors. Two digital Tektronix TDS 2024C 200 MHz units were available, as well as an analogue Gould 20 MHz OS300 unit. Each of these had useful attributes for different purposes.

The analogue instrument can be adjusted more quickly, and the direct relation between sweep time and visual display intrinsic to this technology means that the signal displayed may be more representative of the average than that displayed by the digital models. This was found to be useful when viewing a periodic but intermittent signal, or a periodic signal with a significant element of noise.

The digital oscilloscopes provide significant additional capabilities, such as those for the capturing of signals, and for the real-time analysis of signals. These last include Fast Fourier Transforms, enabling the measurement of the frequency spectrum associated with a signal.

2.2.2 Optical measurements

Measurements of optical emission were made using various instruments. The detectors used all have their own different spectral sensitivities, and so these are illustrated in the following descriptions for reference.

2.2.2.1 Spectrometers

Two spectrometers were used for making measurements of the spectrally-resolved light emitted from the plasma. These were very different instruments, each having

attributes making them more or less suited to the making of measurements at different conditions.

Horiba FHR1000 spectrometer:

This was the larger spectrometer used, which is sensitive to the ranges of wavelengths between 250 nm and 750 nm, or 250 nm and 999 nm, depending upon the grating used. This instrument allows for adjustment of the widths of entrance and exit slits, and the positioning of mirrors so as to cause the intensity of different wavelengths to be observable at the exit. These are motorised, and may be programmed so that the intensities of a progressive series of wavelengths may be recorded using a photo-multiplier tube. Slit widths were set to 0.2 mm for most measurements, which was found to be the minimum required to enable sufficient levels of light to fall upon the photo-multiplier tube.

Ocean Optics USB4000:

In contrast to the FHR1000, this instrument is spectrometer and detector in one small package. It works using a rotating prism and an array of photo-detectors encapsulated in an IC chip. This enables simultaneous recording of information about the entire wavelength range between 180 nm and 890 nm, making this instrument the faster way of measuring the spectral content of light across such a large range of wavelengths, by far.

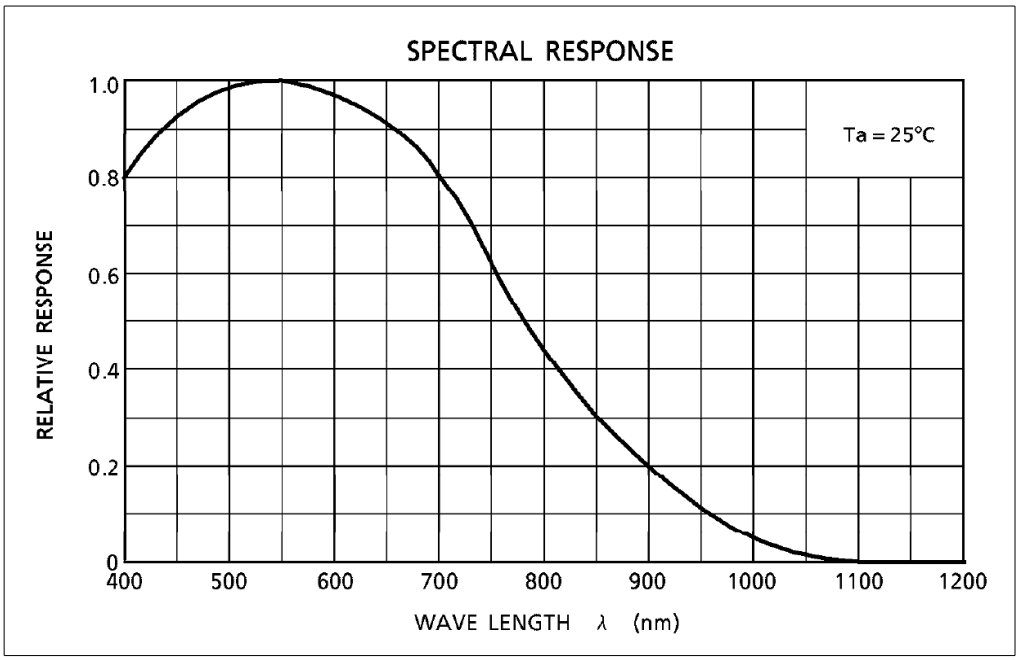

Fig. 18. Spectral response of Toshiba TCD1304 detector chip in Ocean USB4000 spectrometer, reproduced from datasheet.

The drawbacks are a lack of resolution, meaning the instrument is not suitable for detailed measurement of line-shape or very low-intensity signals. It also has a very different spectral response to the other detectors. Ocean Optics do not publish the spectral response for the instrument, but that for the detector chip is provided on the

datasheet, reproduced in Fig. 18; this curve does not however include the effect of additional filtering, which appears to further alter the response considerably. Fig. 19 shows spectra recorded using both this instrument, and the FHR1000 and photo-multiplier arrangement, using light from a similar source. Two ranges of wavelengths are illustrated for each case, showing the FHR1000/photo-multiplier system to be relatively far more sensitive to light at shorter wavelengths. The variation in relative intensities of lines between 750 nm and 800 nm evident in the measurements made with the two instruments is also considerable, as is the difference in wavelength resolution.

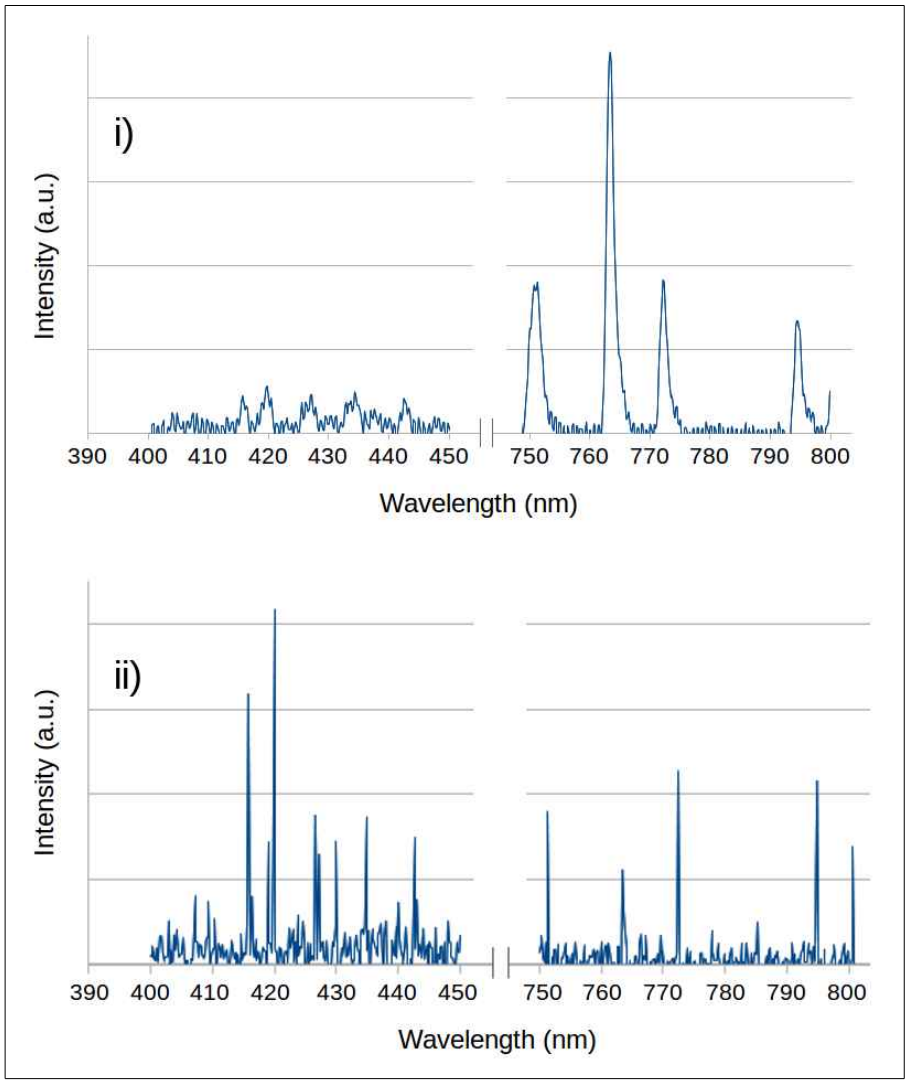

Fig. 19. Emission spectra from argon discharges operating at similar conditions, corresponding to pressures of between 9.3 mTorr and 9.6 mTorr, and as measured using i) Ocean USB4000 spectrometer and ii) FHR1000 spectrometer and PM tube. Signals shown for different wavelength ranges have same vertical scale in each case.

This variation illustrates the need for caution in comparing measured results, and as a rule any comparison of the relative intensities of spectral lines is only made between measurements made using the same equipment.

2.2.2.2 Optical set-up

Mounting arrangements:

In the making of measurements of optical emission, it was at times convenient to use optical components such as lenses and filters. In order to facilitate this, an adjustable arrangement for optics was set up, using a long optical rail that allowed for a range of measurements to be made at different focal lengths. This rail was held normal to the chamber, and was mounted upon a motorised translation stage with a direction of travel parallel to the chamber. The position of the translation stage could be controlled and monitored by a digital stepper motor control. This entire assembly was in turn mounted upon a vertically-adjustable stage.

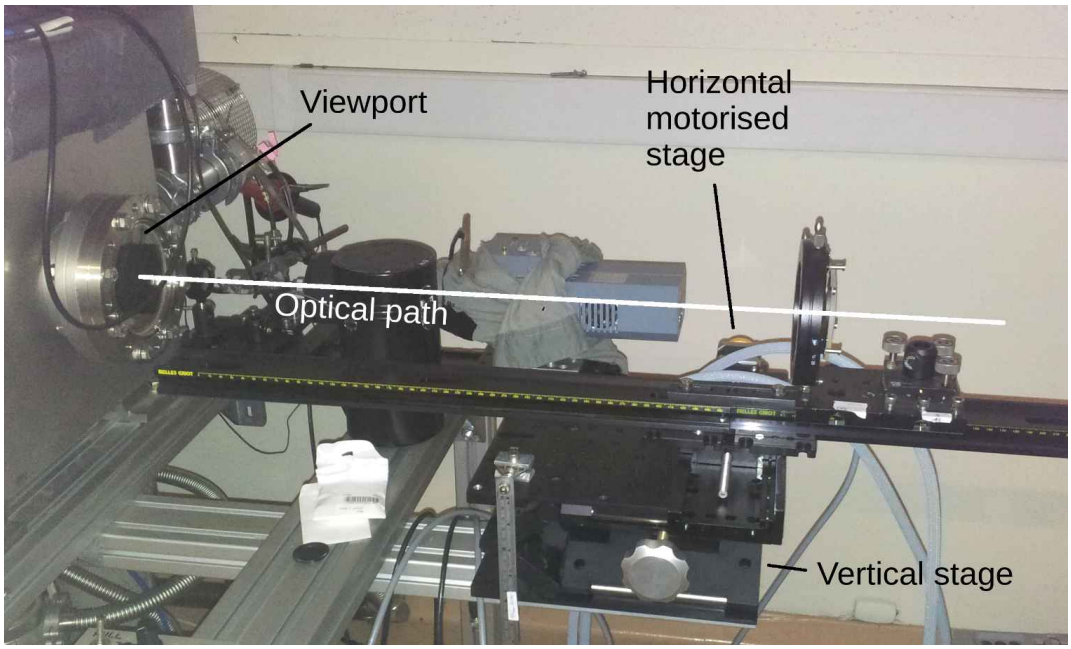

Fig. 20. Photograph showing arrangement for making optical measurements

An annotated photograph of the set-up described is shown in Fig. 20. In this image, the long black piece of apparatus beneath this line is the optical rail. A line is drawn to indicate the optical path, which passes through a holder for a large lens positioned towards the right hand side of the rail, with the mount for an optic fibre positioned slightly further to the right of this. When in use, this fibre mount was located further still to the right, out of frame.

2.2.2.3 Optical detectors

Horiba DPM-HV photomultiplier:

This photo-multiplier tube assembly was used attached to the FHR1000 spectrometer. The spectral composition of light may then be recorded by monitoring the output of the tube via the proprietary software installed on a PC, as the

spectrometer causes a progressive succession of wavelengths to be incident upon the detector. The photo-multiplier tube itself is a Hamamatsu R928. The spectral response of this tube is illustrated in Fig. 21.

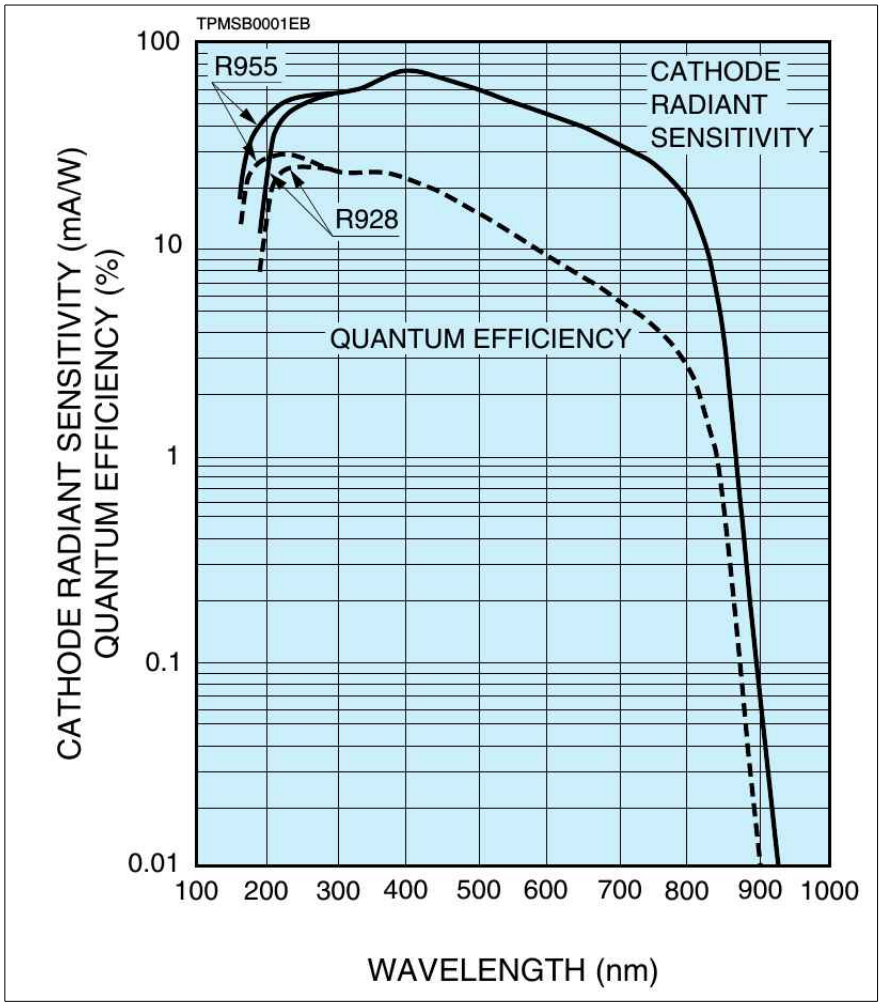

Fig. 21. Spectral sensitivity of the photo-multiplier tube used in the Horiba detector unit. Reproduced from datasheet

Photodiode detector:

An Osram SFH213 photodiode was used with a simple amplification circuit to provide a signal of time-varying emission that could be viewed on an oscilloscope. This same piece of equipment was also used to record the optical signal received from the active cathode current sensor described above. The spectral sensitivity of this component is shown in Fig. 22.

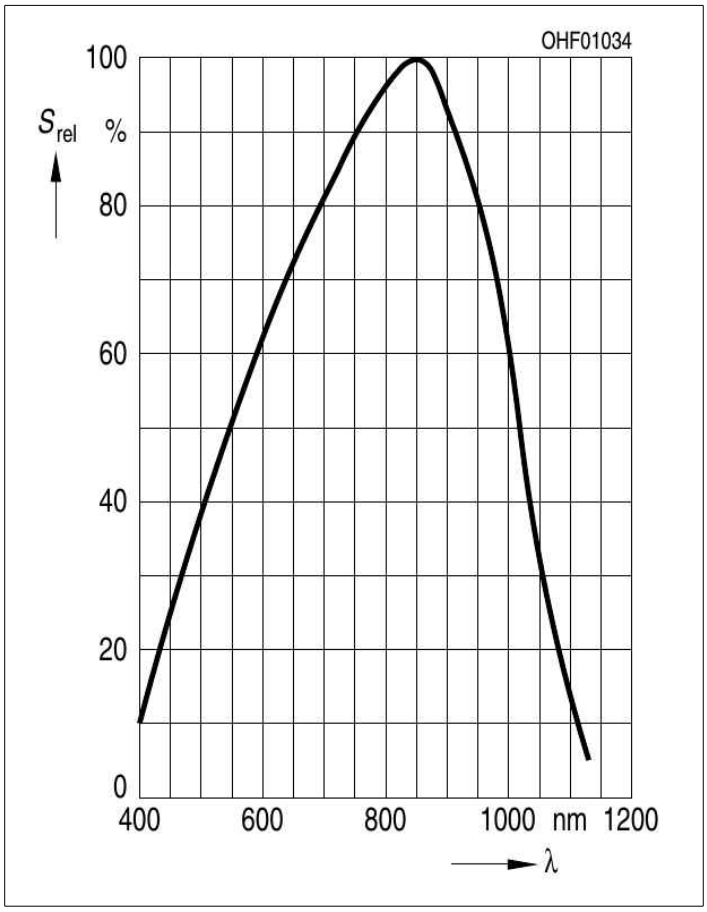

Fig. 22. Spectral response of Osram SFH213 photodiode. Reproduced from datasheet.

2.2.2.4 Cameras and filtering

Three different cameras were used for recording levels of optical emission.

Andor DH520 ICCD camera:

This camera could be coupled to the FHR1000 spectrometer, enabling the simultaneous capture of spectrally-resolved light across a limited range of wavelengths. It could also be used with 35 mm optical lenses for imaging spatial distributions of emission. With a lens fitted, the transmission of the system is subject to considerable additional filtering at UV wavelengths.

The camera is equipped with a type 'W' photo-cathode and an intensifier system, which in theory enables extremely fast shuttering. Unfortunately, the camera unit and associated digital electronics were not functioning sufficiently well for this capability to be used. These issues also meant it was not possible to trigger the camera by external means, but sequences of exposures could be recorded with a maximum repetition rate of around 2 Hz.

The Andor camera system allows for noise reduction in various ways, which are implemented in both hardware and software. The intensifier enables the exposure time to be relatively very short; this acts to minimise the signal-to-noise ratio. The sensor also may be cooled to -15 °C, which reduces the thermal noise contribution to the measured signal. Additionally to these measures, the camera control software allows for the recording of a 'dark spectrum', which refers to the sensor noise profile at conditions corresponding to the exposure and intensifier gain settings for an image, but with no light incident upon the detector. This profile may be subtracted from the image, so removing characteristic noise from the signal.

The spectral response for the photo-cathode is shown in Fig. 23.

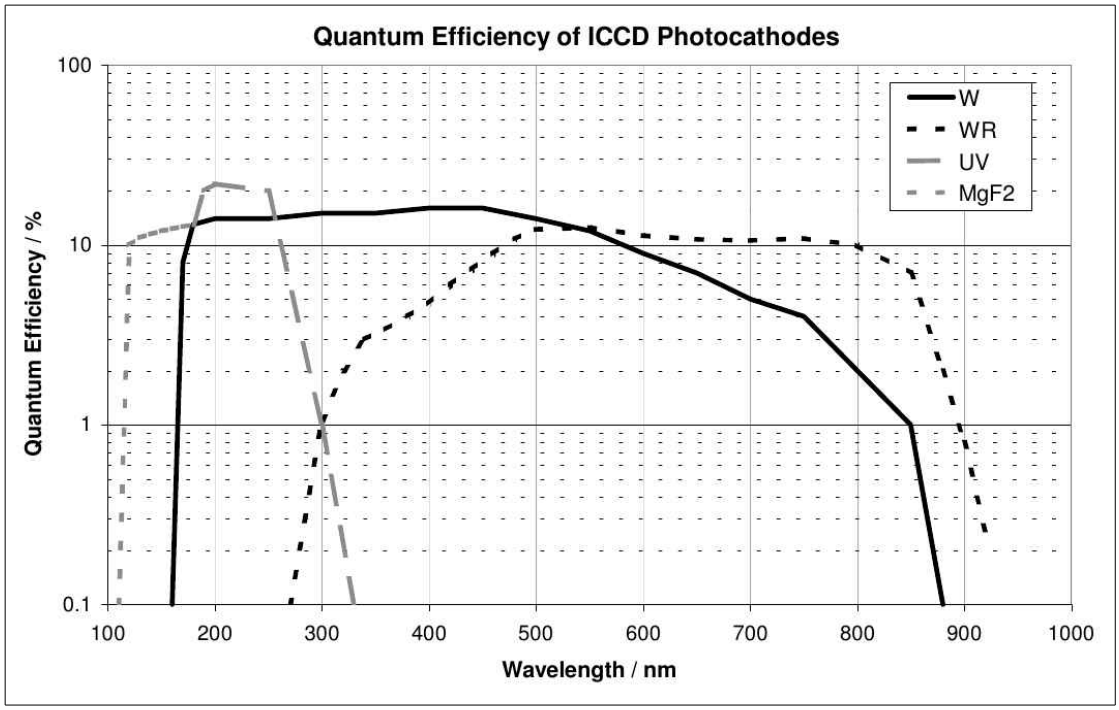

Fig. 23. Spectral response of Andor DH520 camera photo-cathode. The camera used was fitted with a type 'W'. Reproduced from Andor literature.

Canon DSLR camera:

This camera enables manual control over exposure settings and, as with the Andor camera, may be used with good quality optical lens arrangements. Two issues are associated with its use in this context, as compared with the Andor system; these are as follow.

The sensor is designed so as to record coloured images, that as far as possible represent those as perceived by the eye. To this end, the light falling upon individual elements of the pixel array is filtered, so that the levels recorded by a given pixel may constitute information about either the red, blue or green content. This means that the overall spectral response is limited to be approximately similar to that of the human eye, which is between 400 nm and 700 nm. It also means that the wavelength

sensitivity may vary across this range, as different wavelengths are transmitted to different degrees by the filtered sensor elements.

The second issue with this system regards the processing of image data that is carried out by the camera. This involves the interpolation of individual pixel values, in terms of both intensity and colour.

Samsung GT-19100 smartphone camera:

This camera was used frequently to record details of the appearance of the discharge, and also to capture dynamic behaviour within experimental runs by making videos recordings of either the appearance of the discharge or the monitoring displays of diagnostics, such as oscilloscope traces.

The ease of use, in both readiness and portability, enabled the recording of much more information than either of the other cameras. The trade-offs for these advantages are limitations, similar to those of the DSLR in terms of variable spectral response and software manipulation of the recorded images. Additional factors to these are the inferior optics and small sensor size of this unit.

Filter:

The spatial distribution of spectral content from optical emission may be measured using a wavelength-specific filter. An arrangement enabling such a filter to be quickly moved in and out of the optical path was devised, in the manner of a spring-loaded shutter, which is shown attached to a camera in Fig. 24.

When in use, this apparatus was shielded from extraneous light with a hood. The action of the shutter could be automated, using a stepper motor and the control unit for the translation stage.

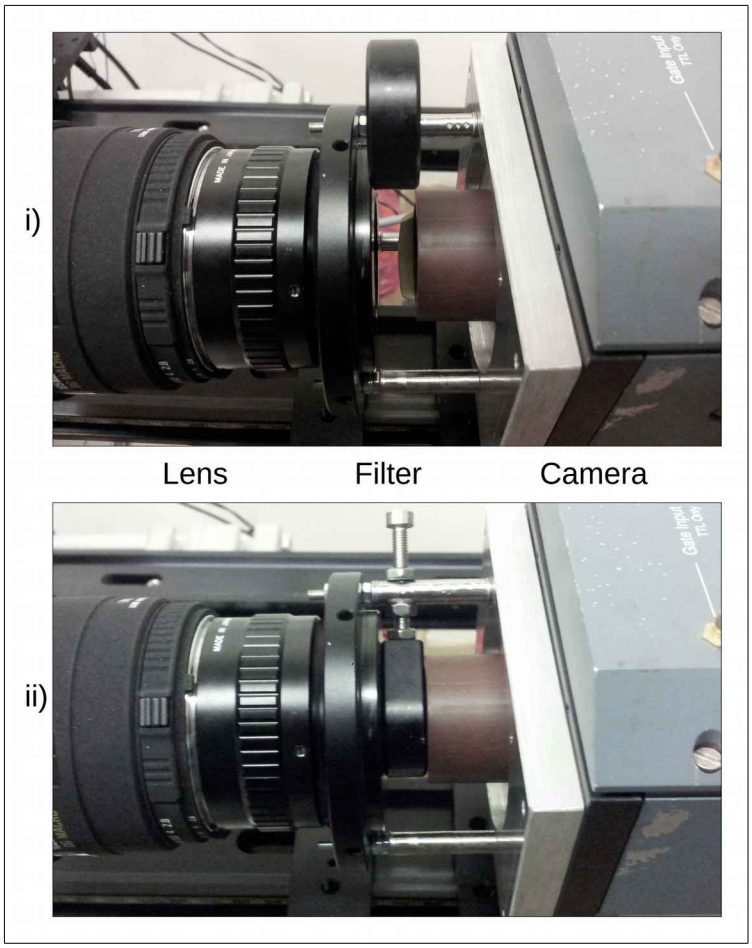

Fig. 24. Filter-shutter assembly used for recording images filtered by wavelength. Filter shown i) removed from optical path; ii) inserted into path. Hood not shown.

Chapter 3
Mode structure

3.1 Introduction

This chapter provides an account of the general operating characteristics of the discharge, observed over a wide range of pressures, and in several different species of gas.

Both the visual appearance of the plasma, and also the cathode voltages required for initiation and sustaining of the discharge, show considerable variation with pressure. This pressure-dependence is not found to occur as a gradual evolution, but rather may be described in terms of a characteristic pressure-dependent mode structure, which provides a convenient framework for the description of discharge characteristics.

The purpose of the research is to investigate plasmas that are sustained by ionic and neutral species, and so the identification of such regimes of operation is important. Attention is therefore directed principally towards the understanding of which species may be active in the processes that cause and sustain these discharge modes.

The structure of the chapter is as follows: in the section following this introduction, a brief account is given of the mode structure in terms of the distributions of optical emission. Some general observations about the stability and other issues affecting operation are also included in this section, and the pressure ranges of interest for the study are defined.

Following this, measurements made of the electrical and optical properties are described, as observed when the discharge is operating in different modes in helium and argon. The vacuum distributions of electric field and potential calculated using a software modelling package are also presented.

The results of these experimental observations are then discussed. The conditions at which the discharge operates are considered, with reference to works from the literature that describe the physical dependences of processes caused by different species. The experimental observations are then examined for evidence that may enable the identification of the species associated with the processes that cause and sustain the discharge, and the implications of the findings are considered.

3.2 Experimental observations and calculations

3.2.1 Overview of mode structure

Across the range of pressures from those associated with conventional glow discharges down to the low-pressure limit for operation with the available apparatus, the mode structure of the discharge is evident as a series of changes in the visual appearance of the discharge. This may be broadly characterised into three regimes, as follows.

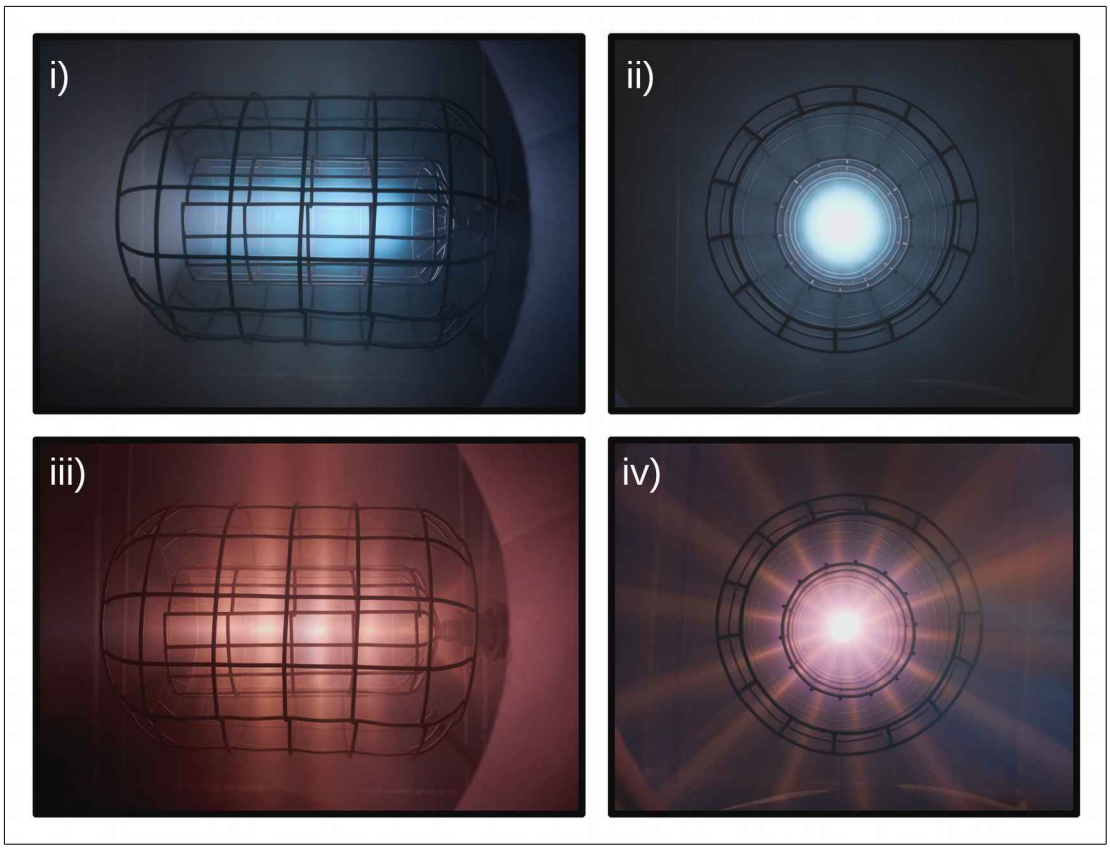

Fig. 25. Photographs of the helium discharge at i) and ii) 300 mTorr; iii) and iv) 30 mTorr

At relatively high pressures, of around a Torr and above, the spatial distribution of emission is generally associated with the region between the electrodes, and voltages are typically a few hundreds of volts. These conditions are similar to those at which conventional glow discharges operate; with the distribution of emission occurring between the electrodes, the discharge in this regime is considered to be similar to these, and it is not investigated further.

At pressures below these, the distribution of emission is found to change, with the bright region becoming principally localised to within the interior of the cathode [Fig. 25 i) and ii)]. This characteristic appearance is then consistently evident across a range of pressures extending down to the tens of mTorr. Voltages are generally in the hundreds of volts across most of this range; these become greater towards the low-pressure limit, but remain smaller than a kilovolt.

If pressure is further reduced, the appearance of the discharge changes again; the glow within the cathode is replaced by a series of radial beams which pass through the apertures of both grids, converging at the central axis and extending to the walls [Fig. 25 iii) and iv)]. A glow also extends from the open end of the cathode at transitional pressures, and this becomes a narrow beam in the low-pressure mode. In this regime, cathode voltage rises quickly from around a kilovolt to tens of kilovolts as pressure is reduced, and the low-pressure limit in this apparatus is determined by the voltage available.

These last two modes of operation shall be further described in the following. The mode occurring at higher pressures, in which the glow is largely confined to within the cathode, shall be referred to as the 'cathode-confined mode'. That occurring at lower pressures, in which emission is localised so as to resemble radial beams, shall be referred to as the 'beam mode'.

The nature of the emission distribution at pressures corresponding to the transition between these modes is interesting. This is illustrated, again using images of the helium discharge, in Fig. 26. At these conditions, the distinct colours of emission that are characteristic of the modes to either side of the transition are both evident, and are noted to be associated with distinct spatial locations. The emission structure is therefore observed to be associated with spatial location as well as pressure.

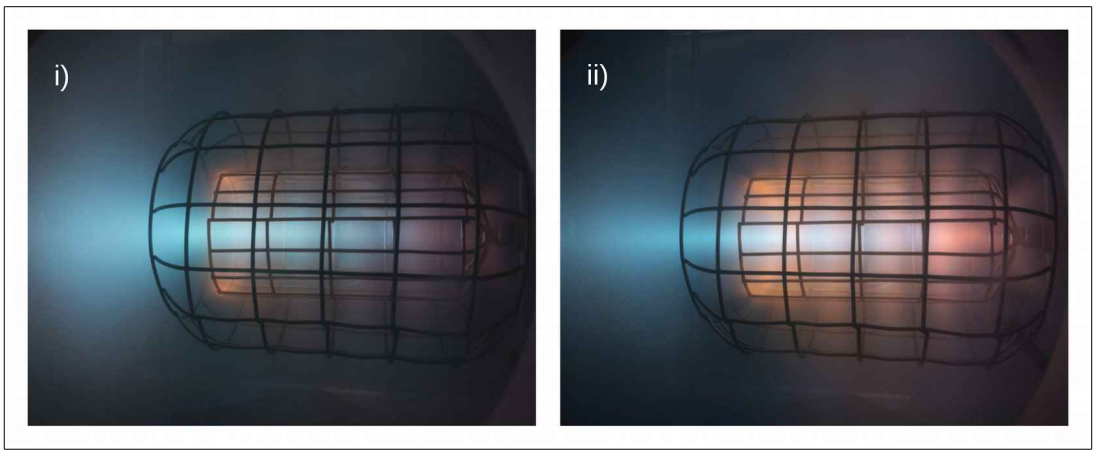

Fig. 26. Photographs of the helium discharge at i) 112 mTorr and ii) 88 mTorr

The evolution from cathode-confined glow to radial beams is observed to be broadly similar in helium, neon, argon and nitrogen, although the mode structure is associated with different specific ranges of pressure in all cases. A similar form is observed in the helium discharge at around four times the pressure of that in argon. The colour of emission in helium makes the transition behaviour much more visibly evident than it is in other species. In argon the cathode-confined mode is observed to be less well-defined in general; there is a relatively narrower range of pressures at which the glow is confined to within the cathode, in particular at higher levels of current. The mode is also found to be less stable, and the discharge may transition out of the mode spontaneously, which has not been observed with helium.

This mode structure is made additionally complex at certain conditions by the appearance of various additional discharge features within the cathode, that are referred to as 'space charge objects'. These may affect the discharge properties to varying extents, and occur over a comparatively narrow range of conditions. They are not discussed further in this chapter, but are treated in detail in Chapters 6 and 7.

In terms of general behaviour, the discharge in the cathode-confined (CC) mode is found to be relatively stable, with little drift in voltage when driving a constant current. In the beam mode, this is different; after switch-on, the voltage may rise as much as two- or three-fold over the course of an hour at a moderate current of 10 mA. This effect is most pronounced after the chamber has been exposed to ambient conditions, although it also occurs to a significant degree after the chamber has been maintained at low pressure for some time with the rotary pump running.

3.2.2 Electrical characteristics

Current-voltage relations and breakdown voltages for the discharge were measured at conditions encompassing operation in both the CC and beam modes, in helium and argon.

3.2.2.1 Current-voltage relations

Current-voltage relations were measured using the following procedure: with the current limit set fully open on the power supply, the voltage was ramped up and down quickly. This was found to be the best way to minimise the effects of voltage drift, but some may be seen to occur on the beam mode data. During operation of the discharge, values of voltage and current from the monitoring outputs of the power supply were recorded using the ADC logging system, as described in the previous chapter, at around 20 Hz. The cathode voltage is obtained from the supply voltage by subtracting the voltage dropped across the 3.9 kΩ ballast resistor. Levels of current were also monitored directly using the active sensor, and logged in the same manner. This was calibrated using a low-voltage current source on the bench.

The helium curves are described first, shown in Fig. 27. These are colour-coded, with blue used for the beam mode and a variety of colours for the CC mode curves, since these are less well-separated. Values for current presented in the figure are those from the sensor.; these measurements were found to generally agree well with those obtained from the supply signal, but occasional instabilities in the discharge cause current to spike above the supply maximum and distort the curves. The supply does not output a signal above the maximum, and so the results from the sensor indicate where this occurs. This behaviour is visible on the curve recorded at 88 mTorr.

At all pressures, levels of current can be seen to increase with voltage. The data are plotted on a log-log scale, and so a straight line indicates a consistent current-voltage relation. The curves show a varying degree of consistency in this respect; the relation evident for the beam mode curves appears to become consistent for currents above a

few tens of mA. A fit line is included on the plot to show the relation evident for the beam mode curve recorded at 29 mTorr. The relation for the higher-current part of this curve is shown to be close to voltage raised to the power 3.7.

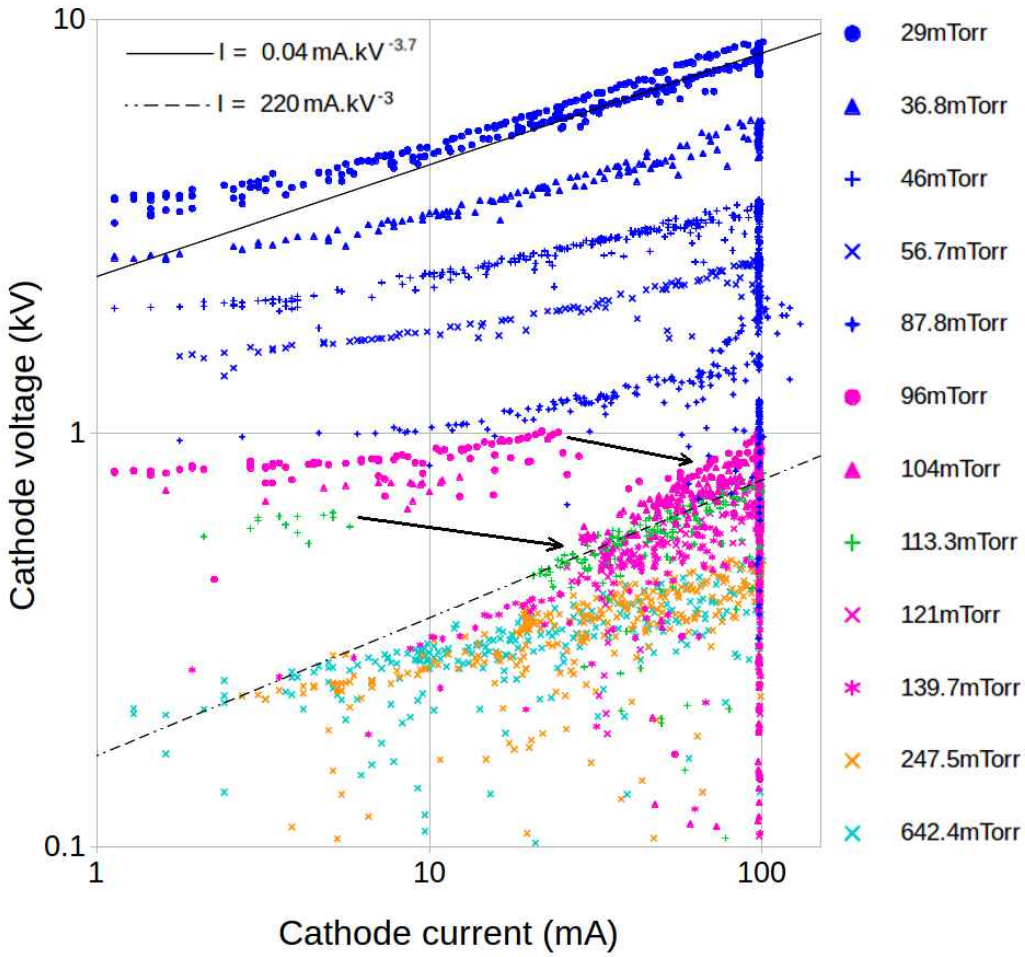

Fig. 27. I-V curves for helium discharges at a range of pressures. Arrows indicate jumps in current and voltage on instigation of the CC mode.

The CC mode curve for 113 mTorr is highlighted to distinguish it from the others, and this may be seen to follow a quite consistent relation. A fit line is also included on the plot to demonstrate the relation followed by this curve, which is close to a voltage-cubed dependence.

The mode structure is most apparent towards the low-pressure limit of the CC mode, where the onset of the mode is indicated by significant discontinuities in the curves. These appear as sudden increases in current, of the order tens of mA. The region in which this occurs is indicated by arrows in Fig. 27. Discontinuities are only evident for these curves at pressures between 96 mTorr and 113 mTorr, although similar behaviour continues to affect operation at pressures up to 250 mTorr, in which the threshold current is smaller than 1 mA.

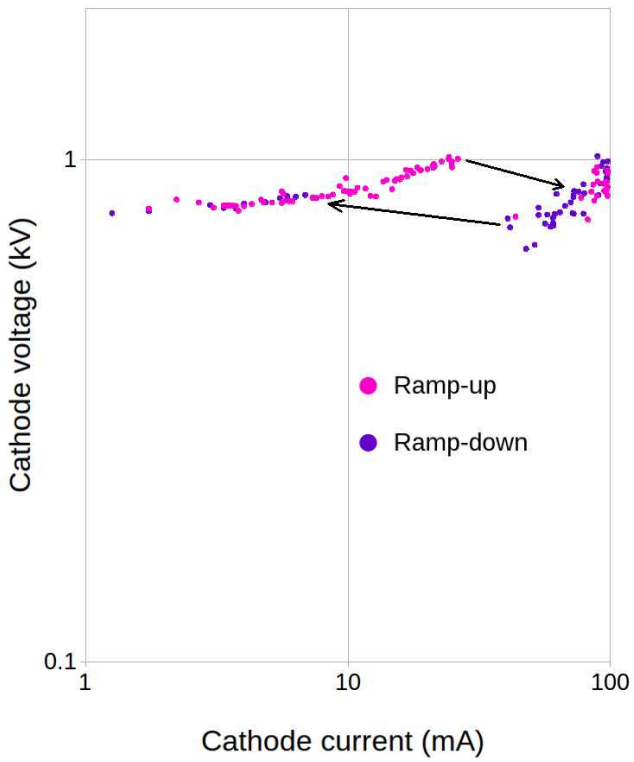

Fig. 28. I-V curve in helium at a pressure of 96mTorr, showing hysteresis associated with CC mode formation and extinction

This behaviour is shown in more detail in Fig. 28, in which the current-voltage curve obtained at a pressure of 96 mTorr in helium is shown in isolation, with outlying data points removed for clarity. During the recording of these values, the discharge can be seen to transition to the CC mode as voltage was increased, and then back again during the ramping down. The extinction of the mode occurs at a lower value of current than that at which it instigates, indicating a hysteresis to be associated with the mode.

When this behaviour occurs, the power supply is initially operating in voltage-limited mode (as described in the previous chapter), in which the output is determined by the voltage control. Should sufficient current be suddenly made available to reach or exceed the supply maximum, the unit changes mode to become current-limited, and voltage is internally reduced so as to maintain the current level to within the supply limit. In this case, the power supply appears to react to a sudden increase in current that reaches the maximum, but to stabilise at a level below the maximum. This occurs during a relatively fast ramping of voltage, and is simply considered to be evidence of a sudden rise in current associated with the appearing of the CC mode.

Whilst the curves for pressures between 100 mTorr and 250 mTorr also show a threshold current for the mode to appear, the mode persists to lower currents at these pressures, and the discharge does not continue to operate once it disappears. The threshold current for the mode is observed to become smaller with increasing

pressure, and at higher pressures the mode appears to form instantaneously at breakdown.

These discontinuities therefore indicate a sudden increase in current to be associated with the appearance of the CC mode. A hysteresis is also found to affect current levels, with the established mode persisting to much lower currents than the threshold for formation.

Current-voltage curves for argon are shown in Fig. 29. These are also plotted on a log-log scale, and blue is again used to indicate beam mode curves. Values of current are those obtained using the active sensor, and unstable behaviour is visible on the 8.4 mTorr curve. The argon curves tend to a consistent current-voltage relation at higher currents, as was observed with helium. In contrast to helium however, the relation at these conditions is similar for both beam mode and CC mode curves; for either mode, the relation is close to voltage raised to the power 2.5.

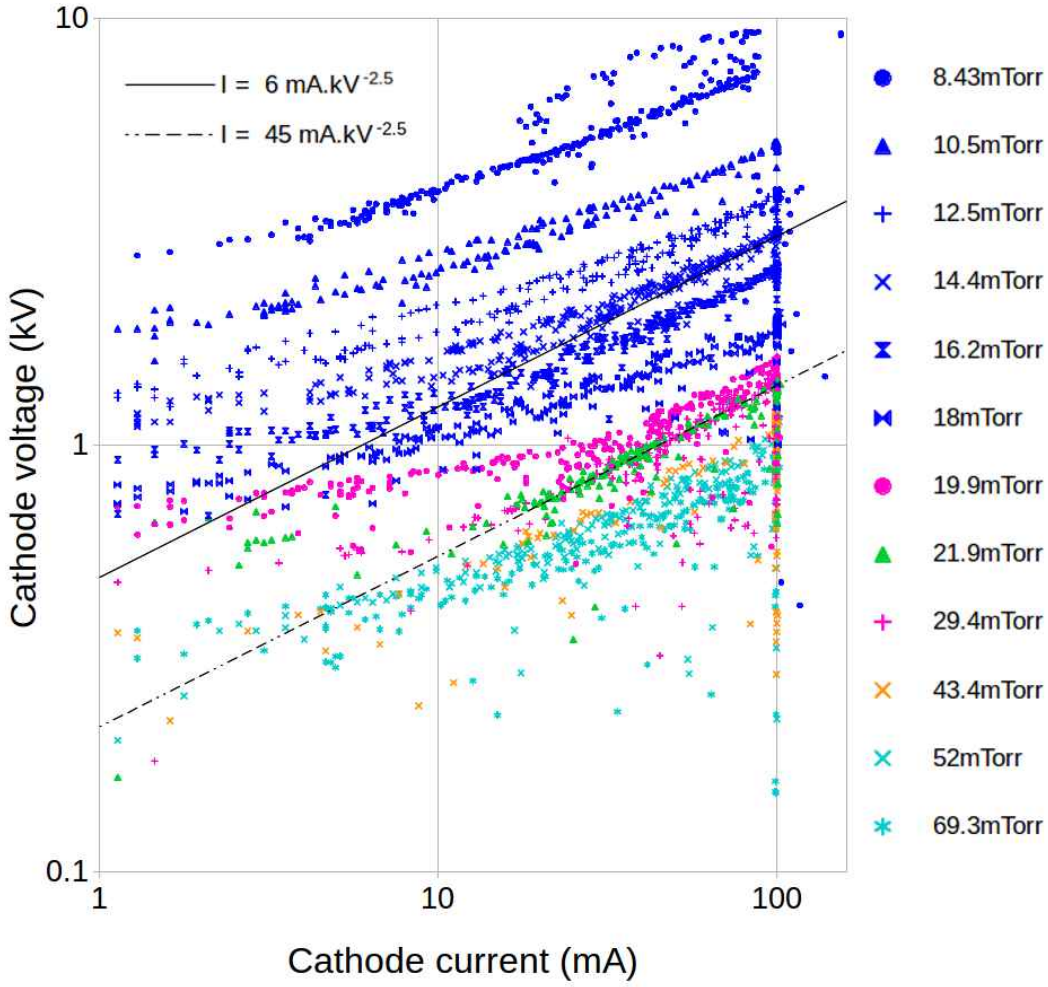

Fig. 29. I-V curves for argon discharges at a range of pressures

The mode structure is also evident in argon, with discontinuities occurring in levels of cathode current when the CC mode appears at pressures around the mode transition. This may be seen for the curve corresponding to 22 mTorr, which has been coloured green for clarity. In argon, the jumps in current are accompanied by little change in the overall current-voltage trend, and the mode transition region is therefore less obvious in Fig. 29 than it was for the helium curves (Fig. 27). The curves for the CC mode, which are those for pressures greater than around 20 mTorr, are observed to correspond to generally higher voltages than those for the CC mode in helium.

3.2.2.2 Breakdown voltage-pressure relations

Helium has a known characteristic for multi-valued breakdown at low *pd*, with a higher-voltage branch measured when pressure is incrementally increased at fixed voltage, as opposed to the more usual method of increasing voltage at fixed pressure (see e.g. [63]-[65]). All measurements in this study, whether in argon or helium, were made using the latter technique.

Before making a set of measurements, the apparatus was first operated at a relatively high power and then left to cool to ambient temperature. This procedure helps to maintain a degree of consistency in conditions and so minimise transient effects; it is noted however, that the significant dependence of voltage upon chamber condition means that any such series of measurements will be a function of this.

Breakdown was defined in Section 1.2 as the point at which a discharge becomes self-sustaining, which may occur at levels of current as small as 10^{-10} A, as indicated in Fig. 2. Without equipment capable of monitoring this order of current, the approach taken was to record the voltage- and current-monitoring outputs from the power supply, whilst voltage was increased until past the point of breakdown, as evidenced by a visible discharge. The recorded data-logs were then examined to ascertain the voltage at which the current level consistently rose above the ADC resolution, which was of the order 10^{-5} A. Upon breakdown at some conditions, levels of current rise immediately to levels considerably in excess of this, and when this was accompanied by a discernible reduction in voltage, the preceding maxiumum value was considered to represent the breakdown voltage. The overall accuracy of the ADC system is estimated to be within a few percent. Pressure was monitored using the CMR375 capacitance manometer where possible, since the accuracy of this instrument significantly exceeds that of the pirani gauge. For pressures greater than arond 90 mTorr, the PCR260 pirani gauge was used, and these measurements are subject to an uncertainty of 15 %..

The values of voltage recorded at breakdown in helium and argon are shown in Figs. 30 and 31. The parameter *d* is considered poorly defined for the discharge because of the electrode apertures, and so the voltages are plotted against pressure, rather than *pd*. The degree of uncertainty associated with the measurements is generally smaller than the size of the markers on the plots, except as indicated for the measurements of higher pressures.

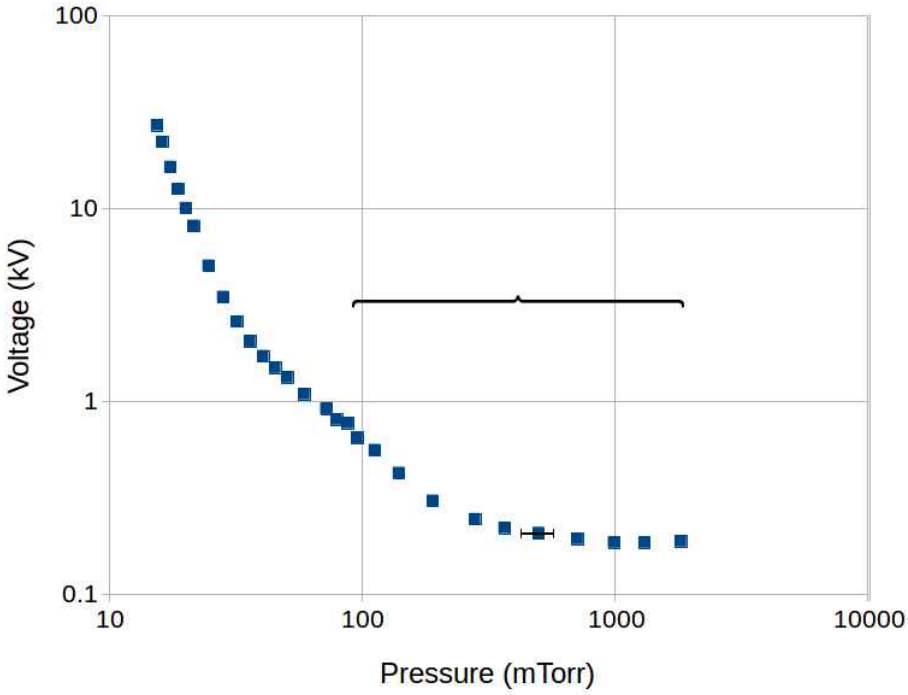

Fig. 30. Breakdown voltages against pressure in helium. Uncertainty in pressure (15 %) associated with use of PCR260 gauge affects bracketed points

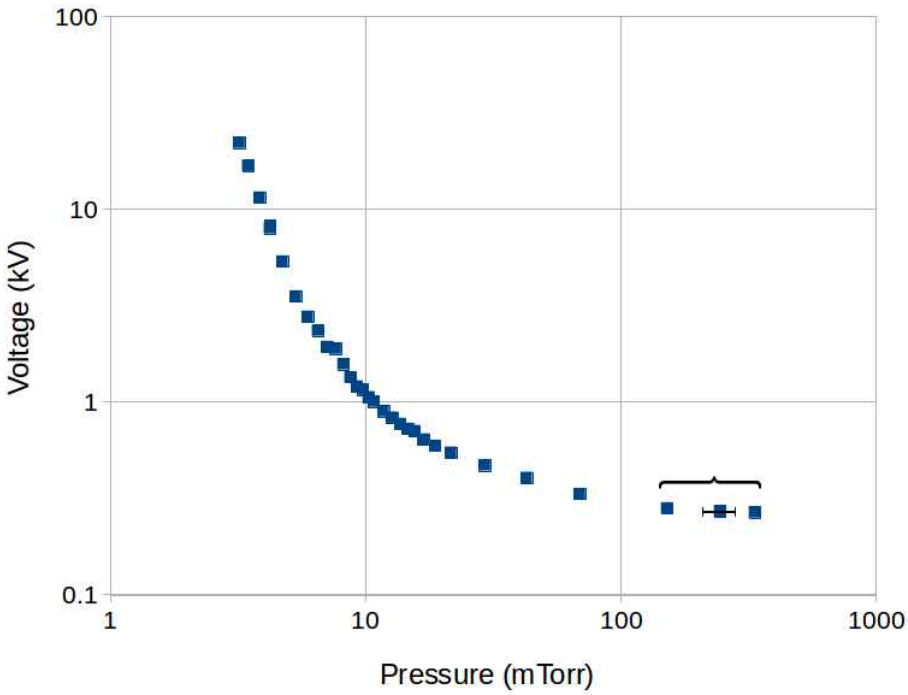

Fig. 31. Breakdown voltages against pressure in argon. Uncertainty in pressure (15 %) associated with PCR260 gauge affects bracketed points

The mode change is discernible as a bump in the curve at a little under a kilovolt in helium, but is much less clear in argon. The difference in this respect between the measurements made in helium and argon is observed to reflect breakdown voltages in argon being generally greater for the CC mode than in helium. This is noted to correspond to the difference in characteristic values of voltage evident in the current-voltage curves for the CC mode also. Visual observations made during the process indicated that when operating at very low currents, the discharge occurs along the longitudinal axis of the apparatus in the higher pressure range, whereas at lower pressures the radial beams are visible.

3.2.3 Optical emission spectroscopy

In this section, the results of measurements of spectrally-resolved optical emission from discharges in helium and argon are presented. Different series of measurements were made at different times, and using different equipment. As noted in the previous chapter, the spectral sensitivity may vary considerably between spectrometers, and so direct comparison is not made between measurements unless obtained using the same equipment. Measurements were generally made using an optical fibre aimed through a glass viewport. In some cases, optics were in place for making other measurements, which meant the light sampled was from a specific location along the axis of the discharge. At other times, light was sampled according to the fibre's angle of acceptance, which is relatively large. A consistent optical arrangement was generally used throughout the making of a set of measurements, and wherever this was not the case, it is specifically mentioned in the following. Prior to the making of each measurement, the discharge was allowed to reach a stable equilibrium, and voltage and pressure noted.

3.2.3.1 Helium

Light was collected from discharges in helium using an optic fibre held close to a viewport, using no additional optics. Emission was sampled at a range of pressures between 400 mTorr and 20 mTorr, which encompasses conditions at which the discharge operates in both modes. The fibre was directed towards the axis of the discharge, aligned with the centre of a row of electrode apertures. The spectra were obtained using the FHR1000 spectrometer and PM tube arrangement, for wavelengths between 250 nm and 750 nm.

Examples of characteristic spectra from CC mode and beam mode discharges are shown in Fig. 32 i) and ii) respectively. The visible spectrum for helium contains relatively few spectral lines, and all of the significant lines appearing in these spectra are helium lines. This has been verified by checking the wavelengths against the NIST Atomic Spectroscopy Database [66]. The strongest visible emission from these discharges is from the spectral line at 501.6 nm for the CC mode, and the line at 587.6 nm for the beam mode. These lines are found to dominate the emission structure for discharges from these modes throughout their respective pressure ranges. Light at these wavelengths is respectively green and yellow-orange in colour, and the relatively small number of lines within the helium spectrum means that these

wavelengths may be identified as being responsible for much of the visible colour of emission. The line at 388.9 nm is consistently strong in both modes. The greatest degree of variation in spectral composition is therefore observed to be found between light collected from the discharge operating in the different modes.

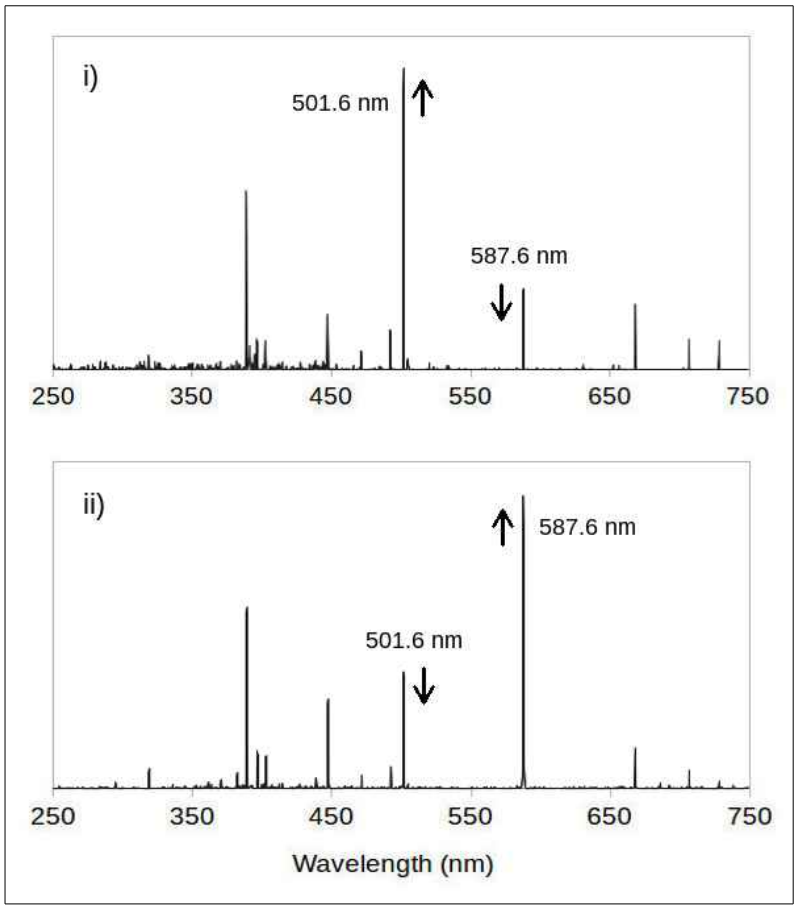

Fig. 32. Optical emission spectra from i) CC mode and ii) beam mode discharges in helium

Levels of recorded emission vary considerably across the pressure range, and so the spectra obtained are normalised in order to compare the emission profiles. The spectra are also subject to a relatively-varying low level of background signal, and the distribution of few lines across a wide range of wavelengths causes this to affect the results of normalisation to total signal significantly. The profile of emission across the range of pressures is therefore assessed by noting the intensities of 15 lines that consistently appear brightest within the spectrum, and normalising amongst this set for each measurement. From the examples in Fig. 32 it may be observed that these will make up the vast majority of recorded spectral emission.

When the relative intensities of the 501.6 nm and 587.6 nm lines amongst this set are plotted, they are found to almost mirror each other (Fig. 33). In both cases, these abruptly change in magnitude across a range of pressures between 100 mTorr and 50 mTorr, which corresponds to the range of pressures just below the low-pressure limit of the CC mode.

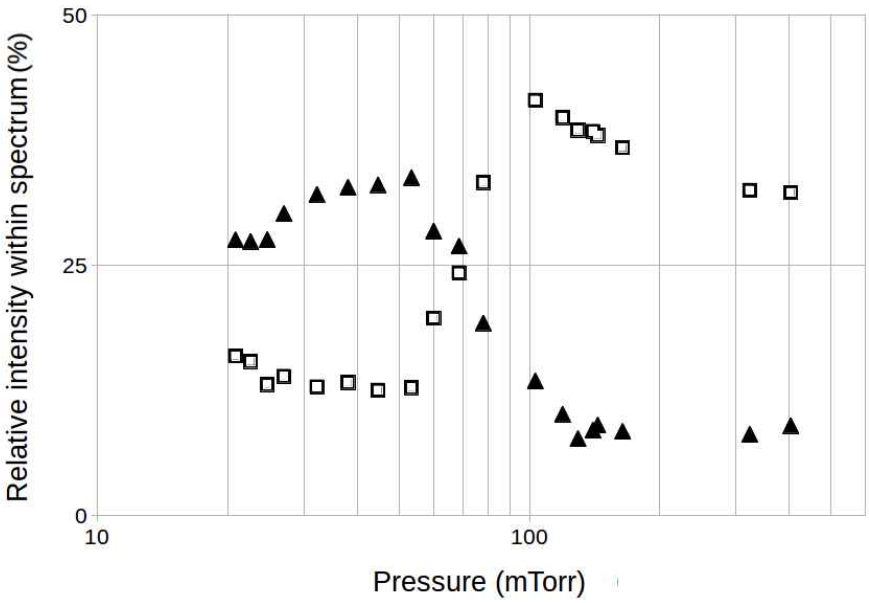

Fig. 33. Variation in relative intensities of 501.6nm (open squares) and 587.5nm (closed triangles) spectral lines in optical emission from the helium discharge at a range of pressures.

3.2.3.2 Argon

Results presented are of measurements made of light emitted from argon discharges on more than one occasion. The spectrum obtained at the conditions of greatest pressure was of light sampled using an optic fibre aimed generally at the axial glow of a CC mode discharge. The other measurements were all made using light sampled from a more specific location, which was on the axis of the discharge, at a displacement approximating to the centre of the row of cathode apertures closest to the open end of the electrode. These measurements were all obtained using the USB4000 spectrometer, since they were also to function as reference spectra for other measurements made using this instrument.

The argon spectra are shown in Fig. 34. These may be observed to have a greater distribution of lines having moderate intensities, and also have comparable signal-to-noise levels, so the results may be normalised to the integrated signal across all wavelengths. When these are compared, comparatively little difference is found between them. This is to some extent an artefact of the spectrometer's wavelength sensitivity; as was observed in the previous chapter, the sensitivity of this instrument is considerably reduced at shorter wavelengths, and so the intensity of the cluster of lines between 400 nm and 500 nm appears correspondingly to be much attenuated. These lines do show some evolution with pressure, although the attenuation and the relatively poorer resolution of the instrument make a reliable characterisation of this difficult.

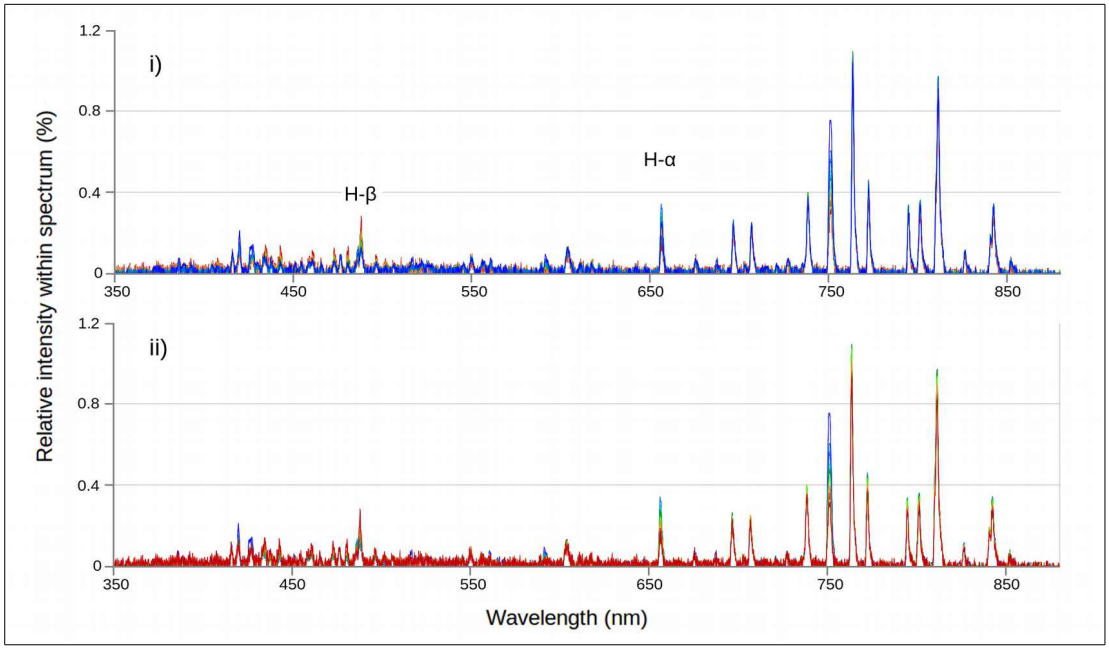

Fig. 34. Normalised spectra from argon discharges obtained at a range of pressures. The spectra are overlaid in order of i) increasing pressure, with highest pressure uppermost, and ii) vice versa, in order to aid comparison. The key to values of pressure is as for Fig. 35

The stronger lines in the spectrum have been checked against the NIST Atomic Spectroscopy Database [66]. Lines in the group having wavelengths mostly between 400 nm and 500 nm are found to be largely argon ion lines, and those between 700 nm and 850 nm are argon atomic lines. The hydrogen Balmer-α and -β lines also appear in the spectra, with a significant and variable degree of intensity that shows no clear relation with pressure.

Of the strong argon lines within these spectra, it is only the line at 750.4 nm that shows much variation with operating conditions. The relative intensity of this line within the spectrum is found to show a monotonic decline at conditions of increasingly low pressure, shown in more detail in Fig. 35. The line shape is an arterfact of the USB4000 spectrometer, and measurements made at lower pressures are subject to an increased element of noise. The evolution of relative intensity within the measured spectrum is however quite clear.

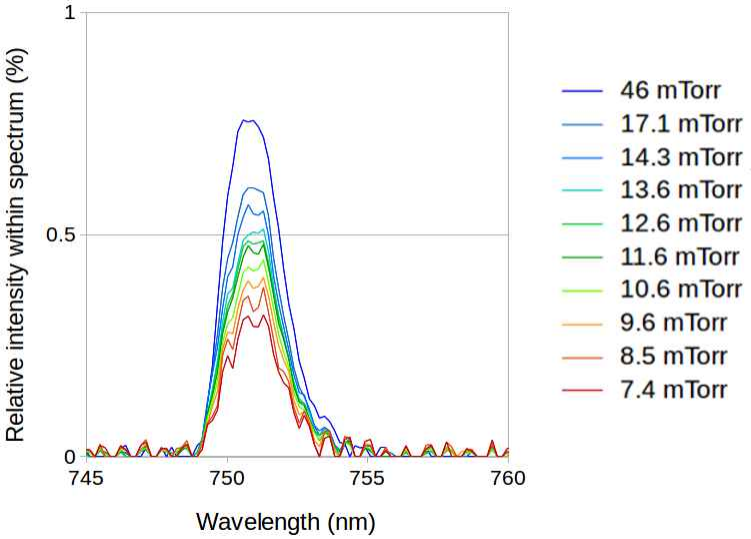

Fig. 35. Zoom of Fig. 34 ii) showing variation in relative intensity of 750.4 nm spectral line within optical emission spectra from the argon discharge at a range of pressures

3.2.4 Vacuum distributions of potential and electric field

In this section the results of calculations made of electric field and potential distributions are presented. The distribution of electric field and potential surrounding the electrodes in the vacuum case, with no plasma present, was modelled in three dimensions using the Comsol software package.

Fig. 36 shows contours of the potential distribution within the chamber, as calculated for two intersecting planes; the relative location of each of these is indicated upon the other with a dashed line. The distributions of electric field occurring along both the line of intersection of these planes and the axial line are also plotted, with values corresponding to a nominal cathode potential of 1 V (Fig. 37).

These plots show the vast majority of the cathode potential to be dropped between the electrodes, causing the electric field distribution across the chamber to be correspondingly peaked in this region. Relatively little variation occurs in the potential in the regions external to the anode or within the cathode interior, and the electric field in these regions is smaller by more than an order of magnitude.

The effect of the grid electrodes may be observed as causing local distortions in the distribution surrounding them, with a distinctive 'bulging' of the contours associated with the apertures of both anode and cathode.

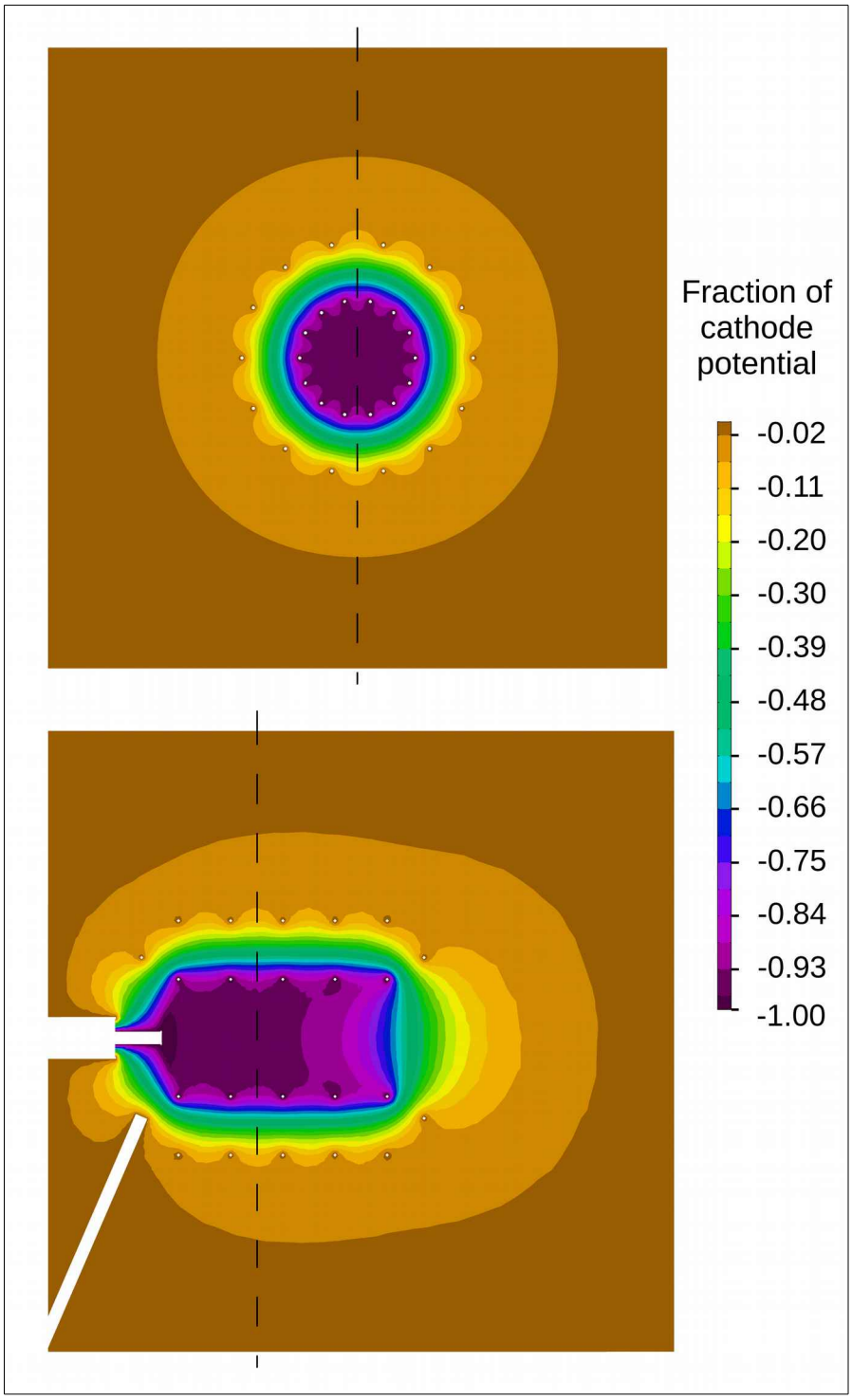

Fig. 36. Vacuum distribution of potential within the chamber, shown as contours upon planes having two different projections. The location of each plane is marked upon the other by a dashed line.

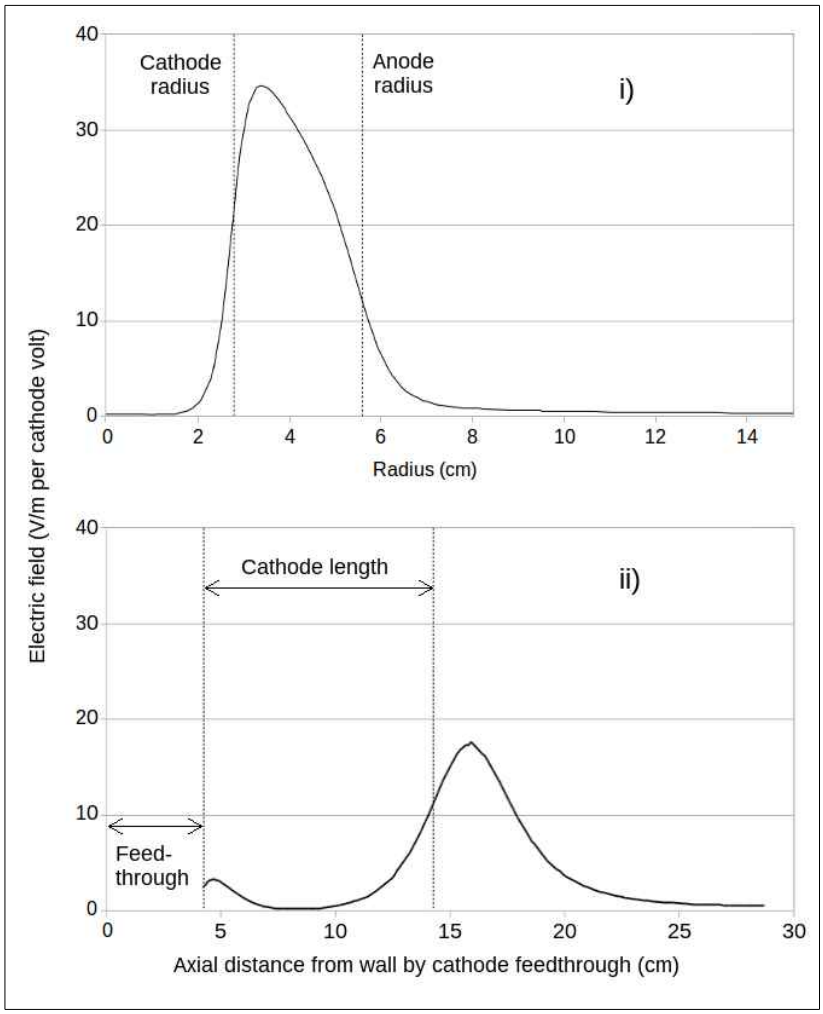

Fig. 37. Vacuum distribution of electric field and potential, plotted i) along a radial chord corresponding to the line of intersection of the two planes in Fig. 36, and ii) along the axis of the entire chamber.

3.3 Discussion

This research project is concerned with the possible utility of plasmas in which reactive processes such as electronic excitation and ionisation are caused by the action of ions and neutrals. The identification of operating regimes that result in the production of such plasmas is therefore of key interest for this initial stage of the project, and so the understanding of the species responsible for plasma processes at work in the two modes is a principal aim. In the following, the measurements and calculations described previously are assessed for evidence that may inform this.

The conditions of voltage and pressure at which the modes are evident are considered first, and these are related to accounts in the published literature describing conditions at which ions and electrons may be expected to become suitably energetic within a plasma to cause reactive processes. The optical emission measurements are then considered, again with reference to the literature. Finally, the nature of the mode transition in helium is discussed in the light of the results of these considerations.

3.3.1. Analysis of conditions

The quantity known as the reduced electric field, or *E/N*, is commonly used to describe the conditions that affect the behaviour of charged particles. In this term, *E* refers to electric field and *N* to the background neutral particle density. In the situation in which a charged particle acquires energy as it drifts in an electric field to then lose it again on having a collision, the energy gained per unit distance is proportional to electric field, and the average distance travelled between collisions is inversely proportional to the density of the medium, and so the *E/N* ratio gives a measure of the energy acquired between collisions.

In a real situation, the energy gained by different particles at given *E/N* conditions is determined by both the path-lengths travelled between collisions and the energy lost when collisions occur. Both of these characteristics vary for different species and also between different *E/N* regimes.

Ions are relatively much more massive than electrons, and so impart energy to the background neutral particles much more effectively than electrons. When ions are drifting in their parent gas, they have a relatively high probability of experiencing charge exchange collisions, in which the ion captures an electron from a background neutral particle. The products of such a reaction are a fast neutral particle and a cold ion, and so this amounts to the transfer of all kinetic energy from an ion to a neutral. Conversely, the much-lighter electrons transfer comparatively little kinetic energy in background collisions. These dynamics cause ions to become energetic at much higher values of *E/N* than electrons, and so the operating conditions at which they are reactive may be characterised in terms of this parameter.

3.3.1.1 Accounts of *E/N* dependences from the literature

Studies have investigated the dependence upon *E/N* for processes of excitation and ionisation, as caused by the activity of both ions and electrons. The findings of some of these are summarised in the following, before an assessment is made of the *E/N* conditions found in the CC and beam mode discharges.

Two bodies of work are found to be particularly useful in describing the *E/N* dependence of gas phase collisions; these are those co-authored by A. V. Phelps, covering processes in helium and argon [63], [67], [68], [70] to high *E/N*, and studies of helium discharges by Hartmann, Donkó and co-workers [64], [65].

In [63] Jelenkovic and Phelps describe the measurement and modelling of excitation and breakdown in a helium discharge at conditions of *E/N* up to 9 kTd (1 Td = 10^{-21} V.m^2). They comment that electron populations are indicated to fail to reach an equilibrium state by *E/N* of around 850 Td, as they start to experience 'runaway'. This refers to the process in which sufficient energy is gained for them become relatively unreactive, and their transport becomes largely ballistic. The authors also plot reaction coefficients against *E/N* up to 100 kTd for ions and neutrals. These are obtained by averaging cross section values over the Maxwellian ion energy distributions that are expected to result from charge-exchanging populations at given values of *E/N*. These results indicate ions to become reactive between 1kTd and 10kTd in helium, and fast neutrals between 10 kTd and 100 kTd.

Further data on helium is found in [64], in which Hartmann, Donkó et al. measure breakdown to *E/N* of around 10 kTd, and model breakdown values to 60 kTd. The projected contributions to ionisation made by electrons, ions and fast neutrals, and contributions to secondary electron production at the cathode made by ions and neutrals, are plotted against *E/N* of up to 100 kTd. These indicate ion-impact ionisation to become important at *E/N* of between 1 kTd and 10 kTd, and neutral-impact ionisation at *E/N* of between 10 kTd and 100 kTd; these values agree with those given in [63]. The neutral secondary electron yield at the cathode is indicated to start to dominate that caused by ions at *E/N* between 20 kTd and 30 kTd. In [65] Hartmann and Donkó describe this model again, and also model the sustaining of a high voltage glow discharge in helium operating at *E/N* of ~16 kTd. This indicates ion-impact ionisation to be more important than that by neutrals at these conditions.

In a study of an argon discharge [68], Jelenkovic and Phelps note that ionisation caused by ions and neutrals dominates that caused by electrons by *E/N* of 15 kTd. In a compilation of cross sections for collisions in nitrogen and argon [67], cross sections for ions and neutrals are again plotted as a function of *E/N* to 100 kTd, using a similar approach to that described above for [63]. These indicate both ion-impact and neutral-impact processes to become significant between 1 kTd and 10 kTd in argon.

These works suggest that we may expect ions to become reactive in helium and argon at *E/N* conditions of between 1 kTd and 10 kTd, with electrons indicated to become less reactive at broadly similar conditions. Fast neutrals are projected to

become reactive in helium at conditions of *E/N* between 10 kTd and 100 kTd, and by 10 kTd in argon.

Ion KE distributions are measured in helium, argon and neon by Rao, Brunt, Olthoff in [69], at *E/N* up to 50 kTd in argon and 20 kTd in helium. Interestingly, these show deviations from Maxwellian equilibrium conditions for argon at *E/N* greater than 20 kTd, and for helium at *E/N* greater than 10 kTd; the energy gain is found to slow as *E/N* increases beyond these values. This work also describes the importance of charge exchange for moderating ion energy at a wide range of conditions.

In order to relate these findings to the conditions that might be found in the CC and beam mode discharges, an assessment is now made of the conditions of *E/N* present in the chamber.

3.3.1.2 Assessment of practical *E/N* conditions

The distribution of electric field calculated for vacuum conditions shown in Fig. 37 indicates the strength of field to vary within the chamber by two orders of magnitude, and so at conditions of fixed pressure, vacuum values of *E/N* will show the same degree of variation. The region in which the CC mode has has been observed to occur is subject to a relatively small electric field from the cathode bias, whereas the radial beams of the beam mode traverse the region of comparatively large electric field within the inter-electrode space.

This leads to the observation that the spatial location of the discharge in these regions serves to maximise the separation in values of reduced electric field, *E/N*, from the already distinct ranges determined by the modes' different ranges of voltage and pressure.

Estimating values of *E/N* for these ranges is quite straightforward at breakdown conditions, since the vacuum distribution of electric field is well-defined. Estimating values for the electric field whilst the discharge is present is a different matter, since plasma may influence this considerably.

For the purpose of assessing *E/N* conditions at breakdown, values of electric field are selected accordingly. For the beam mode, the electric field across half of the inter-electrode space is noted to have a value in excess of of 30 V/m per cathode volt (Fig. 37), which corresponds to around 85 % of the maximum. This value is used to calculate the electric field for beam mode *E/N* estimates. For the CC mode, the assessment of relevant electric field is made harder by the fact that the vacuum field in the cathode centre is negligible, and yet the field closer to the cathode radius is considerably stronger. The relatively-weak field caused by the electrodes in the cathode centre will also be more easily changed by the presence of the plasma, and for the purpose of this exercise, a nominal value for electric field is assigned an order of magnitude smaller than that for the beam mode.

Values are calculated for CC mode conditions corresponding to 300 mTorr in helium and 40 mTorr in argon, with typical cathode potentials of 400 V and 700 V respectively. For conditions representing the beam mode, pressures are chosen to be 25 mTorr for helium and 8 mTorr for argon, with a corresponding cathode potential of 10 kV in either case. The density, N, in units of m^{-3}, may be obtained from the pressure, by re-arranging the ideal gas law:

$$p = N\,k_B T \quad \rightarrow \quad N = \frac{p}{k_B T} \qquad (1)$$

in which p refers to pressure in Pa, k_B is the Boltzmann constant in units of $J.K^{-1}$ and T is temperature in K (1 Pa = 7.5006 mTorr; a nominal temperature of 300 K is used). The results of these calculations are shown in Table 1:

	CC mode		**Beam mode**	
Fill species:	Helium	Argon	Helium	Argon
***E/N* (kTd):**	0.124	1.63	373	1164

Table 1. Typical values of E/N estimated for high- and low-pressure operating conditions corresponding to the CC and beam mode discharges in our apparatus

The variation between the estimates for typical conditions corresponding to the CC and beam modes is noted to be of around three orders of magnitude. Recalling that a change in relative significance from electron processes to ion and neutral processes may be expected to occur somewhere between 1 kTd and 100 kTd for breakdown, these estimates indicate the ranges of *E/N* associated with the two modes to be at least consistent with the mode transition representing a general change from electron- to ion-driven processes. Indeed, the estimated values of *E/N* corresponding to beam mode conditions are sufficiently great to make it seem exceedingly unlikely for breakdown in this mode to be caused by electron processes.

The processes acting to sustain the discharge are expected to be broadly similar to those causing breakdown, and so whilst values of *E/N* will be somewhat different in the discharge, it seems quite likely that these considerations will apply more generally. The nature of the processes at work in the CC mode are less clear however, since the estimated values of *E/N* are much closer to the regime in which such a transition between active species may be expected to occur. The measurements made of optical and electrical characteristics are therefore examined for further evidence regarding the processes that may be operating in the two modes.

3.3.2 Electrical characteristics

In measuring the current-voltage and breakdown voltage-pressure relations, the electrical behaviour across the operating pressure range was found to be broadly similar in helium and argon discharges, with the visible change in distributions of emission observed at the mode change accompanied by various changes in electrical characteristics. Discontinuities are evident in voltage-current curves in both helium

and argon, due to a current threshold associated with the low-pressure limit of the CC mode. This suggests some efficiency to be associated with the establishment of the CC mode. A change in trend of breakdown voltage-pressure relations is evident at the mode change in helium, and CC mode voltages are observed to be consistently relatively greater in argon. Conclusive interpretation of the electrical measurements is made difficult however, by the change in distribution of emission that accompanies the mode change, and no firm evidence regarding the nature of the underlying processes at work is taken from these results.

3.3.3. Optical emission spectroscopy

The results of the optical emission measurements described in Section 2.2 showed characteristic pressure-dependences to be evident for light of certain wavelengths. This was found to be the case for the argon line at 750.4 nm, and the helium lines at 501.6 nm and 587.6 nm.

In the literature concerning excitation processes at high *E/N*, specific mention is made of the 750.4 nm argon line and both of the helium lines. In [70], spatio-temporally resolved measurement of argon spectral lines at high *E/N* is shown to demonstrate production of light at 750.4 nm to be due to electrons, as compared to other strong lines in the spectrum that are shown to result from excitation by fast neutral species.

This lets the evolution in relative intensity of the 750.4 nm line observed in spectra from the argon discharge, as shown in Figs. 34 and 35, be associated with a decline in electron activity at increasingly low pressures. Whilst these results are consistent with a progressive reduction in electron activity at increasingly low pressure, they do not conclusively demonstrate the nature of processes acting to sustain the two modes.

The helium lines at 501.6 nm and 587.6 nm have been found to make up significant fractions of the visible emission from the CC and beam modes respectively. The contribution made by these lines to overall levels of emission in the visible range was found to change quite abruptly across a range of pressures immediately below those of the CC mode range (Fig. 33), suggesting this change to be representative of the processes causing excitation in the two modes.

In [68] Phelps and Jelenkovic consider excitation processes that give rise to the 501.6 nm and 587.6 nm spectral lines, as measured in a drift tube at different *E/N* conditions. They calculate values for excitation coefficients as functions of *E/N*, by averaging cross sections over energy distributions. The results of this indicate emission caused by electrons to have a relatively-larger component at 501.6 nm (at all *E/N* plotted, to 10 kTd), and that ion-impact excitation will result in relatively more emission at 587.6 nm (from threshold at a few kTd, with the difference becoming smaller by 100 kTd). For emission caused by neutrals, the coefficients are of similar size for both lines at lower values of *E/N* (around 10 kTd), with that for 501.6 nm becoming relatively larger at higher values.

Before these results may be applied to the interpretation of the measurements made here, it is noted that the experiments in [68] are carried out at optically thick conditions, and so the analysis corrects for the effects of excitation transfer. The optical measurements reported in this chapter were made at a relatively wide range of pressures, and the effects of this are considered in the following.

The effects of excitation transfer are associated with the process known as radiation imprisonment, in which radiation from transitions to the ground state may then become re-absorbed by background neutrals; this causes the effective lifetime of the upper state to be increased [71]. When such a level may also transition to levels other than the ground state, resulting in visible emission, this effect therefore causes the intensity of these visible lines to become greater with pressure, since some of the excitation energy that would otherwise be lost via transitions to ground (causing invisible UV radiation) is re-directed into production of visible photons [72].

Should the upper state have a principal quantum number, *n*, greater than 4, then energy levels with same *n* but different angular momentum and spin are spaced sufficiently closely in energy for excitation to be transferred to these via collisions [73]. The effective increase in excited lifetime enables this to happen so as to populate triplet states that are not resonant with the ground state. These would be otherwise immune to the effects of radiation imprisonment, and a variable pressure-dependence for different visible lines results [74].

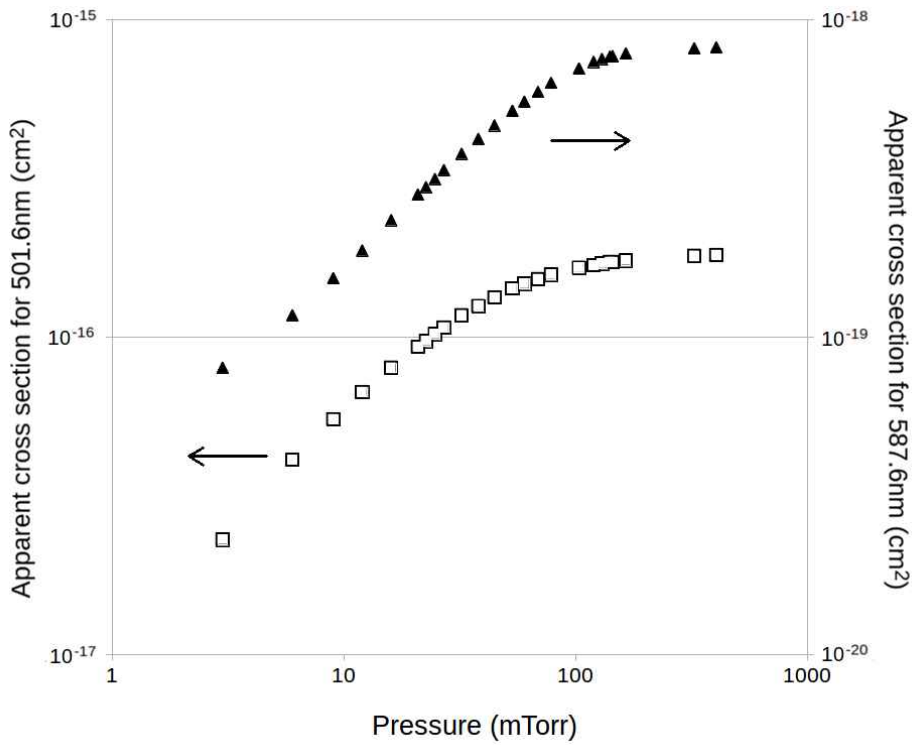

Fig. 38. Apparent cross sections for excitation of 501.6 nm (open squares) and 587.6 nm (closed triangles) of helium by 100 eV electrons at different pressures. Data from [74].

The apparent cross section for excitation of the 587.6 nm triplet line by 100 eV electrons, as measured by Jobe and St.John [74], is shown to have slightly more of a pressure-dependence than the 501.6 nm line (Fig. 38). This means that, although the experimental conditions are likely to vary considerably in optical opacity, the species-dependence indicated for excitation of these two lines at a Torr will be expected to hold similarly for these conditions also.

The change in emission structure associated with the mode change in helium is therefore considered to represent a change in principally-active species. Because ions and electrons become reactive at conditions of different *E/N*, and because significant local variation occurs in such conditions, this may cause a spatial separation of regions in which either species is active. In helium, excitation caused by the two species results in emission at sufficiently different wavelengths to make this localisation visibly apparent, which may be observed by considering the distributions of emission evident at conditions corresponding to the mode transition, as illustrated by the photographs in Fig. 26.

It should be noted that, whilst these findings enable us to perform a quick visual diagnosis of species reactivity in helium, this interpretation of the emission structure is made possible by the different magnitudes of the cross sections being insufficiently distorted by other effects within this discharge. This might not hold for different types of plasmas, for example those with a particularly high electron density, since any significant metastable populations will be expected to affect the spectral distribution of emission [75].

3.3.4 Summary

In considering how these distributions of emission relate to the distribution of electric field within the chamber, the cathode-confined glow is observed to occur in the region along the central axis of the cathode, where little electric field is caused by the electrode bias. The radial beams, however, follow the orientation of the strongest electric field within the chamber, in the annular inter-electrode region. These modes therefore occur in very different *E/N* conditions. Analysis of the ranges of *E/N* likely to be associated with these indicates conditions in the region in which the beam mode occurs to be associated with reactive processes caused by ions and neutrals.

The characteristic spectrally-resolved emission structure evident in light from helium and argon discharges at increasingly low pressures is found to reflect an evolution in excitation processes from those caused by electrons to those by ions or neutrals. The correlation observed between the spatial distribution of the emission structure in helium and the distribution of *E/N* conditions demonstrates the CC mode emission structure to be associated with electron activity, and emission from the beam mode plasma to be associated with ion and neutral activity. Making an analogy between the *E/N* dependence of processes for excitation and ionisation, the processes sustaining the CC mode more generally are considered to be caused primarily by electrons, whilst the beam mode is considered to be principally sustained by ion- and neutral-driven processes.

The cathode-confined mode may therefore be described as an electron-driven mode that occurs towards the upper *E/N* limit for electron-driven glow discharges in our apparatus. It is visually characterised as having a well-defined region of intense emission located in the central region of the cathode, with little significant change in electrical characteristics over a relatively wide pressure range.

In the beam mode, the radial beams traverse the zone of high electric field between the electrodes, with the dependence of reactivity upon *E/N* conditions letting us expect that the discharge is sustained significantly by activity occurring in this region. They also pass through the electrode apertures, suggesting that these paths are selected for in the efficient sustaining of the discharge. The equivalence of mass between ions and the background neutrals will result in efficient transfer of momentum in collisions; this, along with the high probability for charge exchange reactions, suggests considerable production of fast neutral species to accompany ion transport. The highly-open grid electrodes and long paths to the chamber walls may allow fast neutral particles produced in the beams to travel further, and so to be relatively more significant, in this type of discharge than those produced between planar electrodes at similar *E/N*.

3.4 Conclusions

In this chapter, some of the principal operating characteristics of a cylindrical Transparent Cathode Discharge have been described. The discharge was generated using DC potentials applied between two grid electrodes, and it was operated in several different gases, over a quite wide range of pressure, voltage and current. Discharge behaviour was monitored using visual observation of the spatial distribution of plasma emission, spectral analysis of this emission, and measurements of discharge voltage and current. In all cases, the apparatus was operated as a self-sustained discharge, with the applied electrode voltage being increased until a continuous self-sustained discharge was present. The low-pressure limit for these observations was set by the limitations on achievable operating voltage.

The device was found to operate in two characteristic modes, distinguished by distinct patterns and colour of emission, different breakdown behaviour and different voltage-current characteristics. The modes were observed to occupy distinct ranges of both cathode voltage and pressure, and different spatial regions within the chamber. The mode occurring at higher pressures and lower voltages has been called the ‘cathode-confined’ mode, and the low-pressure, high-voltage mode the ‘beam’ mode, since these terms describe the visual appearance of the emission distributions in each case.

The cathode-confined mode is characterised by strong emission only in the region enclosed by the cathode. For helium, this mode was present for pressures between 100 mTorr and 1.5 Torr, while for argon the pressure range was between 20 mTorr and 50 mTorr. Current-voltage relations towards the low-pressure limit of this mode show its formation to be associated with a current threshold, which either does not apply throughout the rest of the operating pressure range, or is too low to be evident.

The beam mode is observed at pressure ranges below 100 mTorr for helium, and below 18 mTorr for argon, and these extend to the lowest pressures for which a self-sustained discharge could be obtained in the apparatus. This mode is visually distinguished by distinct radial beams of emission, passing through the apertures of both electrodes and extending to the walls of the chamber.

Analysis of optical emission together with the *E/N* dependences for electron- and ion- or neutral-induced processes of excitation and ionisation led to the conclusion that the cathode-confined mode is predominantly sustained by electron-impact ionisation and excitation, whilst the beam mode is sustained by collisions of high-energy ionic and neutral species with the background gas. In this experimental set-up, the emission associated with beam formations starts to appear during the mode transition and is evident throughout the lower-pressure range, and so the presence of the beams is directly associated with the occurrence of an ion-reactive plasma.

This is a very useful distinction to be able to make for this research, since it constitutes the identification of the operating regime of interest for the obtaining of a plasma in which ions and neutrals are principally-active species. A reactive discharge in which properties such as radical density and energy are determined by ion-impact excitation may generate reactive plasma with significantly different properties from conventional sources, in which electron-impact collisions originate all the reactive processes. The separation of the modes by pressure is also significant, since there are few plasma sources for which the reaction mechanisms can be easily switched between electron-driven and ion-driven collisions. Further studies, however, are necessary to investigate the nature of collisional processes in this system, particularly in molecular gases, before the utility of such a source can be determined.

The predominance of charge-exchange reactions for ionic species lets us infer the existence of a high-energy neutral population, accompanying the ion-driven discharge, which observation is consistent with the spatial extension of the beams to the chamber walls. From this, it is concluded that the beams are responsible for carrying significant thermal energy from the inner regions of the apparatus to the chamber walls. This opens up the possibility of this source being developed further, perhaps in a different geometry, as a source of energetic neutral beams. However, further studies of the beams, including more detailed measurements of their properties and investigation of the mechanism which generates them, is needed to identify any potential applications.

Previous IEC work has concentrated upon the lower-pressure regime, with the research motivation making the upper limit to this range of little interest, although Hirsch does describe the existence of a hollow-cathode type discharge [7]. No study has previously documented the nature of the transition from electron to ion/neutral processes in an IEC device. This work shows where this transition occurs in the overall mode structure, and how it is evident in discharge parameters.

Chapter 4
The Cathode-Confined mode

4.1 Introduction

In the preceding chapter, the investigation of two discharge modes apparent at different, consecutive ranges of pressure indicated them to represent discharges primarily sustained by electron-impact processes at higher pressures, and processes caused by ions and neutrals at lower pressures.

This research is directed towards the operation of a plasma source in which reactive processes are caused by the activity of ions and neutrals, and so the electron-driven mode, called the cathode-confined mode, constitutes an undesirable mode of operation for this purpose. An understanding of the nature of the processes that cause its appearance, and the dependences of these upon the device configuration, may therefore inform the practical engineering of a stable source. This makes these areas of interest for the purposes of this study, and they are addressed in this chapter.

Consideration of some characteristics of the CC mode, i.e. its confinement within a semi-transparent cathode, the discontinuities in current and voltage evident upon its appearance and its operation at the upper range of *E/N* conditions for electron-driven activity in our set-up, suggests that it may bear some resemblance to hollow cathode-type discharges, as has been suggested for other higher-pressure IEC plasmas [7]. Should this be so, the sustaining processes may be expected to involve a confining effect exerted upon electrons by the negative potential of the cathode; secondary electrons emitted from the cathode and accelerated across the cathode-to-plasma potential, that lose sufficient kinetic energy via inelastic collisions, may become confined within the plasma-cathode field structure. Energetic electrons so confined may then lose their remaining kinetic energy to further electronic excitation and charge generation as they undergo more collisions, with the ion flux incident upon the cathode releasing fresh secondary electrons to sustain the plasma. This mechanism is known as the 'hollow cathode effect', and the extent to which it may sustain the CC mode discharge is investigated in this chapter.

The discharge is first characterised in terms of distributions of current and optical emission within the chamber, in order to gain some insight into potential structure and charge flow. These measurements are described in Section 4.2. The operation of the hollow cathode mechanism might be expected to cause discharge properties to show a dependence upon the physical form of the cathode, and so in Section 4.3, the effect of enclosing the open cathode end with a wire grid is explored. The experimental findings are then considered in Section 4.4 along with relevant theoretical principles, and the implications for a future source outlined.

4.2 Electrical and optical characteristics of the CC mode

4.2.1 Current distributions

The measurements described in this section are those made of various currents flowing within the chamber volume when the discharge is in operation. In the previous chapter, the cathode current-voltage relation of the CC mode was described. In the following, the results are presented of corresponding measurements, made simultaneously, of currents collected by the anode and by collectors positioned in axial and radial locations within the chamber.

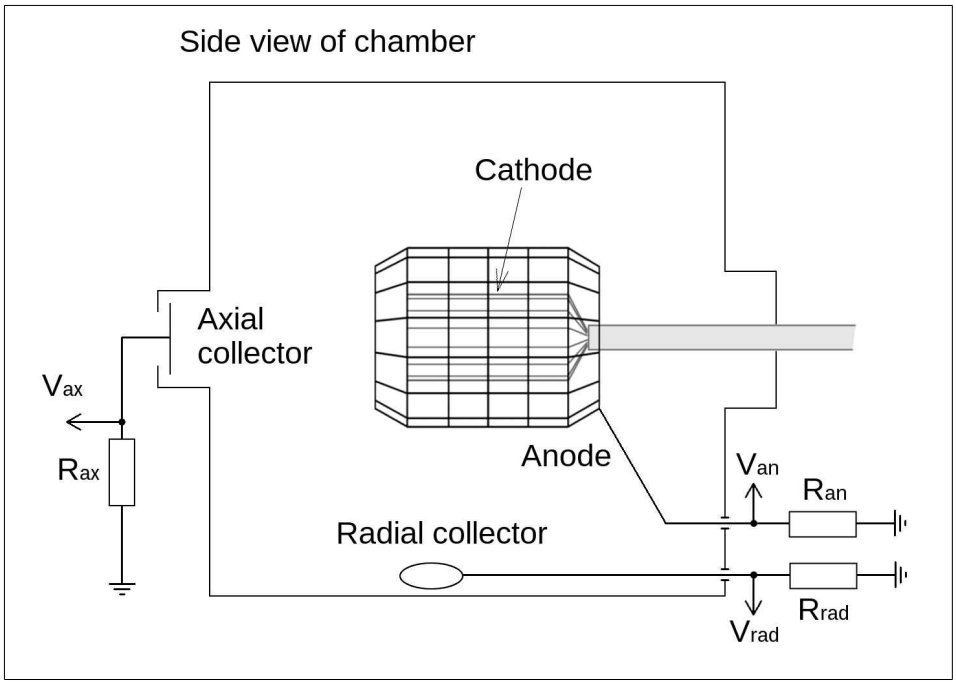

Fig. 39. Diagram showing electron current monitoring system

These collectors were located aligned axially with the electrodes and displaced radially from the end row of cathode apertures, as described in the set-up chapter (diagram reproduced in Fig. 39). For these measurements, the KF40 blanking plate was used as axial collector, and the radial collector was a stainless steel disc with a diameter of around 3.5 cm. This was located on the floor of the chamber and held at an angle approximately normal to a radial chord.

The procedure followed in making these measurements was as described previously; values of voltage from the power supply monitoring outputs were logged using an ADC system whilst the cathode voltage was varied quite rapidly, repeated out at a range of different pressures. Current collected by the anode, and current incident upon the collectors were measured by recording the voltage developed across small resistances to ground.

With the ADC reference voltage set to be around 2.7 V, the resistances were chosen so as to be large enough to provide adequate resolution and small enough to

generally enable the recording of the full range of values. From Ohm's Law, currents were then calculated by $V = IR$ [i.e. $V_{axial} = I_{axial} x R_{axial}$; $V_{anode} = I_{anode} x R_{anode}$ and so on].

Before proceeding to describe the results of these observations, the relations between currents flowing in the chamber are briefly outlined. Cathode current is essentially ion current, drawn from all regions throughout the chamber subject to the negative influence of the cathode. The ion current, as monitored at the cathode, is augmented by the secondary electron current caused as electrons are ejected from the electrode surface due to ion impact, since the power supply does not differentiate between incoming ion current and outgoing electron current. The metered cathode current, I_k, may therefore be written:

$$I_k = I_i \times (1 + \gamma_{SE}) \qquad (2)$$

in which I_i is ion current, and γ_{SE} refers to the secondary electron yield per incident ion. The secondary electron current flows to the anode and chamber walls, as does all primary electron current resulting from ionisation within the chamber volume. The primary electron current is noted to be equal to that of the ion current, since both of these result from the same ionisations; this makes the total electron current equal to the metered cathode current:

$$I_k = I_i \times (1 + \gamma_{SE}) = I_e \times (1 + \gamma_{SE}) \qquad (3)$$

in which I_e is primary electron current. The axial and radial collectors intercept fractions of the wall current according to their area and the flux density at their respective locations. The anode, axial and radial currents are therefore all expected to be principally electron currents.

Measurements made in helium are presented first, followed by those made in argon. Data are shown for both the CC mode and the beam mode. This aids comparison between them, and the observations made here concerning the differences evident between the modes may also be referred to in the discussion of the beam mode in the next chapter.

4.2.1.1 Helium

The cathode current-voltage relation is reproduced from the previous chapter, to aid comparison, as Fig. 40. This shows curves at a range of pressures that extends to pressures well below the low-pressure limit for the CC mode to instigate; the beam mode curves are all coloured dark blue so as to distinguish them from the CC mode curves.

The appearance of the CC mode was noted to be accompanied by discontinuities in the current-voltage curves, at conditions approaching the low-pressure limit for the mode to form. This behaviour was illustrated in further detail in the previous chapter (see Figs. 27 and 28), in which the appearance of the CC mode was observed to cause a sudden increase in current. The persistence of the mode was also noted to be associated with a hysteresis, as once in operation it will continue to be evident at currents smaller than the threshold for formation.

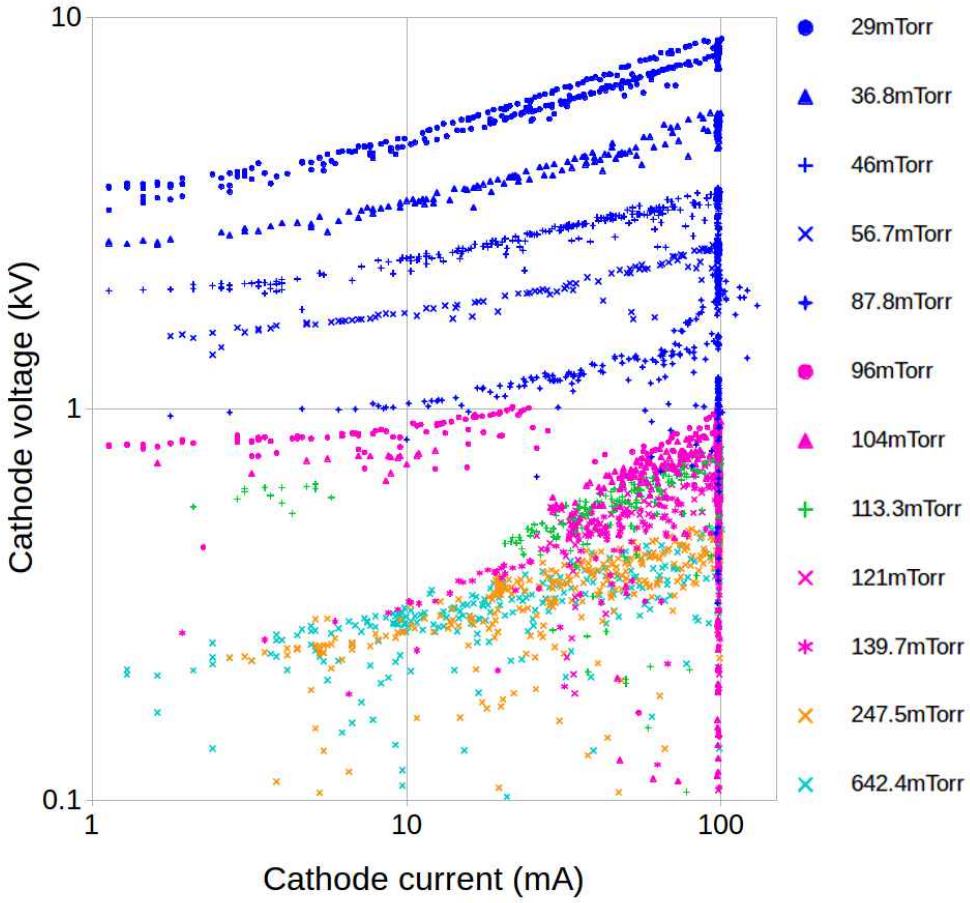

Fig. 40. Cathode current-voltage curves for the discharge in helium, at various pressures. Beam mode curves are coloured blue to distinguish them from the CC mode curves.

The plots showing the dependence of anode current, and currents to axial and radial collectors, upon cathode voltage are shown in Figs. 41 i) - 43 i). These are also represented on a log-log scale, and the curves follow the same colour-pressure coding as those in Fig. 40. The data for these currents is also plotted against cathode current for each case [Figs. 41 ii) - 43 ii)], to show proportionality with cathode current; these plots are on linear scales.

Before describing these further, it is noted that the magnitudes of anode current for the two CC mode discharges at pressures greater than 200mTorr become greater than the limit of the ADC recording system. Unfortunately, time constraints did not allow for the repeating of these measurements using a smaller resistance. This may be observed most apparently in Fig. 41 ii), where the build in anode current at these pressures suddenly halts at around 7mA. The corresponding points in the current-voltage plot [Fig. 41 i)] are indicated with arrows, the direction of which roughly indicate the trends.

Anode current:

The anode current-cathode voltage relation is observed to be very different in the CC and beam modes (Fig. 41), and to be evident as such to either side of the discontinuities associated with the mode change. For CC mode discharges, this relation evolves considerably with pressure. Since the cathode current-voltage relation is quite consistent for the CC mode (Fig. 40), this pressure-dependence may be observed as the changing proportionality between anode and cathode current illustrated in Fig. 41 ii).

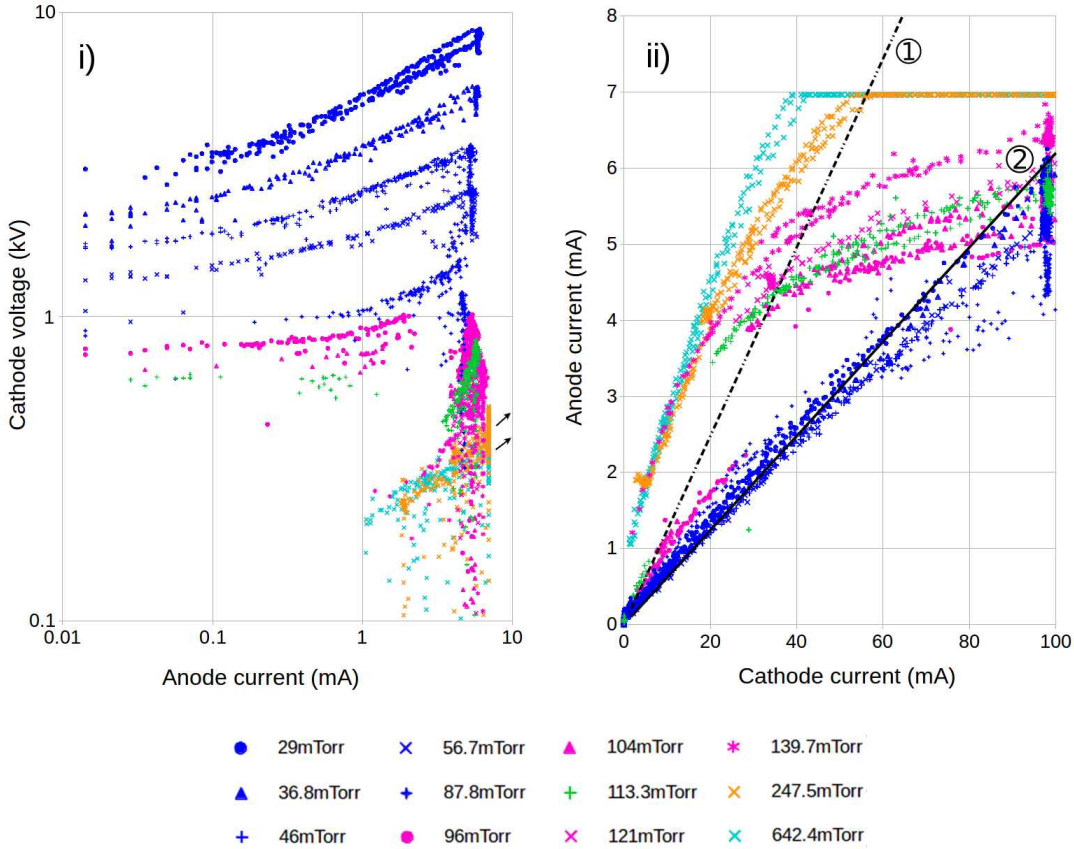

Fig. 41. Anode current for the discharge in helium, at various pressures. Beam mode curves are coloured blue to distinguish them from the CC mode curves. Anode current-cathode voltage curves are shown in i); values of anode current are also plotted against cathode current in ii). Current voltage plots have log-log scales, current-current plots have linear scales.

At conditions of relatively small cathode current, and for discharges operating in either the CC or beam modes, anode current is observed to be proportional with cathode current, although this proportion is considerably greater for the CC mode. In the beam mode the proportionality is largely preserved at conditions of higher current, but for currents greater than around 20 mA in the CC mode, anode current builds at a progressively smaller rate than cathode current. This effect becomes more pronounced at conditions approaching the low-pressure limit for the mode.

Two lines are drawn on the plot of anode current against cathode current in Fig. 41. ii), marked ① and ②, to illustrate consistent fractions of cathode current. The significance of these is as follows: since the anode grid surrounds the cathode, and also surrounds much of the visible activity within the CC mode discharge, the electron current to the anode will flow largely from locations within its radius. The anode grid has a circumferential geometric transparency of around 87.6 %; this is as calculated for the four rings of apertures making up the main part of the electrode, neglecting the end rings and axial apertures. Assuming straight-line trajectories, the fraction of an azimuthally isotropic radial flux of electrons, originating from an axial line source, that might be expected to be incident upon the anode is therefore 12.4 %. If this is assumed, for the sake of the exercise, to be equal to the entire electron current within the discharge, (from Eqn. (3), p. 68, this will be equal to the metered cathode current), then this fraction is that represented by the line marked ①. The other line, marked ②, represents half of this fraction.

From consideration of these, it may be observed that at conditions of low to moderate cathode current, levels of anode current in the CC mode discharge are greater than the fraction of a radially-directed isotropic flux intercepted by the electrode, even should this flux represent all electron current in the discharge. At these conditions, anode current appears to represent an active collection of electron current by the anode. At conditions of increasing cathode current, this fraction becomes progressively smaller, and this relative reduction in anode current is observed to become generally greater at conditions of lower pressure within the CC mode range.

To briefly consider the different relation evident in the beam mode; in this case, anode current remains quite consistently proportional to cathode current at all pressures. The proportionality of this is roughly consistent with the interception of an isotropic electron flux that is directed radially-outwards, having a magnitude of around half of metered cathode current. This cannot be concluded to be the case from this, but it places the relation illustrated between anode and cathode currents into some context.

Axial current:

The currents collected at the radial and axial collectors are now considered, beginning with axial collector current (Fig. 42). Axial current levels from the CC mode discharges are observed to be very small compared to those from the beam mode, with quantities collected generally smaller than a tenth of a milliamp. To place the magnitudes of these into some kind of context, the area of the axial collector is calculated to be around 1.4 % of the area of the end wall in which it is situated; were the axially-collected levels to represent the intercepted fraction of an isotropic flux of even density incident upon the wall, they would indicate total levels of this flux to be generally smaller than 10 mA.

That this is representative of a relatively-small proportion of electron current flowing axially from the discharge in the CC mode is noted to be consistent with the relative lack of axial emission evident in the photographs of Fig. 48.

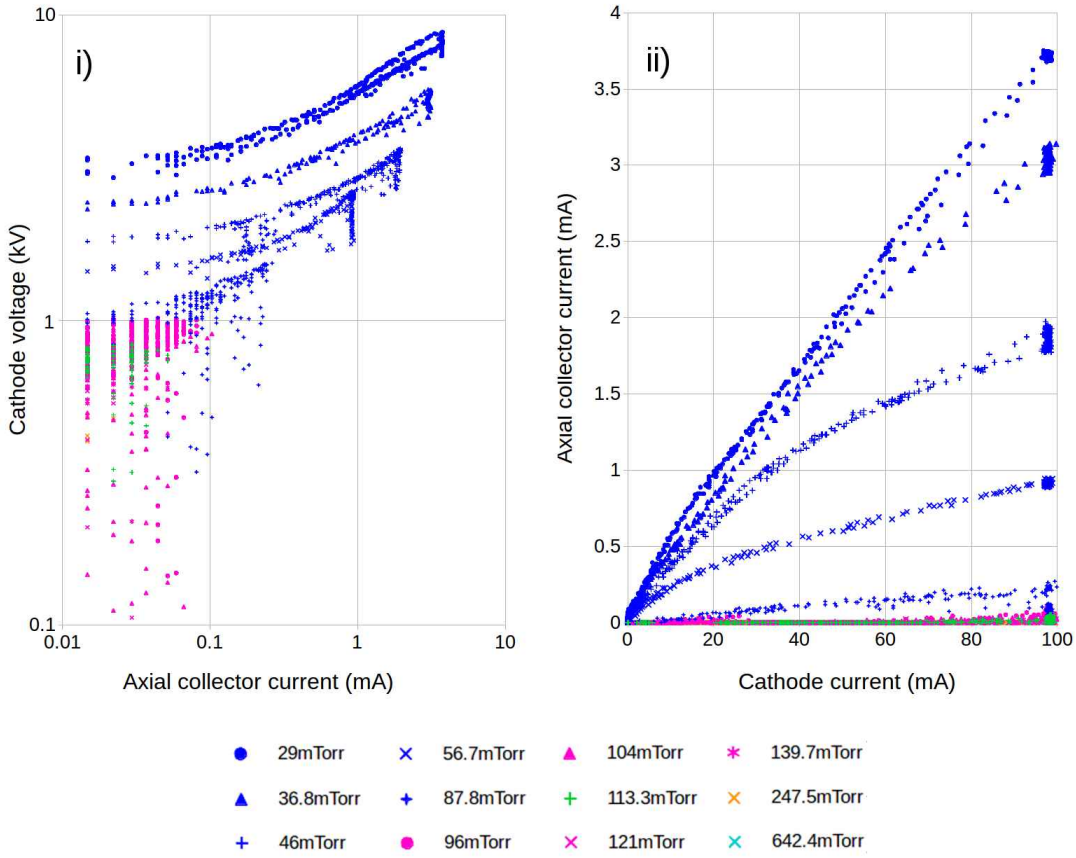

Fig. 42. Current to the axial collector for the discharge in helium, at various pressures. Beam mode curves are coloured blue to distinguish them from the CC mode curves. Axial collector current-cathode voltage curves are shown in i); values of axial current are also plotted against cathode current in ii). Current voltage plots have log-log scales, current-current plots have linear scales.

The magnitude of electron current incident upon the axial collector becomes increasingly significant at progressively low pressures in the beam mode, which is associated with the presence of the axial electron beam. This beam is noted to become more focussed upon the collector at progressively lower pressures, and so the increasing proportion of cathode current represented by axial collector current during operation at these conditions is consistent with this.

Radial current:

The current incident upon the radial collector during CC mode operation is now considered, with this data plotted in Fig. 43. The radial current-voltage curves are observed to be quite similar in appearance to the cathode current-voltage curves. When plotted against cathode current, radial current is indeed found to show a close proportionality with cathode current, as may be observed from the linear relations evident in Fig. 43 ii). This is also the case for the beam mode relation, with a relatively small difference in proportionality evident between the two.
Lines are drawn on the plot of radial collector current against cathode current [Fig. 43 ii)], which describe constant proportional relations in a similar way to those in Fig. 41 ii). In this case, the corresponding fraction of cathode current is calculated by

assessing the areal fraction of a cylindrical surface, concentrically surrounding the electrodes and having a radius such that it includes the collector surface. The longitudinal dimension for this surface is given a nominal value of 12 cm, but it is noted that since that of the flux of electrons is poorly-defined, this is subject to a degree of uncertainty. Similarly to those shown in Fig. 41 ii), the line marked ① represents the radial collector current that would result from an intercepted fraction of an isotropic, radially-directed flux of electrons equal to the entire electron current from the discharge. The other line, marked ②, again represents half of this fraction.

Significantly, the results of this analysis show both anode and radially-collected currents from beam mode discharges would bear a similar proportionality to cathode current, were they indeed to represent intercepted fractions of an isotropic flux according to their respective areas, and were this flux to be of the order of half of the total discharge electron current.

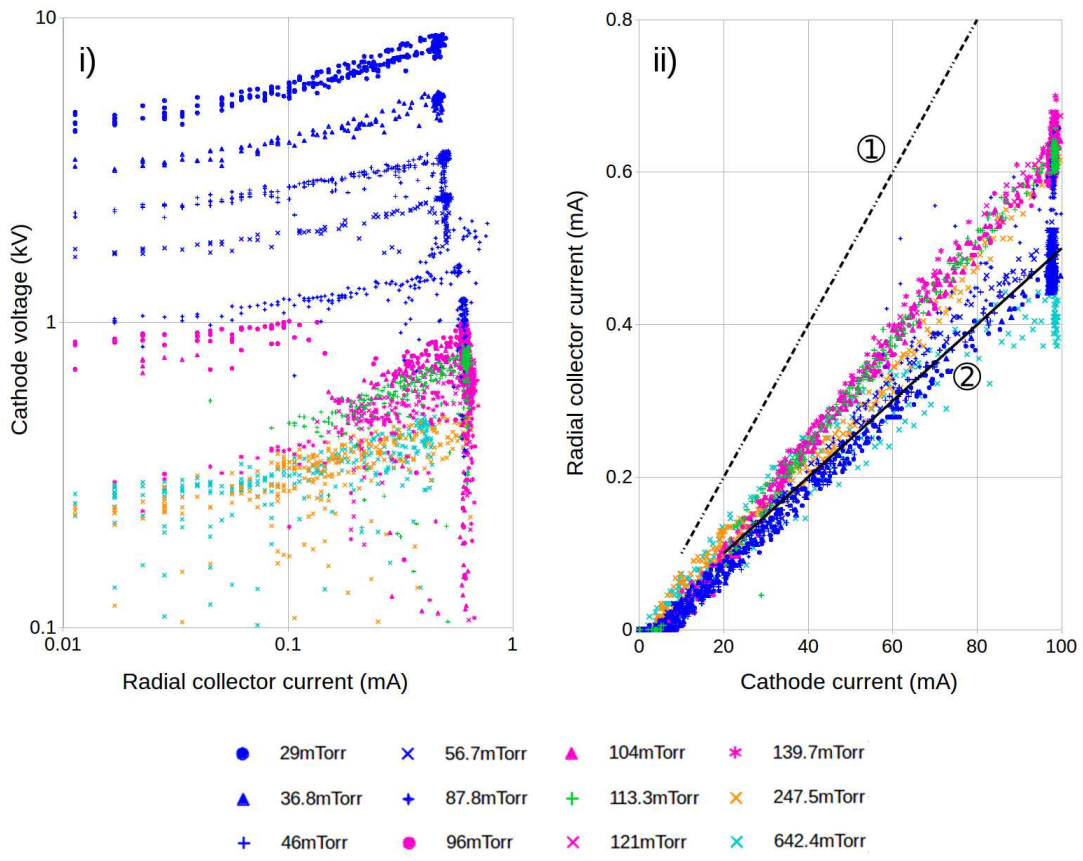

Fig. 43. Current to the radial collector for the discharge in helium, at various pressures. Beam mode curves are coloured blue to distinguish them from the CC mode curves. Radial collector current-cathode voltage curves are shown in i); values of radial current are also plotted against cathode current in ii). Current voltage plots have log-log scales, current-current plots have linear scales.

The consistent proportionality of radial collector current with cathode current from CC mode discharges indicates that, whatever mechanism is the cause of the variation seen in anode current, this does not affect the current to the radial collector.

4.2.1.2 Argon

The same currents as measured in argon discharges are now considered, since some significant differences are evident. These are presented in the same manner as the helium data, with anode and collector currents again plotted against both cathode voltage and cathode current.

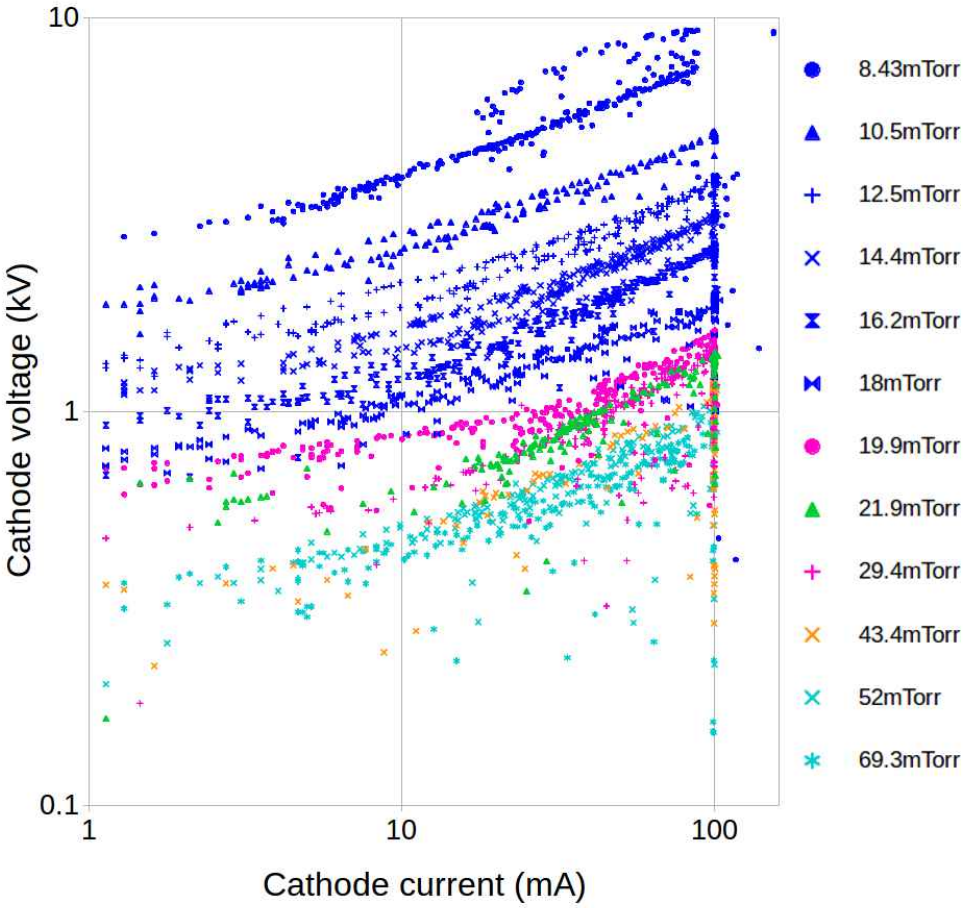

Fig. 44. Cathode current-voltage curves for the discharge in argon, at various pressures. Beam mode curves are coloured blue to distinguish them from the CC mode curves.

As for helium, the cathode current-voltage relation is first reproduced from the previous chapter, as Fig. 44. This was noted to be broadly similar to the behaviour found for helium, with some differences evident in the scaling. The magnitude of voltages corresponding to the CC mode were observed to be generally somewhat greater in argon, making the mode structure less obvious for these curves when compared with those for helium. The curve at 8.4 mTorr was interrupted by a space charge object-related instability, causing flicker and a scatter of data-points at voltages generally in excess of those on the curve. Points corresponding to this may be recognised as such on the following plots.

Anode current:

The anode current-voltage relation measured from argon discharges is plotted in Fig. 45 i). The curves corresponding to the CC mode appear quite different to those for the beam mode, with levels of anode current limited to significantly smaller values. A strong hysteresis is evident for the CC mode curves at pressures of around 20 mTorr, causing these to follow an unusual form.

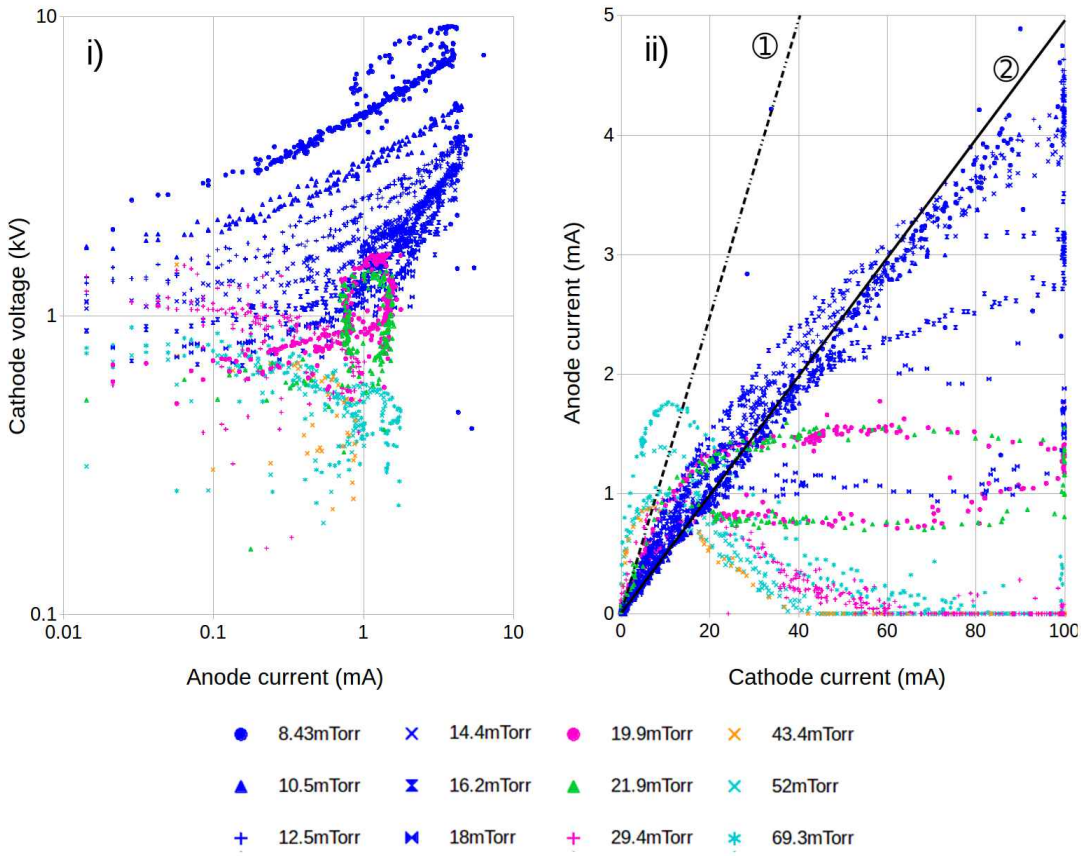

Fig. 45. Anode current for the discharge in argon, at various pressures. Beam mode curves are coloured blue to distinguish them from the CC mode curves. Anode current-cathode voltage curves are shown in i); values of anode current are also plotted against cathode current in ii). Current voltage plots have log-log scales, current-current plots have linear scales.

This behaviour is not reflected in the cathode current-voltage relation, and so when plotted against cathode current, the levels of anode current from the CC mode show a proportionality with cathode current that evolves significantly with conditions [Fig. 45 ii)]. This may be described as follows: at conditions of very low levels of cathode current, anode current can be seen to rise fast with cathode current. This is noted to be similar to the behaviour seen in helium. The rate of anode current-build relative to that of cathode current then becomes progressively smaller. This is again similar to the behaviour seen with helium, but is observed to occur at conditions of relatively much smaller cathode current. For the argon curves, this trend continues until anode current actually starts to decrease, and at higher pressures levels of anode current fall to become negligible. For lower pressures in the CC mode range, a hysteresis

accompanies this variation in levels of anode current, causing the anode current-cathode voltage curves to appear as a loop.

Lines are drawn on the argon anode current-cathode current plot [Fig. 45 ii)] representing similar proportional relations to those shown for helium in Fig. 41 ii). In this case, the line marked ① again represents total electron current as an isotropic radial flux intercepted by the anode fill factor, but the line marked ② represents 40 % of this, rather than half. Beam mode curves are observed to increasingly follow this second relation at progressively low pressures.

Axial current:

The axial collector current-voltage relations for argon (Fig. 46) show a relatively small level of axial current to be evident from CC mode discharges, as was found to be the case for discharges in helium.

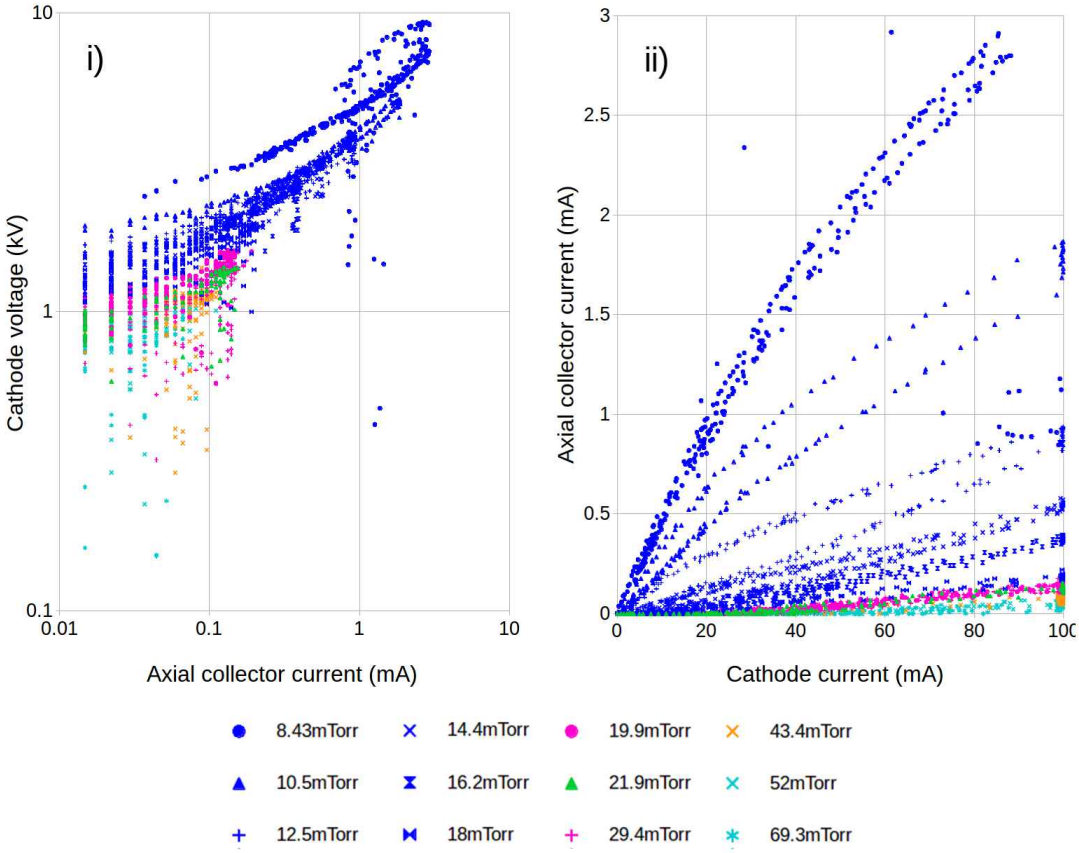

Fig. 46. Current to the axial collector for the discharge in argon, at various pressures. Beam mode curves are coloured blue to distinguish them from the CC mode curves. Axial collector current-cathode voltage curves are shown in i); values of axial current are also plotted against cathode current in ii). Current voltage plots have log-log scales, current-current plots have linear scales.

Radial current:

As was found for helium, the radial collector current-voltage curves in argon resemble the cathode current-voltage curves quite closely. When plotted against cathode current, the levels of radially-collected current show a much closer proportionality to cathode current than the anode current does. In contrast to the relation observed in helium however, the CC mode curves show a weakly-changing relation with cathode current, with the proportion represented by radially-collected levels becoming smaller at conditions of greater cathode current. Despite this, the beam mode and CC mode curves are observed to constitute an overall quite similar proportion of cathode current. The radial collector current appears to be subject to an increased degree of fluctuation in argon, as compared with helium.

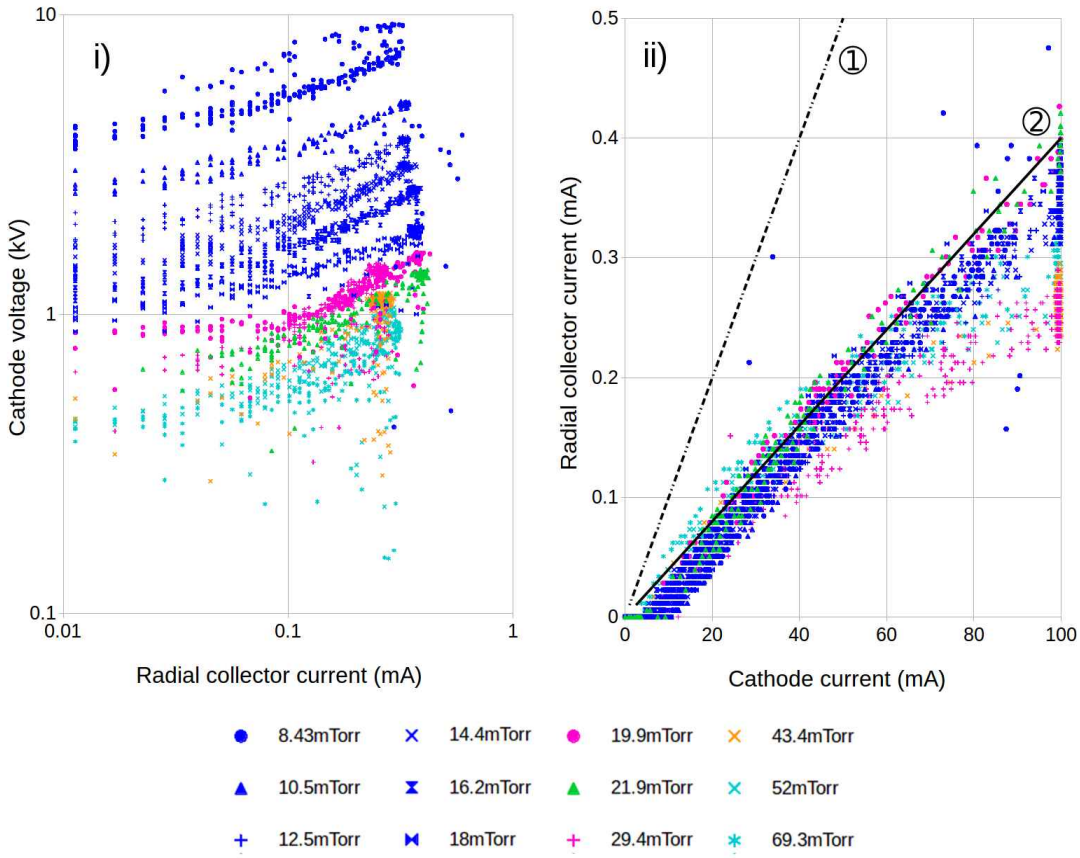

Fig. 47. Current to the radial collector for the discharge in argon, at various pressures. Beam mode curves are coloured blue to distinguish them from the CC mode curves. Radial collector current-cathode voltage curves are shown in i); values of radial current are also plotted against cathode current in ii). Current voltage plots have log-log scales, current-current plots have linear scales.

Lines of consistent proportionality are drawn on the radial collector current-cathode current plots in Fig. 47 ii) in the same way as was done for anode current in Fig. 45 ii); the line marked ① again represents total electron current as an isotropic radial flux intercepted by the collector, and the line marked ② represents 40 % of this.

This analysis indicates the proportionality evident between cathode current and both anode current and radially-collected beam mode currents to be consistent with the interception of an isotropic, radially directed electron flux, according to the areal projection of electrode and collector. In the argon discharge, this electron flux would have a magnitude of around 40 % of total electron current, whereas that in helium would be around half.

The broad similarity in radial collector current-cathode current proportionality evident between the curves from either mode shows this to be relatively insensitive to the mode structure.

The relatively small areal coverage of the chamber walls by the collectors, and the anisotropic distributions of emission within the chamber make these quantities subject to a significant degree of error, and they are treated as qualitative. They nonetheless provide insight into the nature of charge low within the chamber, indicating electron current to be predominantly radial at all conditions. The characteristic difference of around 20 % between the radial currents in helium and argon do not appear to have a converse effect in axial current.

4.2.2 Optical emission distributions

In this section, distributions of optical emission are considered, as evident at a range of pressures extending from the low-pressure limit of the CC mode, at around 100 mTorr, to a pressure of several Torr, at which the mode is no longer recognisable. For this purpose, images of the discharge in helium are used. These correspond to discharges operating at currents of between 10 mA and 30 mA. The distribution of emission evident from a discharge may be expected to show some change with this degree of variation in current; this however has been observed to be small, when compared with the change in distribution observed at different pressures. It will therefore not significantly affect the overall trends observed across this relatively large range of pressures.

Photographs of the helium discharge are presented in Fig. 48. These images are first described, and then the distributions of signal recorded in some of the photographs are quantified. The technique used to do this is outlined before the results are assessed.

The photographs shown in Fig. 48 represent the distributions of emission evident from both an axial perspective, and also as viewed from the side of the discharge axis. These lateral projections of the emission show the extent to which emission may be observed in the region located further along the axis external to the electrodes. The emission that is evident in this region is considered briefly, before describing the images of the axial projection of the distributions.

The photographs taken at a the lowest pressure of 112 mTorr correspond to conditions at which the CC mode only instigates at higher currents, and these images

show the discharge during operation below this threshold, when the CC mode is not established. These, and to a lesser extent the images corresponding to the next-lowest pressure of 143 mTorr, show the increased axial emission that is characteristic of operation at lower pressures in the CC mode range. The relative lack of axial emission at pressures below 200 mTorr is noted to be consistent with the small levels of axial current evident from the discharge at these conditions (see Figs. 42 and 46).

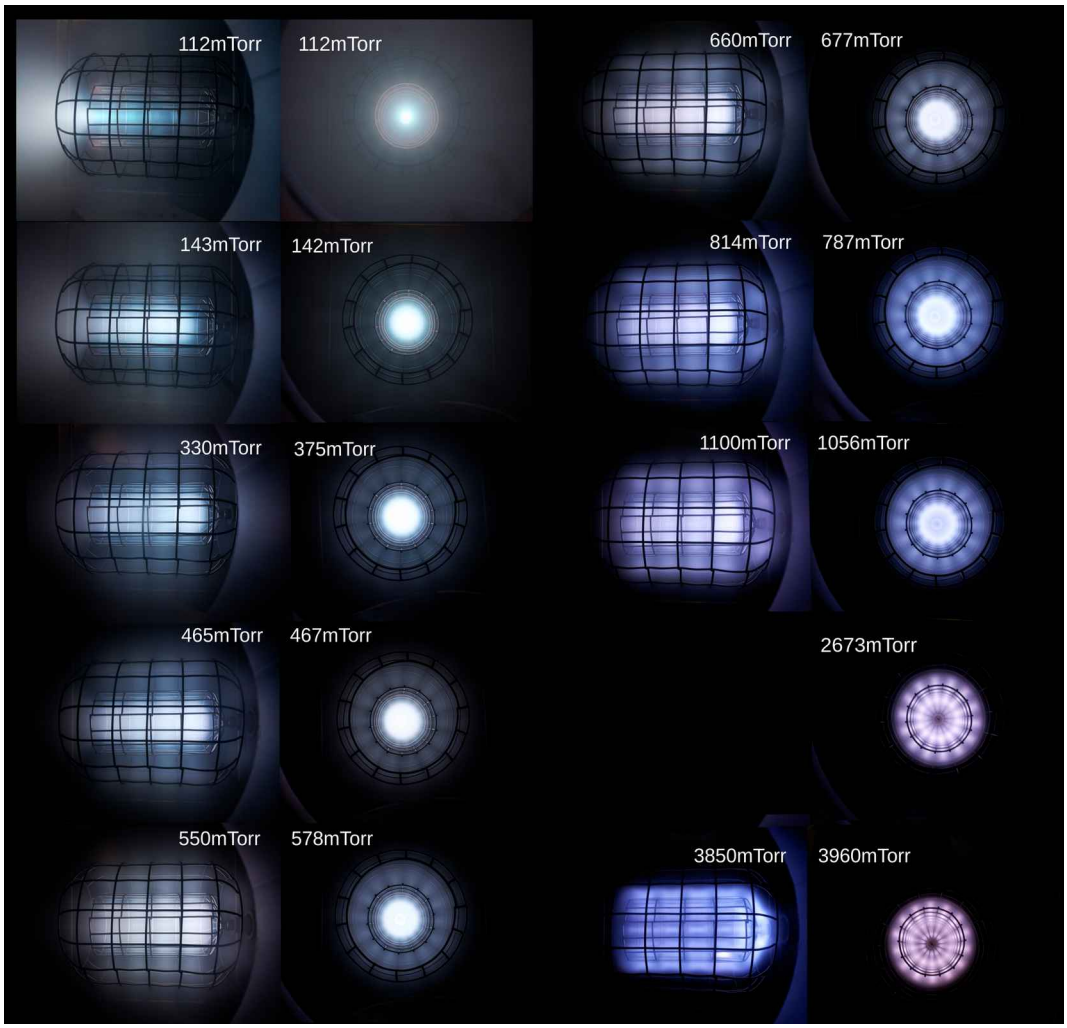

Fig. 48. Photographs of the discharge at progressively higher pressures in helium, showing the evolution of optical emission distribution. Pairs of images have been selected that show the discharge from the side, and from along the axis, at conditions of similar pressure. No side view at ~2.5 Torr was available

The images obtained from an axial perspective show the progressive change in distribution that occurs both within the cathode radius and in the region surrounding the cathode. The progression evident at conditions of increasingly low pressures may be broadly characterised as a shift in the distribution of strong emission, occurring from the region surrounding the cathode to the region within its radius. Some of the details of this are as follow.

The photographs taken at conditions of greatest pressure, of around 4 Torr, show the distribution of emission to consist of a series of radial discharges passing through the cathode apertures.

As pressure is reduced, the parts of these that project into the cathode interior are observed to become brighter, so that by a pressure of around 1 Torr, these form a continuous ring of emission within the cathode, encircling the axis and within its radius. Levels of emission from the central region enclosed by this ring are observed to be also bright, but notably less so than from the ring, which constitutes the region of brightest emission evident..

The progression in this pattern over the range of pressures between 1 Torr and 500 mTorr may be characterised in terms of a progressive reduction in the intensity of emission occurring within the cathode apertures and in the inter-electrode region, and also as an increase in brightness within the central region of the cathode. The intensity of emission in this central region becomes comparable to that of the bright ring, so that by 500 mTorr, the bright emission within the cathode appears as one homogeneous region. The reduction in emission from the region immediately surrounding this lets the overall pattern evident at this pressure be described as consisting of a central, bright region within the cathode, surrounded by a relatively darker region that extends across the region between the electrodes, with little emission evident beyond the radius of the anode.

At pressures between 500 mTorr and 140 mTorr, the region within the cathode remains similarly bright, and the emission occurring between the electrodes becomes less significant. A degree of emission is also observed to occur in the region surrounding the anode at lower pressures.

4.2.2.1 Analysis procedure

In the interest of assessing the relative importance of processes occurring within the cathode, it is useful to consider the degree of emission that occurs here, as compared with that occurring in other regions of the chamber.

This may be characterised by a simple analysis of the distribution of signal recorded in photographs. Before describing the procedure and results of this analysis, it is noted that issues relevant to the analysis of emission distributions recorded in photographs are considered in Appendix 2. These explain that, in order to extract meaningful information regarding the distribution of plasma processes, careful consideration must be made of factors such as the effect of foreshortening, and the spatial distribution of spectral content.

Accordingly, an assessment is first made of the extent to which the distributions of emission apparent in the photographs may be considered representative of those occurring within the chamber. Issues regarding spectral dependence are considered afterwards.

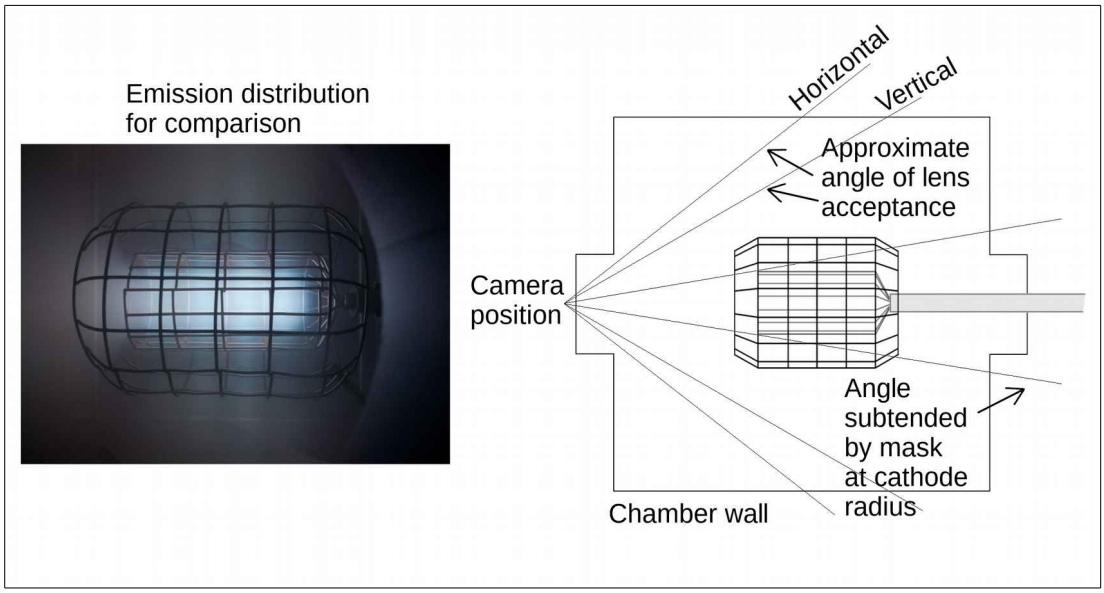

Fig. 49. Geometry of the camera, discharge and chamber. Side view of emission distribution shown for comparison

It is observed that for most conditions illustrated in Fig. 48, the images represent a largely cylindrical discharge; emission occurs principally in the region within and radially surrounding the electrodes, and the distributions are largely symmetrical about the axis. The photographs used for the analysis are those taken from an axial perspective, which therefore approximate to a radial distribution integrated along the line of sight. The geometry associated with the flattening of the real distributions into these images is shown in Fig. 49, also used in the example given in Appendix 2.

This geometry informs the extent to which the photographs may be considered representative of the depth-integrated radial distribution. The camera may be seen to have a relatively wide-angle lens. This enables a significant portion of the chamber interior to be within the field of view, with the trade-off being a considerable degree of foreshortening due to perspective.

With reference to the side-view photograph included in Fig. 49, it is noted that most, but not all, emission will fall within the camera's angle of acceptance, since the spatial distribution of emission external to the cathode tends to be either on-axis or radially surrounding the electrodes. In cases where significant emission occurs along the axis from the electrodes (such as that illustrated), the results will be subject to an increased degree of error.

In order to quantify the signal within the photographs, a short program was created using Processing, which is an application oriented towards the creation and manipulation of visual and interactive media. The facility for accessing and altering the pixel values of an image makes it an ideal tool for the analysis of emission distributions in photographs. Details of this are also included in Appendix 2.

4.2.2.2 Results of analysis

The results of the analysis indicate the proportion of signal originating from regions external to the cathode in these photographs to range from 54 % to 67 % (Figs. 50, 51). The higher values in this range are those corresponding to the photographs of discharges at lower pressure, with that corresponding to the lowest pressure (142 mTorr) differing most significantly from the others. Consideration of the distributions of emission as viewed from the side (Fig. 48) indicates that the results at this pressure may be affected by the degree of emission occurring in the axial region beyond the open end of the cathode.

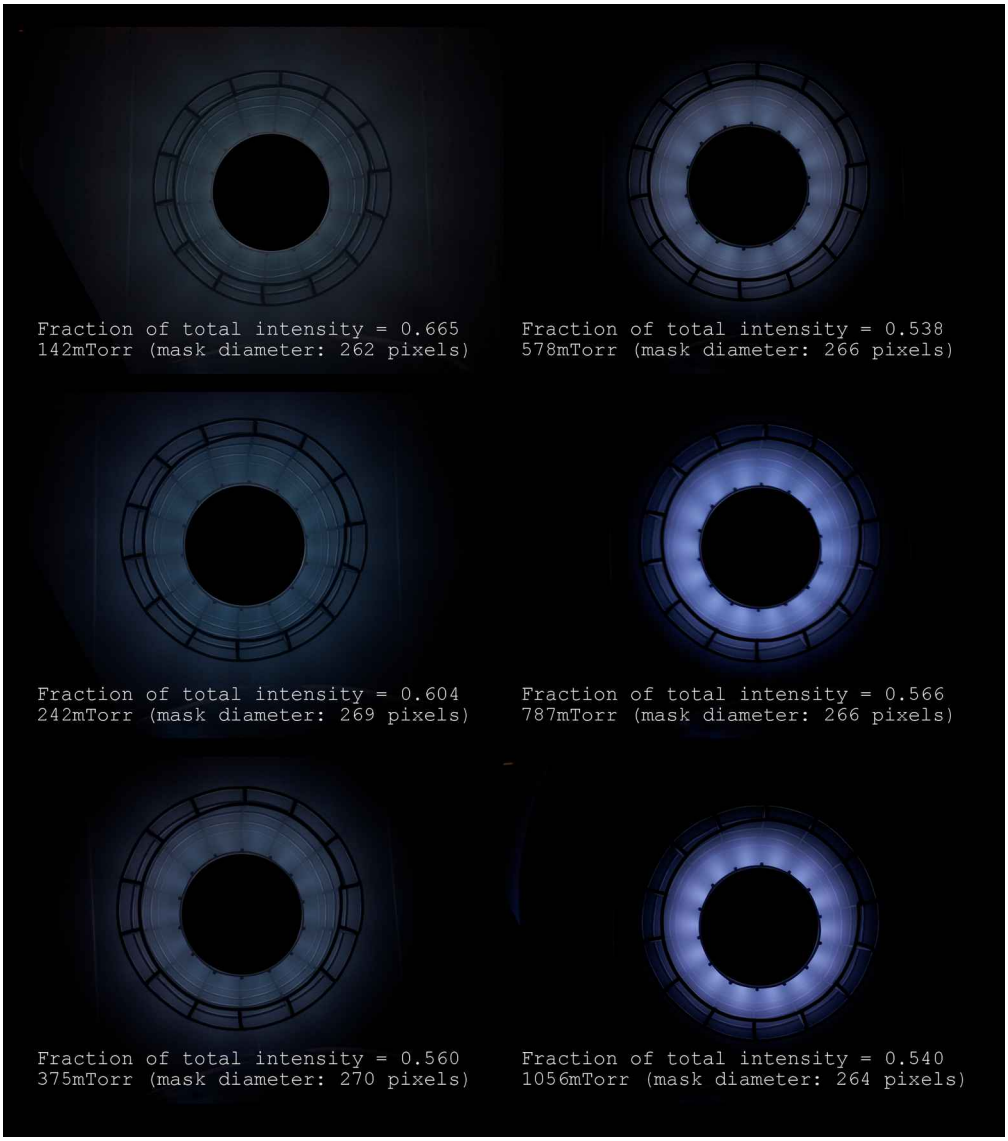

Fig. 50. Photographs of discharge at different pressures, with mask applied to cathode interior, showing fraction of signal originating from outside the cathode

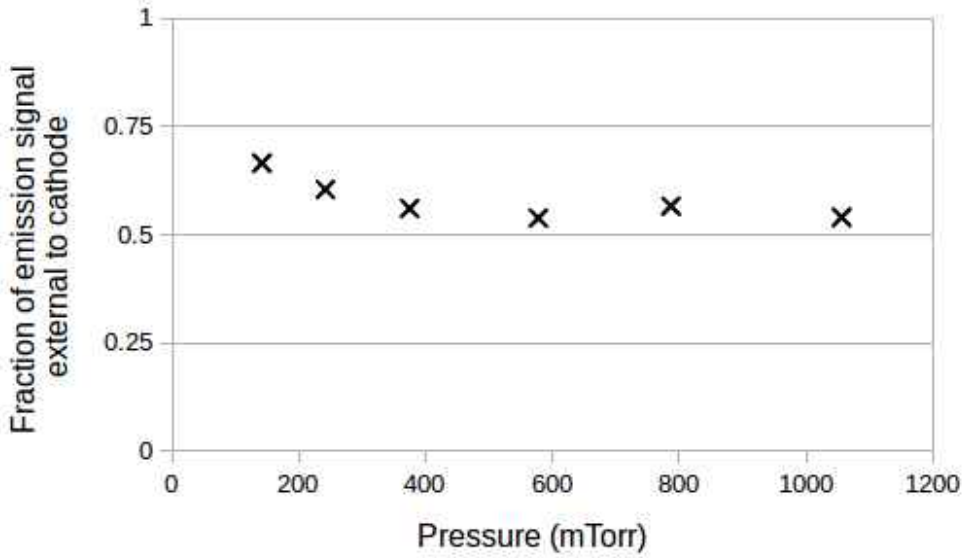

Fig. 51. Results of analysis of emission distributions within photographs, as shown in Fig. 50

It is noted that the incomplete coverage of the chamber interior, and also the effects of foreshortening, will both act to cause a degree of under-estimation of the extent of emission external to the cathode. The effect of foreshortening is also observed to disproportionately affect the results for distributions in which emission is relatively more significant in the region immediately surrounding the cathode. These cases are those found at higher pressures, and so the effect of this source of error is expected to be relatively greater for these conditions.

Whilst these results are not considered to be quantitatively precise, they are an instructive illustration of non-intuitive outcomes resulting from integration of different emission densities over different areas. The relative brightness of emission in the inter-electrode space evident at conditions of at higher pressure appears to the eye to represent a much greater proportion of total signal than the more diffuse emission that extends to larger radius at conditions of lower pressure; this analysis shows that, at least for the distributions of signal in the photographs, this is not so.

This property is found to be quite insensitive to conditions of pressure; the progressive brightening with increasing pressure that is so noticeable in the inter-electrode space appears to be largely offset by the accompanying reduction in intensity at larger radius. Across the operating pressure range up to a pressure of one Torr, the fraction of emission originating from within the cathode is indicated to remain roughly consistent, despite the perceived trend to the contrary.

4.2.2.3 Assessment

Regarding the extrapolation of these results to the assessment of overall distributions of excitation and ionisation activity; again with reference to Appendix 2, it is noted that this is in principle valid, but that the results may be subject to any significant variation in spectral content between the masked and unmasked areas, and also to any such variation that may evolve with pressure.

The fact that the images represent an evolution in conditions of pressure means that any such factors will be expected to also evolve across the range. The possible difference in this respect between masked and unmasked areas might cause a general offset to the results, and the trends indicated across the range may be additionally influenced. The results are therefore considered to be broadly representative in this regard, but that this is subject to the above qualifications.

Despite the uncertainties involved, the analysis is considered to be sufficiently representative to characterise the distributions of emission in terms of a significant fraction of total levels originating in locations outside of the cathode, and that the magnitude of this may be more than half. By analogy between processes of excitation and ionisation, this taken to indicate that a substantial fraction of current generation occurs in regions external to the cathode, and also that the relative location at which this occurs becomes increasingly localised to within the anode radius at conditions of increasing pressure.

In summary, this consideration of the pressure-dependence of emission distributions shows emission within the cathode to evolve first from separate regions associated with discharge elements passing through the apertures into an annular region, and then into a central glow. Processes occurring within these regions are discussed later in the chapter. A less obvious feature of these distributions is that a consistently large part of the emission originates from regions external to the cathode. Understanding the distribution of processes occurring in the CC mode discharge requires consideration of this property also.

4.3 Operation with a fully-enclosed grid cathode

4.3.1. Rationale

In this part of the chapter, attention is turned to the processes operating within the cathode, and in particular, the influence that the geometrical form of the cathode has upon the discharge. It has been hypothesised that the CC mode discharge is sustained to some extent by an effect of electron confinement in the fields surrounding the plasma, and these fields are maintained to some degree by the cathode grid wires. Should this effect be occurring to any significant degree, then observable discharge properties might be expected to show a dependence upon the degree of enclosure of the cathode internal space. A principally defining feature of the cathode in this respect is the open end, and it is noted that the effect of enclosing this will be to significantly increase the overall degree of enclosure, without otherwise altering the

existing geometry. The effect of this was tested by the construction of an alternative cathode. This was similar to the primary one, except in having the open end enclosed by wire struts, so that the resulting fill factor was comparable to that of the rest of the cathode.

The effect this alteration was observed to have upon the CC mode, the beam mode, and the nature of the transition between them is described in the following. This description concentrates upon the helium discharge, since the mode structure is well-defined both in electrical characteristics and colour of emission. The argon discharge is also referred to, more briefly.

4.3.2 Experimental set-up

In order to investigate the effect of the terminal aperture of the cathode, a second version was constructed, identical to the first except in having both ends similarly enclosed (Fig. 52). This cathode will be referred to in the following as the 'enclosed' cathode. The original cathode will be referred to as the 'open' cathode, for clarity. This electrode was fitted to the experimental apparatus described previously. No other changes were made.

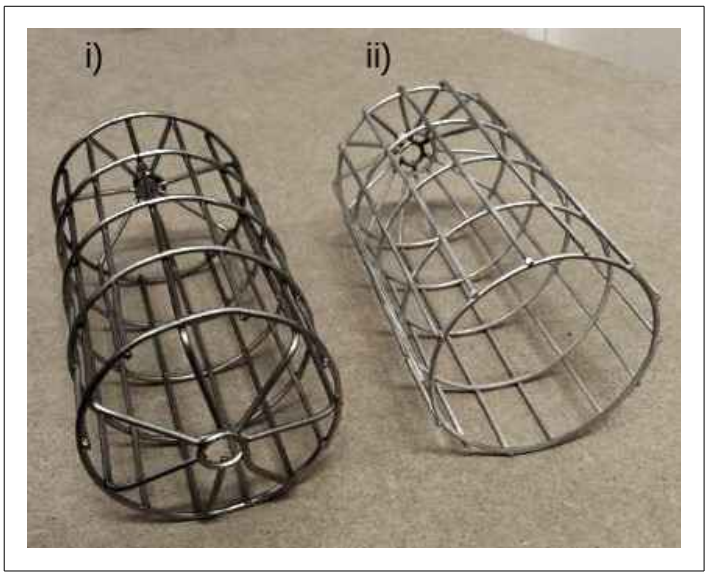

Fig. 52. The form of the i) enclosed, and ii) open grid cathodes

The change in calculated vacuum potential distribution caused by this alteration is mostly apparent as an increased degree of symmetry in the distribution within and around the end of the cathode (Fig. 53).

Whilst the vacuum distributions show a relatively small degree of change, they may become considerably altered by the presence of space charge. It is noted that the presence of the additional grid wires at the end of the enclosed electrode will cause the local potential in the axial area of this region to be subject to significantly greater influence from the cathode, regardless of any accumulation of space charge.

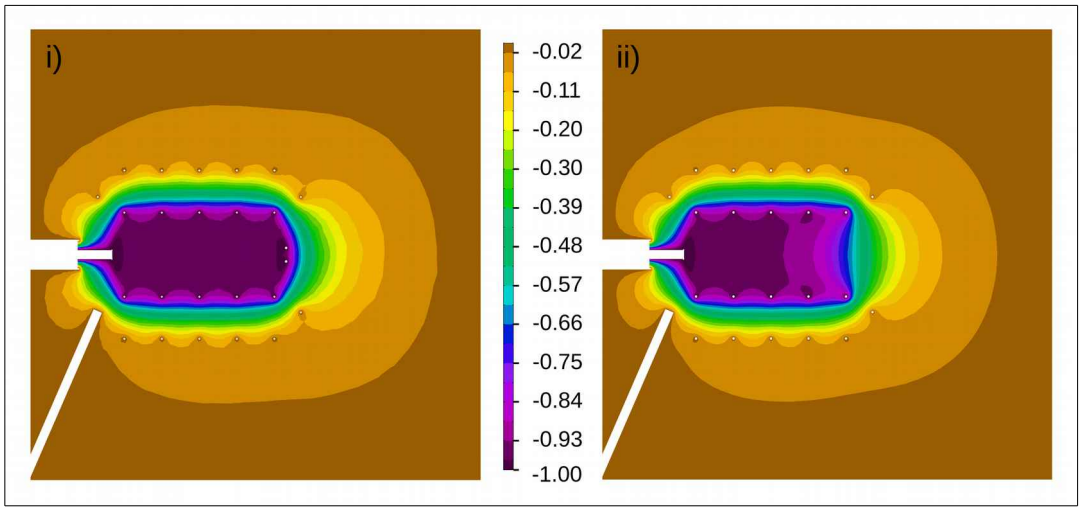

Fig. 53. The vacuum potential profile of the set-up with i) enclosed, and ii) open grid cathodes. Units correspond to fraction of cathode potential

4.3.3. Experimental findings

The apparatus fitted with the enclosed cathode was operated at a range of pressures, corresponding to those previously associated with both the CC and beam modes. The discharge characteristics in this arrangement are initially described in terms of the mode structure observed in helium, as compared with that described for the set-up with the unaltered cathode in the previous chapter. This is illustrated with photographs and current-voltage curves.

Following this, a brief description is made of the corresponding behaviour observed in argon, and then attention is given to some additional features of the discharge observed to accompany operation in the enclosed cathode.

4.3.3.1 Visual appearance of modes

The CC mode was found to also appear during operation of the discharge with the enclosed cathode. Its appearance in this case is visually similar to that observed in the open cathode, but with the additional feature of one or more plume-shaped formations. These are connected to the CC mode glow, and emerge from terminal apertures of the cathode (Fig. 54). This form is observed to appear similarly at a wide range of conditions, of both cathode current and pressure.

During operation with the enclosed cathode, at current levels smaller than the threshold for the CC mode to instigate, the beam mode discharge appears quite similar to that described previously for operation with the open cathode. In beam mode operation with the enclosed cathode, the principal difference evident also concerns an additional feature, which in this case is a bright beam, that is observed to propagate outwards from one of the terminal apertures of the cathode. This beam replaces the axial electron beam, that was noted to be evident in normal beam mode

operation in Section 3.2.1, and is observed to appear significantly brighter than this. It emerges normal to the plane of the aperture, and continues in a straight line to impact the wall. In some instances this primary beam may be accompanied by one or two additional formations, of similar appearance but generally less bright, and associated with other terminal apertures of the cathode. In helium the beam is noted to be bright green in colour. Significant local heating occurs at the site of impact, causing the 10 mm-thick stainless steel chamber wall to become very hot in minutes.

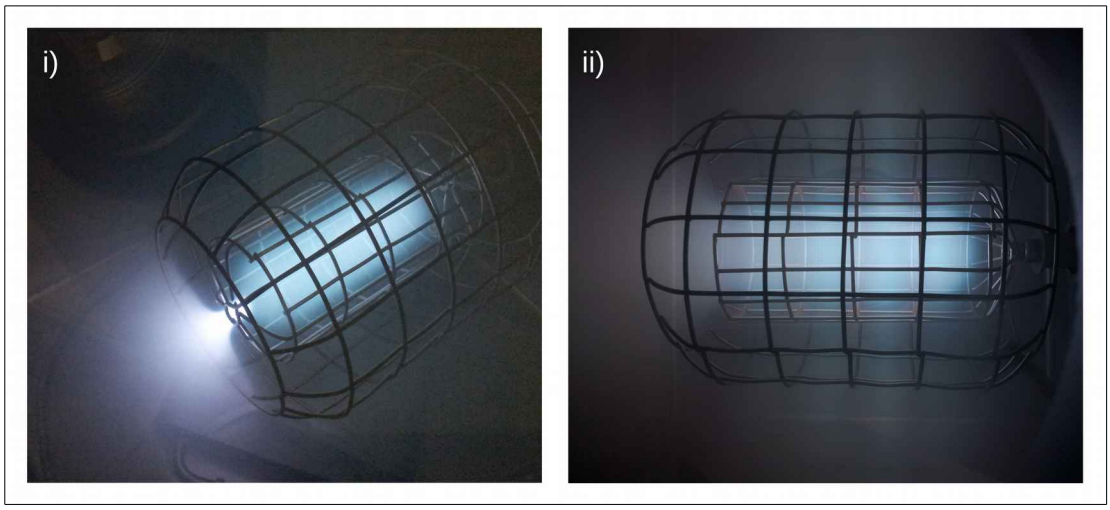

Fig. 54. CC mode discharge in helium, in i) enclosed and ii) open cathodes showing effect of enclosure of cathode end. i) is at 145 mTorr, 8 mA; ii) at 147 mTorr, 35 mA

Upon the appearance of the CC mode this beam disappears, to be replaced by one or more plume-shaped formations as described above. Fig. 55 shows photographs of the appearance of the helium discharge, i) in the CC mode and ii) just prior to transition to the CC mode, at a pressure of around 50 mTorr.

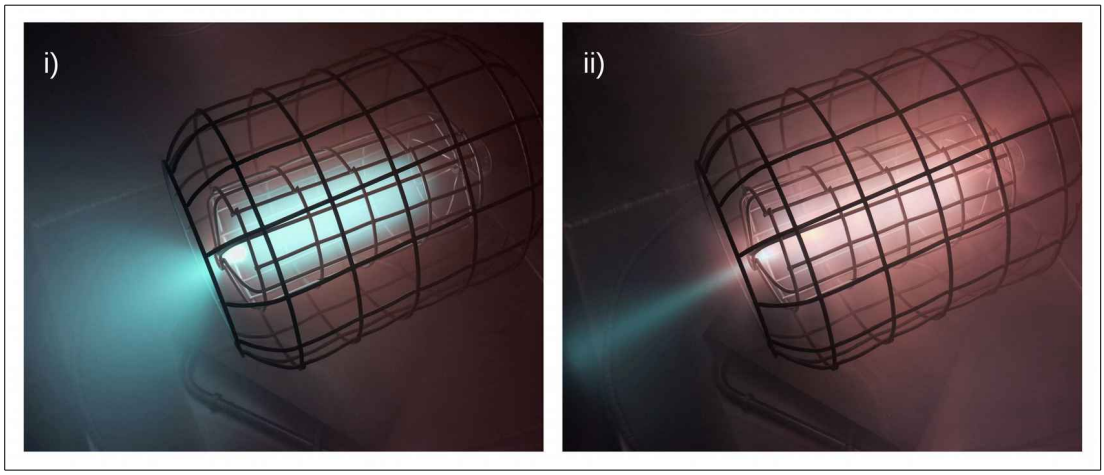

Fig. 55. Helium discharge at 50 mTorr with enclosed cathode; i) in CC mode, showing plume; ii) before CC mode instigation, showing beam.

4.3.3.2 Current-voltage relations and pressure-dependence

Current-voltage relations are shown in Fig. 56 for operation of the discharge with i) the open cathode, and ii) the enclosed cathode, at different pressures in helium. These were recorded using a similar procedure as for the results presented in Section 1.1.

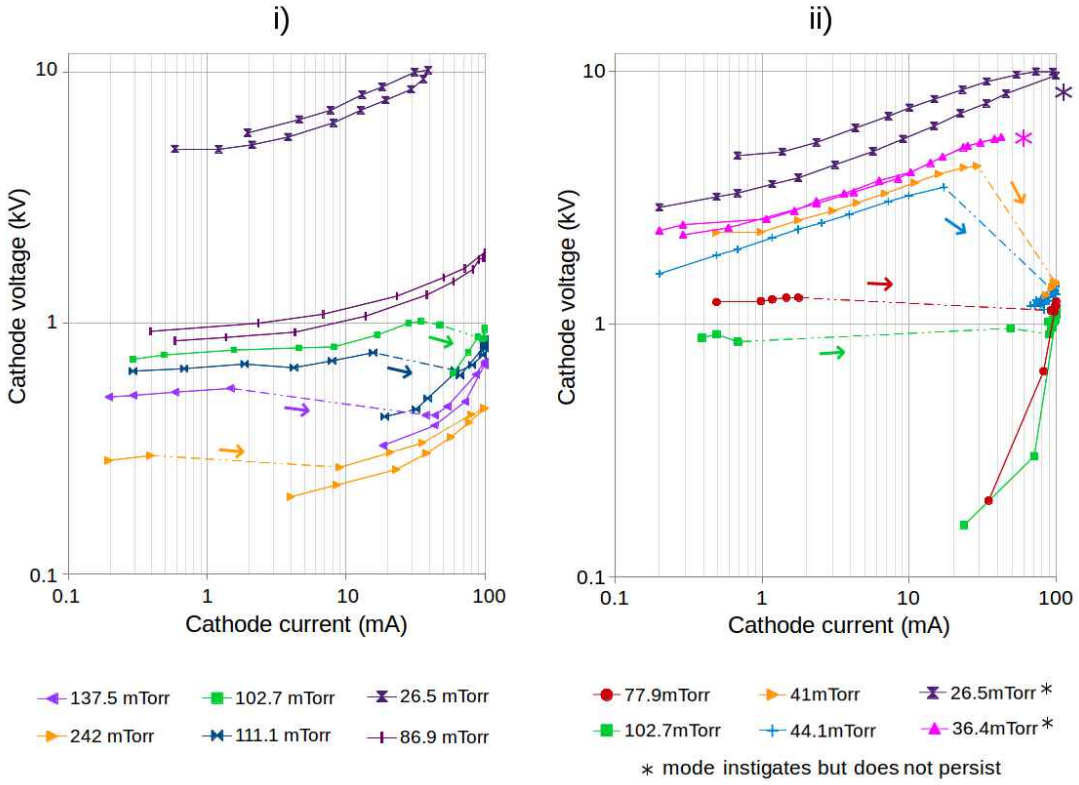

Fig. 56. Current-voltage curves in helium at various pressures, measured during operation with i) open cathode and ii) closed cathode.

In operation with the open cathode, an apparent current threshold affects the mode's formation at pressures below around 250 mTorr. Curves are shown for pressures encompassing the range at which this threshold is evident, and one curve is also shown for the pressure corresponding to that at which operation became limited by the voltage available (10 kV), which was 26.5 mTorr. The current threshold is noted to increase at conditions of progressively lower pressure, until a limiting pressure is reached at around 100 mTorr, below which the mode does not appear. When the current threshold is reached and the CC mode appears, a jump in cathode current occurs which is evident as a discontinuity in the current-voltage curve. These are indicated in Fig. 56 i) with arrows. For the curve obtained at 26.5 mTorr, the voltage reaches the power supply limit of 10 kV at a current of around 40 mA.

In operation with the enclosed cathode, a current threshold for the CC mode is also observed to occur at certain pressures, and in Fig.56 ii) curves are again shown for pressures that encompass the range at which this is observed. This range is noted to occur at significantly lower pressures than was found for the open cathode, which are

between 100 mTorr and 40 mTorr. The discontinuities associated with the appearance of the CC mode in this case are also indicated by arrows.

Not only is the operating pressure range for the CC mode found to be different for each cathode, but the discharge is also found to behave differently in the low-pressure limit. With the open cathode set-up, the low-pressure limit for the mode occurs as the threshold current exceeds the supply limit of 100 mA, and the mode simply does not appear at pressures below this. In operation with the enclosed cathode, it is observed that whilst the mode will persist at pressures as low as 40 mTorr, it will also instigate at pressures significantly lower than this. This was observed to occur at pressures as low as 26.5 mTorr, which was the lowest pressure tested; the low-pressure limit was not ascertained. In this extra-low-pressure range, the mode extinguishes almost immediately and then re-instigates, causing a flickering effect.

4.3.3.3 Mode transition behaviour

In the helium discharge, an interesting effect is associated with the mode change occurring at pressures of below around 50 mTorr. At these conditions, there is found to be a critical level of cathode current, somewhat below the threshold for the CC mode to spontaneously appear, above which a distinctive, relatively slow temporal evolution in discharge parameters is observed to occur. This evolution, which is repeatable, occurs over a period of several seconds and results in the appearance of the CC mode.

During this period, the level of cathode current is observed to gradually rise whilst voltage remains constant. The colour of emission within the cathode interior is also observed to change, becoming progressively more green, until the CC mode instigates. This additional rise in current may also be observed in the different behaviour evident in the current-voltage curves obtained at 26.5 mTorr (Fig. 56). In operation using either cathode, the voltage-dependence of smaller currents is similar. For the open cathode, levels of current reach 40 mA by the 10 kV supply limit. For the enclosed cathode, the current-build becomes relatively greater at currents above 10 mA, so that in this case the supply maximum of 100 mA is reached before the voltage limit.

4.3.3.4 Enclosed cathode discharge in argon

The previous description focussed largely upon the discharge in helium. The discharge was also operated in argon, and showed similar behaviour in the following respects: the CC mode was found to be evident at a range of pressures, the lower limit of which was considerably smaller than that observed in operation with the open cathode, and a similar association of a plume formation with the CC mode, and beam formation at other conditions was also found to be evident.

With the enclosed cathode, the CC mode was found to form at pressures as low as 5 mTorr in argon, and to do so at comparatively low threshold currents, making it hard to operate the discharge in the beam mode at any appreciable power.

The discharge was also briefly run in argon with a set-up further altered by removal of the anode grid. This investigation was not carried out in any particular detail, but the behaviour within the cathode appeared to show little difference; the two modes were found to be evident in the same way in operation at a pressure of 7mTorr, and the plume and beam formations were observed to be associated with the modes in the same way as that found with the anode grid in place. The only visual difference observed in this case was that the plume formation would occasionally appear located so as to pass through one of the lateral cathode apertures.

4.3.3.5 Additional discharge features

In the above description, additional features of the discharge were noted to distinctly accompany operation in the beam and CC modes when using the enclosed cathode. These resemble a beam and a plume respectively, and in either case are observed to pass through one of the terminal apertures of the cathode. In passing through an electrode aperture, both the plume and beam formations connect the region of bright emission within the cathode with the space outside it. The parts of these formations passing through the aperture are observed to be consistently somewhat narrower in argon than that in helium, and this appears to be independent of current. Single instances of either formation tend to appear, although in both cases a multiplicity has been observed, with each instance located within a separate aperture.

Both the beam and plume formations shown in Fig. 55 i) and ii) emerge from a cathode aperture located directly away from the point of view of the camera, and so details of these features are hard to see. Stills from a video recording of the same behaviour are shown in Fig. 57, since in this case the formations occur in a location in which they are more easily observed. The discharge represented in these images was obtained in argon, when the anode grid had been removed for separate reasons. As noted above, this did not affect the visual appearance of the discharge, and the features illustrated in Fig. 57 are generally representative of those occurring in either helium or argon, and with or without the anode grid.

It is observed that principal differences between these formations concern their shape and associated dimensions. In both cases, a small region of relatively intense emission is observed to be proximate to the cathode interior glow. In the case of the beam formation this is considerably smaller than for the plume, and in argon is notably more yellow in colour than the purple-blue beam with which it is connected. The entire structure of the beam feature is noted to remain co-linear with the beam, and to be oriented normal to the plane of the aperture. For the plume formation, the bright region proximate to the CC mode glow is more blob-like in appearance, and the entire feature may curve as it passes through the aperture. The variation in this respect is evident in the still images in Fig. 57.

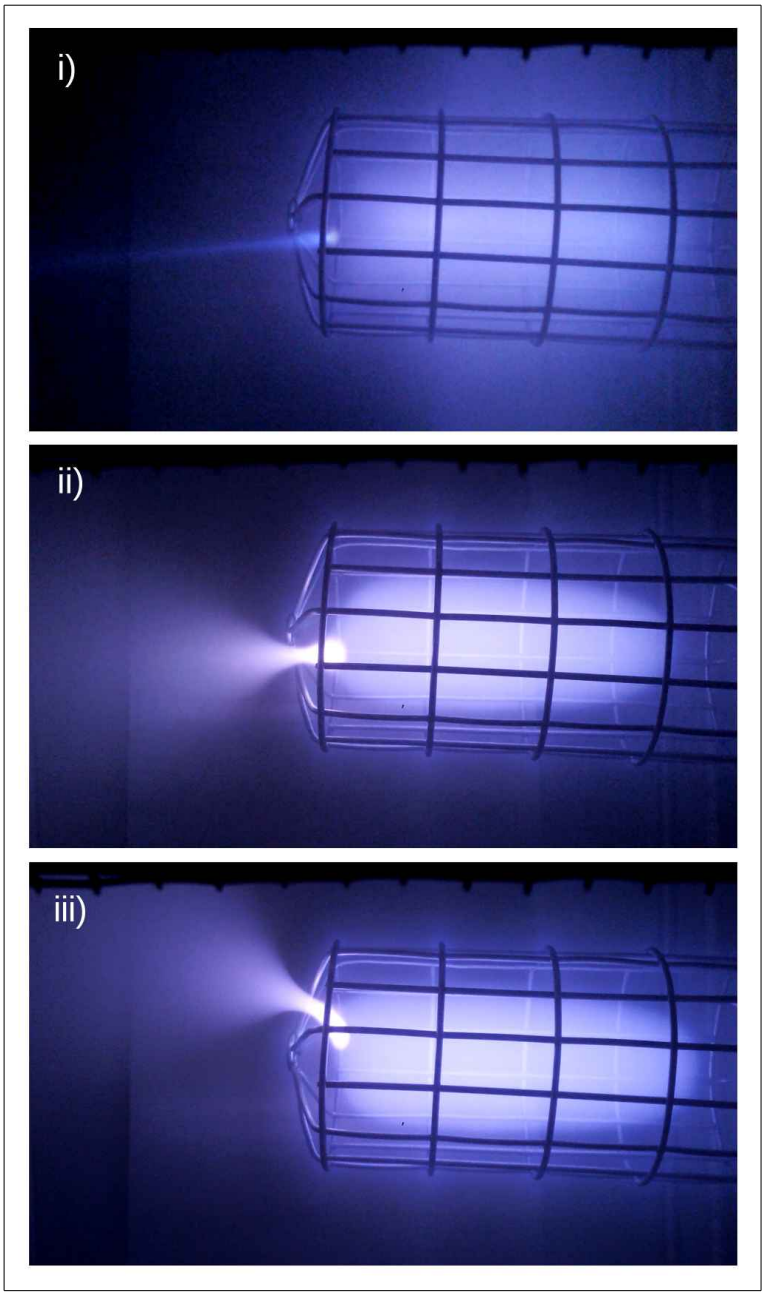

Fig. 57. Still images taken from a video recording showing the i) beam and ii) plume formations associated with operation using the enclosed cathode, as are evident to either side of the mode transition. The emission levels in ii) and iii) are considerably brighter than those of i); the photographs do not reflect this. Discharges in argon at around 7 mTorr.

4.4 Discussion

In the previous two parts of this chapter, various experimental observations of the CC mode discharge have been described. The first of these was concerned with measurements of the distributions of current and optical emission evident at conditions of different pressure. In the second part, the effects upon observable discharge properties found to result from the experimental modification of the cathode were characterised, in order to explore the physical dependences involved.

A primary objective for this work is to investigate the extent to which the CC mode discharge may be sustained by the confinement of electrons within the cathode. Confinement of electrons is known to be important in hollow cathode discharges, and so it is useful to gain some understanding of this property. The following discussion therefore starts with a summary of characteristic properties of these, and how the principles of their operation might apply in the case of grid electrodes.

The distributions of current and optical emission observed for the CC mode discharge are then considered within this framework, along with the findings concerning the dependence of discharge properties upon electrode geometry.

4.4.1 Hollow cathode effect and grid electrodes

Hollow cathodes

The action of electrons confined within the cathode field is known to sustain the hollow cathode family of discharges, and in this section the basic operating principles of this type of discharge are summarised. This material refers to some of the principal characteristics described by Oks in [76], and also to some research background material from [77].

Hollow cathode discharges have been the subject of much study. A simple description of the important processes and the physical dependences of these is taken from the first chapter of a book about plasma cathode electron sources [76], in which the use of hollow cathode discharges as such sources is discussed.

These discharges are noted to be appropriate for this application because of a high degree of ionisation, and that this results from the dynamics of fast electrons emitted from the cathode that then become electrostatically confined within the plasma. This occurs because the plasma is largely bounded by regions of cathode fall (Fig. 58). Secondary electrons emitted from the cathode become energetic as they cross this region into the plasma, and so may cause ionisation and excitation in collisions with the background gas particles, as occurs in a conventional planar discharge. Critically for the hollow cathode discharge, energetic electrons that reach the boundary of the plasma are reflected by the cathode fall, and so continue to play a role in the discharge, rather than being lost from the volume. This is known as the 'hollow cathode effect'.

The establishment of a discharge sustained by this confinement effect is noted to be accompanied by an abrupt decrease in discharge operating voltage and increase in discharge current. Significantly, it is observed that this may only occur when the electron mean free path exceeds the characteristic dimension of the cathode cavity.

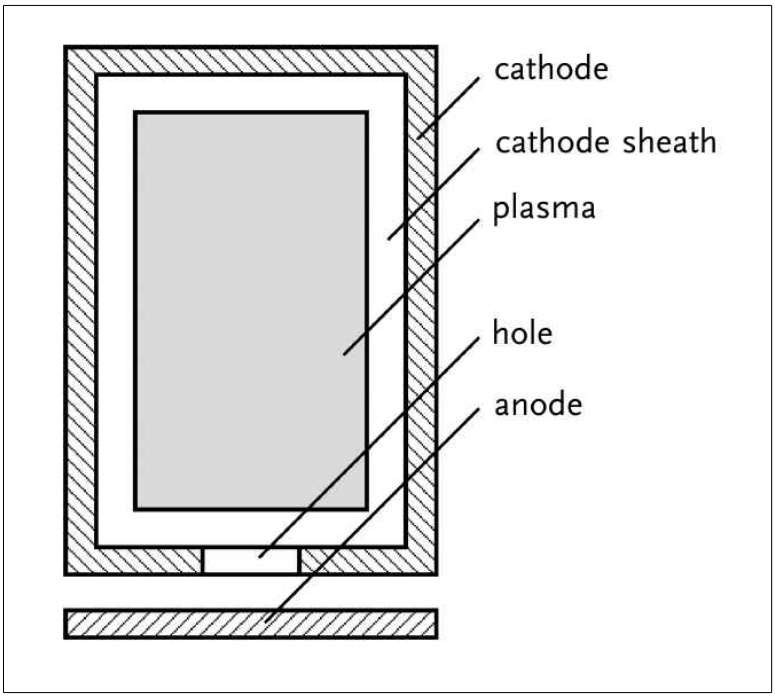

Fig. 58. Diagram of characteristic arrangement of electrodes for the formation of hollow cathode discharges. Reproduced from [76]

Electrons produced in ionisations occurring within the plasma volume are effectively confined within this region by the potential fall across the cathode sheath. Since ions are extracted across this, the electron population will accumulate if there is no corresponding region of electron extraction, and alter the potential so that the discharge is not viable. In the configuration of Fig. 58, electron extraction to the anode is accomplished via a gap in the cathode and the sheath.

The dependences of discharge parameters upon the form of electrodes illustrated are characterised in terms of the ratio between the area of the extraction hole and the area of the inner surface of the cathode. In general, the reduction of this ratio is described to enhance the confinement of fast electrons, since these may only escape through the hole. This is observed to reduce the limiting pressure at which the discharge will operate, and to require a smaller operating voltage.

However, it is also observed that should this ratio become smaller than $\sqrt{m_e/m_i}$ (m_e and m_i referring to electron and ion masses respectively), then a positive extraction potential is required, and that this produces a double layer at the extraction region. A double layer is a type of potential structure that is associated with a step change in plasma conditions, involving a similar change in potential. These structures are discussed in more detail in Chapter 6. The structure has a surface area larger than that of the hole, and acts to accelerate the slow electrons until they may

pass through the reduced aperture in sufficient numbers to balance the ion current to the cathode. This counters the reduction in limiting pressure and voltage, and a minimum in values of these has been shown to be associated with this ratio of hole-to-cathode surface area.

Grid electrodes

The grid cathode has clearly significant differences in form to that illustrated in Fig. 58, in that it is largely perforated. The effects of this have been shown to result in a degree of distortion in the vacuum potential distribution, and the regions of space within the apertures are noted to be subject to variation in potential caused by the presence of space charge. These perforations also result in a considerable reduction in the physical surface area of the cathode.

Despite such perforation, grid electrodes may still successfully confine electrons and so enable the sustaining of discharges assisted by the hollow cathode effect, although this is noted to be more accurately referred to as the electrostatic trapping effect [77]. The principle of electrostatic confinement of a plasma by a negatively-biased grid is illustrated in the diagram in Fig. 59, adapted from [78], which is explained as follows.

Electrostatic confinement by a biased grid occurs when the dimension of the sheath between plasma and grid becomes greater than half of the grid-wire spacing interval, by the application of a sufficiently negative bias. Once this condition is met, the lower-energy plasma electrons may not escape through the apertures, and the plasma is confined [78], pp. 317-319. Charge transport from the confined plasma occurs as the Maxwellian distribution of electron energies, and the relatively-high electron flux upon the boundary (by virtue of their relatively-smaller mass) causes one higher-energy electron to escape for every extracted ion (the plasma potential self-adjusting to maintain this).

The plasma boundaries illustrated in Figs. 59 b) and c) show a clear resemblance to the confinement of the central glow by the cathode, as depicted in photographs of Fig. 48 that correspond to conditions of moderate and lower pressures respectively.

Summary

In summary, the 'electrostatically-trapped electron' (ETE) effect is understood to be a broader term describing similar processes to the 'hollow cathode effect', that may be applied to the confinement of electrons within a grid cathode. The hollow cathode electron confinement effect is generally noted to be accompanied by an abrupt decrease in discharge operating voltage and increase in discharge current, and this is described to occur only when the electron mean free path exceeds the characteristic dimension of the cathode cavity.

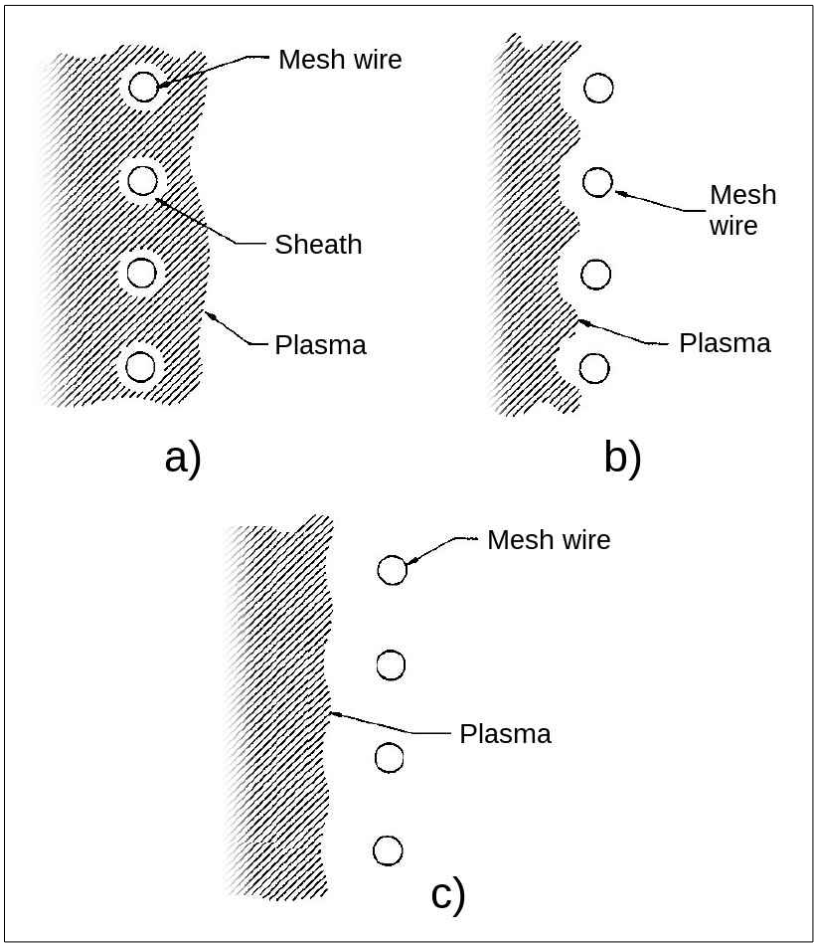

Fig. 59. Diagram showing progressive stages of plasma confinement by an increasingly negative bias applied to a grid. a) low bias voltage causing separate ion extraction sheaths to form at each wire and plasma to pass through grid; b) moderate bias voltage causing coalescence of sheaths and electron confinement; c) high bias voltage causing plasma surface to become planar. Adapted from [78] p.318

The dependence upon the physical form of the apparatus shown by the properties of such discharges is described to be determined in particular by the ratio between the inner surface area of the cathode and the effective area of the part of the boundary through which bulk electrons are extracted. When the effect occurs for discharges obtained using grid electrodes, it is noted that these may generally act to confine plasma when the thickness of the sheath surrounding the wires becomes equal to half of the spacing between them.

These insights are now applied to the consideration of the results of experimental observations made of the CC mode plasma, before then considering the effects of cathode modification.

4.4.2 Potential structure and charge flow in the CC mode

In this section, the characteristic distributions of current and emission described in Part I are considered. Any relevance for the degree of ETE effect occurring is noted, before the making of a more general assessment of this.

4.4.2.1 Current distributions

Anode current shows a varying relation with cathode current at different conditions of pressure and current, and the degree of this variation is found to be associated with the operating mode. Radially-collected current shows a largely linear relation with cathode current that is little changed between mode, with a modest increase in proportion evident in the CC mode curves for pressures smaller than 200 mTorr, as compared to curves obtained at either beam mode or higher-pressure conditions. These characteristics are interpreted in the following. The general relation between axial and radial current is initially considered, before examining the anode current characteristic.

Axial current vs. radial current

The levels of axially-collected current associated with the CC mode discharge are consistently smaller than 0.1 mA, reaching this magnitude only at conditions of cathode current of the order 100 mA and pressures towards the lower limit. From the area of the collector, these levels would represent the intercepted fraction of an isotropic current density incident upon the entire surface of the end wall of the chamber of total magnitude smaller than 10 mA. The current density incident upon the collector is considered extremely unlikely to be maintained over such an area, and so axial current from CC mode discharges is characterised as constituting significantly less than 10 % of total electron current. Total levels of anode current are also considerably smaller than 10 %, with the possible exception of the helium discharges at higher pressures, in which the ADC maximum of 7 mA was exceeded. These properties enable the observation that, regardless of the variation seen in anode current, most electron current will be incident at the walls that surround the electrodes in a radial projection.

The linearity with cathode current shown by the radially-collected currents when the discharge is operating in the CC mode indicates that the radial collector current represents an intercepted fraction of this wall current. The proportionality with cathode current evident in the measurements made in helium, according to the area of the collector and estimated area of the flux, are consistent with around 65 % to 70 % of total electron current, rather than the 80 % to 90 % suggested by the levels of axial and anode current.

There is considerable uncertainty however, concerning the longitudinal extent and degree of isotropy in the radial electron flux surrounding the electrodes. Measurements were only made with the radial collector in one location, and so any variation in the radial electron flux distribution was not discerned. These

uncertainties mean that the discrepancy mentioned above could easily be due to inaccuracy in the estimation of the electron flux distribution.

It is noted that the proportion of cathode current represented by radially-collected levels in the argon CC mode discharge is smaller than that in helium, by around 40 %. Levels of axially-collected current are somewhat greater in argon but remain small overall, and so this difference does not appear to represent a large-scale shift from radially- to axially-directed current. According to the above interpretation, the difference could represent either a different distribution of electron flux, or a degree of ion current to the collector that is relatively more significant for the argon discharge.

Anode current

Anode current is found to behave very differently from the radially-collected current. Since the anode surrounds the cathode radially, and the majority of emission (and by association, charge generation) originates from within its radius, the current it collects may be expected to represent an intercepted fraction of the overall radial electron current. The variation in the fraction of cathode current represented by anode current at different conditions is therefore interpreted as being an indication that the radial electron current experiences a varying degree of focussing through the anode apertures or attraction to the anode grid. This effect shows a dependence upon operating conditions, with anode current found to represent an increasingly small fraction of cathode current at conditions of progressively low pressure and progressively greater levels of cathode current and voltage, when the discharge is operating in the CC mode.

4.4.2.2 Potential structure

The principal finding from the measuring of current distributions is that the majority of electron current from the CC mode discharge flows radially to the walls surrounding the electrodes, and this has implications for the understanding of the potential structure of the discharge. The measurements indicate a significant electron current to be radially-extracted from the CC mode plasma, as well as the ion current. In the CC mode plasma, the majority of the electrons within the plasma are products of ionisation, and so will have relatively little kinetic energy at the plasma potential. The electron energy distribution will therefore consist of both a low-energy thermal population and the higher-energy secondary electrons.

For the ETE effect to be operating, a degree of radial confinement of the more energetic secondary electrons must occur, and so thermal electrons might be expected to be radially confined, and escape the cathode via the open end instead. The measurements of axial and radial electron currents however show this not to be so. The radial extraction of electron and ion currents must therefore occur as described by Humphries [78] (and illustrated in Fig. 59), indicating the periodic variation in background potential caused by the discrete cathode grid wires to be important for the simultaneous radial extraction of both ions and electrons. This implies that the plasma potential may not exceed the potential within the cathode

apertures by more than a value within the energy range of the electron population's temperature.

Further insight into this behaviour is found in the description of the dynamics of electron outflow from the cathode discussed in the work of Ohnishi and co-workers [43]. They consider a spherical grid cathode, that is subject to an influx of positive space charge from a collisionless radial ion current, causing a virtual anode to appear within its interior. It is reasoned that should an element of ionisation occur within the cathode, the electrons so created will be confined within this region of positive potential, and accumulate until the potential is lowered sufficiently for a route to exist for them to flow out of an aperture to the wall, and so enable steady-state operation. This theory is tested by a particle-in-cell modelling code, and the results show electron outflow to occur through a small area within the centre of the aperture, in the form of a relatively narrow beam. Although this finding is for different conditions of voltage, pressure, gas species and geometry, there are clear similarities in the more general conditions of electrons born within a grid electrode that are observed to flow outwards through the apertures.

Experimental evidence for this is found in [20], in which probe measurements show evidence of electrons accelerated from within the cathode, and the microchannelling phenomenon is observed to persist to conditions of higher pressure at which the beams of the star mode are no longer apparent.

For this to account for the observed pressure-dependence of levels of anode current, it suggests that the increased incidence of collisions at higher pressures causes the electron beam to become scattered before it reaches the anode. This is in accordance with the relative increase in optical emission seen in the region between cathode and anode at higher pressures.

Whilst the varying dependence of anode current upon conditions of cathode voltage and current might represent an evolution in the nature of electron extraction, but the more extreme behaviour seen in argon, in which anode current drops to zero, suggests a different effect may also be operating. For the cessation of all electron current to the electrode, the potential within the aperture is indicated to rise above ground, so that electrons are locally repelled from the anode. Repeating the measurements with anode voltage recorded in a bipolar ADC channel may show an ion current to the anode at these conditions.

4.4.2.3 Beam mode comparison

To briefly consider how the distributions of current change in the beam mode: in helium, the proportion of cathode current represented by the radial collector current during operation in the beam mode is smaller than that in the CC mode. In argon, there is little difference between the modes in this respect, and the fraction of cathode current in either mode is relatively smaller than in helium.

It seems significant that in both species, the currents collected by the anode and radial collector bear a similar proportionality to cathode current, were they to represent intercepted fractions of an isotropic flux according to their respective areas. This apparent agreement is treated with a degree of caution, since measurements were only made with the radial collector in one location, and because of uncertainties concerning the longitudinal extent and degree of isotropy in the radial electron flux surrounding the electrodes. The agreement however between the magnitudes of anode and radial collector current and their respective areas, when the linearity of both of these with cathode current is also considered, constitutes strong evidence that these currents do represent interceptions of the same flux.

The proportionality shown by these currents suggests a flux of the order of half of the total discharge electron current in helium, and around 40 % in argon. Given the considerations above regarding electron transport through the cathode apertures, and the decrease in anode current that is associated with this at conditions of progressively lower pressure, the anode current at beam mode pressures is not expected to contain many electrons born within the cathode, and so this current is expected to be made up of the secondary electron flux from the cathode and electrons created in the inter-electrode volume.

4.4.2.4 Summary

It can be said for certain that the small axial current, and the magnitude and linearity of radially-collected current with that of the cathode, indicate the majority of electron current to flow radially for CC mode discharges. This has implications for the extraction of electrons from the plasma boundary; since these must be able to escape via the apertures, the plasma potential may not be more positive than that within the apertures by more than a value within the electron temperature range.

This in turn has significance for the degree of ETE effect that may be operating within the cathode-confined plasma, since secondary electrons incident at an aperture will be able to escape regardless of the energy they have lost. In the following section, the degree to which this effect may be occurring in the CC mode discharge is considered further.

4.4.3 Secondary electron current

For the CC mode discharge to be conceivably sustained by the ETE effect, a sufficient fraction of the secondary electrons that result from the ion flux upon the cathode must be confined with sufficient energy to cause enough ionisation to maintain the ion flux. In order to consider these dynamics, the nature of the secondary electron current is initially considered, both in terms of its likely magnitude, and the direction of its flow. Following this, the collisional dynamics for these electrons are also considered, and the likelihood for their confinement assessed.

4.4.3.1 Magnitude of secondary electron current

From (4.1) it is clear that the magnitude of secondary electron current will be the fraction of the ion current determined by γ_{SE}, the secondary electron coefficient. Values of γ_{SE} are found to vary considerably with surface condition [79], [80], and to a lesser extent, with target material [79]. Yields from ultra-clean surfaces are reported to be relatively small, and to be considerably enhanced by the presence of a surface monolayer of adsorbed gas. The electrode surfaces in this case are cleaned by ion bombardment, but impurities will be present. Values of γ_{SE} reported in [81] are for helium incident on gold [Fig. 60 i)], of a comparable cleanliness to the experimental surface. [79] indicates that the values for stainless steel may be around 20 % smaller than those for gold. It is apparent that the value of γ_{SE} may change significantly with impacting energy, for both ions and neutral species, although this is less so at lower incident ion energies.

Corresponding values for argon are provided in [82]; these are found to be considerably smaller than those for helium [Fig. 60 ii)]. This difference is an order of magnitude at electronvolt energies, although this difference is indicated to become smaller at progressively greater energies, becoming a factor of 3 by 500 eV.

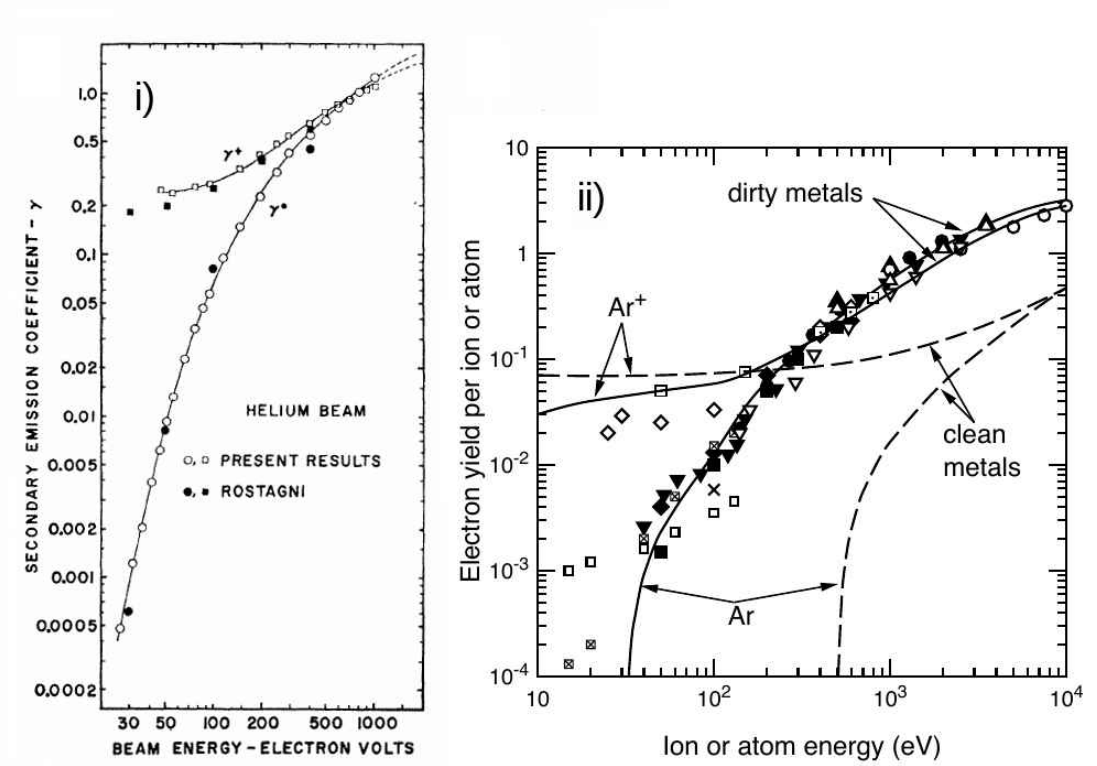

Fig. 60. Secondary electron coefficient for i) helium ions and neutrals incident on contaminated gold surface, reproduced from [81]; ii) argon ions and neutrals incident upon clean and contaminated surfaces, reproduced from [82]

In order to estimate the value of γ_{SE} that may be expected in CC mode operation, an assessment is made of the range of ion energies likely to be incident upon the cathode. Analytic expressions for ion temperature as a function of *E/N* are given for helium in [63], and for argon in [82]. Expressions for modelling values of γ_{SE} as a function of this are also given in these references. These expressions predict ion energy to remain in the 10's eV at *E/N* as high as 10 kTd, which from the estimated values in Chapter 3 is considered high for the CC mode. At these conditions γ_{SE} is indicated to be around 0.24 for helium ions, and 0.07 for argon ions, when incident upon contaminated surfaces. It is observed that γ_{SE} shows relatively little dependence upon energies of this order, and so these values are considered to be reasonable estimates.

Before moving on to consider the likelihood of secondary electrons becoming confined, it is noted that a value of 0.24 for γ_{SE} implies around four helium ions to be incident upon the cathode for every secondary electron emitted, and many more so for argon. This difference makes it harder to account for processes in the argon discharge, and so the following discussion will be primarily concerned with the dynamics in helium. The differences implied for argon will be briefly considered afterwards.

The electric field immediately surrounding the cathode grid wires will be largely radial, and so secondary electrons emitted from the surface might be expected to be ejected in all directions, according to the location of ion incidence. It seems reasonable to expect secondary electrons emitted from the exterior surfaces of the cathode to be more likely to drift outwards than to travel into the cathode interior, and so these will not be expected to have any effect upon processes operating within the cathode.

From the distributions of emission, a significant degree of ionisation is expected to occur in locations both external and internal to the cathode, and so the ion flux will be expected to arrive at the cathode in significant numbers from these respective regions. This suggests that the part of the secondary electron current that is directed within the cathode will constitute only a part of that which is emitted.

4.4.3.2 Collisional dynamics for secondary electrons

The fraction of the secondary electron current emitted from the inside surfaces of the cathode will be accelerated inwards across the sheath and into the plasma. Any of these electrons that do not experience inelastic collisions will become decelerated in the opposite sheath, but will not be completely slowed until reaching the cathode potential. These electrons will therefore have a high probability for being lost from the cathode, unless they are incident upon the grid itself.

Conversely, should an electron experience inelastic collisions, the reduction in kinetic energy will cause it to be reflected from a lesser potential rise than that to the cathode, and so increase the probability for confinement. As noted above, this

probability will however remain negligible for incidence at the part of the cathode boundary from which the bulk electron extraction occurs.

Elastic collisions may be expected to have some effect also. Even if these collisions do not result in an ionisation, the angle of scattering may cause the electron's path length within the cathode to become longer, and so increase the probability of an ionising collision occurring before the electron is lost. An increased angle of incidence at the cathode boundary may also increase the probability for an electron to be confined, since a smaller part of its velocity will be radially directed. Collisional processes are therefore indicated to be important for any degree of electron confinement that occurs.

The ETE effect was noted in Section 4.4.1 to affect hollow cathode discharge properties only when the electron mean free path for ionisation, or ionisation length, exceeds the characteristic dimension of the cathode cavity. Given the likelihood that non-ionising collisions may also affect this dynamic for the grid cathode, mean free paths are calculated for both ionising collisions, and for any collisions at all to occur, at various pressures in helium. This is done using the following definition for mean free path, λ_{mfp}:

$$\lambda_{mfp} = \frac{1}{N\sigma} \qquad (4)$$

Where σ refers to the cross section and N is the number density of the background gas. The density is again obtained from the pressure by re-arranging the ideal gas law, as was done in Section 3.3.1, using Eqn. (1).

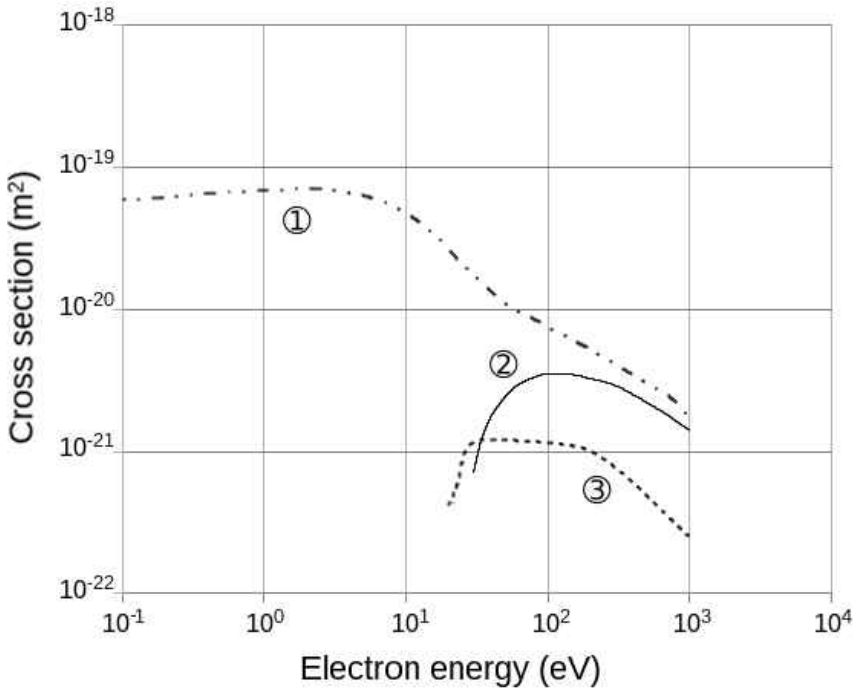

Fig. 61. Cross sections for ① total momentum transfer; ② ionisation; and ③ excitation, for electrons in helium [83]

The cross sections for ionisation and for total momentum transfer are taken from [83] These are plotted, along with that for excitation, in Fig. 61. The cross section for electron-impact ionisation for helium is noted to show less than 20 % variation for electron energies between 60 eV and 300 eV, and so as long as the magnitude of cathode fall remains within this range, the ionisation mean free path will be largely determined by the pressure. An ionisation cross section size of 3.13×10^{-17} cm^2 is used, which is around 90 % of the maximum. The cross section for total momentum transfer shows more variation, and mean free paths are calculated for cross section sizes as given for electron energies of 50 eV, 100 eV and 300 eV.

The mean free paths, as calculated for a series of trial pressures, are shown in Fig. 62. The cathode diameter is indicated, and also the approximate dimension of the plasma, as suggested by the dimension of the region of bright emission. The realistic dimension over which a collision needs to occur for there to be much chance of confinement is likely to be somewhere between these. For the approximate cross section size used, the ionisation length is indicated to become equal to the cathode diameter at a pressure a little smaller than 200 mTorr. It is indicated to become larger than the plasma dimension at a pressure of around 250 mTorr, which is roughly the pressure at which the current-voltage relation starts to show a current threshold.

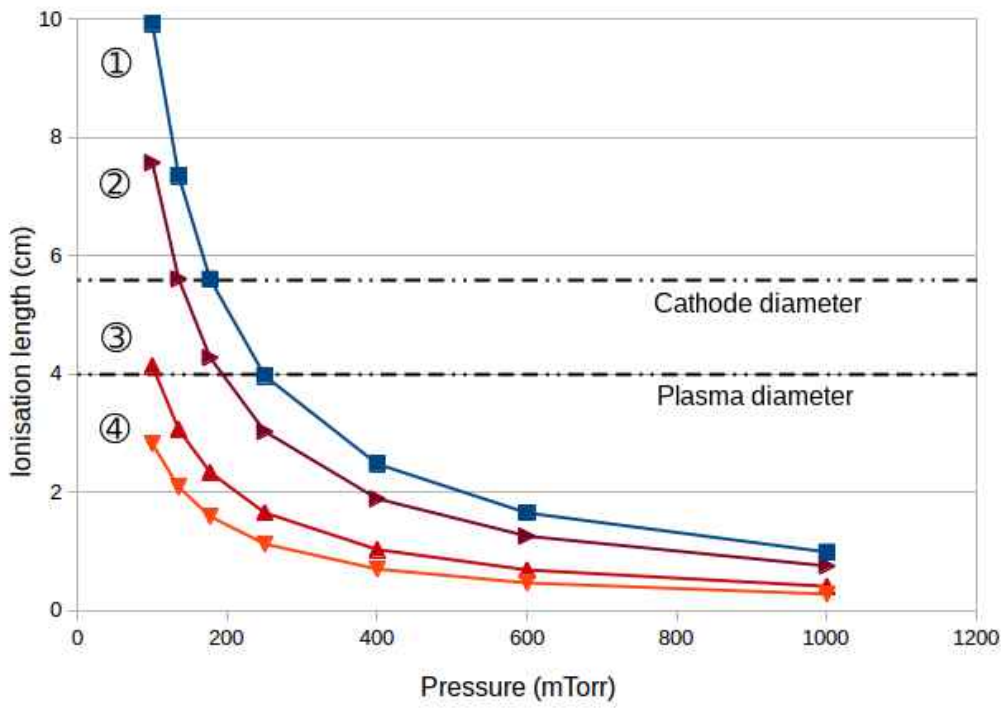

Fig. 62. Pressure dependence for ①, ionisation length for electrons calculated as described in the text; ②-④, collision lengths for electrons at 300 eV, 100 eV and 50 eV respectively.

The probability for any collisions to occur can be seen to vary quite significantly with electron energy, particularly for energies greater than 100 eV. At these energies, collisions are more likely to be ionising, and so the total cross section becomes closer to the size of that for ionisation.

The ETE effect was noted in Section 3.1 to affect hollow cathode discharge properties only when the electron mean free path for ionisation, or ionisation length, exceeds the characteristic dimension of the cathode cavity. The low-pressure limit for the CC mode occurs at a pressure of around 100 mTorr, at which pressure the ionisation length for secondary electrons is around twice the dimension of the cathode. For electrons having energies greater than 100 eV, this pressure corresponds roughly to that at which they start to become unlikely to have any collisions before reaching the other side of the cathode.

This suggests that an element of the ETE effect is likely to be operating at pressures below around 200 mTorr to 250 mTorr, as indicated by the ionisation length becoming longer than the cathode dimension. The interpretation of the general collisional path lengths is somewhat conjectural without knowing the electron energies. It may be observed however that the low-pressure limit for the mode occurs at conditions roughly corresponding to those at which electrons having energies greater than 100 eV start to be unlikely to have a collision during a transit of the cathode.

From the photographs in Fig. 48, it may be noted that for pressures greater than around 500 mTorr, the intensity of emission at the very centre of the cathode starts to become reduced, relative to that in the bright region more generally. This is observed to correspond to the ionisation length becoming significantly smaller than the cathode radius, indicating the bright emission visible within the cathode interior at these conditions to be associated with the ionisation length.

The cross section for excitation is smaller than that for ionisation, by a quite consistent factor of around 5 at these energies (Fig. 61). The corresponding excitation length will therefore be 5 times longer than that for ionisation, and so for the emission profile to show this association with the ionisation length suggests emission to be rather determined by the potential structure within the cathode.

The apparent association between the location of this and the ionisation length suggests the potential structure to be itself determined by the location of ionisation, although the dynamics of ion influx through the cathode apertures will also be expected to contribute to this. The 'hollowing' of the emission profile is therefore considered to be indicative of a splitting that occurs in an otherwise relatively positive potential profile within the cathode, occurring at pressures greater than around 400 mTorr to 500 mTorr.

4.4.4 Hollow cathode effect in the CC mode discharge

In summary, consideration of the generation and dynamics of secondary electrons within the CC mode discharge suggests that the numbers of these may represent around a fifth of cathode current in helium, and a considerably smaller fraction in argon. The fraction of this secondary current that becomes directed inwards to transit the cathode interior is expected to bear some relation to the fraction of total ion flux that is incident upon the interior surfaces of the cathode.

This convergent part of the secondary electron flux is noted to be subject to a varying degree of direct confinement by the cathode, depending upon the location at which it encounters the boundary radius. This is indicated to be so by the condition of relative parity between the potential within the cathode apertures and that of the plasma, as required to account for the observed bulk electron extraction in a radial direction.

The 'hollow cathode' or ETE effect is noted in [76] to be associated with discontinuities in discharge operating voltage and current, and in this respect shows a similarity to the behaviour of the CC mode discharge towards the low-pressure limit. The effect is predicted to become significant only as the ionisation length exceeds that of the characteristic confining dimension, which is calculated to indeed be the case at the conditions at which these discontinuities are observed. Consideration of the dynamics of scattering collisions suggests these to be important for electron confinement, as well as those causing ionisation, since the low-pressure limit for the mode appears to coincide broadly with the total collisional mean free path becoming similar to the cathode dimension, at least for electrons with energies of 100's eV.

The analysis of optical emission distributions indicates a considerable fraction of total levels of emission to occur within the cathode and, as mentioned previously, this is expected to represent a considerable degree of ionisation. The relatively small magnitude of internal secondary electron current indicated to be produced by the ion current resulting from this ionisation, and the relatively long ionisation length at such conditions, indicate this degree of activity to be only consistent with an element of electron trapping.

A few considerations regarding the mechanics of this are noted in the following paragraphs, before moving on to consider the effect of the cathode modification experiment.

If a general parity is assumed between the relative degree of ionisation occurring within the cathode and that of the inwardly-directed element of the secondary electron flux, then the value of γ_{SE} suggests that the secondary electron flux within the cathode must cause around 4 ionisations per emitted secondary electron, in order to maintain an equilibrium in this region. The ionisation length at most CC mode pressures is in excess of one quarter of the cathode diameter, and so this figure implies an element of electron confinement to occur throughout most of the range.

It should be noted that this figure describes the number of ionisations per secondary electron emitted, and so must therefore become larger if any of the energetic secondary electron flux is lost at the cathode boundary. The considerable losses that may be expected to result from the aperture potential structure suggest that this will occur to a significant degree. At conditions of lower pressure, when the ionisation length exceeds the cathode, the losses might be expected to be relatively greater, since this will cause more electrons to be incident upon the boundary before losing energy to inelastic processes.

For energies above threshold values, the number of exciting collisions will be expected to be approximately a fifth of that for ionisation, from the relative magnitudes of the respective cross sections. The magnitude of kinetic energy expended by a secondary electron in causing the nominal 4 ionisations will therefore be somewhat greater than the 4x24.6 eV required exclusively for ionisation, and so will correspond to a potential fall that is closer to 120 V.

The expected electron losses will cause this figure to increase, so that those that become most effectively confined may cause sufficient ionisations to make up for these losses. There is a physical limit however to the degree to which this may occur, since the plasma potential is not expected to become much more positive than ground. This may be appreciated from the considerations regarding electron extraction discussed above in section 3.2, in which it was observed that electrons born in ionisations occurring within a region of relatively positive potential will accumulate until the potential structure bounding the region is altered sufficiently for them to escape. In the present context, this requires the plasma potential to be not more positive than ground, except by a value within the range of bulk confined electron temperature.

Typical cathode voltages are between 300 and 500 volts, which are greater than the no-loss potential figure of 120 V by a factor of between 2.5 and 4.2. In the limit of the plasma potential being close to ground, this still implies a degree of electron confinement in which every third or fourth secondary electron becomes sufficiently trapped on average for all of its kinetic energy to be expended in inelastic collisions. This seems quite high in the light of the considerations made above regarding the likelihood of losses, suggesting that the escape routes for the bulk electrons must constitute relatively small gaps in the enclosing potential structure.

This analysis equates the ion flux incident upon the inner surface of the cathode with the rate of ionisation occurring within the cathode. If an element of the ion flux originating from locations external to the cathode is transported through the apertures of the electrode to be then incident upon its inner surface, then the internally-directed secondary electron population will be increased accordingly. The assessments of emission distributions suggest the limiting case for this effect might see ion flux upon the inner surfaces increased by a factor of maybe two, but this assessment is noted to be very approximate.

In argon, the situation is made more difficult to understand by the comparatively small values predicted for γ_{SE}. These do not approach the magnitude of the value used in the above assessment of the helium discharge until impacting energies of several hundred eV, which are not projected to occur at the relevant conditions.

It is noted however that the emission distributions in argon have not been recorded, and that these might indicate a relatively larger fraction of emission to occur external to the cathode; were the same conjectured process of ion influx via the apertures to function in such a case, then the magnitude of cathode-plasma potential fall required could be mitigated further. The cathode voltages associated with the CC mode in

argon have been noted to be significantly greater than in helium, which difference is likely to also reflect this difference in γ_{SE}.

4.4.5 Physical dependence on cathode structure

The experimental modification of the cathode was designed to affect the degree of electron confinement that might be expected to occur within the cathode. Observations of the effect upon operating characteristics caused by this modification indicated it to be significant.

The effect of enclosing the terminal aperture was found to considerably extend the low-pressure operating range of the CC mode, and to assist the mode to form at pressures constituting the lower limit of the range in the open cathode. This is considered to be further indication that confinement of electrons by the cathode grid does assist in the sustaining of the CC mode, since the effect of the cathode modification is to increase the degree of enclosure of the space within the electrode with regions of negative potential.

In the previous sections, the degree of loss of secondary electrons has been indicated to be a limiting factor in operation of the discharge, and so this result indicates the open cathode end to be a loss route for energetic secondary electrons, despite the lack of bulk electron transport evident axially.

4.4.5.1 Mode transition

In helium it was observed that as current levels approach the threshold for the CC mode to form, emission from within the (enclosed) cathode central region becomes progressively more green, which is interpreted as an increase in emission due to electron-impact excitation within the cathode. This progression is also associated with a moderate rise in levels of cathode current, indicating the increase in emission to be accompanied by a corresponding increase in ionisation.

This behaviour clearly represents an increase in electron activity within the cathode, and from the understanding gained so far, this is considered to indicate an increasing quantity of secondary electrons experiencing inelastic collisions within the cathode.

Whether this dynamic is associated with an increasing flux of secondary electrons directed within the cathode, or an increasing cross section for an existing flux, or indeed some combination of these factors is not clear. It may be observed however that the progression results in the appearance of the CC mode, with associated step changes in voltage and current, and that this is likely to indicate a critical point to have been reached in the evolution in conditions. It is observed that this evolution represents a shift in the relative distribution of ionisation to within the cathode, suggesting that this may be associated with the subsequent instigation of the mode.

4.4.5.2 Beam and plume formations

The modification made to the cathode was also found to result in the appearance of additional discharge features passing through one or more apertures of the cathode. These were observed to take a characteristic form that was specific to the discharge mode, and this association was found to be similarly evident in helium and argon.

These features are described to resemble a plume in the CC mode and a beam in the beam mode. In the helium discharge these formations are bright green in colour, which is associated with a predominance of the 501.6 nm spectral line. In the previous chapter it was established that observed levels of the 501.6 nm and 587.6 nm helium lines in these discharges are a reasonable indication of electron and ion activity, and so the colour of these features indicate them to be caused by electron activity.

The association of the electron beam with the mode structure of this discharge bears similarities with accounts of hollow cathode electron beam sources found in the literature; this link between higher-pressure IEC operation and hollow cathode plasma electron beam sources has been made previously by Hirsch [7].

In a study of the production of energetic electron beams using a perforated hollow cathode [84], a considerable heating effect was demonstrated in the melting of metal samples. This is consistent with the heating of the chamber wall described above. The perforations in the grid cathode are considerably larger than those of the gauze used in [84], but the beam is extracted through an aperture of more comparable size. Significantly, the study finds that the discharge is capable of switching between a high- and a low-impedance mode, with the electron beam present only in the high-impedance state.

Another study of a hollow cathode plasma electron beam source also describes a 'low-impedance' or 'normal hollow cathode' mode, which is found to disrupt the operation of an 'electron beam' or 'high-impedance' mode [85]. This causes voltage to drop and current to rise, which is analogous to the discontinuity in current-voltage that is observed to accompany ignition of the CC mode. The CC mode would appear to be the analogue of the 'low-impedance' or 'normal hollow cathode' mode described in these works.

Further similarities with the findings of [84] are evident regarding the differences in operating characteristics of discharges in helium and argon. The authors of [84] report difficulties in operating the argon discharge in the electron beam mode stably and at higher power levels, which is consistent with the relatively lower current threshold for CC mode instigation in the enclosed cathode.

The presence of the additional features observed in operation with the enclosed cathode suggests that bulk electron transport in this case is not via the longitudinal apertures in the same way as indicated to occur with the open cathode. Unfortunately this may not be verified by measurements of the current transported axially in these

features, or the current to a radial collector, since these diagnostics were not in operation at the time that the experimental observations were made.

The implied extraction of electrons via these formations does suggest however that they are instrumental in the removal of electrons born within the cathode interior, that would otherwise accumulate until the potential became lowered to that of the cathode apertures.

These considerations, along with the comments regarding the physical dependences upon electrode geometry made in [76], suggest a possible interpretation of this behaviour as follows: operation with the enclosed cathode may causes the potential structure that facilitates ambipolar charge extraction in the open cathode discharges to be altered in such a way that the ratio between electron extraction area and cathode inner surface area becomes equal to $\sqrt{m_e/m_i}$.

For the 'conventional' hollow cathode discharge occurring in apparatus such as that illustrated in Fig. 58, such a constriction of the exit aperture is noted to result in the formation of a double layer that bulges into the plasma, allowing for both a larger surface area for electron extraction, and a potential rise to accelerate these electrons through the gap. The electrode configuration at which this occurs is noted to be optimal for the operation of the discharge, and to be associated with a minimum in operating pressure and voltage.

As a test of this theory, the inner surface area of the cathode is approximately evaluated, considering the wire members to be adequately represented in this respect by rectangular elements having the small dimension equal to the wire diameter of 1.6 mm. The resulting area is calculated to be around 43 cm^2. For argon, this implies an optimal electron extraction area of 0.16 cm^2, and for helium an area of around 0.5 cm^2; these areas correspond to circles of respective diameters of 4.5 mm and 8 mm.

Consideration of the diameter of the features as they pass through the cathode apertures indicates that these figures describe the cross sectional areas quite closely. This is illustrated in Fig. 63, in which the small dimension of a cathode aperture is also indicated in one photograph to aid the perception of the plasma dimensions.

This agreement is considered to be significant, and to confirm the functional nature of these features as mechanisms by which electrons are extracted from the plasma. This also confirms that the plasma potential in these discharges may become more positive than that within the cathode apertures. Before concluding this discussion, brief consideration is made of the different characteristic forms of these extraction features, as seen in the different modes.

The shape of a jet, or beam, that is extracted from a spherical IEC discharge is illustrated using photographs in [23]. In this account, the formation is described to evolve from a plume at conditions of higher pressure, to become a beam at lower pressure. This evolution is attributed to a loss of electron energy occurring in collisions at high pressures, which causes the electrons to spread by charge repulsion.

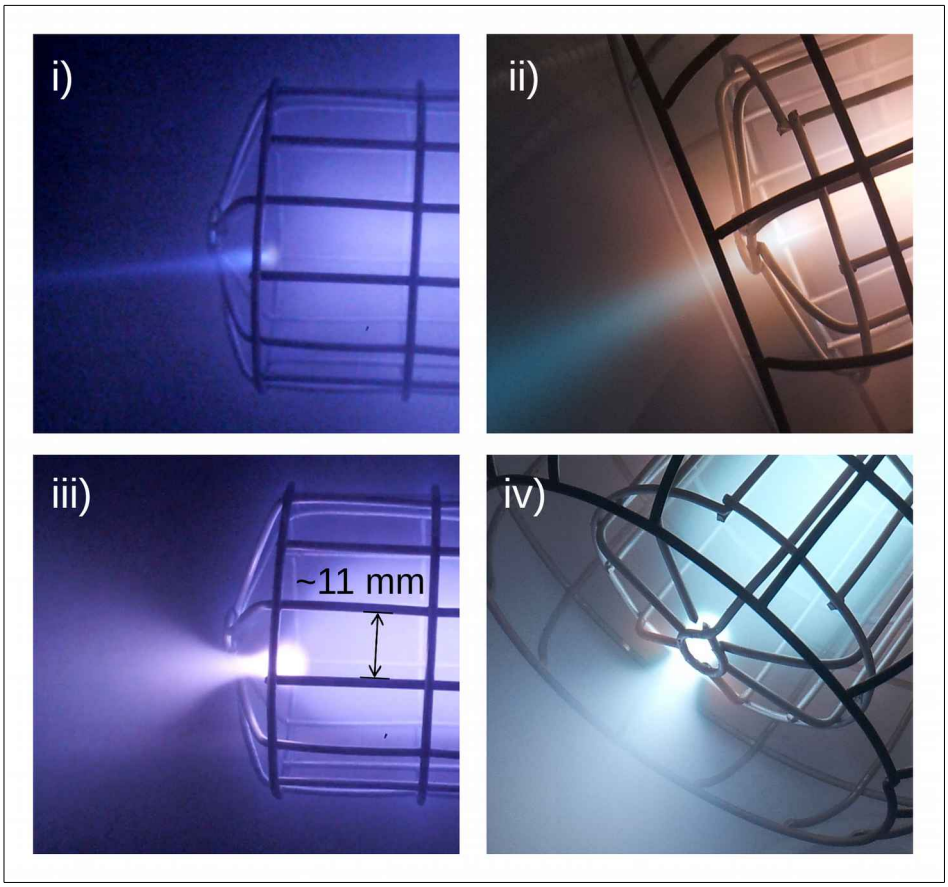

Fig. 63. Electron extraction feature evident in helium and argon. i) beam in argon at 7 mTorr; ii) beam in helium at 51 mTorr; plume in argon at 7 mTorr; iv) plume in helium at 56 mTorr. The dimension indicated in iii) is a characteristic dimension for these apertures

By analogy, this would suggest the electrons in the plume formation to have relatively smaller energies than those in the beam formation. This is consistent with the observed heating effect of the beam, which indicates these electrons to be energetic. The form of these features is clearly not a function of pressure in these cases, since this is unchanged at the mode transition, and so an apparent difference in electron energy will rather be associated with the accelerating potential.

The nature of the formations has been indicated to enable the transport of electrons from a region of relatively positive potential within the cathode, across a region of more negative potential within the region of the aperture, to the region of more positive potential in the region external to the cathode. The function of the double layer in the extraction of electrons is described in [76] as being twofold, comprising both the creation of a larger surface area for them to be drawn from and also a potential for their acceleration. The electron energies implied by the shape of the formations in the region external to the cathode indicates a greater accelerating potential to be associated with the beam mode formation. This suggests that the magnitude of the potential barrier is greater in this case, appearing to require the electrons to be accelerated to energies sufficiently greater than this barrier for them to be 'fired' across it. This would seem consistent with the greater cathode potential in the beam mode, and also with the relatively smaller degree of ionisation expected to

be occurring within the cathode, since this constitutes a significant generation mechanism for electrons. The narrow profile of the beam associated with the beam mode discharge is comparable to that observed in low-pressure operation with the open-ended cathode, although the details of the extracting structure are not apparent in that case. The similarity suggests that the electron beam plays a similar functional role in both cases, with the additional structure required for transport across the potential barrier created by the additional enclosing of the cathode end.

In Chapter 1, the $\sqrt{m_e/m_i}$ ratio was observed to relate the velocities of ions and electrons that have similar energies. The appearance of this ratio in this context therefore suggests the energies at which ions and electrons are extracted from the plasma to be of similar order. These energies correspond to the potentials that accelerate the currents away from the plasma, which for the ions will be the voltage across the sheath. For electrons, the extracting potential is therefore indicated to be of similar magnitude to the sheath potential, but of the opposite polarity. This would therefore accelerate the electrons to energies sufficient for them to be transported across the negative sheath.

The relative sizes of the terminal elements of the formations within the cathode would also seem to agree with this interpretation; since that associated with the beam mode is characteristically smaller, this is consistent with a relatively high-potential low-current interface, whereas in the CC mode the larger surface area is indicative of a relatively lower-potential, high current connection.

In short, these interfaces appear to be high- and low-impedance analogues of each other, which might be expected, since they appear as electron extraction mechanisms for regions of discharges that might be characterised as high-voltage and ion-rich, and low-voltage and electron-rich respectively.

Returning very briefly to the evolution of emission within the cathode associated with conditions leading to the mode transition, the observations made above regarding conditions of potential within the two modes suggest that this evolution will represent the potential within the cathode becoming more negative. In this context, the increasing levels of electron-induced emission are therefore likely to represent an increasing cross section size as electron energies become smaller.

4.4.6 Implications for stability and electrode design

In operation with the open cathode, the low-pressure limit for the CC mode to exist corresponds broadly to the pressure range at which the ion/neutral beam activity starts to become apparent, and so in this set-up the evolution with pressure appears as a transition from one regime to the other. With the closed cathode however, this is not the case, with the CC mode appearing at conditions otherwise clearly associated with the ion-driven discharge. This has implications for the reliable operation of a source intended to create an ion-driven reactive plasma chemistry, since a switch to the CC mode will be expected to also switch the plasma properties to those of an electron-driven discharge.

It seems therefore that the open cathode end may contribute significantly to the stability of the ion-driven beam mode plasma, particularly when operating at higher currents. This in turn has implications for the design of electrodes in a system intended to provide ion and neutral reactivity, as it implies that the cathode must allow for a sufficient rate of escape of secondary electrons to prevent the electron-driven CC mode from establishing.

4.5 Conclusions

In this chapter, the electron-driven discharge mode that has been called the cathode-confined, or CC mode has been investigated. The focus has been upon the nature of the processes operating within the discharge, and the physical dependence upon the form of the electrodes.

Measurements were made of the distributions of current and optical emission associated with operation of the discharge in this mode, and considered with reference to characteristics of the so-called 'hollow cathode' or 'electrostatically-trapped electron' (ETE) effect. Consideration of the characteristic ionisation length, as compared with the diameter of the cathode, and the discontinuities evident in current-voltage behaviour at low pressures, indicate this effect to be instrumental in the sustaining of the discharge at these conditions. At conditions of greater pressure, it seems likely that the relative degree of emission observed to occur within the cathode is caused similarly.

The experimental modification of the cathode in such a manner designed to increase this effect is found to considerably enhance the low-pressure limit for operation, which is consistent with the observations above. This modification has also allowed the observation of additional features of the discharge, appearing in the form of a beam and a plume, that have been identified as playing a role in the extraction of electrons from within the region of relatively positive potential within the cathode interior. The functional nature of these features offers significant insight into fundamental dynamics of operation of grid cathode discharges, and this has been found to agree with observations and interpretations made elsewhere in the IEC literature.

It is concluded that the CC mode discharge shows significant similarities to certain hollow cathode-type discharges described elsewhere, and it has been found to be practically assisted by an increased degree of cathode enclosure. These associations identify it to be sustained to a significant extent by the processes commonly referred to as the 'hollow cathode effect', and which is attributed to the increased path-lengths of secondary electrons experiencing a confining effect from the cathode field.

The efficiency associated with this effect means that the characteristics of the discharge are relatively sensitive to the degree of enclosure of the cathode. The design of the cathode is therefore indicated to be important in the engineering of the mode structure of this discharge.

It has been noted that IEC discharges at higher pressures have been previously described as 'hollow cathode' type discharges, but no previously-published work has illustrated the relative importance of the cathode geometry for either avoiding or encouraging this mode to form. This will be important for applications that require the creation of a plasma having properties specific to the operating mode, such as the operation of an ion-reactive plasma source.

It is not clear how important the asymmetrical degree of enclosure found in the open-ended cylindrical geometry is for the stability of the beam mode, and further work is required to understand this dependence more fully.

Chapter 5
The Beam mode

5.1 Introduction

In Chapter 3, the low-pressure mode structure of the discharge was described as consisting of two principal modes, each being associated with operating conditions that occupy distinct ranges of *E/N*. Spectroscopic analysis of optical emission from the discharge in helium showed the mode occurring at conditions of lower *E/N* to be sustained by the action of electrons, whilst emission from the higher-*E/N* mode indicated it to be sustained by ions and/or neutral species. The electron-driven discharge was called the cathode-confined mode, and this mode has been described more fully in the previous chapter. The discharge occurring at the conditions of relatively high-*E/N*, that was referred to as the beam mode, is of particular interest for this research, because of the energetic populations of ions and neutrals. This mode is described in more detail in this chapter.

This is approached in a similar fashion to the investigation of the CC mode made in Chapter 4, in which distributions of current and optical emission were considered, and the effects of altering the electrode configuration observed. Information concerning the dependences of discharge characteristics upon electrode and chamber geometry, and upon operating conditions of pressure and voltage, will be valuable for the understanding of the nature of discharge operation in this mode.

The first part of this account is concerned with the distributions of current within the chamber. Following this, observations of the distributions of optical emission are described. The beam mode discharge was previously characterised in terms of a distinctive pattern of optical emission, consisting of spoke-like beams, oriented radially so as to pass through the apertures of both electrodes. Observations are made of the beam elements of these distributions, and an assessment is also made of the broader distribution of emission within the chamber. The formation of the radial beams is then investigated by exploring the dependences of this mechanism upon the physical form of the electrodes. Finally, a description is made of optical phenomena associated with the presence of hydrogen in beam mode discharges.

The wider significance of these observations is then discussed, concentrating upon the processes that are indicated to be important for the operation of the discharge, and the mechanics that lead to its appearance. The behaviour of the hydrogen is considered, and a possible explanation for this suggested. Finally, the general appearance of the beam mode discharge is noted to bear a clear resemblance to the 'star' mode discharge described in spherical single-grid devices in the literature. The relation between the findings reported in this chapter and the descriptions of mode structure reported elsewhere in the IEC literature is discussed.

5.2 Experimental observations and analysis

In this first section, measurements of optical and electrical characteristics of the beam mode plasma are described. Before proceeding to details of the experimental work, the electrode assembly and the beam mode plasma obtained are first described in more detail.

5.2.1 Current distributions

In the previous chapter, measurements were presented of electrical characteristics obtained at a wide variety of pressures, including those at which the discharge operates in the beam mode. These results were not separated by mode, in order to facilitate the observation of characteristics specific to the mode structure, and some mention was therefore made of the characteristics evident in the beam mode curves. The procedure used to make these measurements, and the results obtained, will not be described again here in their entirety. A brief summary is given of the procedure and set-up, and the important aspects of the measurements relevant to the operating of the beam mode are reiterated. Figures are reproduced to illustrate these, although the descriptions made previously of the CC mode behaviour will not be repeated.

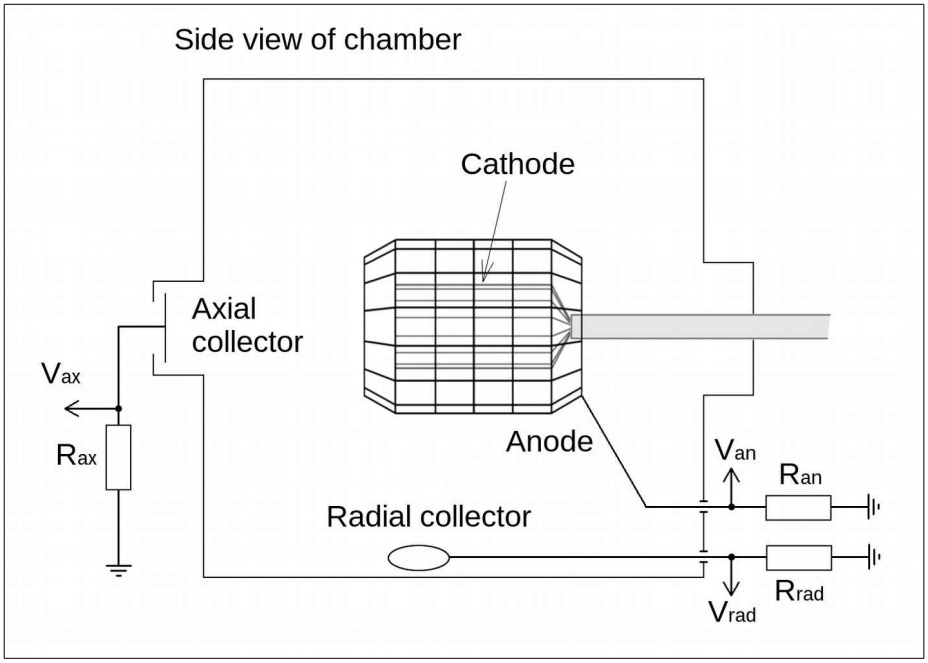

Fig. 64. Diagram showing electron current-monitoring system

The procedure followed in the making of these measurements was described in Section 4.2.1. Measurements were recorded of cathode current and voltage, and of currents collected by the anode and by two collectors positioned within the chamber. One of these collectors was aligned axially with the electrodes, and one displaced radially from the end row of cathode apertures (as in the diagram reproduced in Fig. 64). The axial collector was a KF40 blanking plate, and the radial collector was a

stainless steel disc of 3.5 cm diameter, located on the floor of the chamber at an angle approximately normal to a radial chord.

Cathode current is noted to consist of both ion current, and the secondary electron current emitted from the cathode due to ion bombardment. Electron current consists of these secondary electrons and electrons produced in ionisation occurring within the chamber volume, and is noted to be equal to the metered cathode current, from Eqn. (3). The electron current flows to the grounded surfaces of the anode and chamber walls, with fractions of this intercepted by the axial and radial collectors according to their area and the flux density at their respective locations.

The measurements of currents to the anode and the two collectors were plotted against cathode voltage, and also against cathode current, in order to show the relative degree of total electron current that they represent. The results for currents to the anode and radial collectors are reproduced first in Figs. 65 to 68, followed by those for the axial collector in Figs. 69 and 70.

Anode and radial currents

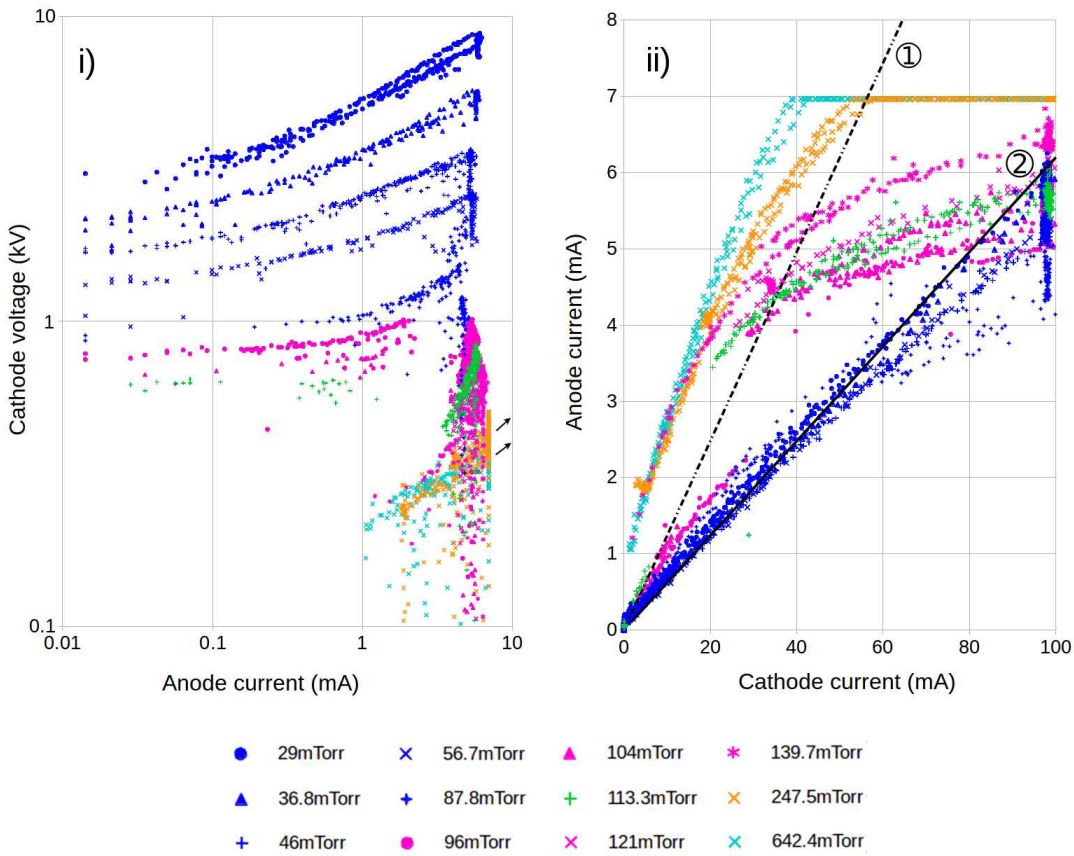

Fig. 65. Anode current for the discharge in helium, at various pressures. Beam mode curves are coloured blue to distinguish them from the CC mode curves. Anode current-cathode voltage curves are shown in i); values of anode current are also plotted against cathode current in ii). Current voltage plots have log-log scales, current-current plots have linear scales.

Two lines are drawn on the plot of anode current against cathode current in Fig. 65 ii), marked ① and ②. These illustrate consistent fractions of cathode current, ① corresponding to the fraction of total electron current from the discharge that would be intercepted according to the anode geometric fill factor, were it isotropically incident upon its surface, and ② to half of this value. Lines are also drawn on the plot of radially-collected current against cathode current in Fig. 66 ii), in order to represent similar quantities. In this case, the corresponding fraction of cathode current is calculated by considering the area of the collector as a fraction of a cylindrical surface, concentrically surrounding the electrodes and having a radius so that it includes the collector surface. The longitudinal dimension for this surface is considered to be 12 cm, but this is noted to be an estimate. As for Fig. 65 ii), the line marked ① represents the radial collector current that would result from an intercepted fraction of an isotropic, radially-directed flux of electrons equal to the entire electron current from the discharge. The other line, marked ②, again represents half of this fraction. Similar lines are included on the plots of measurements made in argon, shown in Figs. 68 and 69, but in these figures, the lines marked ② represent 40 % of the currents indicated by the lines marked ①.

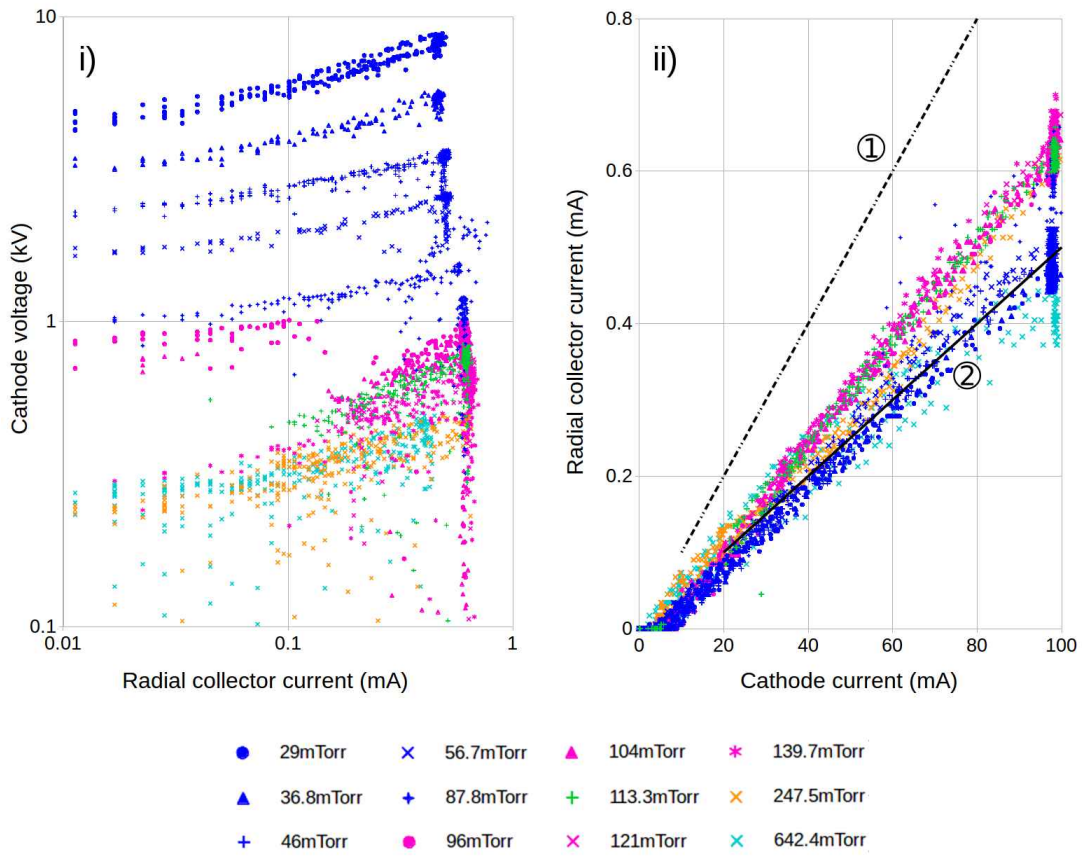

Fig. 66. Current to the radial collector for the discharge in helium, at various pressures. Beam mode curves are coloured blue to distinguish them from the CC mode curves. Radial collector current-cathode voltage curves are shown in i); values of radial current are also plotted against cathode current in ii). Current voltage plots have log-log scales, current-current plots have linear scales.

The principal finding for the beam mode was that, in both helium and argon, the currents collected by the anode and radial collector were both consistently proportional to cathode current. This suggested that the anode intercepted a fraction of an electron current that was also incident at the radial collector. By making a rough estimate of the areal extent of this radially-directed electron current, and assuming an isotropic distribution, the areal projections of the anode and the radial collector were found to correspond with the levels of currents that they collected.

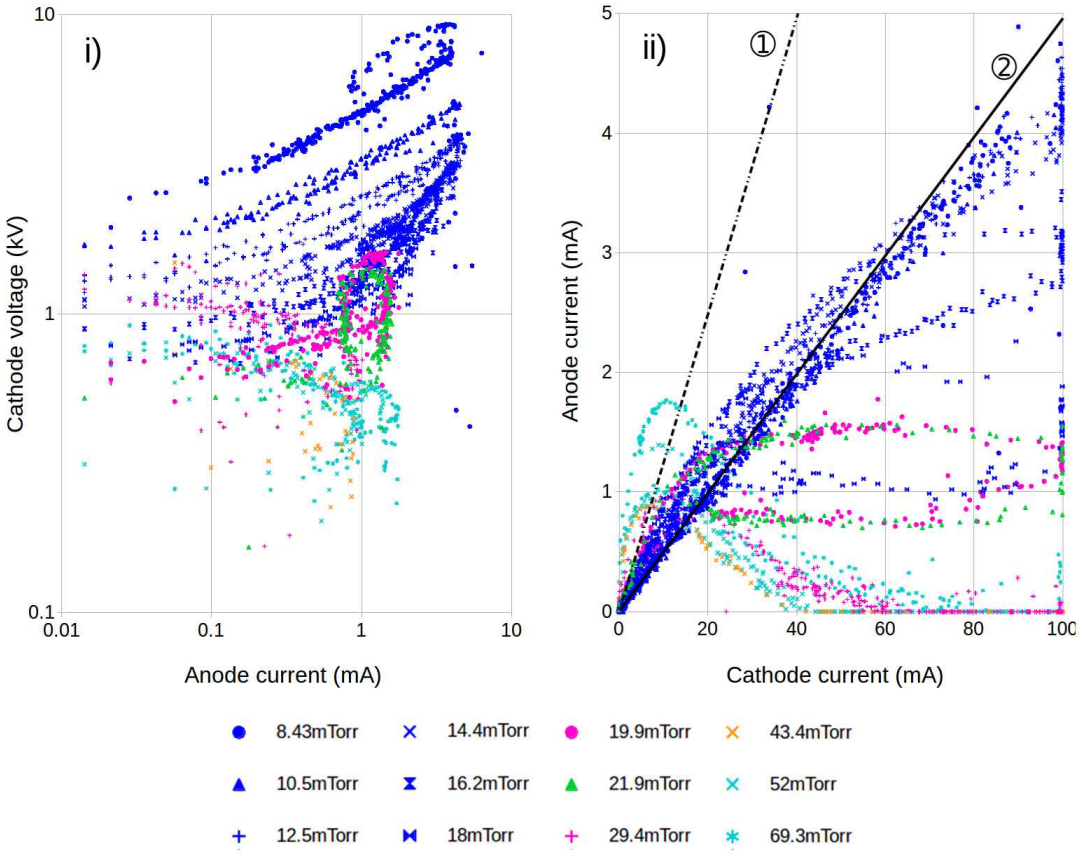

Fig. 67. Anode current for the discharge in argon, at various pressures. Beam mode curves are coloured blue to distinguish them from the CC mode curves. Anode current-cathode voltage curves are shown in i); values of anode current are also plotted against cathode current in ii). Current voltage plots have log-log scales, current-current plots have linear scales.

Despite the uncertainties concerning the longitudinal extent and degree of isotropy in the radial electron flux, this agreement between the magnitudes of anode and radial collector currents and their respective areal projections was noted to be an indication that these currents may represent interceptions of the same flux. At conditions of higher pressure, when the discharge was operating in the CC mode, measurements showed anode current to represent a proportion of cathode current that varied considerably, and that also generally became smaller at conditions of lower pressure

or conditions of greater cathode voltage and current. Since levels of radial collector current were found to remain proportional to cathode current, the radial outflow of electrons from the cathode apertures was indicated to experience an increasing degree of focussing through the apertures of the anode at these conditions. This interpretation is in qualitative agreement with the results of modelling work done by Ohnishi and co-workers [43], and with probe measurements made by Meyer and co-workers [20].

The proportionality shown with cathode current suggests the magnitude of this radial electron flux would be of the order of half of the total discharge electron current in helium, and around 40 % in argon.

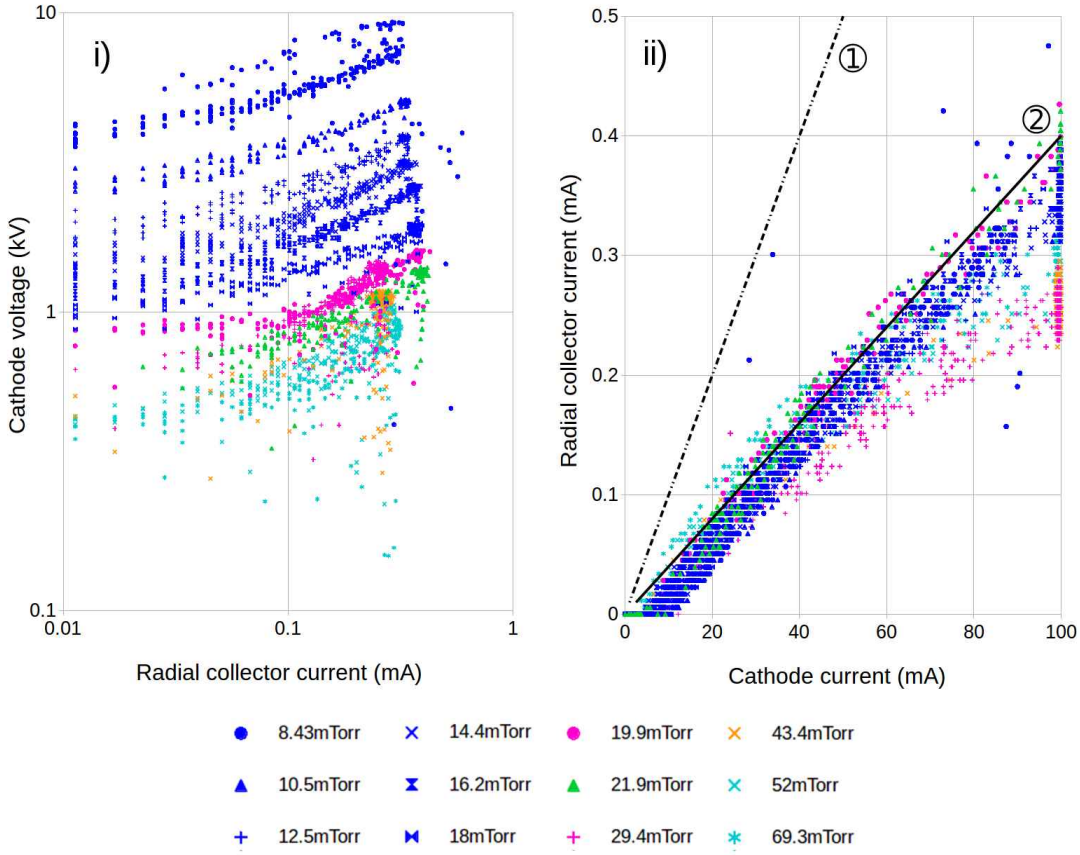

Fig. 68. Current to the radial collector for the discharge in argon, at various pressures. Beam mode curves are coloured blue to distinguish them from the CC mode curves. Radial collector current-cathode voltage curves are shown in i); values of radial current are also plotted against cathode current in ii). Current voltage plots have log-log scales, current-current plots have linear scales.

Axial current

The magnitude of electron current incident upon the axial collector was found to only become significant in the beam mode, and to become increasingly so at progressively low pressures. This is associated with the presence of the axial electron beam; this beam is noted to become more focussed upon the collector at progressively lower pressures, and so the levels of collected current will to some extent represent the increasing proportion incident upon the collector. This is illustrative of the relative nature of the axial collector current, which is not considered to represent total levels of axial current consistently between instances of operation at conditions of different pressures.

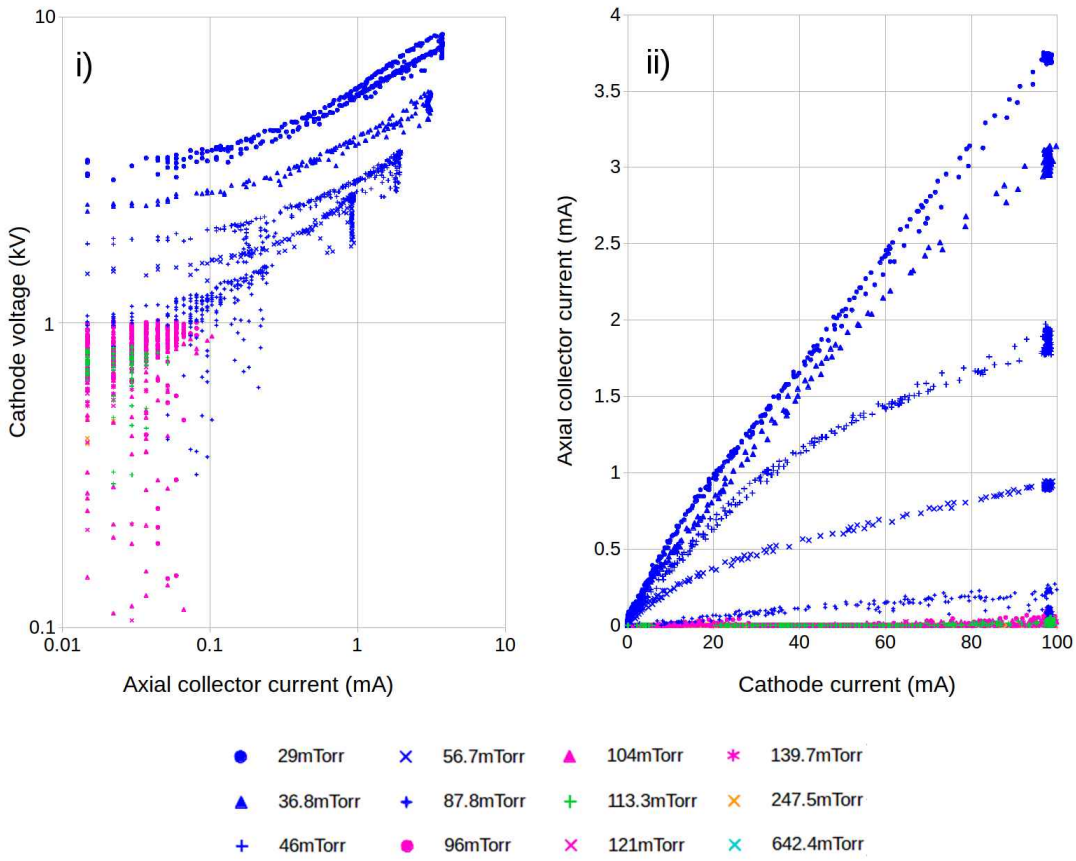

Fig. 69. Current to the axial collector for the discharge in helium, at various pressures. Beam mode curves are coloured blue to distinguish them from the CC mode curves. Axial collector current-cathode voltage curves are shown in i); values of axial current are also plotted against cathode current in ii). Current voltage plots have log-log scales, current-current plots have linear scales.

The presence of the axial electron beam indicates that, in the beam mode, some electrons born by ionisation within the cathode are transported to the wall by this mechanism, rather than through the cathode apertures. This would imply that the potential structure within the cathode may be more positive than the aperture value, and so may differ in this respect from the modelling in [43].

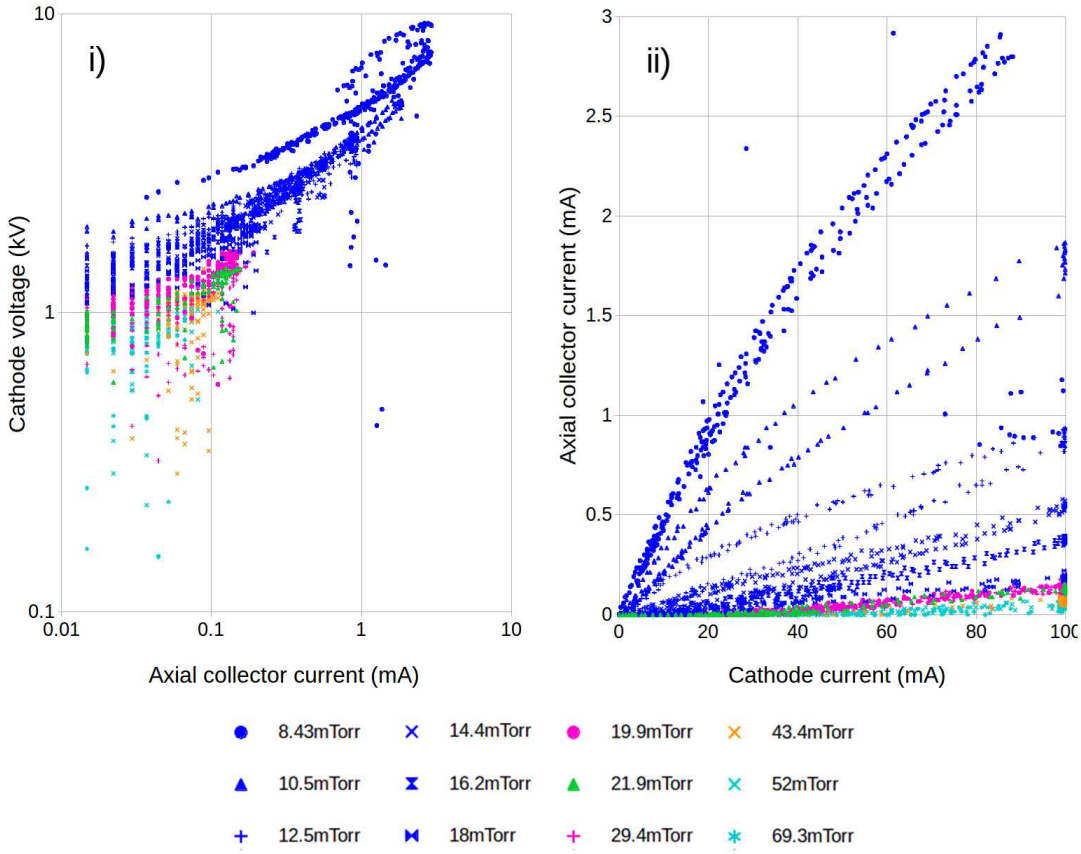

Fig. 70. Current to the axial collector for the discharge in argon, at various pressures. Beam mode curves are coloured blue to distinguish them from the CC mode curves. Axial collector current-cathode voltage curves are shown in i); values of axial current are also plotted against cathode current in ii). Current voltage plots have log-log scales, current-current plots have linear scales.

This interpretation suggests that at beam mode conditions, few of the electrons produced within the cathode contribute to the radial electron current, which is therefore indicated to be composed of secondary electrons and the electrons born in the region external to the cathode radius. This suggests that the equating of anode and radial collector current according to their respective projections may not be accurate, since the significant levels of emission observed to be evident in regions external to the anode implies the radial electron current to be augmented by ionisation occurring in the region beyond the anode radius.

5.2.2 Optical emission distributions

In this section, photographs of distributions of emission from beam mode discharges are presented and analysed. Observations are first made concerning aspects of these distributions relating to the radial beams, before the more general distributions of emission are considered in order to assess the distributions of activity in different regions of the chamber, as was done for the CC mode emission in the last chapter.

5.2.2.1 Radial beam emission

The beam mode discharge is characterised by distinctive patterns of optical emission, that appear as a series of radial, beam-like lines. These pass through the apertures of both electrodes, to converge at points along the central longitudinal axis of the discharge. The regular ordering of the apertures causes the beams to also be arranged in a very regular fashion, as may be seen in the photographs in Fig. 71.

The electrodes are made from stainless steel wire having a diameter of 1.6 mm. In being made somewhat roughly by hand, there are irregularities in the geometry of the electrodes, as is most evident in photographs taken from an axial perspective [e.g. Fig. 71 i)]. The electrodes were made from pre-welded square mesh, and so the regularity of this helps to maintain an even distribution of apertures over the electrode surfaces. In operation, the means of support for both anode and cathode were subject to mechanical and thermal stresses, which at times made it difficult to maintain the best achievable alignment. It was however found to be generally possible to maintain a sufficiently good degree of alignment for beams to pass through both sets of apertures during operation of the discharge.

In Fig. 72 the individual beams passing through the inter-electrode region are seen to be composed of a bright core remaining a consistent millimetre or so in diameter, and surrounded by a more diffuse glow. The photographs in Fig. 71 i) and ii) show the more diffuse component of the beams to extend radially outwards to the chamber walls, with a still-lower level of emission generally evident throughout the region outside the anode.

In some photographs of distributions of optical emission, such as in Fig. 71 i), a distinctive shadowing effect is apparently associated with some of the grid wires. The effect is made apparent by the regular cylindrical geometry of the electrodes when viewed from an axial perspective, and is particularly visible on the right-hand side of Fig. 71 i). The shadows appear to be cast in a radially-outward direction, and take the form of straight lines projected from longitudinal members of the electrodes.

This effect is also evident in the photograph shown in Fig. 73. This image also shows the change in the pattern of emission that was observed to occur when the electrodes became misaligned during an experimental run, with the cathode displaced relative to the anode. The effect of this can be seen to cause some of the beams to become apparently split, into one component limited to within the anode radius, and another that projects further.

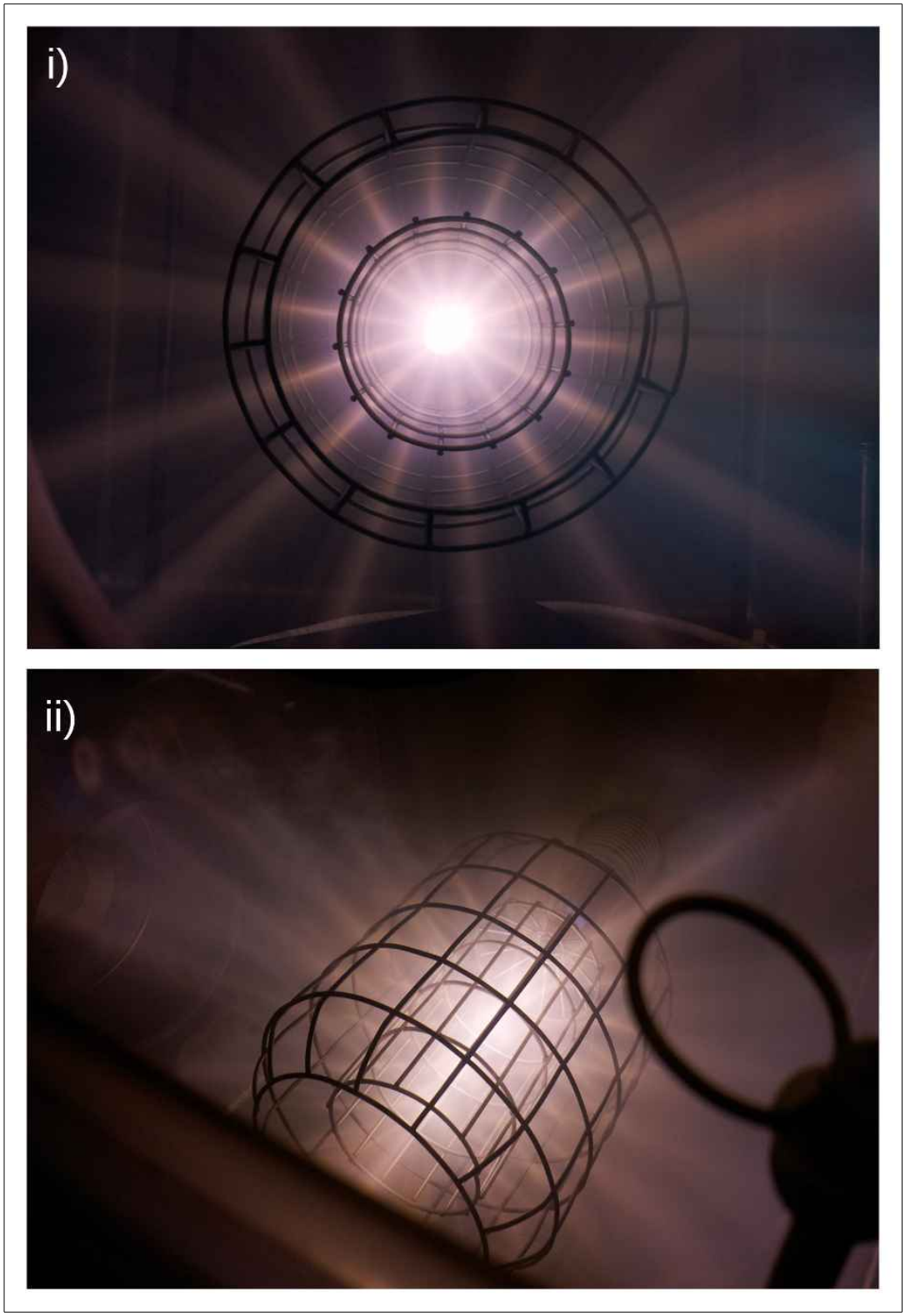

Fig. 71. Beam mode in helium, with electrodes concentrically aligned and apertures radially aligned. i) view along axis showing beams to be radially coincident with apertures; ii) perspective view

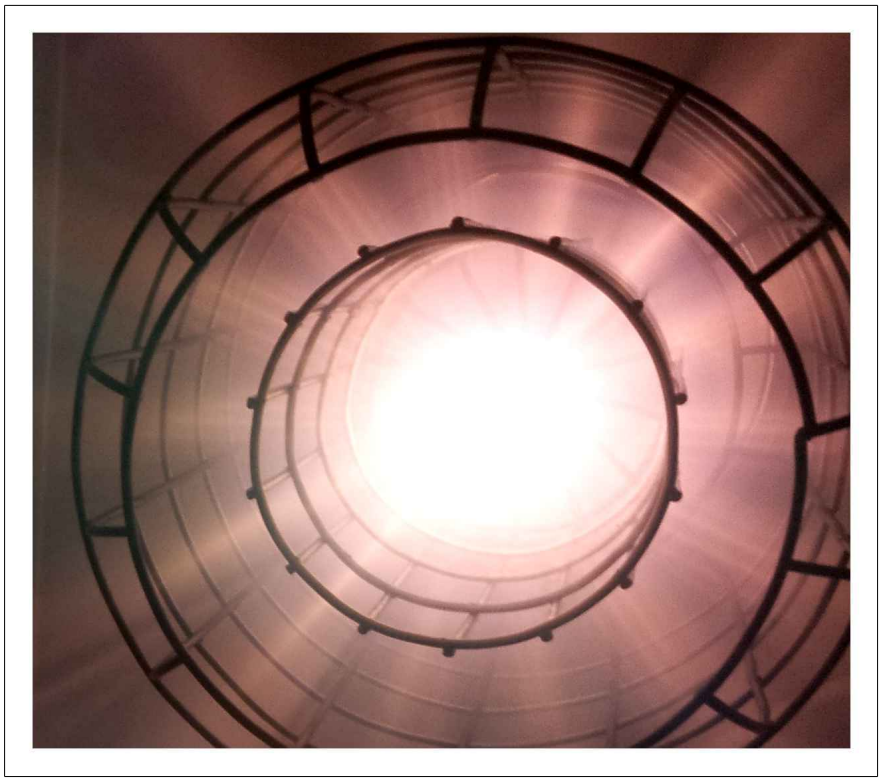

Fig. 72. Detailed view showing small diameter of beams within inter-electrode region

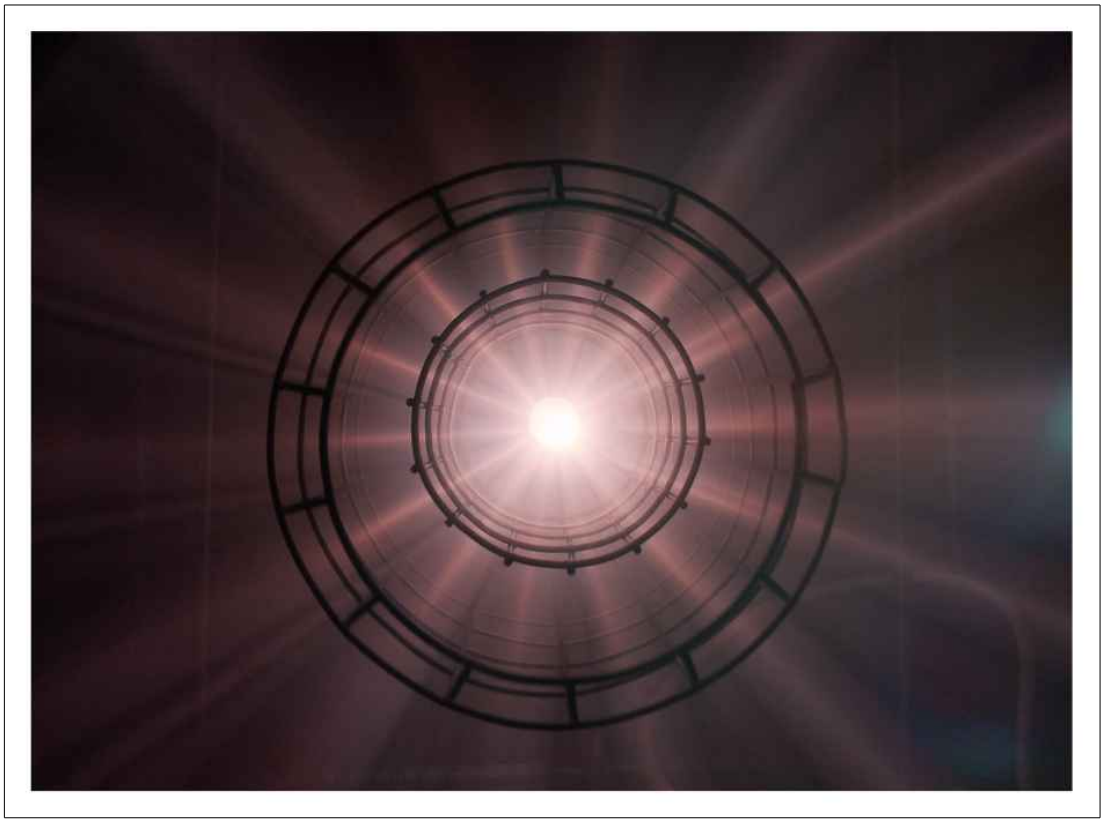

Fig. 73. Image of helium discharge during electrode misalignment, with cathode displaced radially upwards.

The processes leading to the formation of the beams, and which cause them to appear as they do, will be addressed in later sections of this chapter. First, consideration is made of the more general distribution of emission within the chamber.

5.2.2.2 Spatial distribution of emission

In the interest of gaining some insight into the relative levels of activity occurring in different regions of the chamber, a similar analysis of the distribution of optical emission as that performed on the photographs of CC mode discharges in Chapter 3 is applied to two different photographs of the beam mode discharge.

The images selected for this analysis are photographs of the beam mode discharge in helium and neon. They are both taken from a similar perspective, but represent discharges operating at significantly different levels of current, and they are also taken using different cameras.

In this case, the distributions of emission appear to be shifted considerably towards the outer regions of the chamber, as compared with those of the CC mode. The chamber is therefore divided into areas of interest using the anode radius as the line of separation.

The procedure followed is as that described previously, and involves the integration of signal within an area of interest, and subsequent comparison of this with the total integrated from within the entire frame. In this analysis the relative contribution made by emission occurring within the anode radius is evaluated. The results of the exercise are shown in Fig. 74, and indicate similar results to within 10 % for both cases, showing around 40 % of the emission signal in the photographs to originate from this location.

The correspondence between distributions of signal evident in photographs and the distribution of excitation processes is subject to various considerations, as outlined in Appendix 2. These concern the distortion in apparent distributions caused by the flattening of the 3D distribution into a 2D image, and the degree of consistency that may be expected between both the apparent and recorded levels of emission within relevant regions.

Errors due to geometrical factors such as foreshortening and to the incomplete coverage of the chamber interior are addressed first. It is noted that the images in Fig. 74 have a somewhat different field of view. The proportion of the image masked is in fact very similar in both cases; the circular masking applied in Fig. 74 i) constitutes 20.3 % of the unmasked area, and in Fig. 74 ii) this was 20.1 %. The differences in composition are therefore not expected to significantly affect the relative outcomes. In both cases, there will be a similar degree of foreshortening effects, and in neither case is all of the chamber interior included within the field of view, although a large fraction is.

Error may also be associated with spectral response and image sensor data processing; regarding these, it is noted that the colour evident in these photographs does not change very significantly, and so this is not expected to make a large difference to the results in these cases.

The distributions of recorded signal are therefore considered to be broadly representative of the distributions of excitation. The overall similarity in this respect is found between instances of the discharge occurring in two different gases, and at currents varying by a factor of five or six. This suggests the characteristic to be a fundamental aspect of the beam mode discharge produced in our apparatus.

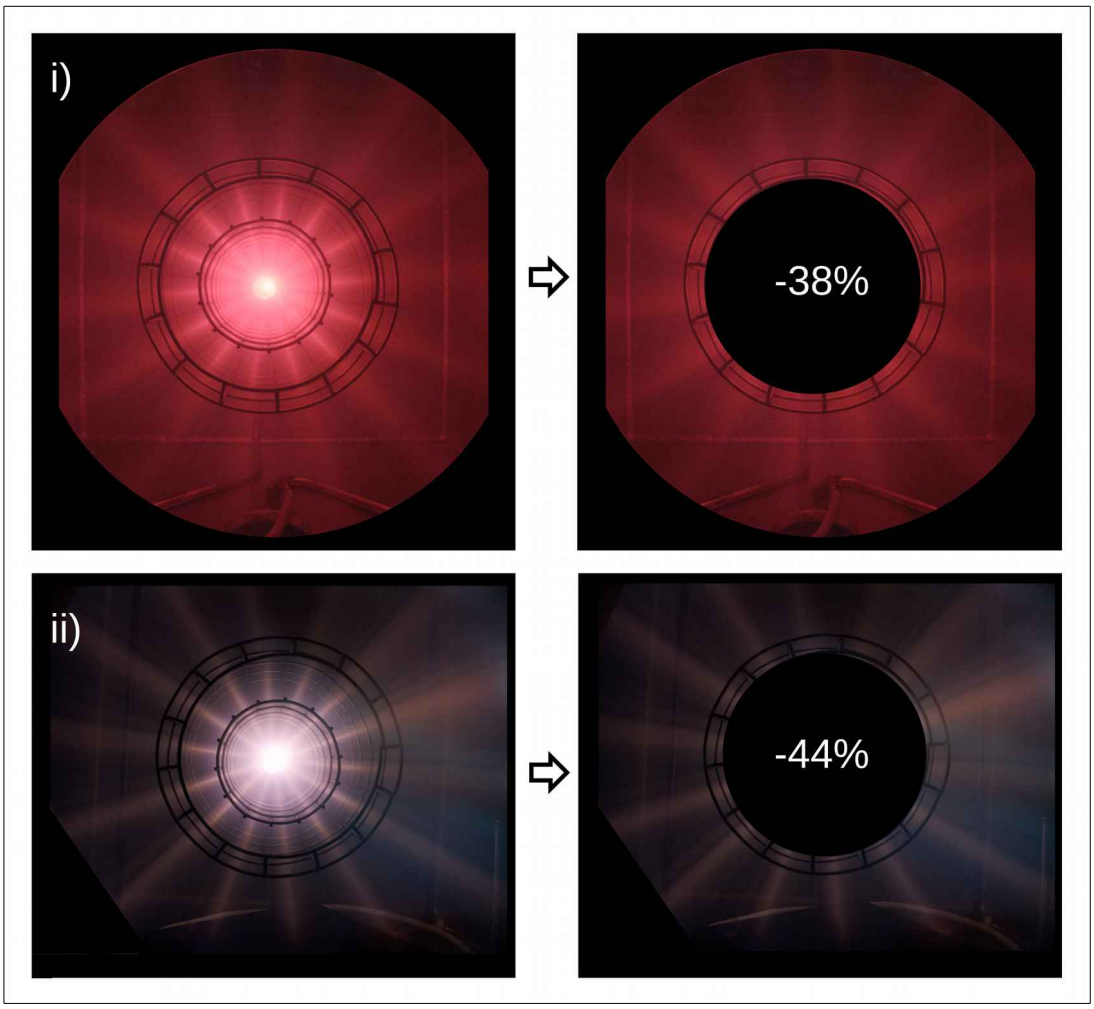

Fig. 74. Reduction in integrated emission levels resulting from the masking of emission from within the anode radius. Images used are of discharges in i) neon, 11.5 mTorr, 3.7 kV, 2 mA; ii) helium, 22.6 mTorr, 8.5 kV, 11 mA.

The distribution of optical emission within the discharge will also bear some relation to the distribution of charge generation by ionisation. To be able to quantify the distribution of this enables an assessment to be made of the relative degree of charge flow occurring in different regions of the chamber, but caution needs to be exercised

in making the link between excitation and ionisation, as also outlined in Appendix 2. For this case, the relevant considerations are as follow.

It was noted that should the energies of principally-active species be close to threshold, levels of excitation might considerably exceed those of ionisation. Any significant difference in the energy dependences for these processes across a wider range of energies might also affect the results, should the energy ranges be disproportionately represented within the areas considered.

As described above, the emission in these discharges is expected to result from ion- and fast neutral-induced processes, from the analysis of spectral content described in Chapter 3. Should both species be contributing to observed levels of emission, the above considerations are made more complicated since these separate processes may represent different relative degrees of ionisation. This will affect the results if not making a similar contribution to recorded levels from the different regions.

The conditions at which ions become sufficiently energetic to cause ionisation and excitation are associated with conditions of relatively high *E/N*. These correspond to the region of the chamber between the electrodes, due to the locally high electric field, and this suggests that the ion-induced emission will occur in this region. The similar colour of emission in other regions suggests this to be caused by fast neutrals.

This will be considered further in the following sections, but for now it is noted that this is likely to be the case, and it is assumed to be so for the purpose at hand. According to this assumption, the emission evident in locations external to the anode radius will represent emission from a flux of fast neutrals travelling outwards to the wall. Emission within the anode radius will also be caused by these neutrals, with an additional component from the ions.

As outlined above, this introduces the possibility of significant error in making an analogy between the distribution of emission and that of ionisation, should the emission caused by ions and neutrals represent different degrees of corresponding ionisation. When the energy-dependences of the cross sections for excitation and ionisation of helium by helium neutrals and ions are considered, these indicate that this may be the case. Fast neutrals are indicated to cause a generally smaller proportion of ionisation than excitation, as compared to these processes caused by ions. These cross sections are shown in Fig. 75. The cross sections for excitation are those to 2^1P, since these are significantly larger than those to other levels.

It should be noted that the extent to which observed levels of emission may be attributed to either species is not quantified, and so the effect of these differences between cross sections is also uncertain.

The results of the analysis in this case are therefore considered to be representative of the degree of excitation that occurs in locations external to the anode but, for the helium discharge at least, these may not be reliably equated with levels of ionisation. Corresponding cross sections for neon have not been found, but values given for argon in [67] indicate much less variation in this respect.

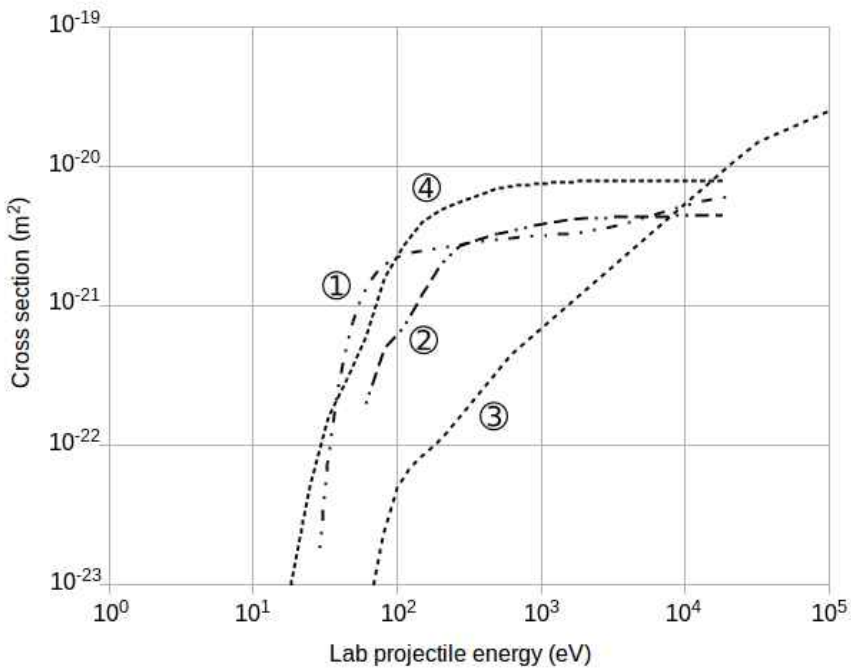

Fig. 75. Cross sections for helium ions and atoms in helium; ion-impact processes of ① ionisation[82], and ② excitation to 2^1P [87]; fast neutral-impact processes of ③ ionisation [81], and ④ excitation to 2^1P [88].

To briefly return to the issue of the current distributions that may be expected to result in the currents collected at the anode and the radial collector; it was noted previously that these both show a quite consistent proportionality with cathode current, and that their respective locations and areal projections suggested that these collected currents may represent intercepted fractions of the same radial flux. This however seemed inconsistent with the degree of current growth projected to occur between the respective radial positions of these collection points.

Upon consideration of the characteristic distribution of emission occurring along the axial length of the chamber during operation in the beam mode (Fig. 76), the apparent discrepancy is explained in terms of the significantly anisotropic nature of this distribution. The degree of emission in the region surrounding the electrodes is considerably greater towards the mid-point of their axial length, and correspondingly significantly smaller towards the end, where the radial collector was located. Since levels of emission will bear some relation to ionisation, this means the current density incident upon the radial collector may be expected to be smaller than the average, and the estimation of overall levels of radial flux will be correspondingly too small.

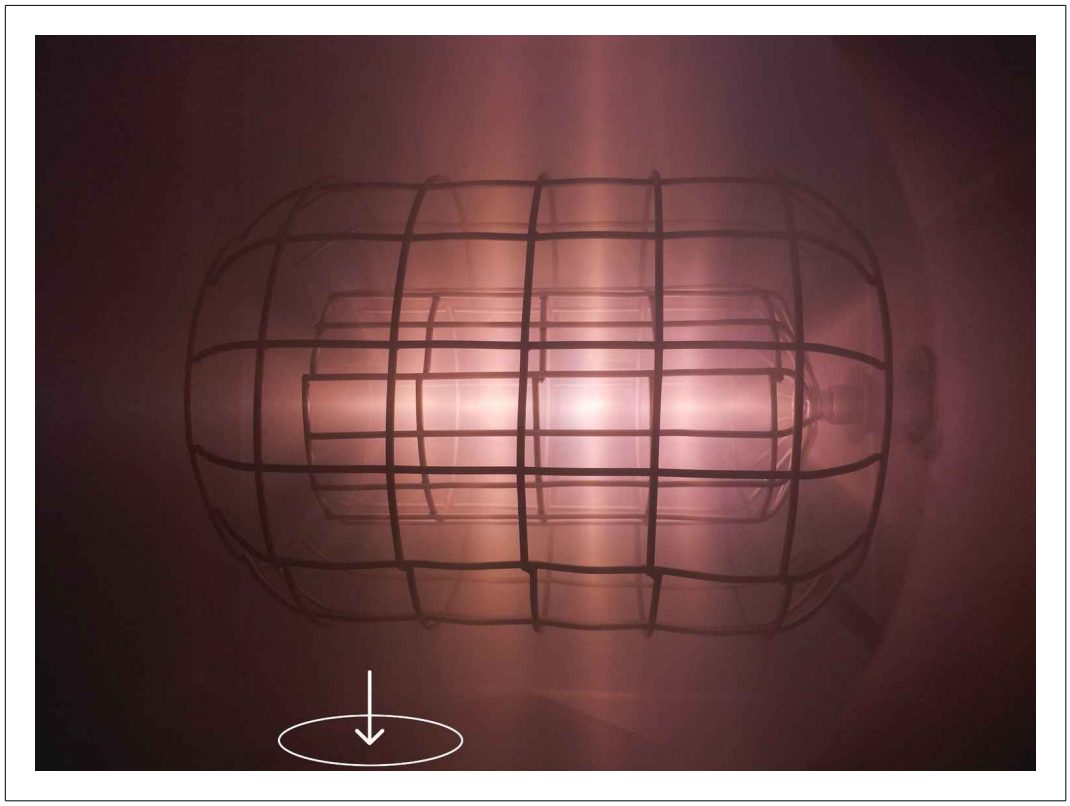

Fig. 76. Photograph of beam mode discharge in helium at around 30 mTorr. The approximate location of the radial collector is indicated by the white ellipse; this is out of frame, as indicated by the arrow

5.2.3 Physical dependences upon electrodes

The defining characteristic of the beam mode plasma is the arrangement of radial beam-like lines of emission. In this section, the reasons for the occurrence of this pattern are examined, by considering the potential distribution within the chamber, and by observing the effect of altering the arrangement of the electrodes.

5.2.3.1 Rotation of cathode

In published accounts of spherical 'star' mode discharges, the spatial distribution of the radial beams is described to be coincident with the cathode apertures. Factors to which the formations of these is attributed include an electrostatic lensing effect, as described above, caused by the distortion of potential surfaces surrounding spherical grid cathodes [21]. In these cases, the focussing effect is exerted upon particles exiting the electrode. During the experimental rotation of the cathode in a star mode discharge, the locations of beams are found to follow those of the cathode apertures [42], showing an association to exist between star mode beam formation and cathode geometry.

In order to observe the relative importance of the potential surfaces surrounding the anode and cathode for the formation of the beams of the beam mode, the effect of altering the alignment of the apertures of these electrodes was observed. This was accomplished by the rotation of the cathode relative to the anode, so as to cause the apertures of each grid to become misaligned with those of the other. This constitutes an angular displacement of the electrodes, and is referred to as such in the following.

The form of the discharge obtained with angularly-displaced electrode apertures was found to be essentially similar to that seen in the aligned set-up. Significantly, the azimuthal distribution of the beams is found to follow that of the anode apertures in this case, showing that in the presence of these two grids the beams are associated with the geometry of the anode, rather than that of the cathode. Fig. 77 shows the form of the discharge obtained with i) aligned and ii) angularly-displaced grid apertures.

Analysis in Chapter 3 indicated emission from the beams in helium to be associated with ion and neutral activity, and this finding is expected to be representative of the mode occurring in all species. The beams are therefore expected to contain ions that are accelerated in a radially-convergent direction across the inter-electrode potential fall. That the locations of these beams follow those of the anode apertures is significant, since it both agrees with this interpretation, and also suggests the anode apertures to be principally important for beam formation.

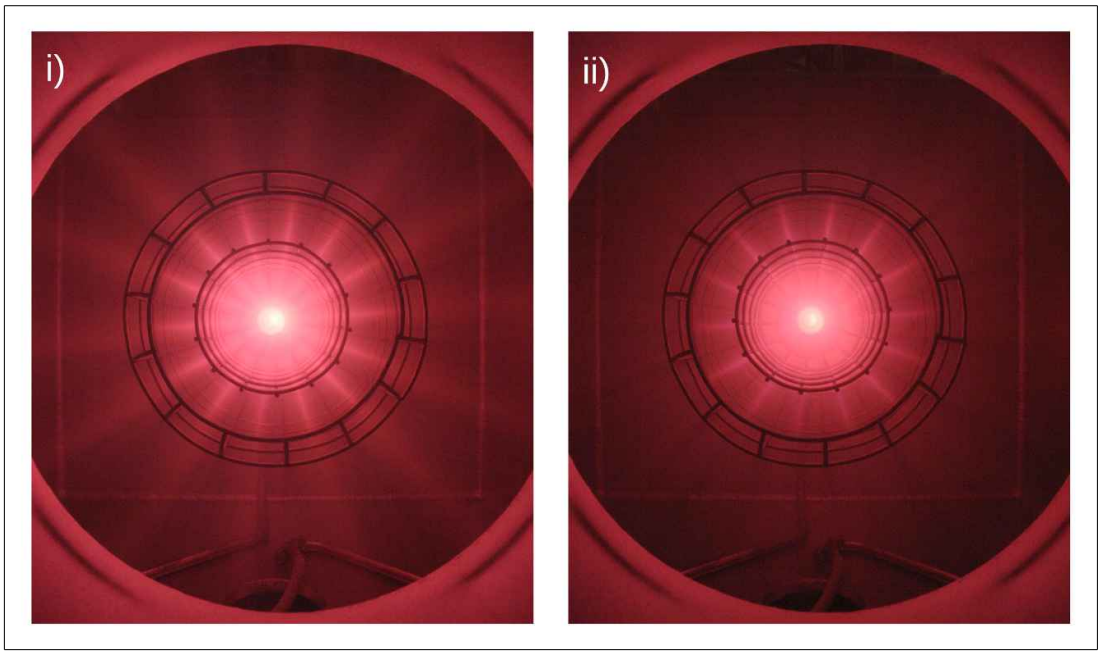

Fig. 77. Beam mode in neon with electrode apertures i) radially aligned, and ii) angularly displaced, showing beams to remain coincident with anode apertures. In ii) it can be seen that an effect of the displacement is to curtail the extension of the beams to large radius. Photographs taken with Canon DSLR

From consideration of the photographs in Fig. 77, the angular displacement of electrode apertures can be seen to have various effects upon the pattern of emission. These include an apparent reduction in the radial extent of the beams, affecting emission in locations external to the anode radius.

These photographs were taken using identical exposure settings on a mounted DSLR camera, to maintain consistency in composition and photo-sensitivity, whilst the discharge was operated at conditions of similar pressure and current. Levels of brightness recorded in the photographs should therefore bear a similar relation to the luminosity of the discharge, and so meaningful comparison may be made between them.

Emission levels recorded in these photographs were quantified in a similar fashion to that described previously. Instead of comparing different areas of the same frame however, similar areas of the two different frames were compared. With extraneous signal from chamber port reflections masked, the total signal recorded in each image was integrated and the two compared. This was then repeated for the emission occurring in regions both within and external to the anode radius.

The regions of the images used are shown in Fig. 78, with relative levels of emission in the rotationally-displaced set-up expressed as fractions of the levels recorded in the aligned images. A general reduction in emission evident in the misaligned case is found to disproportionately affect the diffuse emission occurring at radii larger than that of the anode. Emission in this region becomes noticeably more azimuthally isotropic when the electrodes are rotationally displaced, and so the reduction in emission associated with the misalignment of the electrodes may be observed to principally affect the diffuse beams evident in the region surrounding the anode.

Interestingly, the voltage required to drive 2 mA in the set-up with aligned electrodes [i.e. the discharge in Fig. 77 i)] was around 3.7 kV, whereas with the angularly-displaced electrodes it was 4.5 kV; some 20 % greater (at pressures of around 11.5 mTorr in neon). This suggests that the change in the distributions of emission also reflects a change in the efficiency of charge generation within the chamber. According to the theory that the emission at larger radius is caused by fast neutrals, the difference in this respect suggests this to be accompanied by a significant degree of ionisation, and that this is also an important source of ion current drawn to the cathode.

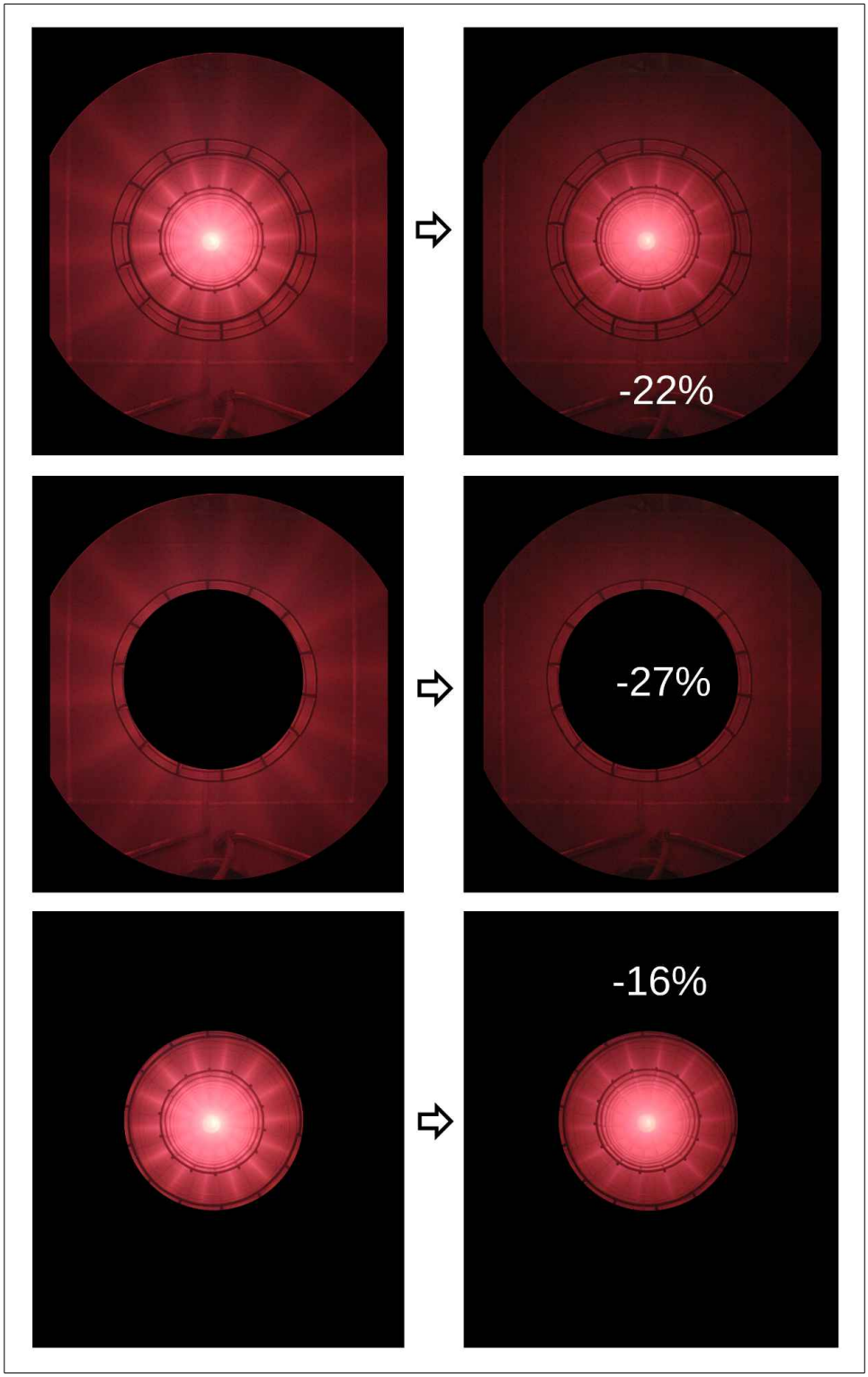

Fig. 78. Regions of the images from Fig. 77 used for analysis of recorded emission levels, with results of the analysis shown as fractional change in levels from the misaligned set-up (RHS images) relative to the aligned case (LHS).

5.2.3.2 Further modification of electrodes

The experiment described above, in which the cathode was rotated so as to cause its apertures to become misaligned with those of the anode, indicated the formation of the beams to be associated with the location of the anode apertures. The pattern of emission evident in the misaligned set-up was found to be consistent with the obstruction of beams by the cathode, with the beam formation mechanism otherwise apparently insensitive to the orientation of the cathode.

This was tested further by the replacement of the grid cathode by a solid stainless steel cylinder of similar dimensions. Fig. 79 i) shows this arrangement of electrodes.

Beams were also found to form in the set-up using the solid cathode, as shown in Fig. 79 ii). This shows conclusively that these beams are not only formed by the effect of the anode apertures, but also that their formation has no critical dependence upon the perforation of the cathode.

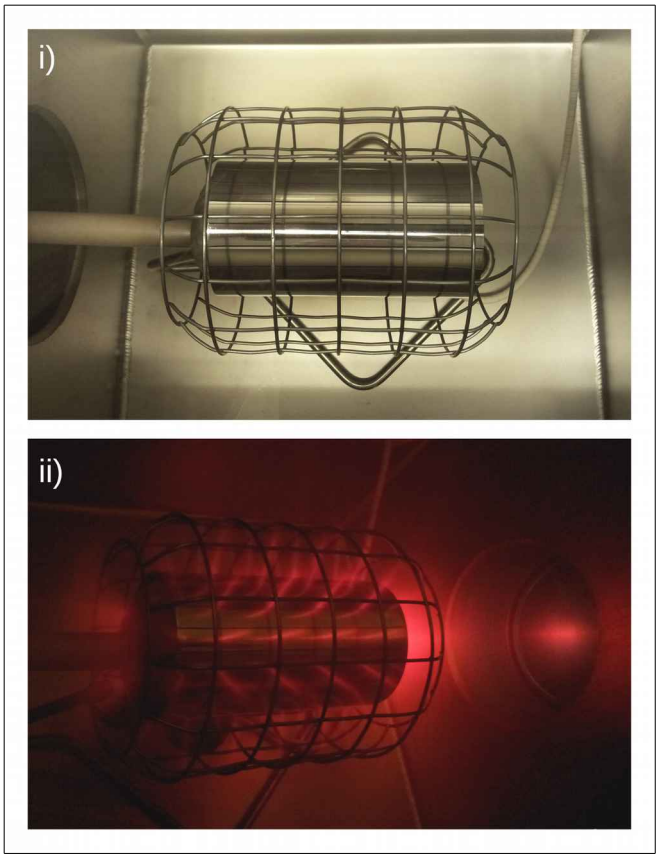

Fig. 79. Beam mode discharge with solid cathode. i) electrodes; ii) resulting discharge, in neon

One final experimental modification of the electrode set-up was made, involving the simple removal of the anode grid, with just the grid cathode remaining in the chamber. This was found to result in the complete absence of visible radial beams.

The discharge that occurs with the anode grid removed was noted above to show no signs of the beam formations. A detailed description of this discharge is not provided here, but it is noted that at the conditions of relatively low pressures and high voltages with which the beam mode discharge is associated, the colour of emission evident from a helium discharge indicates the plasma produced in this arrangement to also contain energetic populations of ions and neutrals.

5.2.4 Energetic hydrogen in beam mode discharges

Measurements made of some properties of the radial beams have been described previously; in Chapter 3, spectrally-resolved light from these was found to correspond to the emission structure characteristic of ion- and neutral-impact excitation. In the course of making such observations, the hydrogen Balmer-alpha spectral line at 656.3 nm (H-α) has been frequently observed to appear in emission spectra from beam mode discharges. The line may appear relatively bright within the spectrum, as may be seen in the argon spectra shown in Fig. 34. It has been observed in discharges occurring at conditions of pressure corresponding principally to the beam mode operating range, in helium, argon and neon. The hydrogen-beta line (H-β) at 486.1 nm is similarly observed.

Over some hours' operation the hydrogen emission is noted to become less bright. This variable intensity suggests an element of the hydrogen concentration in the chamber to be associated with desorption from contaminated vessel surfaces, as well as any degree of impurity introduced with the backfill. The gases used for this are high purity, and any contamination will be of the order of small fractions of 1 %. It is however difficult to relate the observed intensity of emission to such quantities, since this would require a detailed understanding of the collisional-radiative processes operating in the discharge, and also the dependence of these upon a varying balance of impurities. This is beyond the scope of this study.

At some conditions, the H-α spectral line has been observed to show a Doppler-shifted profile. This is interesting because the effect is caused as photons are emitted from a moving particle, with the velocity directly affecting the degree of observed shift. Analysis of measurements may therefore determine this velocity, and so constitute a direct measurement of the kinetic energy of the hydrogen. The phenomenon has therefore been the subject of some attention, and observations are presented below.

5.2.4.1 Doppler-shifted H-α spectral line in beam mode emission

When viewed along the line of a radial beam in a beam mode discharge in helium, the H-α line appears to show a clear, excessively Doppler-broadened profile that is observed to become progressively more shifted at increasing voltages [Fig. 80 i)]. Possible confusion with the He II line at 656.0 nm is eliminated, by comparison of the central unshifted wavelength with that of the H-α line appearing in non-helium discharges. These wavelengths are found to be the same in spectra obtained in

different species using the same equipment, and so the identification is made independent of spectrometer calibration. The spectra shown in Fig. 80 i) were obtained using the FHR1000 spectrometer and PM tube. These results were obtained by averaging several scans made with integration times of several seconds per point, taking around half an hour for a complete capture. With the power supply running in current-limited mode, the voltage was held constant as far as was possible for the duration, by making small adjustments to gas flow.

The phenomenon could not be reliably detected in neon; when using the Andor ICCD camera, apparent hints of a signal could not be resolved from noise, and these were not clarified by repeated accumulations. An unshifted line at 656.3 nm was clearly evident however. Similar difficulties were encountered in argon, although it was found possible to record Doppler wings of a much lower intensity relative to the central peak, as compared with those in helium. The best results were obtained using the ICCD camera, making several hundred accumulations of half-second exposures; these are shown in Fig. 80 ii). These show a much greater shift for comparable voltages to those in helium, and were only observed at conditions having generally low cathode voltages.

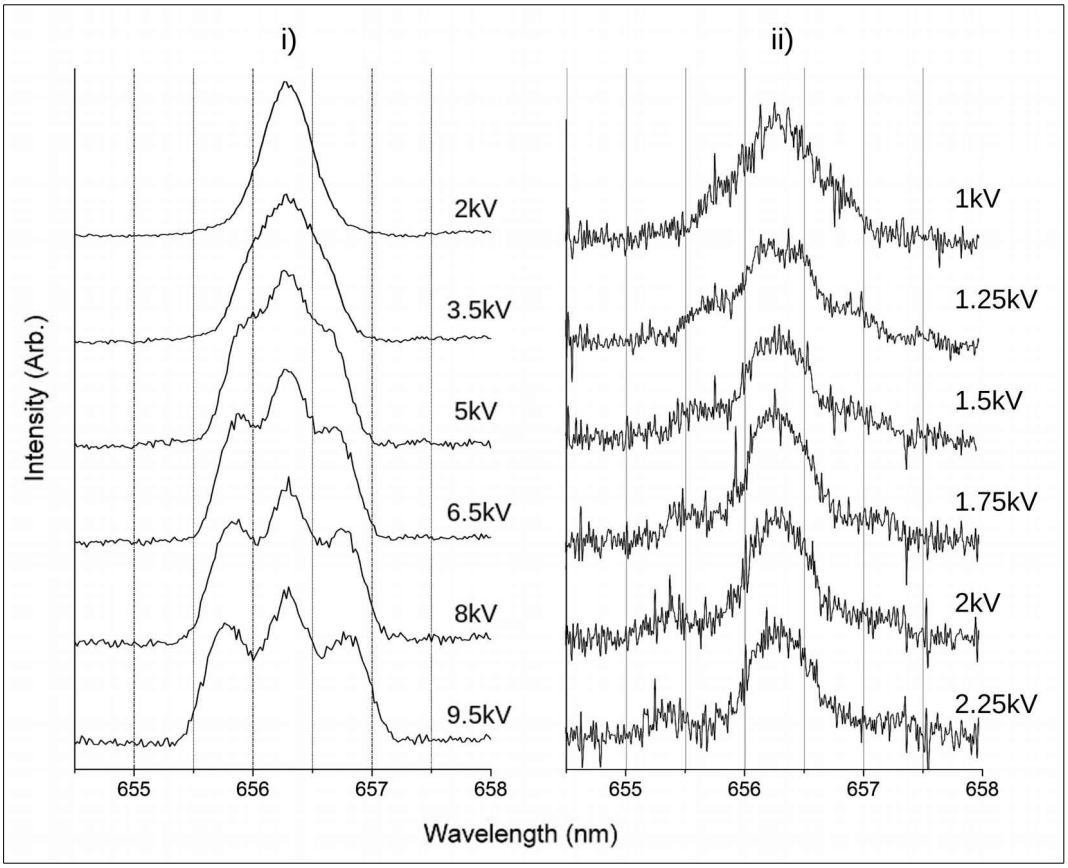

Fig. 80. Doppler-shifted H-α spectral line observed at different voltages in i) helium and ii) argon discharges. Profiles were recorded at different spectrometer settings and so are not to scale.

The spectra were fitted with Gaussian profiles to determine the degree of Doppler shift, as shown in Fig. 81. The cumulative curve obtained by addition of the three peaks fitted is found to be a good match for the measured profile, indicating the signal to originate from a considerably mono-energetic population of emitters. The energy of the fast hydrogen emitting the radiation, ε_H may then be calculated using

$$\varepsilon_H = \frac{1}{2} m_H \left(\frac{\Delta \lambda \, c}{\lambda} \right)^2 \tag{5}$$

in which m_H is the mass of the hydrogen, c is the speed of light, λ is the unshifted wavelength and $\Delta\lambda$ the Doppler shift.

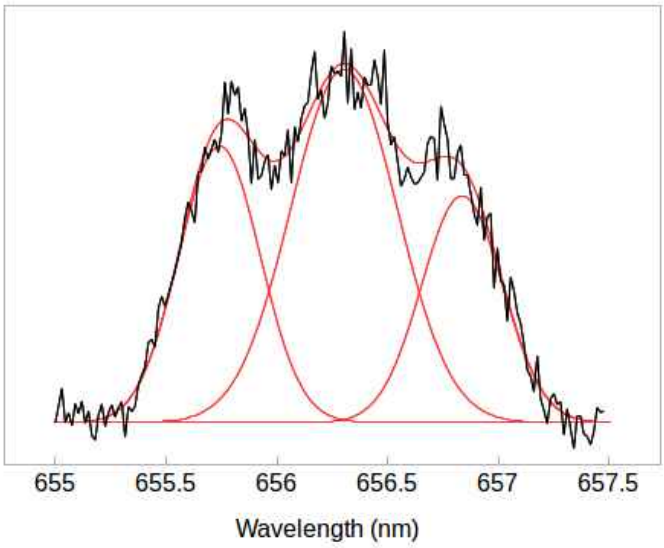

Fig. 81. Doppler-shifted H-α line from 10 kV helium discharge, fitted with three Gaussian profiles

The energies calculated for the spectra shown in Fig. 79. indicate the hydrogen to be very energetic in the argon discharges, relative to the cathode potential. These are indicated to to rise to around 50 % of cathode potential (Fig. 82).

The implied energies in helium correspond to a very much smaller fraction of cathode voltage. These are also shown in Fig. 82, as calculated for the spectra in Fig. 79. In both cases, the energies appear to represent a rising fraction of cathode fall at lower voltages within the range, which then remains at a relatively constant value. This behaviour is clearer in the results from helium discharges, for which this fraction is around 3 % of cathode potential.

Spectral lines emitted from the parent species were examined for evidence of any further Doppler-shifted profiles, but none were identified. From (5.1) the degree of Doppler shift will be smaller for heavier particles having the same energy, and such shifts are indicated to be small for energies attainable in argon discharges.

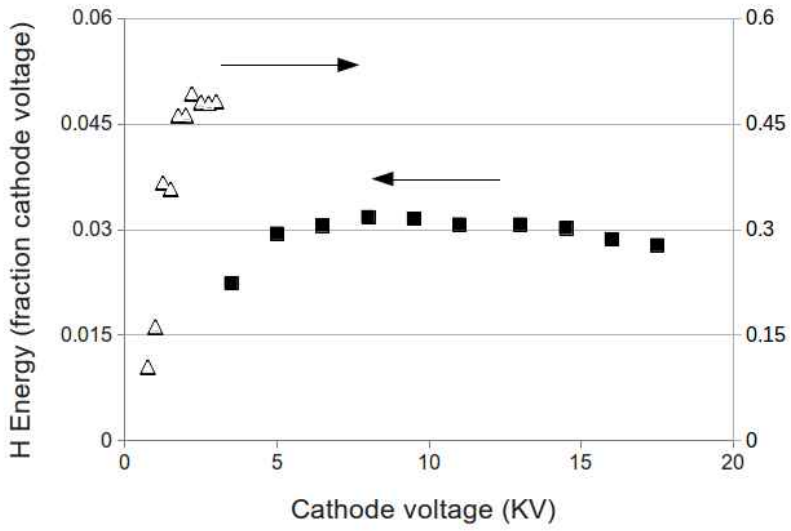

Fig. 82. Energies of atomic hydrogen indicated by Doppler shift, expressed as fraction of cathode voltage. Open triangles, in argon; closed squares, in helium. The scale for energies in argon is 10x that for helium.

As an example, for helium, the magnitude of Doppler shift that would be expected in light emitted at at 587.6 nm by a neutral having an energy of 1 keV would be smaller than 0.5 nm. The line-widths observed are considerably larger than this, and so even if a degree of shift were to affect these it would be difficult to deconvolute from other factors influencing the profiles, such as Stark broadening in the strong electric field. Given the relatively-large contribution expected to be made to observed spectral line intensities by the effects of radiation imprisonment, as outlined in the Discussion section of Chapter 3, any Doppler-shifted element of the emission may also be expected to be of a much smaller intensity than the unshifted component arising from this process, which would make it much less obvious still.

These results are considered significant, since they demonstrate the existence of fast ionic and neutral species within the discharges. The phenomenon was further investigated for evidence concerning the dependence of the signal upon spatial location within the chamber. In the making of further observations it was decided to concentrate upon the helium discharge, since the signal was easier to record and analyse.

5.2.4.2 Radial and axial dependence of H-α emission

Further observations of the H-α profile evident in light emitted from helium discharges were made from an axial perspective. The spectra shown in Fig. 80 and Fig. 81 were all obtained using an optic fibre aligned as far as was possible with a radial beam; in these measurements the Doppler-shifted wings appear to be quite symmetrical, although some slight accentuation of intensity of the blue wing is consistently observed. When viewed from the axis of the discharge however, the emission at 656.3 nm is quite different. A Doppler-shifted H-α line is still evident,

and the wings appear to show a similarly degree of shift; the intensity of the blue wing however appears to be reduced by around half, and that of the central peak increased by a factor of roughly four. Examples of these different line-shapes, as are evident using identical spectrometer settings at similar discharge conditions, and plotted to the same scale, are shown in Fig. 83.

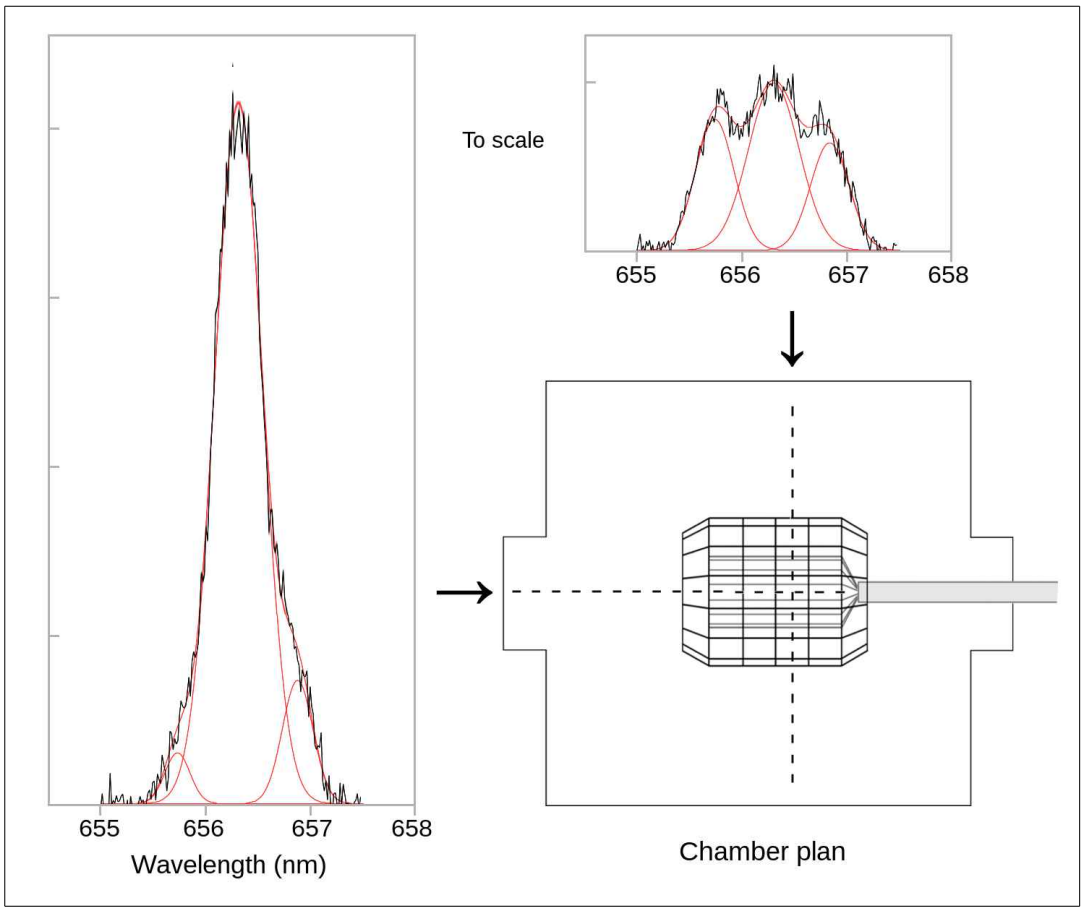

Fig. 83. Examples of H-a spectral line as viewed from axial and radial perspectives. The spectra are shown to scale, and are representative of relative collected intensities at similar operating conditions.

Observations of a Doppler-shifted H-α line, appearing in a glow discharge and having wings of similarly-asymmetrical intensities are described in [89]. In this work the influence of reflected light is considered, and it is noted that observations of e.g. the red-shifted emission from an emitter moving away from the observer will be accompanied by any component of the forward-directed, blue-shifted light that is reflected back from the chamber surfaces. A degree of such reflection will therefore result in the observation of both red- and blue-shifted wings from a uni-directional emitter; in conditions of perfect reflectivity, these Doppler wings will be of identical intensity.

The experimental set-up in [89] involved a highly-polished cathode, the reflectivity of which was a consistent and measurable quantity. Conditions in the TCD chamber are less consistent in this respect; after an argon discharge, interior surfaces are

generally covered with freshly-sputtered electrode material, whereas after operation in helium the surfaces tend to become considerably darker. Surfaces that will reflect light are also less uniform in nature; these will be various combinations of walls, ports and the electrode assembly when viewing from either perspective. A deconvolution of reflected components in these spectra is therefore not attempted. The principle however indicates the observed asymmetry between red- and blue-shifted wings in the axial line-shapes to be consistent with emission resulting from a particle flux directed exclusively away from the line of sight, given a reflective albedo of around half. Should any component of the blue-shifted wing be produced directly by emitters moving towards the point of view, then the albedo is required to be smaller.

According to the above observations, and assuming at least some degree of reflectivity to be affecting the observed line-shape, the Doppler-shifted H-α light as viewed along the axis is indicated to be emission resulting from a predominantly unidirectional flux of fast particles. The relatively-greater intensity of the red-shifted wing identifies this flux as being directed away from the point of view.

The Doppler-shifted H-α light observed from a radial perspective shows a similar degree of shift to that observed axially, and so is expected to be produced by similar processes. The reflective albedo will be of similar order along axial and radial directions in the chamber, and so the obvious interpretation of the more symmetrical profiles obtained radially is that these correspond to a superposition of signal from both the proximate beam and the one on the opposite side of the electrodes. This symmetry is of course missing for the axial perspective. By the same analogy to the processes operating axially, the direction of travel of emitting particles in the radial beams is expected to be converging towards the axis of the discharge.

These considerations offer a satisfactory interpretation of the different relative intensities of red- and blue-shifted Doppler wings when viewed from axial and radial lines of sight; the Doppler-shifted emission is indicated to result from a population of fast hydrogen travelling along the axis of the discharge towards the cathode, and also a population travelling in a radially-convergent direction in the region of the chamber surrounding the electrodes.

If viewed perpendicular to the direction of travel, the wavelength of light emitted from these fluxes will be unaffected by the particle velocity, and so will appear unshifted to the observer. This suggests interpretation of the intensity of the unshifted peak, as viewed from one perspective, to be caused by the flux that produces the Doppler-shifted emission when viewed from the other. The relatively larger intensity of this central peak as viewed axially would correspond to the accumulated emission from the series of convergences of radial beams that occur along the axis of the cathode.

However, further consideration of the Doppler-shifted radial profiles indicates that this interpretation of the relative height of the central peak may not be correct; reasons for this are outlined in the following.

5.2.4.3 Spatial distribution of radial H-α emission

The measurements made from a radial perspective are of light collected from along the line of a beam, and therefore these levels are representative of emission integrated along the beam-length. The measurements were made using an optic fibre held close to a viewport, with no additional optics used, making the resulting angle of acceptance relatively large. The value for this given by the manufacturer (Ocean Optics) is 25.4 degrees [90]. An idea of the effect of this is given by shining light down the fibre and observing the size of the spot of illumination projected; this is eight or nine cm in diameter at the opposing chamber wall. The effect that this geometry will have upon the degree of light collected from sources other than the beam the fibre is aligned with is illustrated in Fig. 84. This shows a substantial component of light collected by the fibre to be expected to originate from other beams, and also that a disproportionately-greater element of this extraneous light will originate from the opposite side of the electrodes. This seems likely to be the reason behind the slightly greater intensity of the blue-shifted peak in the radially-obtained profiles, as compared to the red-shifted one.

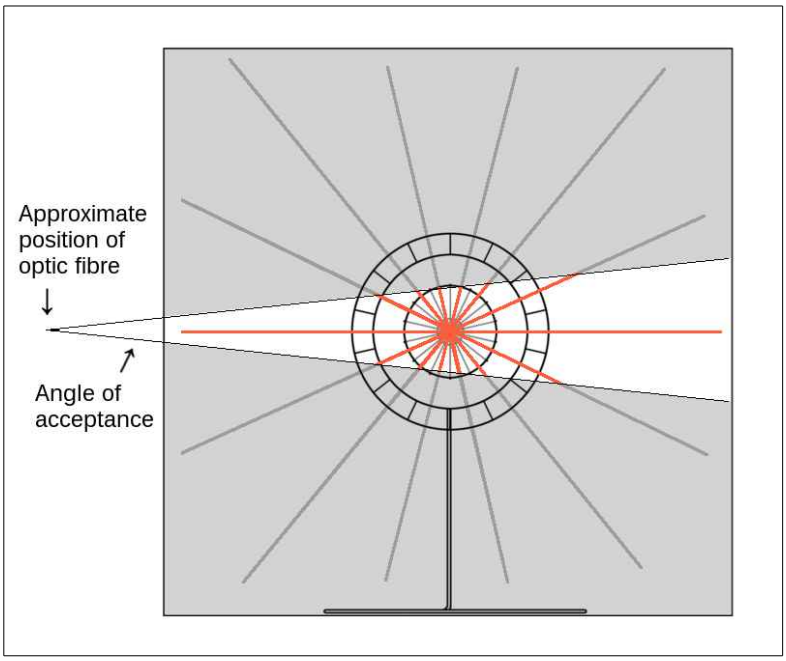

Fig. 84. Diagram showing the approximate angle of acceptance of the optics used to collect the Doppler-shifted light. Portions of beams that fall within the cone of acceptance are highlighted.

The fitting of Gaussian profiles to the Doppler wings has indicated a substantially mono-energetic population to be causing the emission. This implies that the majority of the Doppler-shifted light is collected is emitted by particles travelling not only at a similar velocity, but also in a similar direction, relative to the line of sight of the fibre. It seems reasonable to assume a good degree of radial symmetry to hold for conditions surrounding the electrode axis; aside from the geometry of the electrodes, the patterns of emission from the discharge indicate this to be generally so. From this, it follows that the emission collected by the fibre that is sourced from an increasingly smaller radius will be expected to increasingly represent a superposition

of variously Doppler-shifted components, corresponding to the different angular components of velocities relative to the line of sight.

Elements of beams indicated to fall within the fibre's angle of acceptance by the geometry illustrated in Fig. 84 include considerable fractions of the neighbouring set of beams; most of the emission from these occurring within the anode radius will be expected to contribute to the collected signal. If the emission is produced evenly along the lines of the beams, it can be seen from the diagram that this component will make a contribution around a third of the size of that from the aligned beam. The geometry of the electrodes means that these beams will be angularly displaced from the line of sight by around 25.7 degrees, which will cause the Doppler-shifted light to appear shifted by a factor of $\cos(25.7) \times \Delta\lambda = 0.9 \times \Delta\lambda$. Again assuming an even distribution of emission, the next set of beams are indicated to make a contribution less than half the size of this, which will appear shifted by around $\cos(2 \times 25.7) \times \Delta\lambda = 0.62 \times \Delta\lambda$.

A rigorous analysis is made difficult due to the uncertainties in geometry and effect of reflections, but these figures are expected to be broadly correct. To satisfy curiosity, the spectrum from Fig. 81 was fitted with seven Gaussian profiles, according to the observations above; these were two principally-shifted peaks, then two further at 90 % of the shift and 33 % of the magnitude, and two further still at 62 % of the shift and 10 % magnitude. The height of the central peak was a free parameter. The best fit obtained by hand is shown in Fig. 85, along with the fit produced by software for three peaks shown previously. The red-shifted peaks were all equally scaled to provide the degree of blue-red asymmetry; the best results were obtained using a factor of 0.85 for this.

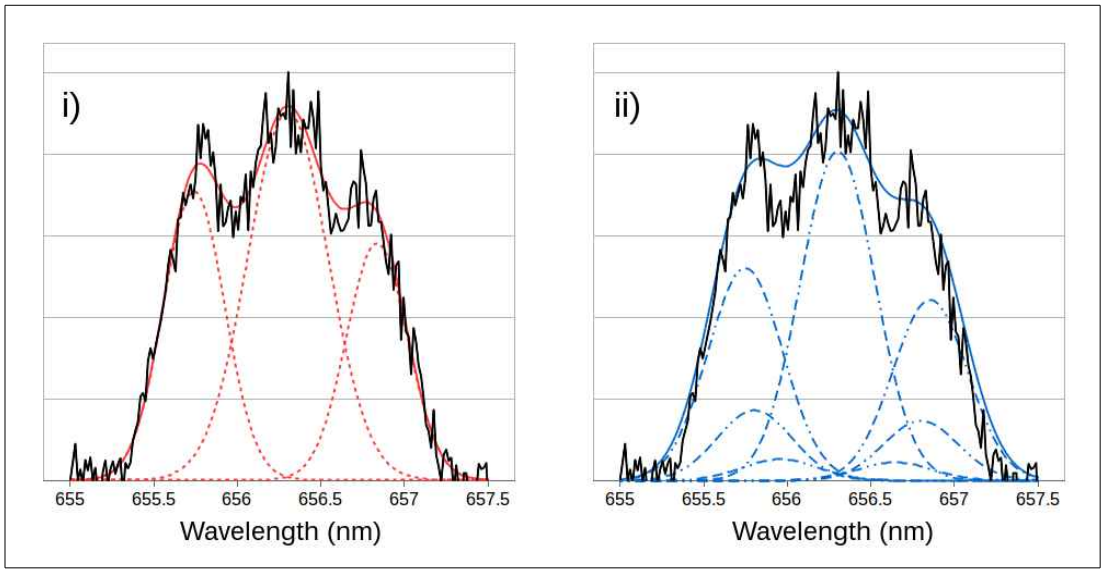

Fig. 85. Doppler-shifted H-α line from 10 kV helium discharge, i) fitted with three Gaussian profiles (as shown in Fig. 81); ii) fitted with seven Gaussian profiles as described in the text

The additional contributions made according to these estimates can be seen to have a generally detrimental effect upon the quality of the fit obtainable. The estimates correspond to the hypothetical situation in which the Doppler-shifted H-α emission is generated evenly along the extent of the beams; the results of the exercise indicate that this is unlikely to be the case, and it is less likely still to be disproportionately sourced from the central region. The analysis rather suggests the emission to be principally sourced from locations having a relatively larger radius.

To return to the question of the relative intensities of the central, unshifted peaks: this is observed to vary considerably between axially- and radially-obtained profiles, and a possible interpretation mentioned above was that the unshifted light evident along the axis might be the same emission that appears Doppler-shifted from a radial perspective. However, the angle of acceptance for the optic fibre, as sketched in Fig. 84, is observed to subtend approximately to the cathode radius at the centre of the chamber. This will be the case similarly for observations made along the chamber axis, and so most of the light collected axially will be from locations having a radius not larger than the cathode. The analysis of the radially-obtained profile suggests very little of the Doppler-shifted light to be produced in the cathode, and so it seems more likely that the unshifted peak represents emission caused by a different process. Furthermore, the interpretation cannot be correct for conditions when no Doppler-shifted peaks are evident; the unshifted line is still visible, for example, throughout the beam mode operating range in neon, and at conditions in argon having voltage levels in excess of 3 kV.

5.2.4.4 Compiled H-α measurements made in helium

Various measurements were made of the Doppler-shifted H-α line in helium discharges; these were made from both axial and radial perspectives, and at conditions of both constant current and various voltages, and constant voltage and various currents. Compiled measurements made from a radial perspective are shown in Fig. 86, and those from along the axis in Fig. 87. The plots may be generally taken to indicate dependence upon current at constant voltage, and on voltage at constant current; where this is not the case, it is indicated as such.

It was generally found to be possible to fit the line-shape with three Gaussian peaks, as shown previously in Figs. 81, 83 and 85. This process is not constrained to set the peaks representing the Doppler wings to be equally spaced from the central peak however, and in a few cases the results of the peak-fitting process showed clearly asymmetrical shifts. This is attributed to noise in the recorded profile upsetting the algorithm used to make the fit, rather than populations having distinctly different energies, and in all cases the average of the two shifts agreed well with the trends shown by other data. The data are presented in Fig. 86 and Fig. 87 as average shifts, with error bars indicating some of the more significant instances of spread between the red and blue shifts as indicated by the peak-fitting process. In many cases this is small enough for the bars to be hidden by the symbols.

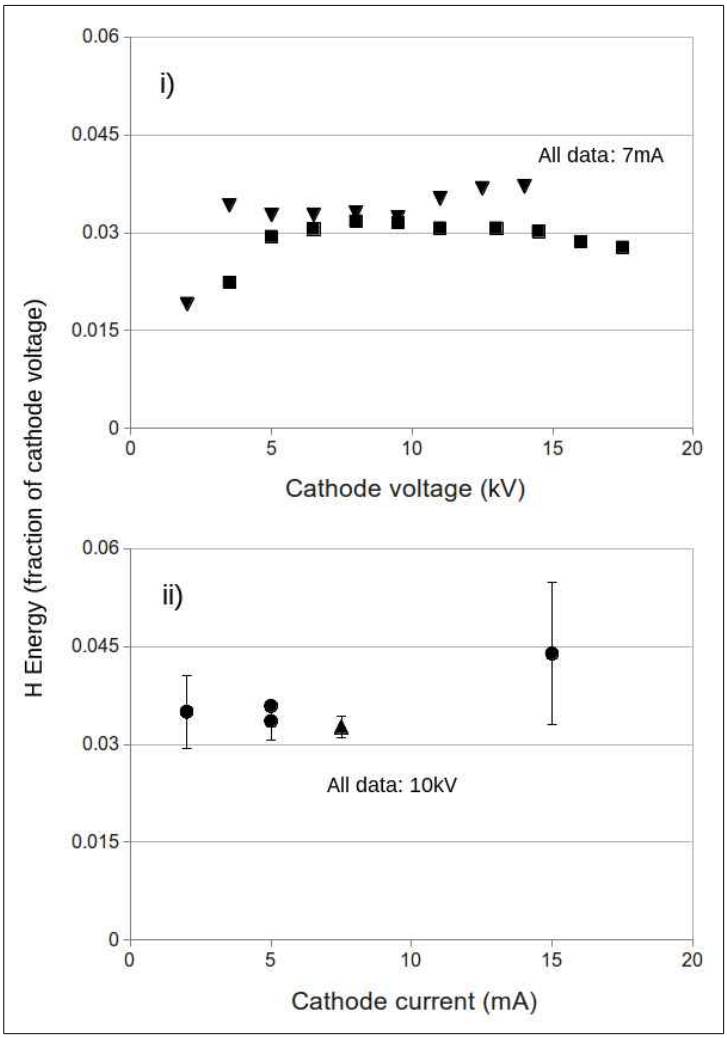

Fig. 86. Compiled measurements of radial hydrogen energy as indicated by Doppler-shifted H-a line in helium, expressed as fraction of cathode voltage. Data is plotted against i) cathode voltage, and ii) cathode current. Different symbols correspond to separate experimental runs; where there is overlap, consistency is maintained between the two plots.

Consideration of the trends in the available data leads to the following observations:

- The measurements made from the radial perspective indicate the energy of the hydrogen to remain a quite consistent fraction of cathode voltage, and for measurements made at one fixed voltage, this shows no clear variation with conditions of different current.
- The measurements made along the axis find the hydrogen energy evident at conditions of increasingly high voltage to represent a fraction of cathode voltage that becomes monotonically smaller. As for the radial measurements, those made at one fixed voltage show no clear dependence upon levels of current.
- All measurements, whether axial or radial, show hydrogen energies to be a few percent of the voltage.

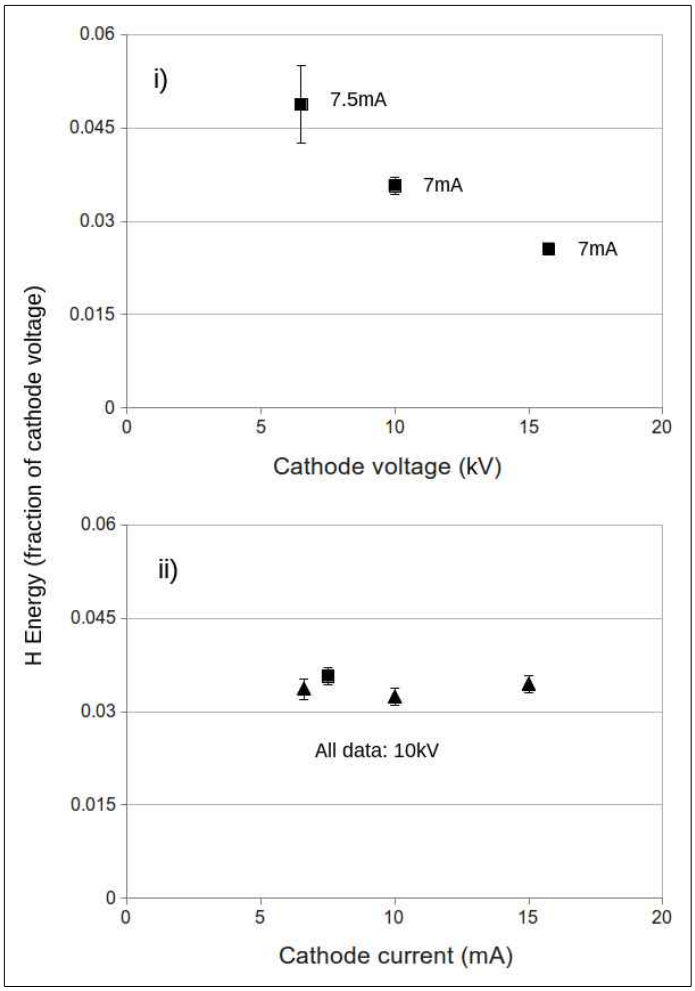

Fig. 87. Compiled measurements of axial hydrogen energy as indicated by Doppler-shifted H-a line in helium, expressed as fraction of cathode voltage. Annotations are as for Fig. 86.

In summary, observations of the Doppler-shifted hydrogen-alpha line in beam mode discharges in helium and argon have shown fast excited hydrogen to be present in these discharges. The hydrogen energies evident vary significantly between these discharges, but appear to show a consistent fraction of cathode voltage in either case. This is around 3 % for helium, and around 50 % for argon. These results suggest the hydrogen energies may not be typical of ion transport more generally, since ion energies will be expected to scale with *E/N* [69]. Possible interpretations of these measurements are discussed in Section 5.3.3.

5.3 Discussion

In the previous part of this chapter, results were described of various experimental observations that have provided some insights into the functioning of the beam mode discharge. Measurements of the distributions of current within the chamber revealed a predominantly-radial electron current, although the appearance of the axial electron beam in beam mode discharges was found to be accompanied by a corresponding

increase in axially-collected electron current. This was noted to imply the potential within the cathode interior to be more positive than that within its apertures.

Analysis of emission distributions indicates a significant element of the processes causing excitation to occur in locations external to the anode radius. The analysis of the beam mode emission structure made in Chapter 3 indicated much excitation to be caused by ions and neutrals, and it was also shown that the conditions at which this may be expected to be most significant will be associated with the regions of strongest electric field within the chamber. The calculated distributions of vacuum potential and electric field also described in Chapter 3 suggest the region of strongest electric field is likely to be found in the region between the electrodes, and these observed characteristics of emission and current flow are consistent with this.

The dependence of the distinctive pattern of radial beams upon the electrode arrangement was experimentally investigated, and this was found to be associated with the anode, showing little dependence upon the form of the cathode. A series of measurements of the Doppler-shifted hydrogen Balmer-alpha spectral line has indicated fast hydrogen to be present in helium and argon discharges, and that the characteristic hydrogen energies are quite different in each case.

The following discussion concentrates largely upon the radial beams that constitute the defining characteristic of the beam mode discharge. A first section is concerned with the inferences that may be drawn from aspects of emission distributions associated with the beams, regarding the distribution of active species causing excitation. The mechanics behind the formation of the beams are then considered, with reference to the vacuum potential distributions within the chamber. The degree of focus apparent in the beams is also considered, and the implications of this for the space charge-induced potential structure located external to the anode explored. A possible interpretation of the measurements of energetic hydrogen within the beam mode discharges is then considered, before a final section addresses how these findings relate more generally to other descriptions of IEC plasmas.

5.3.1 Fast neutrals in the beam mode discharge

In this section, the photographs of distributions of optical emission from beam mode discharges shown previously in Fig. 71 i) and Fig. 73 are further considered. In these photographs, a distinctive shadowing effect was observed to be associated with some of the grid wires, and it was noted that this effect is made apparent by the regular cylindrical geometry of the electrodes. Fig. 71 i) is reproduced as Fig. 88 i), in which the shadows may be seen to be cast in a radially-outward direction, taking the form of straight lines originating from longitudinal members of both anode and cathode grids.

The eclipsed emission is therefore indicated to be caused by an outwardly-directed flux of an exciting species. The straight lines of shadow show no signs of deflection, despite not being aligned with the aperture centres. This would indicate particle trajectories within the flux to be little affected by local electric fields, which is also

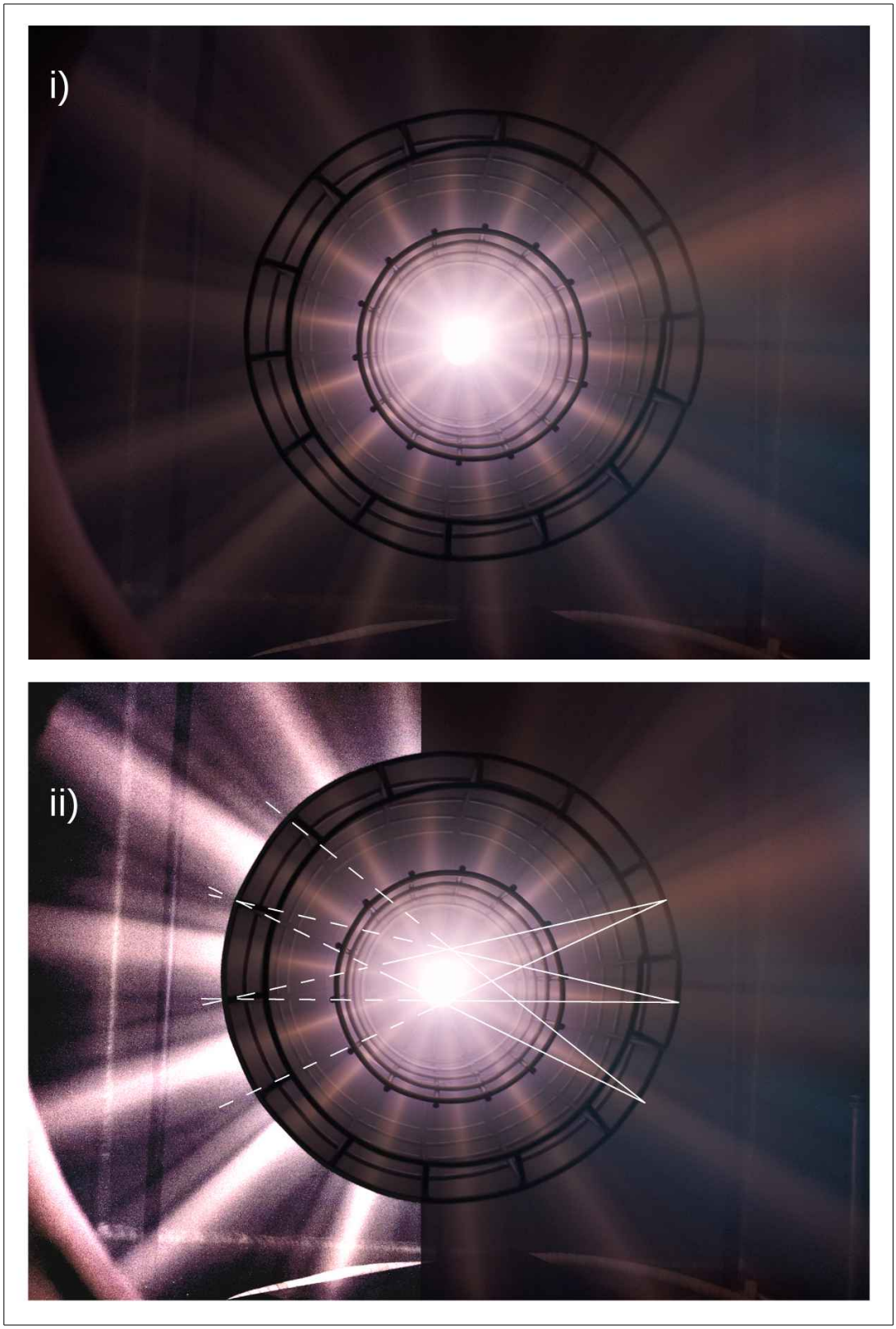

Fig. 88. i) Image of helium discharge, 22.6 mTorr, 8.5 kV, 11 mA, reproduced from Fig. 71; ii) the same image, with contrast levels increased on the left-hand side to clarify the 'double-shadowing' effect from longitudinal members of the anode, and annotated to show the geometry behind this.

suggested by the casting of shadows in a similar direction by electrodes of both polarities. This apparent insensitivity to electric field indicates the exciting species causing the shadowed emission to have no electric charge, and so it may be concluded that the diffuse emission shadowed by the grid wires is caused by a radial fast neutral flux directed outward to the wall.

Another artefact of this grid-shadowing effect is the forming of two distinct shadows from the same longitudinal member of the anode, referred to here as 'double shadowing'. This is less obvious, but may be observed on the left-hand side of the same image. The photograph is reproduced as Fig. 88 ii), with the phenomenon in this area of the photograph made more apparent by enhanced levels of contrast. Lines are also drawn extending the geometry so as to indicate the origin of the flux. It seems clear that the shadows are also cast by the fast neutral flux causing the diffuse beam emission beyond the anode radius, and so their dual nature indicates this fast neutral flux to be radially anisotropic. Rather, it is shown to be composed from a series of individual fluxes aligned with beams located on the diametrically opposite side of the electrode assembly.

This mechanism is illustrated further in the image shown previously in Fig. 73. This image is reproduced as Fig. 89 i), and shows the effect of a misalignment of the electrodes, in which the cathode was displaced relative to the anode. The effect of this was described to separate one or two of the beams into two components, with the radial extent of one component being limited to within the anode radius, and the other continuing to the wall. In Fig. 89 ii), the photograph is overlaid with arrows drawn to illustrate the trajectories of one set of opposing beams. This is consistent with the characterisation of the beams as being composed of both an inwardly-directed ion component, and a counter-streaming fast neutral component originating from the opposing ion beam.

According to this understanding, the splitting of the beam occurs as the electrode asymmetry causes opposing ion beams to become unaligned with each other. The component of the split beam that extends to the wall is the emission caused by the fast neutral flux, whilst the component evident only within the anode radius is be the inwardly-directed ion beam. In the splitting of the beam, this ion component is noted to remain azimuthally aligned with the centre of the anode aperture.

This evidence means the emission that makes up different parts of the beams is considered to be caused predominantly by the activity of ions and neutrals respectively. The accounts of ion transport in [69] indicate this to be characterised by ions losing the majority of their kinetic energy via charge exchange and momentum transfer collisions with the background gas, at all of the pressures of interest for this study. This is because ions have similar masses to neutrals, and so momentum is easily transferred in scattering collisions, and also because of the predominance of charge exchange reactions [69]. In this process, a fast ion captures an electron from a background neutral, and so becomes a fast neutral, leaving a slow ion behind.

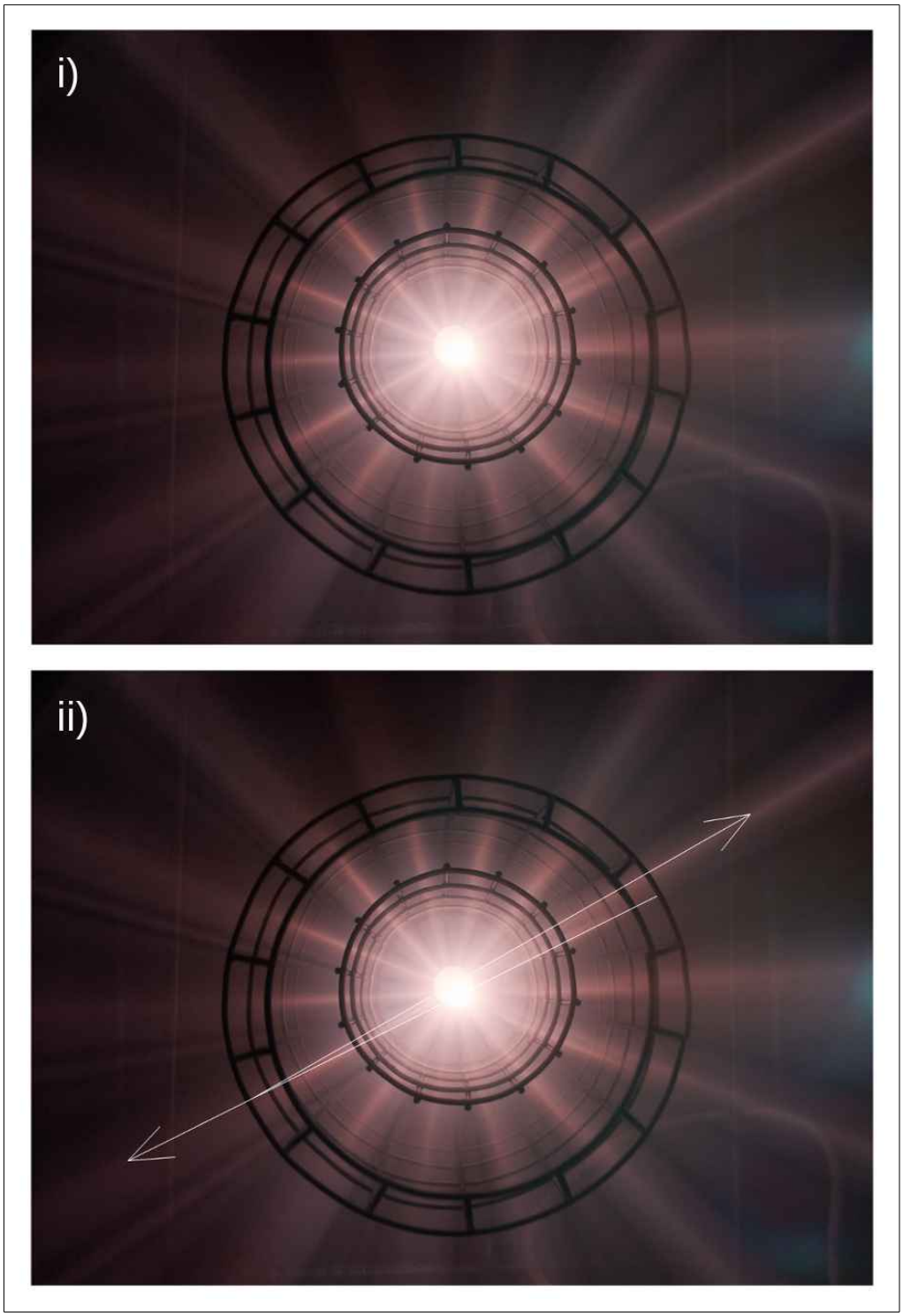

Fig. 89. i) Image of helium discharge, 22.8 mTorr, 15 kV, 12 mA, with cathode displaced radially upwards. An effect of the misalignment may be seen to cause the spatial separation of some beams on the right-hand side of the picture into two components; ii) the same photograph, annotated to show the trajectories of a set of misaligned opposing beams

In Chapter 3, the background conditions of *E/N* associated with the beam mode discharge, and the spectral content of visible emission, were both found to indicate this mode to be sustained by the activity of ions and neutrals. The colour of the emission in both components is observed to be similar. With the production of fast neutrals occurring along the length of the ion beam, their population will be expected to make an increasing contribution to levels of emission along the beam path as it crosses the inter-electrode space. The emission associated with the beams does not appear to be deflected by the cathode, despite the beam passing close to the grid in some cases. This may also be observed in the photograph of the neon discharge in angularly-displaced electrodes in Fig. 77, and suggests that either the beams are effectively space charge neutral at around the cathode radius, or that the majority of the emission at this point is produced by neutrals.

The observations made above confirm the importance of fast neutrals in this discharge. Because these are not decelerated by electric fields, they will transport energy to the walls causing excitation and ionisation to occur along these trajectories.

5.3.2 Radial beam mechanics

In the previous section, consideration of emission distributions external to the anode radius showed the beam-like pattern evident in this location to be caused by fluxes of fast neutrals. Evidence was also found to show these fluxes of energetic neutrals are produced in the transport of ion beams across the inter-electrode region on the opposite side of the device.

In this section, the mechanics of the formation of these ion beams is considered. Experiments described in Section 5.2.3 showed these beams to remain azimuthally-aligned with the apertures of the anode grid, in contrast with accounts of the beams of the 'star' mode discharge in the literature [42], in which the beams are noted to remain aligned with apertures of the cathode. Other accounts of star mode discharges, e.g. [21], associate their formation with an electrostatic lensing effect caused by the apertures of the cathode. In order to investigate the mechanism for the formation of radial beams of the beam mode, vacuum potential distributions for this electrode arrangement are considered in the following.

5.3.2.1 Beam formation

The potential distribution surrounding the electrodes, with no plasma present, was presented previously in Chapter 3, as Figs. 36 and 37. Contour plots of the distributions surrounding the standard electrode arrangement are reproduced in Fig. 90. The distribution calculated for the electrode arrangement without the anode grid being present is shown for comparison in Fig. 91.

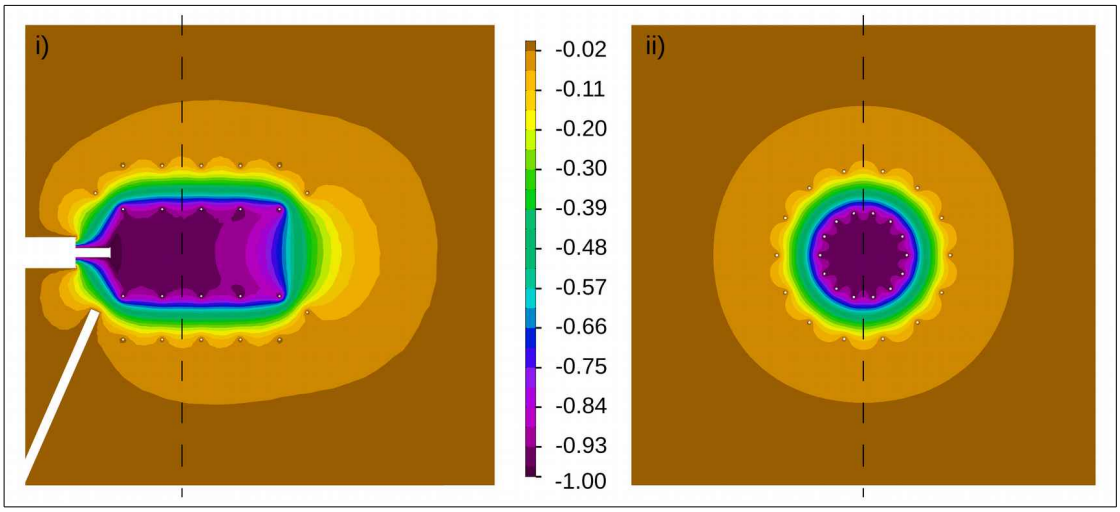

Fig. 90. Potential distribution surrounding the electrodes with no plasma present; contour plots of i) axial, and ii) radial sections. Dashed lines on each indicate the relative position of the plane of the other. Units are fractions of full cathode potential

As noted previously, the majority of the potential fall occurs in the annular region between the electrodes, causing the electric field to be strongest within this region. The effect that the anode and cathode grids have upon the potential distribution is evident as a series of distortions within the vicinity of the apertures, that resemble 'bulges' in the potential surfaces. These are directed away from the region of relatively strong electric field into the cathode interior and the area surrounding the anode, and are clearly associated with the periodic construction of each electrode. The distribution calculated for the electrode arrangement without the anode grid (Fig. 91) is observed to result in a much more even distribution of potential within the chamber.

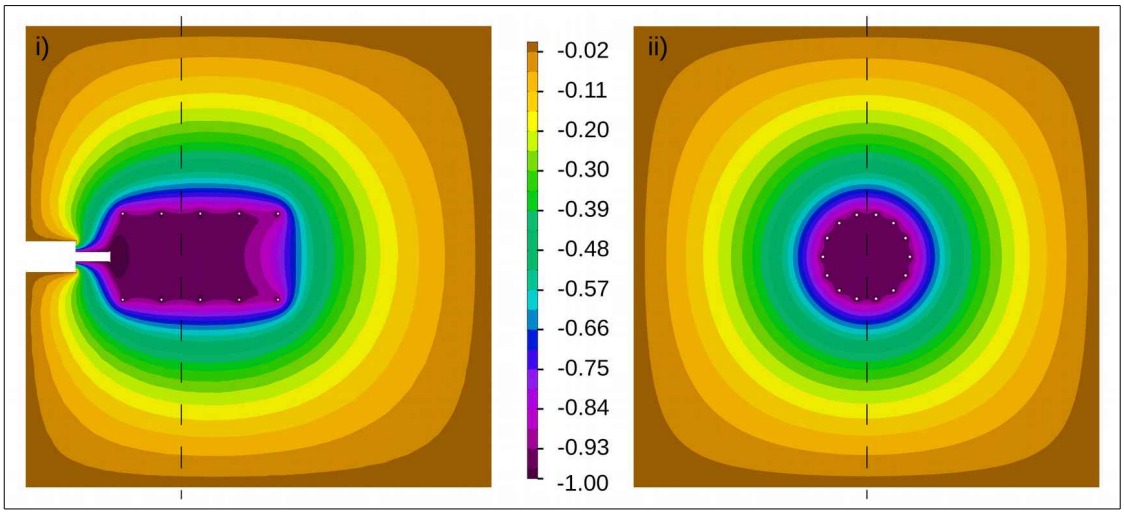

Fig. 91. Potential distribution surrounding the electrodes with no plasma present; contour plots of i) axial, and ii) radial sections. Dashed lines on each indicate the relative position of the plane of the other. Units are fractions of full cathode potential

Charged particles are subject to a force that is aligned with the direction of the electric field, which is normal to equipotential surfaces, such as those illustrated in Fig. 90. This means that the distortion of these surfaces will act as an electrostatic lens for particles drifting across them. According to this principle, the potential surfaces that occur around the anode apertures will act to focus particles flowing inwards towards the axis, and those around the cathode apertures will focus particles travelling outwards. The surfaces around the apertures of the anode are therefore considered to provide the means by which ions travelling inwards are focussed into the beams.

From the contour plots of the vacuum potential distribution in Fig. 90, the surfaces that act to focus the ion flux through the anode apertures are indicated to occur at a magnitude of around 6 % of cathode potential. The modelling software allows for the rendering of a potential iso-surface, and such a surface is illustrated for the 6 % surface in Fig. 92. Consideration of this reinforces the perception of a cylindrical array of electrostatic lenses. It is observed that the potential surface within the axial region located beyond the extent of the electrodes will also act to funnel any ion flux from this region towards the axis.

In contrast to the surface illustrated in Fig. 92, those that occur within the annular inter-electrode region are smooth and cylindrical (Fig. 90), and so beams formed within the lensing regions at the anode radius will continue to experience a degree of azimuthal focussing as they are transported inwards. The narrow contour spacing is indicative of the relatively strong electric field in this region, which will be expected to cause the drifting ions (and the fast neutrals they produce) to become sufficiently energetic for significant excitation of background neutrals and visible emission to occur.

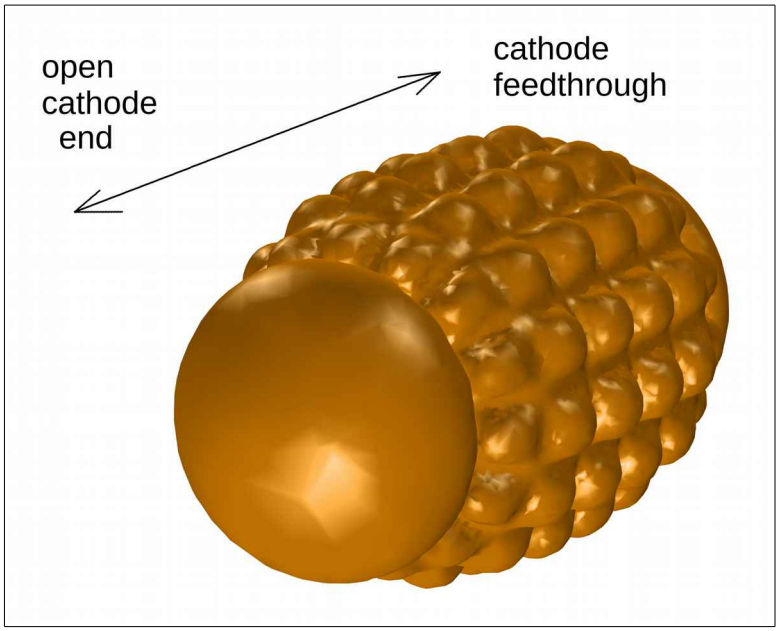

Fig. 92. The equipotential iso-surface within the chamber, with no plasma present, that corresponds to around 6 % of full cathode voltage.

Before leaving this consideration of the effects of the anode, the wider influence of this grid upon the conditions within the chamber is briefly considered. The more even spacing of the contours in Fig. 90 corresponds to a smaller magnitude of electric field, and so the distribution of this is significantly affected also.

This is illustrated in Fig. 93, in which the distributions of electric field are plotted for the cases both with and without the anode grid being present. The effect of the anode grid may therefore be noted to not only cause the focussing surfaces associated with its apertures, but also to significantly localise the distribution of electric field within the chamber, causing the magnitude of this to be significantly increased in the annular region surrounding the cathode. These distributions will of course be expected to be altered, perhaps very significantly, by the presence of the plasma. It is noted however that they represent conditions at breakdown, and the clear association between radial beam formation and the vacuum distribution, for the case with the anode grid, suggests that significant elements of the vacuum distribution may persist during discharge operation in this case. This is considered further in the following section.

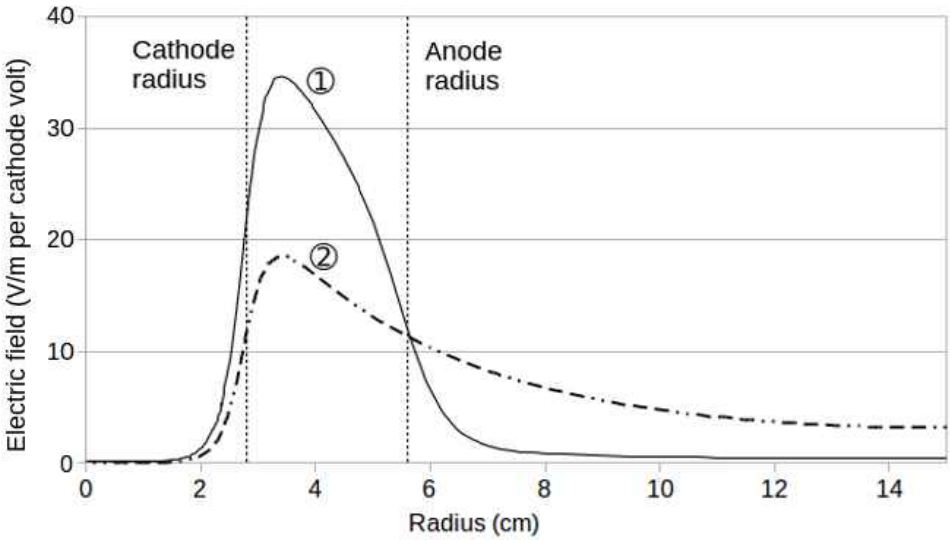

Fig. 93. Vacuum distributions of electric field radially surrounding the electrode axis; with anode grid present; with anode grid removed. The radial line corresponds to the line of intersection between the planes of the potential distributions, as shown in Fig. 90 and Fig. 90.

5.3.2.2 Beam focussing

In section 5.2.3 the azimuthal distribution of the beams was found to follow that of the anode apertures, and the above consideration of the electrostatic lensing properties of the anode apertures has suggested an explanation for how they are formed. This indicates ions in the beams to be transported from a source population beyond the anode radius, which is in agreement with the analysis indicating considerable levels of excitation to occur in this region, since it is reasonable to expect a corresponding degree of ionisation.

The distribution of the component of beam emission attributed to the ions may be seen more clearly in the case in which it has become spatially separated from the counter-streaming neutral beam, as shown in Figs. 73 and 89, and also in the case where the neutrals have been obstructed by the angularly-displaced grids in Fig. 77 ii). Sections of these photographs that show an individual beam in isolation are reproduced in Fig. 94. Interestingly, the beams appear to be well-focussed by the time that significant emission occurs. The relatively well-defined circumference of these beams suggests that a significant fraction of the ions born outside the anode radius may be funnelled into the beam.

A more detailed examination of the potential distribution is made, by sketching lines normal to the contours. These will approximate to the direction of force exerted upon charged particles by the electric field, although actual ion trajectories will be additionally affected by an ion's momentum, and also by any alteration to the local electric field made by space charge. In the limit of momentum limited by many collisions, at conditions of very low current however, trajectories might be expected to follow similar lines. This sketch is also shown in Fig. 94. Comparison between the photographs and the contour diagram in Fig. 94 is complicated somewhat by the degree of foreshortening in the photographs, but the radial extent of bright emission in the beams can be seen to broadly correspond to a location at which the focussing effect close to the centre of the aperture will be mostly complete, but at which a significant degree of convergence is still occurring in the surrounding region. Only those ions arriving at the 6.5 % contour in the region marked 'A' would end up in the bright region of the beam, whilst those arriving within the surrounding region indicated by the label 'B' would remain less well-focussed.

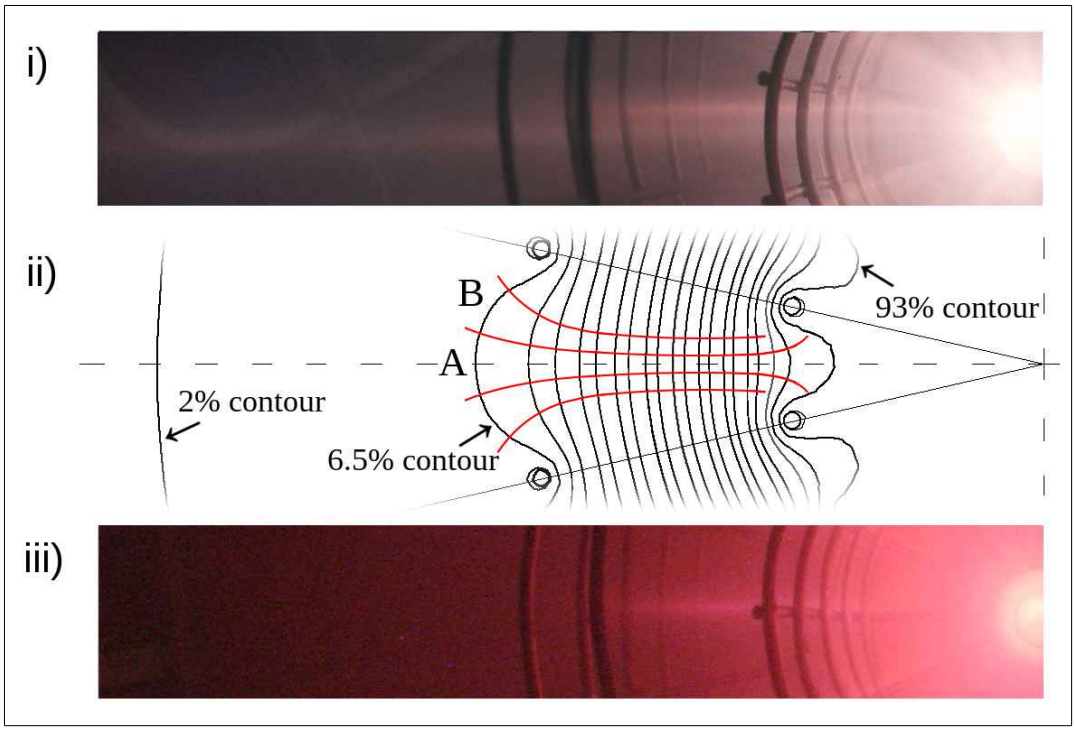

Fig. 94. Photographs of radial beams from discharges having i) translational and iii) rotational misalignment of electrode apertures, with ii) plot of potential contours for comparison.

The relatively-narrow line of bright emission within the beam therefore might suggest the ions in these beams to be sourced from a relatively narrow sector of the region beyond the anode, which would seem to imply the operation of selection mechanisms, such as those discussed in [21], involving a preferential location of ionisation along the beam line. Both of the photographs in Fig. 94 however show this not to be the case. For the neon discharge obtained with the electrode apertures displaced angularly [Fig. 77 ii)], levels of emission surrounding the anode are largely isotropic, which is taken to indicate a quite isotropic source of ion current. In the misaligned case shown in Fig. 94 i), the line along which the neutral-induced emission is evident is clearly separate from that of the ion beam. The relative intensity of emission in the core of the beam suggests a significant degree of pre-focussing to occur at larger radius than the 6.5 % contour.

At conditions of greater pressures, corresponding to operation in the CC mode, the electron current to the anode was found to fall to zero in argon (described in Chapter 4). This was considered to represent a degree of ion accumulation occurring in the region around the anode, of a sufficient magnitude to cause the grounded anode grid to appear relatively negative, and so attract more ion current than electron current. Whilst this is not found to occur in the same way at beam mode conditions, the above analysis has indicated a considerable proportion of emission to occur at locations beyond the anode radius, and the degree of focussing in the beams suggests much ion current flows from this region. A significant degree of ionisation occurring in a region of relatively low magnitude of electric field might be expected to result in positive charge accumulation at these conditions also, and so the effect that this might have upon the degree of beam focus is considered.

The effect of ion accumulation was investigated using the same modelling software as used for the calculating of potential distributions shown previously. The vacuum potential distribution illustrated in Fig. 90 shows a relatively small proportion of the potential to be dropped in the region external to the anode. For this exercise, the accumulation of positive space charge sufficient to cause the potential in this region to become equal to ground was simulated, by modification of the enclosing chamber geometry; this was altered to be a cylinder, co-axial with the electrodes, and having a radius that could be varied so as to represent differing degrees of potential accumulation. Since the chamber wall is held to ground for these calculations, the modelling of the wall in this way equally represents a boundary of positive space charge at ground potential.

The potential distributions for cases having the regions $r > 6.5$ cm, $r > 8$ cm, $r > 10$ cm and $r > 15$ cm clamped to 0 V were calculated. The largest radius of these corresponds to the case in which the distribution is little changed, since the chamber diameter is 30 cm. The software is able to display visualisations of electric field lines; plots of these were produced, and certain ones selected to demonstrate the degree of compression resulting from the electrode apertures. These are field lines that originate from points azimuthally coincident with the radial projection of grid-wires, and also lines that originate from points half-way between these and the aperture centreline. These lines all correspond to the distribution evaluated along the plane indicated by the dashed line in Fig. 90 i).

These field lines are assembled on a single plot, in order to give some idea of the differing degree of compression of electric field lines across the inter-electrode space resulting from the change in boundary geometry. The results show an increasingly small degree of focus may be expected as the radius of the grounded source region becomes smaller, and that the dependence of this effect upon radius also becomes more significant at smaller radius (Fig. 95).

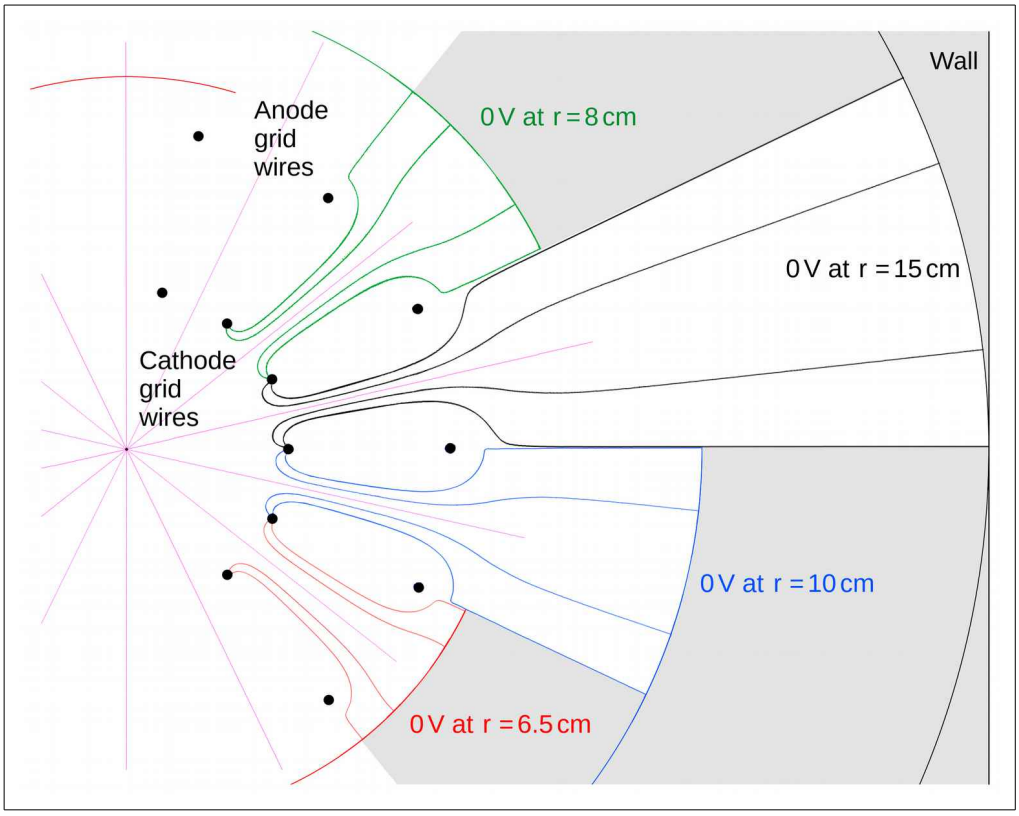

Fig. 95. Diagram illustrating azimuthal compression of electric field lines through anode apertures, showing effect of imposing a cylindrical ground potential at various values of radius external to that of the anode.

The conclusion of this exercise is that these distributions crudely simulate the effect of an annular region of positive space charge occurring at larger radius. The effect of this is observed to simply reduce the degree of focussing that may be expected to occur for the formation of the beams. Some positive accumulation occurring at larger radius than 10 cm might be expected to cause relatively little change to beam formation, but at progressively smaller radius than this, the effects will be expected to result in a significant degree of spread in the beams. The degree of compression illustrated is simply too small however, even for the case of largest source radius, to explain the observed beam diameter, since this is closer to the separation between the inner pair of field lines illustrated for this case.

Radial electron current generated within the cathode will be expected to follow a similar, counter-streaming course to the ions, because the focussing-defocussing effect of the electrode apertures will also operate to some extent in the reverse direction. There will also be a mutual electrostatic attraction between these two

currents, and it might be theorised that this may contribute to the significant degree of focussing apparent in the radial beams. However, the much smaller mass of electrons means that they will travel much faster than ions, and will therefore be expected to have a relatively small effect upon the potential distribution, except for locations in which they must accumulate to overcome a potential barrier, as described in the previous chapter. There is no particular reason to expect this to occur in the beams, since the vacuum electric field is directed in such a way to enable electron extraction and ion injection across the inter-electrode region.

A more likely explanation for the observed degree of focussing apparent in the radial beams is suggested by consideration of the nature of ion extraction that may be expected to occur from a supposed source population distributed in the region surrounding the anode. Ions will be extracted from this region through the apertures of the anode, and so this flow will be drawn from the parts of the source region corresponding to radial projections of the anode apertures. This will be expected to occur to a lesser extent for ions residing in the regions of the chamber coinciding with the radial projection of the anode grid wires towards the walls, and so the anisotropic nature of ion extraction caused by the anode apertures might conceivably create further focussing potential surfaces in the distribution of positive space charge.

It seems that an element of such an effect must be invoked to explain the degree of focus observed in the beams. This suggests that whilst the vacuum potential distribution is important, it is the alteration of this distribution caused by the plasma that enhances the focussing of the beams.

5.3.3 Interpretation of H-α emission from helium discharges

The hydrogen measurements concern the dynamics of an impurity species within these discharges. This makes them additionally interesting, since any future application of this technology for process applications will be likely to use more complex molecular fill species, in which a wide variety of minority species may result from fragmentation. The very different behaviour that appears to occur for hydrogen in helium and argon would appear to demonstrate that charged minority species may show very different dynamics, depending on the reactions that may occur with the parent gas and other constituents.

In the following discussion, possible explanations are considered for the observations made in helium discharges. In order to start to consider this, it is helpful to review what can be said for certain: the Doppler-shifted light indicates emission from fast hydrogen, having energies of the order of 100's eV. The fast hydrogen must first have been accelerated; this will be expected to have occurred in the electric field, whilst in a charged state. The direction of travel indicates the hydrogen to have been positively-charged. After reaching the energies indicated, the hydrogen ions have become both neutralised and electronically excited, in order to then be able to emit the observed photons.

In considering the dynamics of charged impurities, it may be observed that resonant reactions between different species are relatively less likely, and so ionised impurities will generally have small cross sections for reactions with the background gas [91]. This translates to the impurities having correspondingly longer mean free paths in helium than would be the case in their parent gases. Any ionised hydrogen in the helium discharge would therefore be expected to reach relatively high energies at these pressures, as compared with helium ions. From the work reported in [69], ion energies in their parent gases are expected to broadly correspond to *E/N* conditions.

The hydrogen energies however remain consistently proportional to cathode voltage at a wide range of pressures, implying the mean free path to remain quite constant. Being independent of pressure, this is uncharacteristic for a collisional process, and so is rather consistent with there being a generally small probability for interaction with helium. For the energies to all be similar, as is indicated by the mono-energetic Doppler profiles, the fast hydrogen is indicated to have traversed the same accelerating path-length before becoming neutralised and excited, regardless of operating conditions. This then suggests the energy profile to be associated with the potential distribution, rather than collisional dynamics. In the following, the implications of these properties for the understanding of this phenomenon are considered. Possible processes by which hydrogen may be produced, ionised, and accelerated to a consistent fraction of cathode potential are outlined, and then the way that these may combine to cause the observed phenomena are considered.

5.3.3.1 Hydrogen production

The apparent intensity of the hydrogen emission is observed to vary with conditions and with time, and at least part of the source of the hydrogen is expected to be desorption from the walls. In [92] the scale of this is noted to be considerably more significant for massive particle impact, and so the fast neutral flux associated with the beam mode discharge will be expected to cause species bound to the walls to be ejected into the chamber. The yields are noted to vary considerably with incident flux and also with time. The species most commonly detected after desorption from typical stainless steel vacuum chamber walls is indicated to be diatomic hydrogen, in quantities that may be considerable, as indicated in Fig. 96.

5.3.3.2 Hydrogen ionisation

The analysis of optical emission described in the previous section indicated a considerable degree of excitation to be caused by fast neutrals in the helium discharge, and it was observed that the majority of this will excite the 2^1P state [88]. The authors of this work note that it is in fact a cross section for UV emission, although they expect contributions from lines other than the 58.4 nm line (corresponding to the transition from 2^1P to the 1^1S ground state) to be relatively much smaller. From the discussion of radiation imprisonment in Chapter 3, these photons will be expected to be re-absorbed by background neutrals. Since there are no transitions other than to ground from the 2^1P state however, there will be no

cascade contributions made to emission at other wavelengths, and the energy will all be re-emitted at 58.4 nm. This means that regardless of pressure, all of these photons will be expected to reach the wall. Significantly for this discussion, the 21.25 eV UV photons emitted as helium relaxes from the 2^1P state to ground will be sufficiently energetic to cause ionisation of any of the species expected to be present in the wall layer.

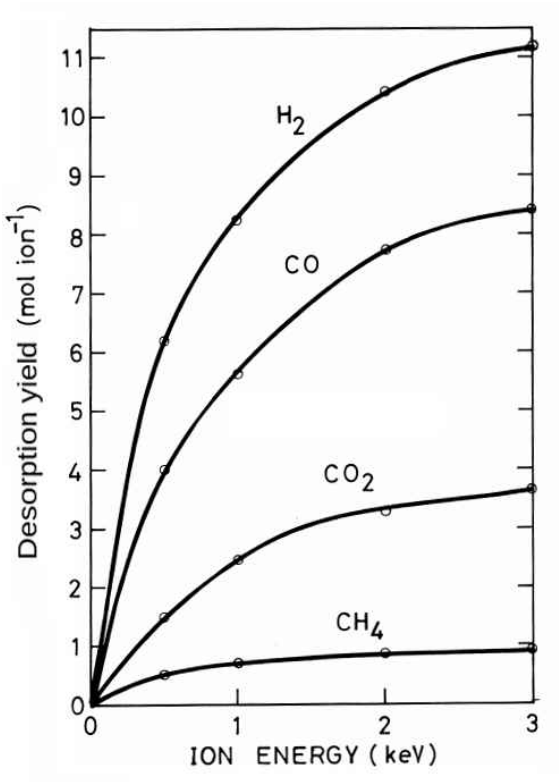

Fig. 96. Species commonly produced in desorption from vacuum chambers under ion bombardment, reproduced from [92].

5.3.3.3 Hydrogen acceleration

If hydrogen is supposed to become ionised at the wall in its diatomic molecular form, and to subsequently become accelerated, neutralised, dissociated and excited to emit the Doppler-shifted light, then the velocities indicated by the Doppler shifts will translate to energies larger than those calculated for atomic hydrogen by a factor of two. This doubles the characteristic fraction of cathode voltage implied by the hydrogen energies measured radially to 6 %.

The vacuum potential distribution along a chord passing through the electrode apertures is shown in Fig. 97. At these conditions, the potential falls slowly in the proximity of the walls and across the region external to the anode, before falling very rapidly in the inter-electrode region; the fraction of cathode potential dropped across the initial, low-field region is observed to be around 6 %.

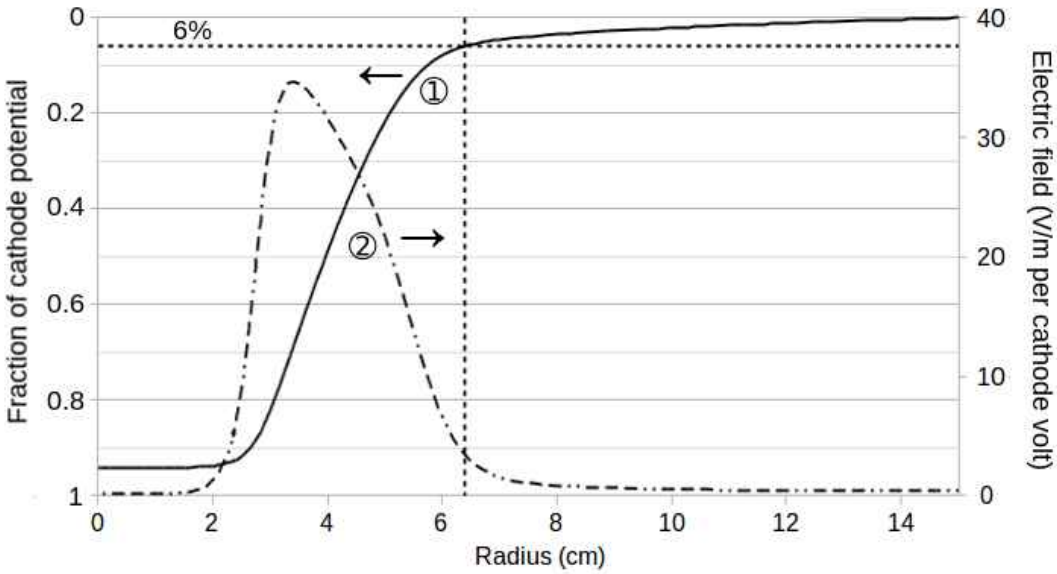

Fig. 97. Potential and electric field distribution along chord passing through electrode apertures. Values are for a nominal cathode voltage of 1 kV. ①, potential; ②, electric field. Dashed marker lines indicate potential of 6 % cathode voltage and radial coincidence with profile.

The same caveats apply to the consideration of vacuum potentials in this case as were outlined in the previous section. As for those considerations, it is noted that the anode represents a local reference for the potential structure, and so it may be that the magnitude of potential fall between wall and anode remains of similar order to the vacuum case. At conditions of background potential at least, the path from wall to anode would constitute a possible acceleration zone, for diatomic hydrogen ions.

5.3.3.4 Hydrogen Balmer-alpha emission

The analysis of the Doppler-shifted H-α emission outlined above suggests it to be produced by a flux of hydrogen that was both directed largely inwards, and also that occupied a location of relatively larger radius in the chamber. Should ionised H_2 be produced at the walls of the chamber by UV photo-ionisation, the considerations of a small probability for interaction with helium and the nature of the potential distribution suggest that this would become an appropriately-directed flux of H_2^+ travelling at the velocity characteristic of the Doppler-shifted emission, when it was located at a consistent radial displacement in the chamber. This location is noted to be coincident with the boundary of the region of strong electric field within in the chamber at vacuum conditions, which is around 1 cm outside the anode.

These observations do not explain why the fast H_2^+ should suddenly become neutralised at this location, but neutralisation must occur if acceleration is to cease. The fast hydrogen neutral must also then become excited, in order to emit the

Doppler-shifted light; for this to occur whilst still directed inwards at relatively large radius, the excitation process would need to be practically immediate.

For the Doppler-shifted emission to result from the flux of H_2^+ therefore, a process must take place that simultaneously neutralises the ions, and leaves neutral hydrogen in an excited state having n=3. The process is indicated to occur with a very high probability at the radius at which the electric field becomes strong, but not to occur in the low-field region at larger radius.

For very strong electric fields, H_2^+ will become dissociated into atomic hydrogen; should this be supposed to occur at the high-field boundary, the products would include neutral hydrogen travelling at the correct velocity to produce appropriately Doppler-shifted light. In a study of H-α emission in ion source plasmas [93], much of the emission is attributed to dissociative excitation of H_2 and dissociative recombination of H_2^+. Whilst this work is concerned with very different plasmas, and so involve quite different collisional regimes, the findings indicate that reactions exist in which H-α emission may accompany dissociation. This process, occurring in the manner outlined above, could therefore result in Doppler-shifted emission such as that which is observed.

Two issues make this interpretation problematic, however. The first of these is that, whilst the electric fields indicated to occur in the chamber are of a considerable magnitude, they will be insufficiently strong to cause dissociation. In [94], the field strengths required are given as ranging from 10^7 V/m for H_2^+ in the uppermost vibrational state to as much as $2x10^{10}$ V/m for the ground state. The smallest of these values is around three orders greater than the fields found at the relevant location in the chamber at the higher-pressure conditions at which the phenomenon is evident.

The second problem concerns the absence of the effect in neon. An abundance of UV photons with wavelengths in the region of 74 nm will be expected to be produced in neon discharges, since these correspond to similar transitions to those producing the 58.4 nm radiation in helium. The neon-produced UV photons will have energies of nearly 17 eV, which is sufficiently energetic to also ionise surface impurities, and so a similar flux of H_2^+ might be expected to be present in neon. The electric fields will be of similar magnitude in neon, and yet no Doppler-shifted H-α light is detected. This suggests a reaction specific to the combination of H_2^+ and helium. The work in [93] indicates that H-α emission may accompany dissociative recombination of H_2^+. The absence of the phenomenon in neon suggests that the helium is important somehow for the process.

These factors all indicate that, in order to agree with the observed behaviour, a reaction is predicted to occur between H_2^+ and the background helium, which results in dissociative recombination of the H_2^+, emission of H-α light, and ionisation of the helium. This reaction will essentially be a charge exchange reaction, and yet charge exchange between helium and hydrogen is not resonant, and so will not normally be expected to occur with anything like the high degree of probability indicated by the observations. Furthermore, there appears to be a strong influence exerted by the strength of local electric field.

For such a reaction to be equivalently probable to symmetrical charge exchange of helium ions in helium, an equivalently-precise energy balance would be implied. In the discussion concerning resonant and non-resonant charge exchange made in [94] however, it is explained that should the non-resonant process be exothermic, then the reaction has no threshold energy and the cross section may be as large as, or even larger than one for a resonant process.

To follow this further is beyond the scope of this study, and without a detailed assessment of the influence of electric field upon the possible reactions between hydrogen and helium, it remains a conjectural scenario. The observations indicate that something quite unusual must be occurring, and this account represents one possible such explanation.

5.3.4 Anode-focussed ion beam IEC mode

Significant levels of reactivity within the beam mode discharge are attributed to fast neutral particles, which are created as ions are focussed into beams by potential surfaces associated with the apertures of the anode grid, and accelerated across the inter-electrode potential fall. The formation of these beams has been shown to be caused as a radially-convergent ion flux, originating from locations external to the anode, becomes focussed into beams by potential surfaces surrounding the apertures of the anode grid. This is in contrast to the selection mechanisms associated with cathode apertures to which the formation of 'star' mode beams are attributed [21], indicating that whilst the beams of the beam mode resemble those of the star mode, the means by which they are formed is significantly different.

This ion beam focussing effect therefore distinguishes the beam mode discharge described here from the 'star' mode discharge described elsewhere. The absence of beams observed with the anode removed indicates the star mode not to be formed at conditions found in this cylindrical geometry. In [21] the star mode is described to be evident in a spherical set-up across a broadly similar range of E/N to that occupied by the beam mode, and so the difference in this respect might be associated with the geometrical form of the cathode.

Aside from being cylindrical, the cathode differs principally from the spherical cathodes used in e.g. [21] in having a relatively-larger aperture at the open end. The enclosing of this open end was found in Chapter 4 to result in the rather persistent formation of the CC mode at conditions of lower pressure, which was attributed to an enhanced hollow cathode effect. At conditions at which this did not occur however, one or more directional electron beams were described to emanate from terminal apertures of this cathode, which may be analogues of star mode beams, according to the modelling work of Ohnishi et al. [43]. In beam mode operation with the open cathode, an axially-directed electron beam is also noted to originate from the open end of the cathode. This axial outflow of electrons suggests that the potential within the cathode interior may be more positive than within its radially-oriented apertures, further distinguishing the beams of the beam mode from those of the star mode.

Whilst parallels exist with star mode, the beam mode described here is clearly a distinct state caused by the presence of the anode grid. The anode effect is twofold; aside from the creation of the beams, this grid also significantly increases the strength of vacuum electric field present within the chamber, almost doubling vacuum values of *E/N* for given conditions of voltage and pressure. This will be expected to significantly increase ion energies within the beams. The effect of the beams is expected to direct ions more effectively into the cathode interior, and so the addition of the anode grid in this set-up is expected to enhance the effective cathode grid transparency. This might be characterised as a shift from the formulation described by Dolan [10] to one more similar to that described by Miley [21].

The beam mode is therefore considered to represent a mode of IEC operation that has not been described previously, and that might be referred to as an 'anode-focussed ion beam' mode. It is noted that the defining characteristic of this mode is attributed to the distribution of potential caused by the form of the electrodes, and so the beam-forming mechanism will be expected to also operate at conditions of lower pressure than those corresponding to the glow discharge regime, provided a source of ions is available in the region surrounding the anode.

5.4 Conclusions

These findings indicate the beam mode discharge to be sustained to a significant degree by the action of fast neutral particles, which are created as ions are accelerated across the inter-electrode potential fall, in beams formed by focussing potential surfaces associated with the apertures of the anode grid.

This understanding is partly arrived at by interpretations of distributions of emission, relying upon the identification of shadowing effects as evidence of fast neutral fluxes originating from opposing beams. Since these shadows may be observed to be similarly cast by both anode and cathode grid wires, this identification is considered unambiguous. Reliance is also made upon the principle that the observed location of emission may be associated with that of ionisation, although it has been shown that details of this relation may be expected to vary between species and conditions.

The focussing of inwardly-directed ion beams by the anode grid is observed to distinguish the beam mode from the 'star' mode described in the literature. The beam mode is therefore considered to represent a new mode of IEC operation, that has not been previously described. This mode is observed in operation at conditions corresponding to the low-pressure part of the glow discharge regime, but the underlying mechanism of anode grid focussing might be expected to influence operation at lower pressures also.

The increase in magnitude of *E/N* associated with the addition of the anode grid will be expected to result in greater characteristic ion energies for same conditions of voltage when operating in the collisional regime. The anode grid focussing effect may therefore allow the accessing of the regime of ion- and neutral-induced reactivity at significantly more moderate requirements of voltage and associated

engineering considerations. With the mechanism of beam formation associated with the anode grid, the form of the cathode is found to be less significant for the operation of the discharge in this mode.

This discharge is considered to be an effective means for creating a significant flux of fast neutrals. The geometry will determine the direction of this; in this cylindrical geometry, it is an axially-symmetrical radial flux, that forms a relatively high density convergence as it passes through the cathode interior, before becoming a flux directed radially outwards. In other geometries, this might be engineered to be different. It is also considered to be an effective means for injecting ions into a grid cathode, since the effects of beam formation will be expected to cause most ions to be incident at the centre of the cathode apertures, and so pass at least some distance into the cathode interior.

The observation of H-α light emitted from beam mode discharges in helium shows characteristic Doppler-shifted profiles to be associated with measurements made from both axial and radial perspectives. A related phenomenon is found also to occur in argon, but the Doppler shifts in this case indicate much greater velocities relative to voltage levels. Analysis of the measurements made in helium suggest one possible mechanism involving dissociative charge exchange between ionised H_2 and the background helium, somehow enabled by the presence of the relatively-strong electric field within the chamber. These observations of varying hydrogen behaviour between instances of this discharge in different fill species are interesting, since they indicate the degree of variation that may be found with more complex plasma compositions.

Chapter 6
Space charge objects I

6.1 Introduction

A variety of space charge configurations are found to occur within the cathode interior during operation at different conditions. These include the CC mode described in Chapter 4, and also various objects that appear more spherical in form. These generally appear during operation at conditions of relatively high cathode current, and at pressures that coincide with moderate to higher pressures in the beam mode range. They show a range of characteristics, occurring in specific locations within the cathode and causing distinctive fluctuations in collected currents. Their observed behaviours show dependences upon both the species of gas used and the arrangement of electrodes employed.

These objects influence the overall operating characteristics of the discharge to a varying extent, which in some cases is as great as that of the CC mode. An understanding of the physical dependences for their formation, the processes that cause them to appear and the effect that they have upon the reactive profile of the plasma is therefore important for the engineering of stable plasma conditions. Insights into the mechanics of operation of different types of collisional IEC plasmas might also make a contribution to the understanding of various modes described in the literature, as outlined in Section 1.4.

A distinction is made between these objects according to their size and apparent level of complexity. The material included in this chapter concerns the smaller objects, which are categorised according to those which appear in the experimental set-up with the anode grid, and those which form in the set-up with the anode grid removed. This is a convenient distinction to make, since although the formations in these two instances are clearly related, they show characteristic differences, from which inferences may be made concerning the conditions at which they occur and the role they play in the discharge. In both cases, these are also observed to develop into larger objects, in a more restricted range of conditions, which are described in a subsequent chapter.

This chapter is structured as follows: in the part that follows this introduction, a general description is given of the objects, in order to provide an overview of the phenomena. Following this, the results of a relatively limited range of measurements are reported, that describe some of the physical characteristics of these structures.

The physical processes to which these characteristics may be attributed are then discussed. In this part of the chapter, fundamental aspects of plasma behaviour that are indicated to be relevant are considered, and reference is made to descriptions of phenomena from both the published literature on IEC operation, and also the wider literature, in which descriptions are found of apparently similar space charge objects occurring in quite different apparatus. The possible analogy that may be made

between these and the objects observed to appear in the plasmas created for this study is then explored.

6.2 Experimental observations

In this part of the chapter, the results of experimental observations of these space charge objects are presented, categorised according to those that appear in the standard experimental set-up, and those that are observed with the anode grid removed. In each case, the description begins with a brief overview of their properties, and the conditions at which they are observed, followed details of the measurements made of their physical characteristics.

The characteristic colour of the visible emission associated with the objects in helium is green. From the understanding of emission structure gained in Chapter 3, this indicates them to be caused by the activity of electrons. This is expected to hold for similar objects observed in different gases, and so efforts have been directed towards the measurement of electrical properties, rather than further investigation of the emission structure.

Properties measured include the waveform and frequency of fluctuations in collected electron currents where these occur, and the effect that the appearance of the objects has upon levels of cathode current and voltage, where this is apparent. Where there are further observable characteristics associated with the behaviour of these objects, a description of these is also included.

Measurements of electrical parameters were made using the ADC system, as described in previous chapters. At the time at which some of these measurements were made, there was no radial collector installed within the chamber, but the currents to anode and an axial collector were always monitored. Many measurements of the time-varying behaviour of these currents were made with only an analogue oscilloscope available, but in some cases it was possible to use a digital model.

During the recording of these measurements, the power supply was operated with the current-limiting control set to the maximum. This means that when current levels are below this limit, which is 100 mA, the supply operates in voltage-controlled mode, with the output determined by the level of voltage selected. Should current levels rise to the limit, the supply then switches mode so that operation becomes current-limited, and the voltage is then reduced internally in order to maintain levels of current to within this limit.

6.2.1 Observations made with anode grid; 'spots'

6.2.1.1 Overview of phenomena

With the anode grid present in the chamber, the beam mode discharge is characterised by the presence of a series of sets of radially-convergent beams. This

mode of operation has been described in the preceding chapter, in which the beams were found to be formed in association with, and therefore to remain aligned within, the apertures of the anode grid. Emission occurs as both ions in the radial beams, and also the fast neutrals they produce, experience collisions with the background gas. The radial lines of bright emission that result extend across the diameter of the cathode, causing regions of intense emission in the locations along the axis at which they intersect.

At conditions of relatively high current, bright 'spots' of emission are found to appear in locations immediately adjacent to these zones of beam convergence. These objects will be referred to as such hereafter. They are relatively small in size, being of the order of 1 cm in diameter, appearing slightly larger in helium and neon than in argon and krypton. Photographs showing examples of spots occurring in helium, neon, argon and krypton discharges are shown in Fig. 98.

With the exception of the neon discharge [Fig. 98 ii)] these photographs all show instances of the occurrence of single spots. In these cases, the spots may be seen to occur in the same axial location within the cathode. This location is almost midway along the axis, and adjacent to the convergence of beams associated with the central band of apertures closer to the cathode feed-through end of the electrode assembly. This is found to be the location at which single spots form, for all cases observed.

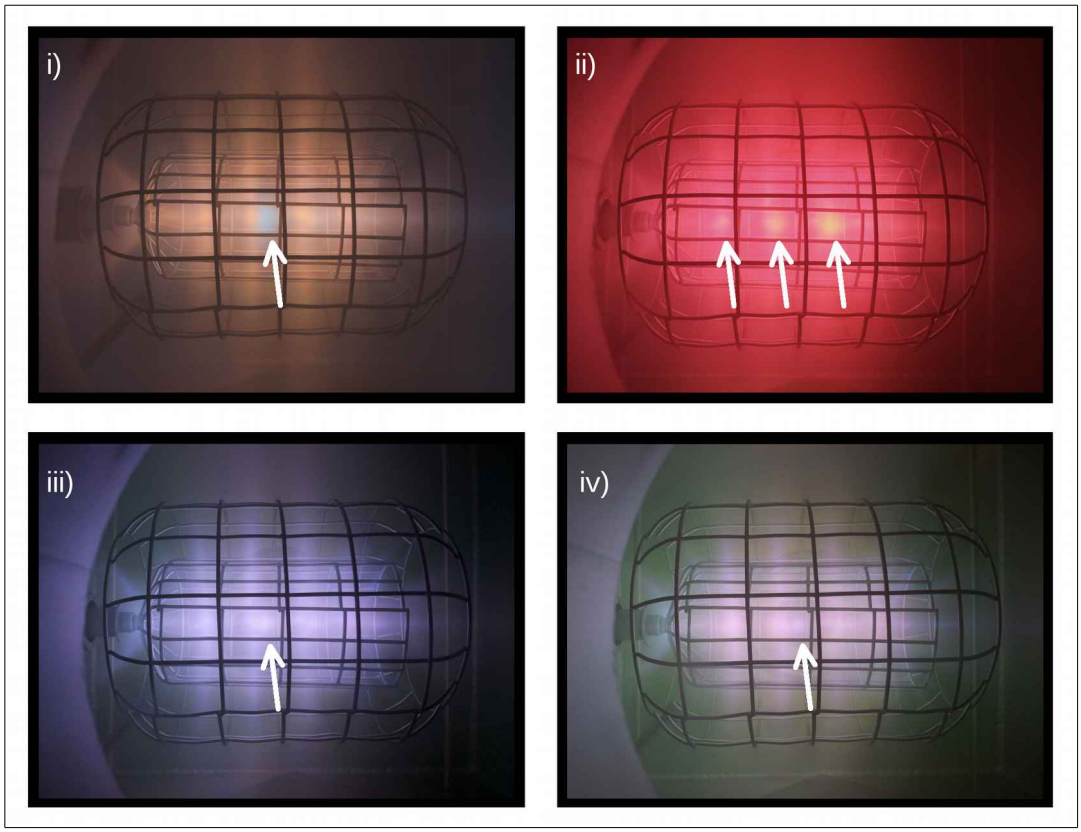

Fig. 98. Examples of spots appearing in i) helium at 41 mTorr, ii) neon at 13 mTorr, iii) argon at 7.9 mTorr and iv) krypton at 11.5 mTorr. Arrows indicate the locations of the spots.

Instances also occur in which the appearance of one spot is either accompanied or followed by the appearance of a second. This has again been always observed occurring in the same location, which is similarly positioned relative to a beam convergence, but in the other central band of apertures. The simultaneous appearance of two spots has been observed in both helium and neon discharges, but not in other species.

Two such spots may be observed in the photograph of the neon discharge shown in Fig. 98 ii), and in this instance these are also accompanied by a further, smaller spot aligned with the end row of apertures by the feed-through. This case is somewhat exceptional, and it is noted that a single spot is most commonly apparent. It is also noted that in all cases the spots do not form around the beam convergence, but rather, immediately adjacent to it.

Spots are noted to occur at a relatively narrow range of pressures that corresponds to more moderate conditions in the beam mode, with typical voltages in the units kV.

6.2.1.2 Spot characteristics

Dynamic current-voltage traces recorded during the apparition of a spot in argon and in neon are shown in Fig. 99. Data are shown for cathode voltage and current, as monitored from the power supply, for the currents incident at the anode and axial collectors, and also for pressure.

In these figures, the cathode current and voltage traces may be seen to follow a progression with time. This generally reflects the adjustments made to the voltage control. These traces also show a consistent degree of fluctuation, with levels of voltage and current frequently dropping to smaller values over a short timescale. These are typically observed during operation of the discharge at a wide range of conditions, and are considered to be an artefact of the power supply regulating its output when driving a plasma load. A degree of fluctuation is also evident in the pressure traces. This reflects a relatively much-smaller degree of variation in the low-voltage signal produced by the pressure gauge at these low pressures.

The instant at which spots appear is indicated by dashed lines, and labelled as such. The level of cathode current at which these spots occur is observed to be quite different in the two cases; the spot in argon appears at a cathode current of a little over 25 mA, and in neon at around 80 mA.

The appearance of these spots is also observed to be associated with a sudden increase in levels of collected current in both cases. The step in cathode current that accompanies the appearance of a spot in neon is observed to be considerably greater than that in argon. For the spot occurring in neon [Fig. 99 ii)], the cathode current is shown to rise by almost 20 mA to reach the power supply limit, and the level of voltage is reduced by the power supply. For the spot in argon, the increase in cathode current is smaller than 5 mA.

Upon the appearance of a spot, fluctuations are observed to appear in the currents collected by the anode and axial collector. This may be seen on the traces for the anode voltage and axial collector voltage on the plots in Fig. 99.

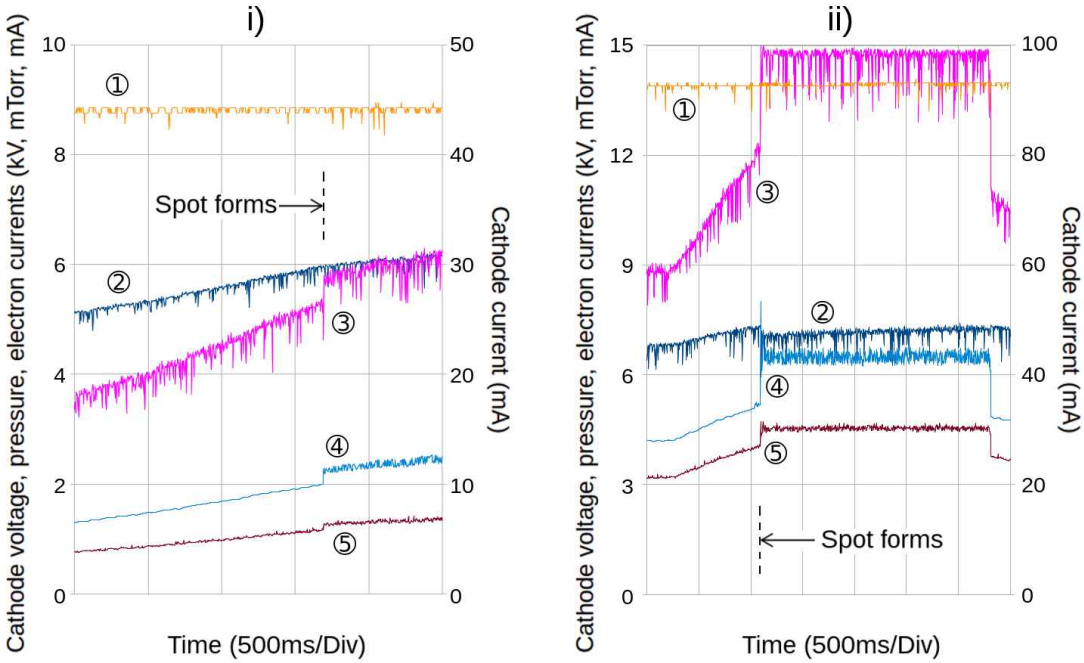

Fig. 99. Dynamic current-voltage traces recorded during spot formation in i) argon, at around 9 mTorr and ii) neon, at 13 mTorr. Key to traces: ① pressure; ② cathode voltage; ③ cathode current; ④ axial collector current; ⑤ anode current. Note different scales

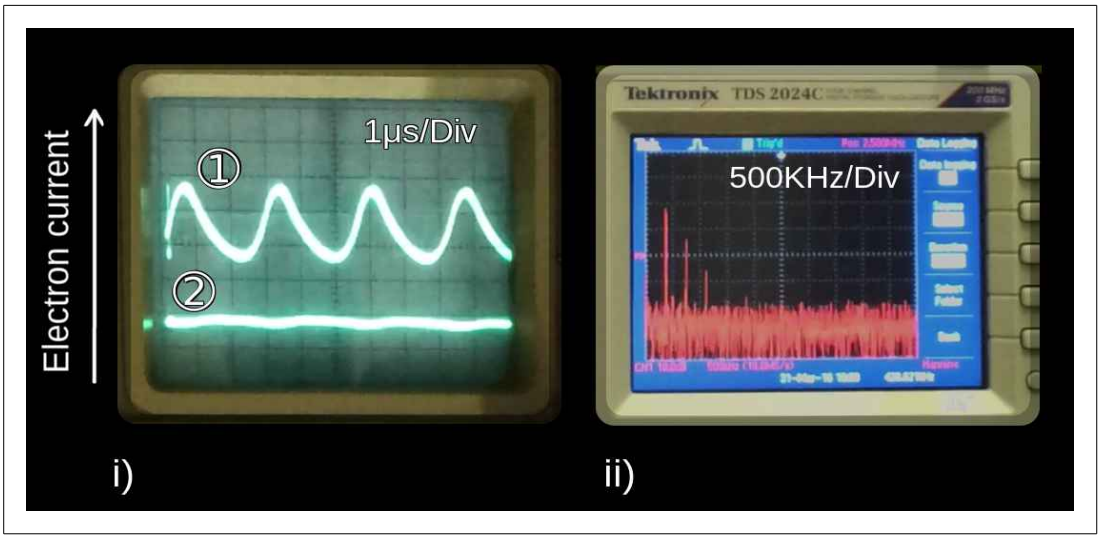

Fig. 100. Fluctuations in electron currents whilst a spot is evident in argon at 8.7 mTorr. i) Waveforms in ① axial current and ② anode current, ii) corresponding power spectrum of axial current (anode current spectrum was similar)

A characteristic waveform of the fluctuations in axial electron current observed whilst a spot is evident during a discharge in argon is shown in Fig. 100, along with its power spectrum. Unfortunately the waveform at the anode is not clear; this is because the behaviour was captured during an experimental run in which oscilloscope settings were programmed to display different fluctuations in anode current from those of the spot, which were of a much greater magnitude. The element that is visible however, shows anode current to vary in a reciprocal fashion with axial current. These fluctuations are found to occur at frequencies in the 100's kHz in all species. Examples of spot frequencies measured in a variety of species are listed in Table 2.

Species:	Helium	Neon	Nitrogen	Argon	Krypton
Frequency:	470 kHz	360 kHz	450 kHz	300 kHz	300 kHz
Pressure:	41.7 mTorr	13 mTorr	9 mTorr	8.7 mTorr	11.5 mTorr

Table 2. Frequencies of fluctuations in axial electron current measured during spots occurring in different gas species

The frequencies are observed to vary little with conditions, except for some occasions when voltage levels have been reduced almost enough to cause the spot to extinguish. The waveforms shown in Figs. 99 i) and ii) correspond to the fluctuations detected at the axial collector whilst a spot is visible in a krypton discharge, and were captured within a few seconds of each other.

The waveform in Fig. 101 i) is the characteristic waveform that appears with the spot, and which generally changes little with voltage-current conditions. As voltage is reduced almost to the point at which the spot disappears, the waveform starts to evolve to become similar to that shown in Fig. 101 ii). The fluctuations are observed to become progressively faster as voltage levels are further reduced, which progression is found to be reversible. It may be observed that the change is associated largely with the decay profile of the waveform, with the rise time remaining quite consistent.

The waveforms shown as Fig. 101 iii) and iv) also represent fluctuations in axially-collected current whilst a spot was evident. These were both captured during a helium discharge, at times around a minute apart from each other. These waveforms show little difference in periodicity, but have notable differences in profile. This occurred without external adjustment having been made to the operating conditions.

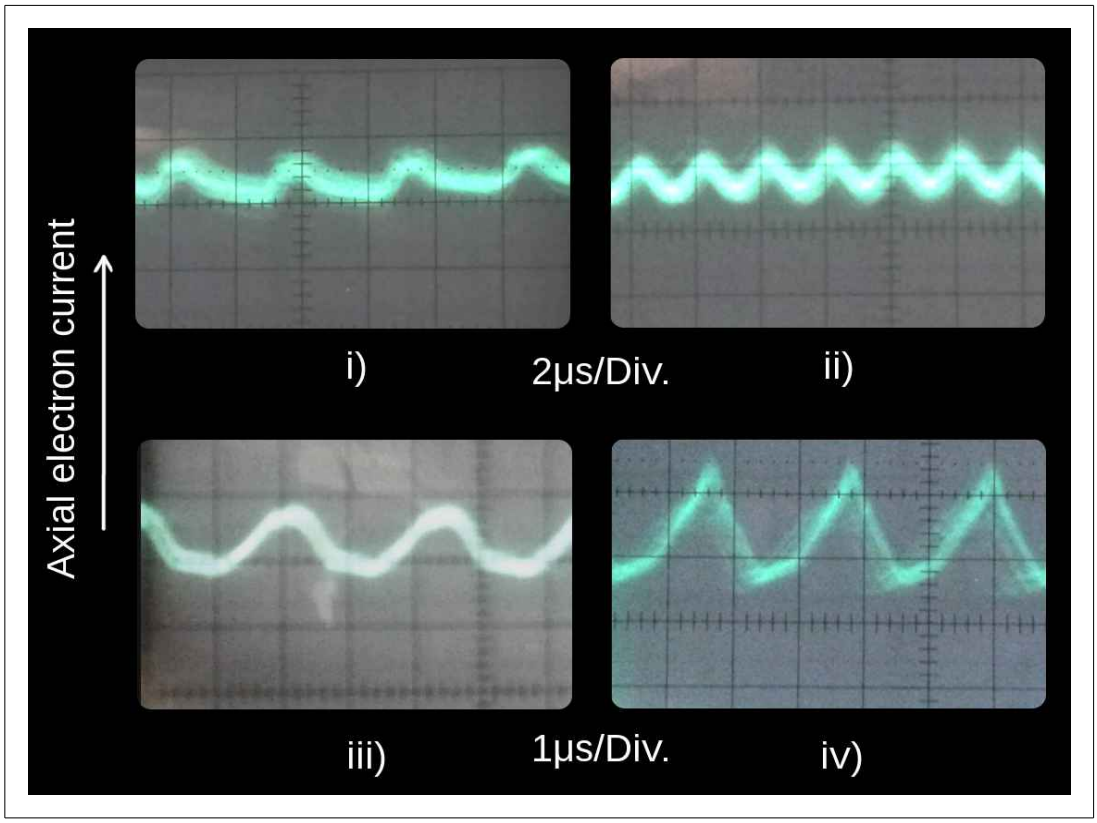

Fig. 101. Examples of waveforms in axially-collected electron current whilst a spot is evident, showing: i) and ii) variation in frequency (krypton, 11.5 mTorr); iii) and iv) variation in shape (helium, 41.7 mTorr)

6.2.1.3 Flicker

At times, the appearance of a spot in helium and neon discharges is accompanied by the discharge visibly flickering. Current-voltage traces recorded during this behaviour (Fig. 102) show cathode current to rise repeatedly to the power supply limit in spikes, before the stable spot appears. Following each spike, the magnitude of all currents dips below original levels, before recovering prior to the next spike.

Some correspondence is evident between these current spikes and the fluctuations in voltage; voltage can be seen to consistently lag the spikes in axial collector current. The data-points in Fig. 102 are spaced by a few milliseconds, and so to be picked up in these traces, the timing of the relation is of this order. This is noted to be a relatively long period of time as compared with the period of the fluctuations, which is some three orders shorter.

The repetition rate of the flicker illustrated in Fig. 102 increases a little over the first few spikes, before becoming quite consistent, at around 15 Hz. This is quite typical, although considerable variation is evident in this respect. At times, the repetition rate has been found to vary with voltage, so that it can be increased until the discharge appears to be steady state.

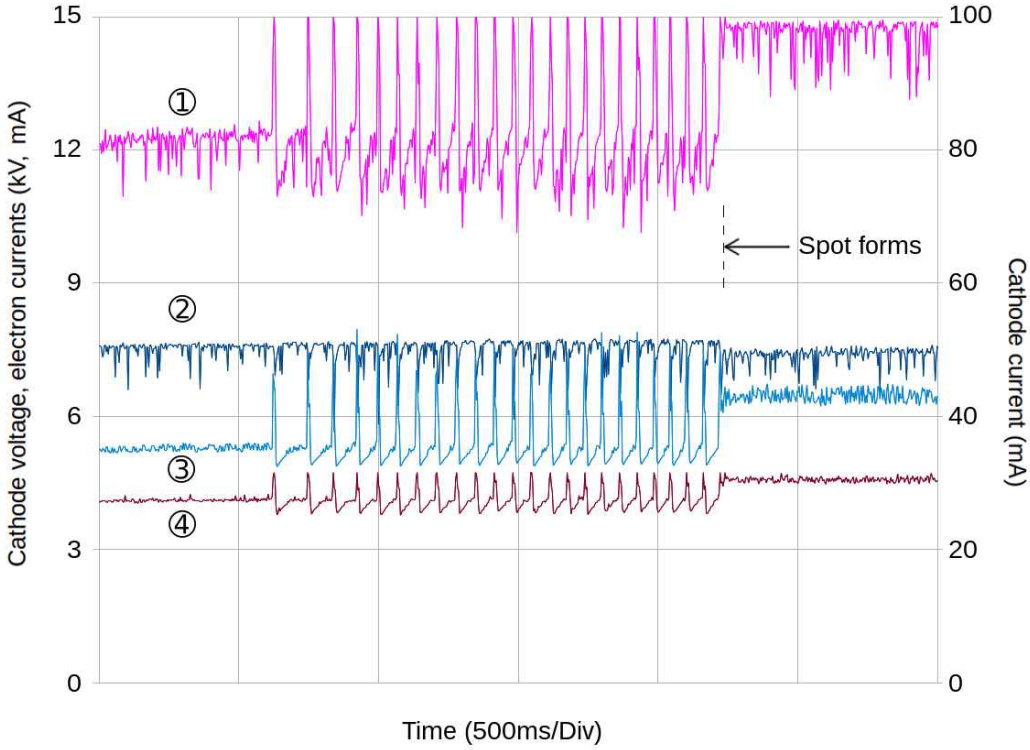

Fig. 102. Dynamic current-voltage traces recorded during flicker behaviour prior to spot formation, in neon at ~13 mTorr. Key to traces: ① cathode current; ② cathode voltage; ③ axial collector current; ④ anode current.

6.2.1.4 Summary

The measurements presented of electrical parameters during the formation of spots in neon and argon show this to be associated with an increase in both cathode current and currents to the anode and axial collector. The simultaneous onset of regularly periodic time-variation in the electron currents is also noted to occur. These constitute characteristic behaviour of these objects, which have been observed to occur in all species of gas in which spots have been observed.

Some characteristic variation is also evident between the properties measured in these species. The spot appears at conditions of considerably higher cathode current in neon, and the rise in current is also observed to be considerably greater in this case. For the gases used, these characteristics are found to be generally evident between the less massive species such as helium and neon, and heavier species such as argon and krypton.

The fluctuations in axially-collected electron current are generally regular, and show few harmonics in the power spectrum. These also show some characteristic differences in waveform between species, concerning the relative lengths of rise time and decay time. Flickering behaviour is sometimes observed in the lighter species, when a spot forms and extinguishes in rapid succession. All measured instances of this have shown current spikes that reach the power supply limit.

6.2.2 Observations made with anode grid removed; 'pea-shooters'

6.2.2.1 Overview of phenomena

In the previous chapter, the effect of removing the anode grid was observed to result in the disappearance of the radial beams. This was noted to be the principal difference between the discharges that occur with and without the anode grid; with this grid removed, the colour of emission in helium indicated the lower-pressure regime to be similarly associated with processes caused by ions and neutrals, irrespective of the formation of radial beams. The axial electron beam characteristic of beam mode operation was also observed to occur in operation without the anode grid.

With the anode removed from the set-up, space charge objects are also observed to appear. In this arrangement, these occur within the open end of the cathode; they are observed to be pea-sized, and approximately spherical in shape. The axial beam appears to be almost attached to the object, which is also surrounded by some additional emission extending radially towards the cathode grid radius. These formations are found to occur in all species in which the discharge has been operated in the set-up without the anode, which include helium, argon, nitrogen and air. The combination of the globe and beam cause the overall form of the structure to be suggestive of a pea-shooter, and so for convenience and clarity they are referred to as such in the following. Photographs showing examples of pea-shooter objects in argon, helium and air are shown in Fig. 103.

The colour of the emission from the pea-shooter object that appears in helium is green, as was noted to be the case for the spot. The emission observed from these objects is therefore also observed to signify excitation caused by the activity of electrons.

In some conditions, the presence of a pea-shooter object is accompanied by periodic fluctuations in electron current incident upon the axial collector. This will be considered in more detail in the following paragraphs, but for now it is observed that whilst this may occur, it is not always the case, and so such fluctuations are not considered to be an intrinsic element of pea-shooter behaviour.

These objects form at a similar range of pressures to the spots. They are observed to appear initially as a very small and barely discernible region of brighter emission in the axial beam, and to become larger and brighter with increasing levels of cathode current until they are of similar size to the spots. As current is reduced, they become smaller until they are no longer discernible. At conditions of higher pressures in the range described above they may appear at cathode currents of the order 20 mA to 30 mA; these threshold currents are a little greater in lighter gases such as helium and neon.

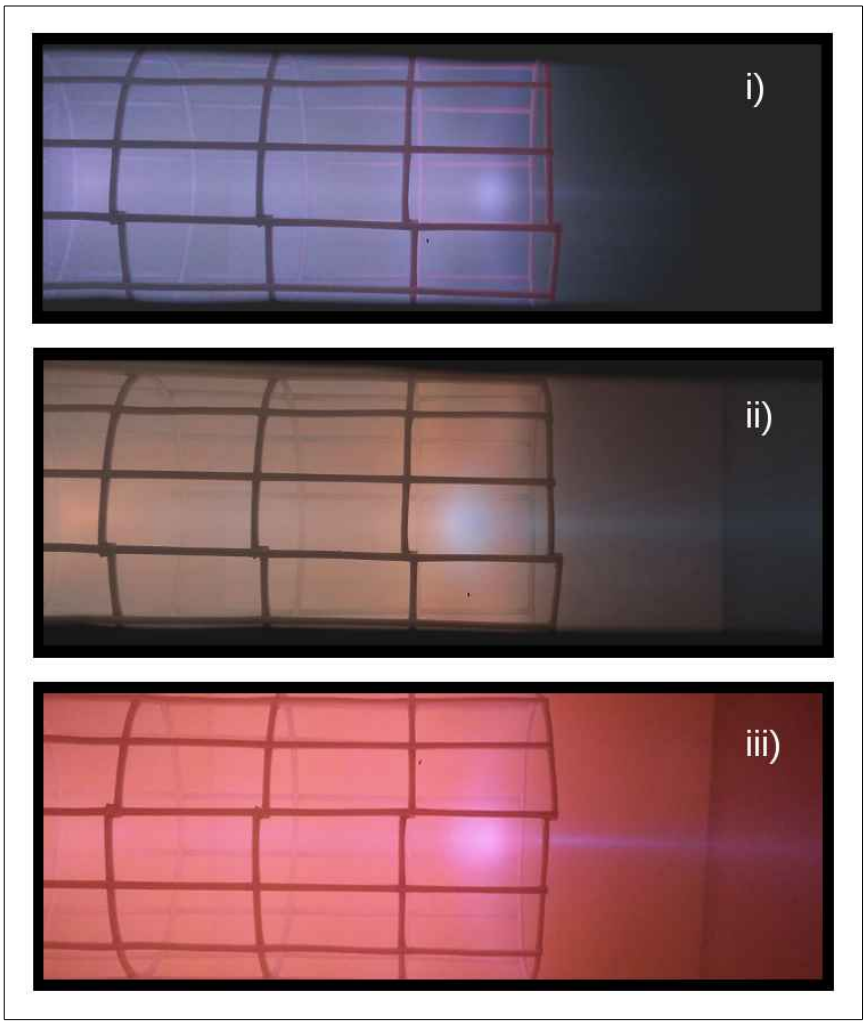

Fig. 103. Pea-shooter objects in i) argon at 9 mTorr, ii) helium at 48 mTorr, and ii) nitrogen at 11 mTorr

6.2.2.2 Pea-shooter characteristics

Pea-shooter objects are found to appear quite gradually, and so no clear discontinuities are evident in the current-voltage characteristic. The objects are found to be sometimes accompanied by oscillations in the current collected by the axial collector. The following observations describe both of these aspects of their behaviour.

Fig. 104 shows stills from a video recording, made during operation in nitrogen at a pressure of 11 mTorr. These images correspond to a period of a few seconds, during which time levels of voltage and current were increased. They illustrate stages in the formation of a pea-shooter object.

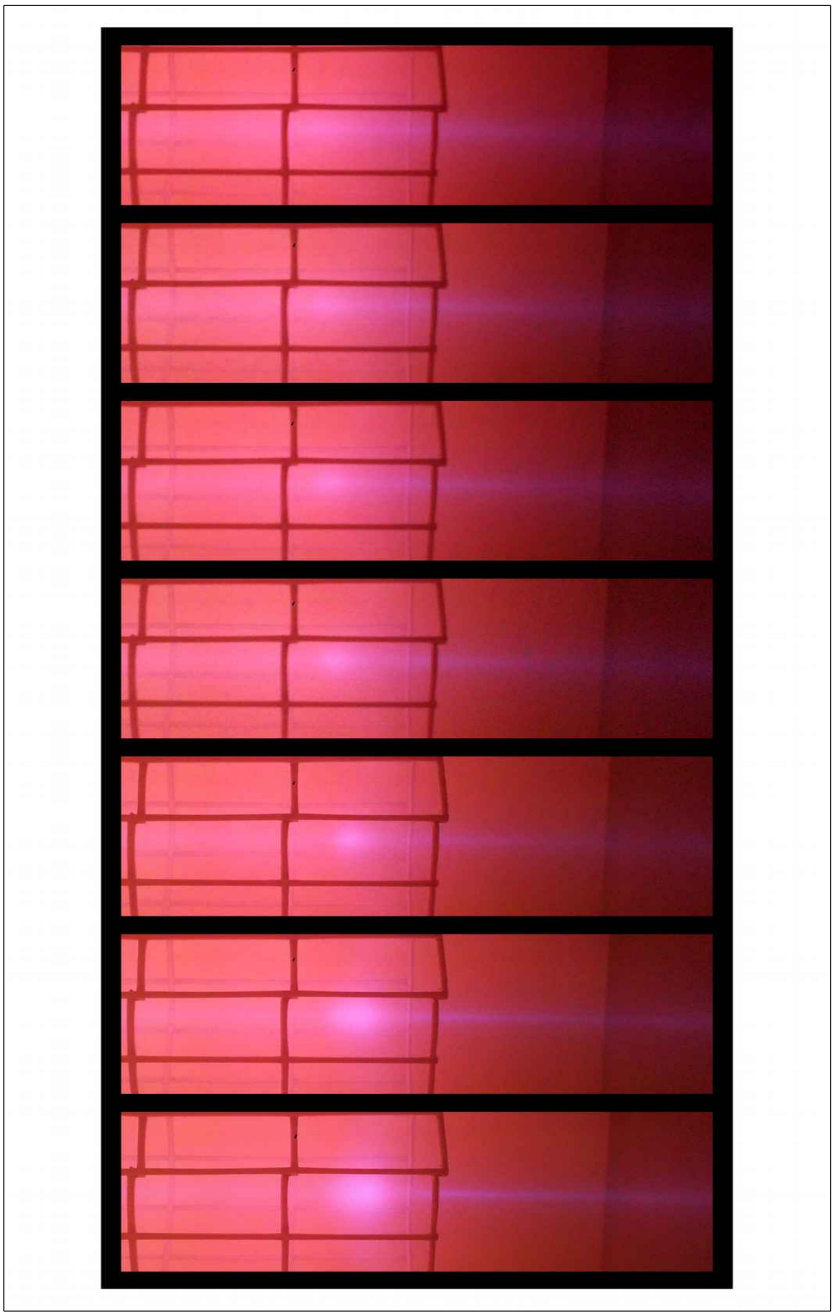

Fig. 104. Stills from a video made of the evolution of a pea-shooter object, forming as levels of voltage and current increase, at a pressure of 11 mTorr in nitrogen. The progression is continuous and reversible.

The pea-shooter object may be observed to grow from a localised area of increased brightness along the axial line. The area at which the object originates is located within the cathode, approximately aligned with the second ring of wire from the open end. As levels of voltage and current are increased, the object appears as a tiny spot of relatively intense emission; with further increase in voltage and current it grows in size, and is also observed to move along the axis towards the open end of the electrode. At this location and size, the incremental progression in both of these

respects is observed to stop. The images in Fig. 104 clearly show the movement along the axis and the growth in size of the object.

Fluctuations are sometimes found to occur in the electron current incident upon the axial collector when a pea-shooter object is evident, but this is not always the case. When these appear, the current waveform has a characteristic spike followed by a notch that is less evident at lower pressures; examples observed during operation at a range of pressures in air, and also in argon are shown in Fig. 105.

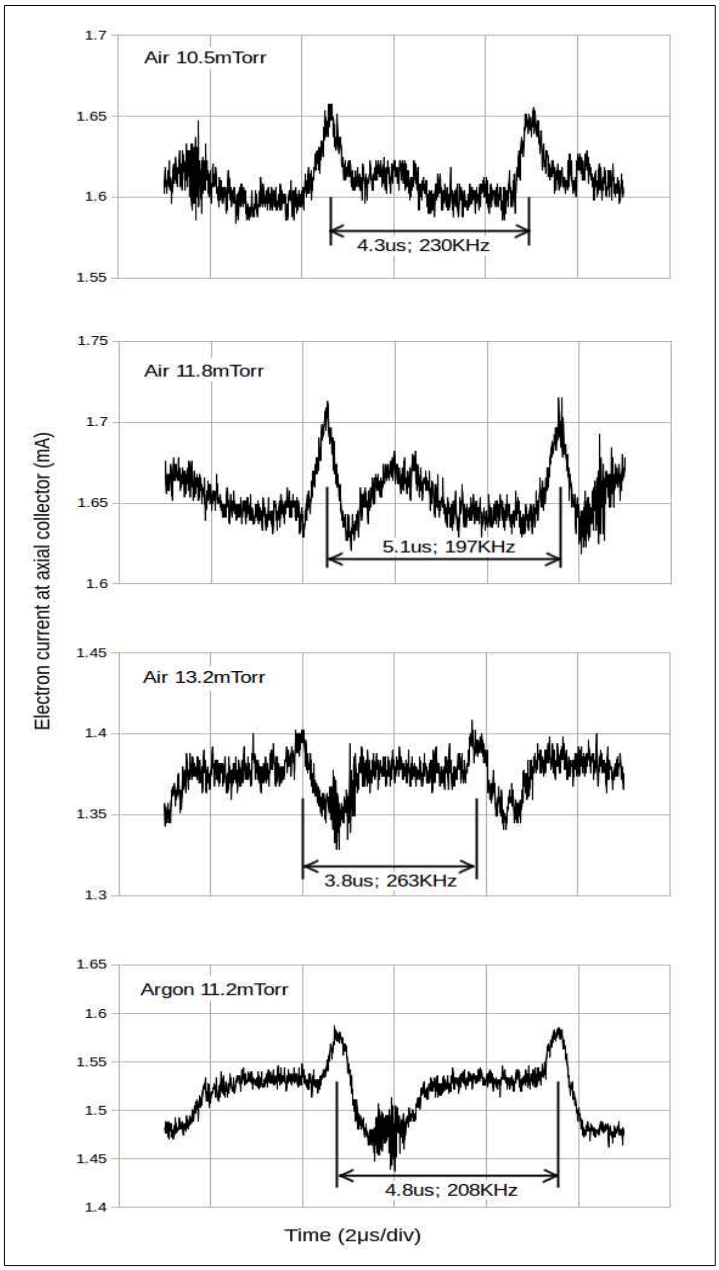

Fig. 105. Fluctuations occurring in electron current to the axial collector associated with pea-shooter objects in air and argon.

The fluctuations are regular, occurring with a period of a few microseconds. The frequencies of these fluctuations are found to vary a little with voltage and current.

In Fig. 106, photographs of the discharge in air are shown, at a range of conditions including those at which some of the measurements in Fig. 105 were made. During this experimental run, the occurrence of the fluctuations was observed to be associated with an additional feature occurring along the line of the axial beam, as seen in Fig. 106 i) and ii). This structure is associated with a change in both colour and distribution of emission associated with the beam. It is observed to occur independently of the presence of the pea-shooter [Fig. 106 i)], but does not cause fluctuations when the pea-shooter object is absent. As levels of voltage and current are increased, the axial location of the structure is observed to move away from the electrodes, towards the chamber wall.

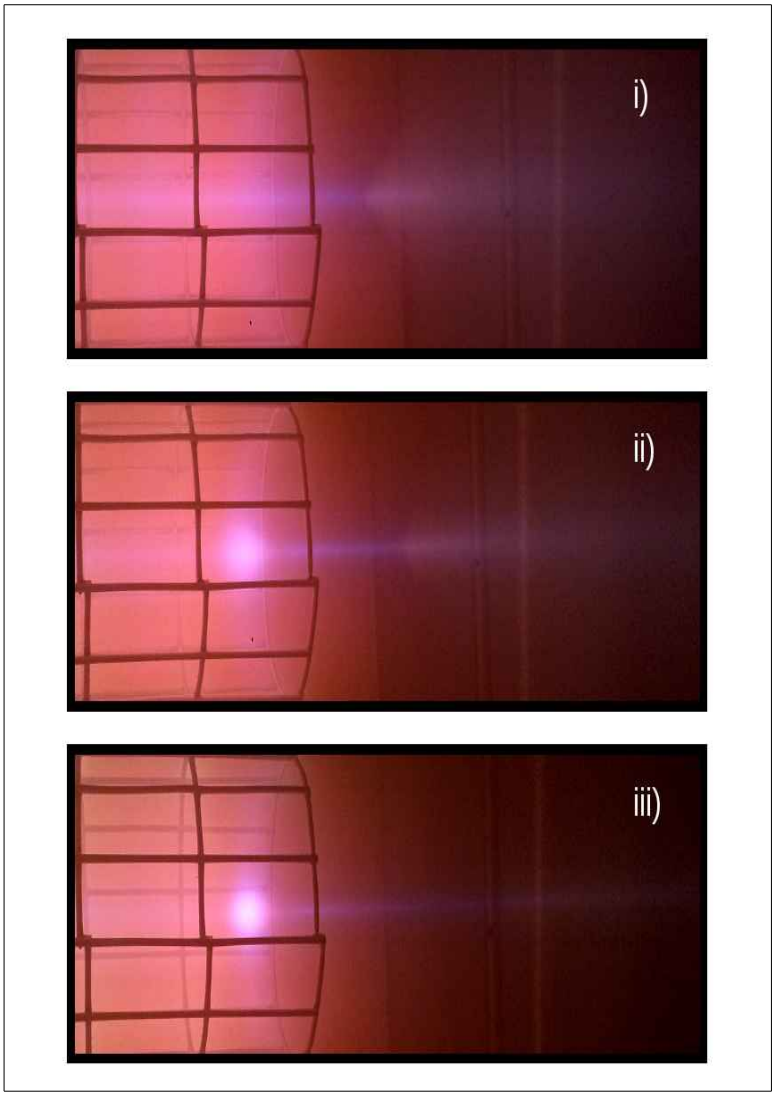

Fig. 106. Photographs of discharges in air, at i) 11.5 mTorr, with no fluctuations evident in axial current; ii) 10.5 mTorr, fluctuations evident (top waveform in Fig. 105); iii) 9.1 mTorr, no fluctuations evident

The nature of this structure is unclear, and the processes that cause it to appear are not further investigated in this study. It is noted merely that the occurrence of fluctuations in axial current in this case shows a clear relation with this feature of the axial beam. This particular discharge was operated in ambient air, and most of the waveforms shown in Fig. 105 were also measured during a discharge occurring in air. Air is composed largely of nitrogen, and the colour of emission from these air discharges is observed to be similar in appearance to those obtained in nitrogen. Ambient air will contain a various mixture of impurities though, and for this reason is not generally used for this experimental work. The observations shown in Fig. 106 are nonetheless included, because they demonstrate a link between the axial beam and the occurrence of fluctuations, and the pattern of emission indicating this happens to be clearly apparent in these images.

Although this behaviour is recorded in air, the variable incidence of fluctuations is observed in other species too, such as argon, and so the behaviour is certainly not an artefact of impurities.

6.2.2.3 Summary

The observations of pea-shooter objects described above show the formation of these objects to occur gradually, and to be associated with a translation in location along the axis within the cathode, in the direction of the open end.

The objects are sometimes accompanied by fluctuations in electron current incident upon the axial collector, and observations indicate the appearance or absence of these to be directly associated with changing conditions occurring along the line of the axial beam towards the wall. When evident, the fluctuations in electron current measured at the axial collector show some variation in waveform, but these characteristically show a spike, that is often followed by a notch. Frequencies measured have all been of the order of a few 100's kHz.

6.3 Discussion

In this part of the chapter, the experimental observations described in Section 6.2 are considered with reference to the published literature. In order to inform the direction of this investigation, the following two observations may be made:

- The optical emission associated with these structures show them to contain populations of electrons that are suitably energetic to cause excitation. The increases in current levels associated with the spots indicate that in these cases ionisation also occurs.
- The pressures at which these objects are observed are similar to those of the extended low-pressure range at which the CC mode was enabled to occur in the enclosed cathode experiment, as described in Chapter 4. The dimension of the objects is also noted to be significantly smaller than the cathode diameter.

These properties are noted to be essentially similar to those that led to the assessment that an 'electrostatically-trapped electron' (ETE) effect was likely to be assisting the CC mode discharge in Chapter 4. In that case, it was shown that the shortest ionisation mean free path that may be expected, for electrons having optimal energies, becomes larger than the cathode diameter.

This was found to occur at pressures several times greater than those at which these observations are made. The diameter of the objects described here is also considerably smaller than that of the cathode, and so it may be appreciated that electron mean free paths will be at least an order of magnitude larger that the dimension of these objects. The highly-localised distribution of emission is therefore considered indicative of an electron population that is not simply confined within the cathode, but confined within the potential structure associated with the object.

It was observed in Chapter 1 that the confinement of charged particles within a spherical potential structure has been of significant interest in IEC research, but that relatively little description was available of phenomena occurring at the collisional conditions described here. In the wider literature however, there are also accounts of spherical space charge configurations, that are described as being associated with anode double layers. These objects are described to occur at a relatively wide range of pressures, including those at which the observations described here were made. They are understood to be sustained by electron activity, and also may occur in a periodically-fluctuating manner, and so an understanding of these may help to explain the phenomena reported here.

The first part of this discussion explores the references in the published literature, both from IEC research and the material concerning the anode double layer objects mentioned above. A brief section also outlines the basic principles of double layers, before the experimental observations described above are considered.

6.3.1 Review of literature and theory

6.3.1.1 Literature

Whilst much IEC work has been motivated by the interest in a particular type of space charge object, relatively little experimental work has been done at pressures as high as those of this study. Some of this work does describe a spherical glow within the cathode, which is often associated with a jet or beam [22], [23]. One account of higher-pressure modes of IEC operation differentiates between two different types of centralised distributions of bright emission. These are called the 'central spot' and 'halo' modes [19], the second of which is noted to be accompanied by a jet. These modes are also described to result from slightly different arrangements of electrodes.

It is not entirely clear from these works whether the jet or halo modes described by different authors describe the same type of structure. It is also unclear whether these modes are more closely related to either the CC mode described in Chapter 4, or to the ion/neutral driven plasma which is the analogue to the beam mode in the set-up

with no anode grid, since both of these are also associated with a jet or beam of electrons. No further reference has been found to a 'halo' mode, or a 'central spot' mode in the IEC literature, and no account describes any characteristic current-voltage relation, or fluctuating behaviour, that might be used to associate these observations with the behaviour recorded here.

In the wider literature however, there are descriptions of space charge objects occurring in a collisional regime, and in a variety of gases, which show more similarities with the phenomena described above. First mention of these in published literature dates back to over a century ago, in which bright spots of emission were reported as appearing attached to the anode of a low-current glow discharge [95]-[97]. More recent experimental accounts indicate these to be capable of evolving to become more complex objects [98], [99].

Similar phenomena, having a range of complexity, have been described as appearing attached to an auxiliary anode immersed in a thermal, un-magnetised plasma generated by external means [100]-[104]. Some reports also describe the persistence of such objects independent of the electrode used to produce them, by means of an applied RF field [103], [105]. The objects are described as consisting of at least one, and in some cases many [98], [99], concentric plasma shells, approximately spherical in shape. Those attached to an auxiliary electrode have been found to display a variety of oscillations in electron current to the electrode [101], [102], [104], [106]. They have been variously termed 'anode spots' [97], 'complex space charge configurations' [102], 'non-linear space charge structures' [101], 'multiple double layer objects' [102] and 'fireballs' [100], [103]. In order to distinguish these from the objects occurring in our experimental apparatus, they will be collectively referred to as 'anode double layer objects' (ADLOs). Some of these works describe the phenomena in terms of a self-organisation mechanism, leading to natural pattern formation; this is also discussed in [107] and [108].

The descriptions of these space charge objects refer to a type of structure that occurs within many plasmas, that is known as a double layer, and so the following account begins with a brief description of these. Some of the experimental observations and analysis presented in [100] are then outlined, since these provide a good framework for understanding some basic dynamics of the objects. Additional observations made in in [103] and [104] are also summarised, which consider the oscillatory behaviour that accompany ADLOs.

6.3.1.2 Double layers

Double layers are also referred to as double sheaths, and the next part of this discussion starts by outlining the processes that cause a sheath to form. It has been noted previously that the relatively much-greater mass of ions causes them to respond more slowly to the force exerted by an electric field than electrons. In most plasmas, this means that electrons have a greater temperature than ions and so, for a quasi-neutral plasma in which ion and electron densities are approximately equal, the electron flux incident across a planar surface within the plasma will be greater than

the ion flux. The greater electron flux incident at the boundary of the plasma means that the plasma potential becomes more positive with respect to its surrounds. This acts to limit electron losses and also to increase ion losses, and so the potential adjusts to keep these equal and preserve quasi-neutrality.

This boundary potential profile is known as a sheath, which is traversed by the more energetic electrons from the plasma and ions accelerated across the potential fall. A sheath is in fact composed of two parts, with ions accelerated to an energy corresponding to half of the electron temperature in a 'pre-sheath' region; this is known as the 'Bohm velocity', and is shown to be required to maintain continuity in ion flux across the sheath in [91] p. 157.

The distinction between 'sheath' and 'plasma' regions is first made by Langmuir, in the same work that a 'double sheath' is also described [2]. In the following paragraphs, a qualitative summary of these descriptions is outlined.

The plasma region is described by first considering how the dynamics of current flowing between biased electrodes are affected by an even distribution of ionisation occurring in the intervening space. Langmuir calculates that should the rate of ion production exceed that of space charge-imposed limit upon ballistic ion transport by a factor of 2.865, then a positive maximum will occur in the potential distribution between the electrodes. This will then confine locally-produced electrons until the potential is reduced sufficiently to result in equal ambipolar losses; the same sheath-plasma equilibrium described above. With a sufficient electrode bias, no electrons cross the cathode sheath and so, at the equilibrium reached, electron current across the anode sheath is equal to the total ion current to both anode and cathode. Two instances of a 'double sheath' are also described, and in order to explain these qualitatively, it is helpful to refer to the potential profiles illustrated in Fig. 107.

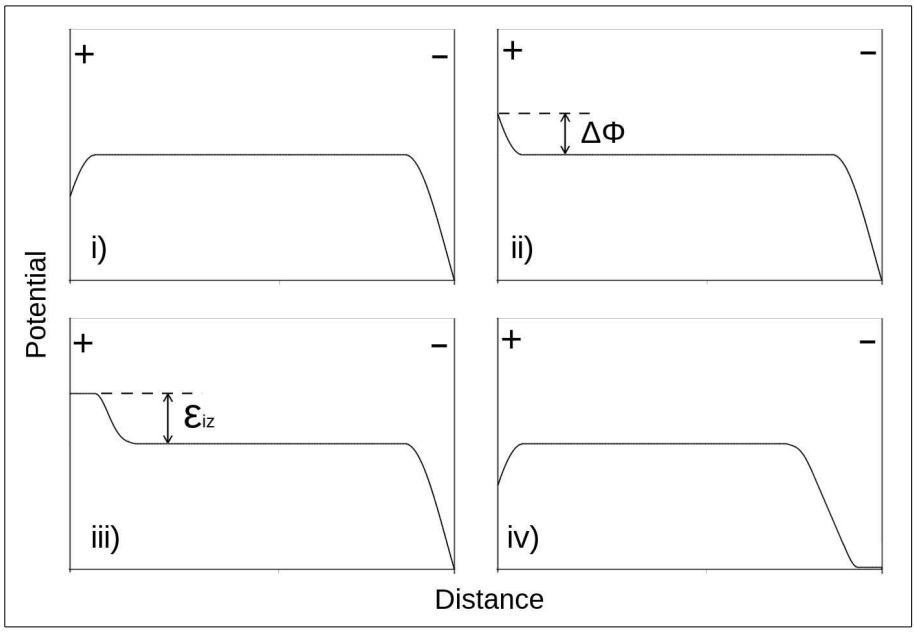

Fig. 107 Potential profiles across a plasma between biased electrodes, illustrating various configurations of sheaths as described in the text.

Fig. 107 i) shows an idealised example of the potential across a quasi-neutral plasma, bounded by positive and negative planar electrodes of equal size, and in which the electron temperature is greater than the ion temperature. This may represent the situation described above, in which ion current flows to both electrodes, and electron current to only the anode. At either electrode, the sheath that forms is a negative sheath, which acts to limit the electron loss from the plasma.

Langmuir notes that should the area of the anode be reduced, this will have the effect of limiting the electron current across the anode sheath. This relaxes the requirement for this sheath to be negative, and a sufficient reduction in area may cause the sheath to become positive [Fig. 107 ii)]. It is also noted that, should the potential fall from the anode to the plasma (marked on Fig. 107 ii) as $\Delta\Phi$) become equal to the ionisation potential of the gas, then ionisation may start to occur in the sheath. The effect of this is described as causing the production of a second plasma within the sheath, which is observed to appear as a luminous, globular spot. This is therefore a description of the processes that give rise to an anode spot. The effect this has on the potential profile is shown in Fig. 107 iii). The anode sheath is now observed to be a double sheath, with two inflections in the potential profile. The magnitudes of the potentials either side of this double layer are separated by a voltage corresponding to the ionisation potential of the gas (indicated on Fig. 107 iii) as ε_{iz}).

The second instance of a double layer described in [2] is illustrated in Fig. 107 iv). This situation occurs when the cathode is heated, so as to create a plentiful supply of electrons by thermionic emission. A sufficient quantity of these electrons will act to neutralise the space charge of the ions in the immediate vicinity of the cathode. This does not affect the magnitude of the plasma potential, since this is determined by the flows from the plasma; what occurs is rather a change in the thickness of the cathode sheath, so that it becomes a double sheath. The limit to this is noted to occur as the electron current from the heated cathode reaches the space charge limit across the sheath.

This is a very brief description, and it is noted that double layers may also occur in locations such as interfaces between different plasma properties, as found at constrictions in the containing geometry or between regions of plasma machines, regions of plasma expansion, and in astronomical and solar phenomena. A review of various experiments and observations is given in [109].

The phenomena that bear some resemblance to the objects described in this study are associated with the anode sheath type of double layer, and these are described further in the following.

6.3.1.3 Anode double layer objects

Experimental observations of anode double layer objects are described in the work by Bin Song et al. [100]. These appear as near-spherical luminous objects attached to an auxiliary disc anode, which is immersed in a plasma created by biased hot filaments in argon, krypton and xenon at a range of background gas pressures

between 0.1 mTorr and 2 mTorr. The principal findings of this work are summarised in the following paragraphs.

The formation of the objects is described to occur when ionisation in the anode sheath causes the local ion density to increase until it is similar to that of the electrons. This then erupts into an unstable spot, or fireball, which flickers until additional voltage rise causes it to become steady-state. This is analogous to the formation of an anode double layer as described above. Probe measurements confirm that the potential dropped across the double layer is indeed slightly greater than the ionisation potential.

The flicker behaviour is explained using time-resolved plots of the plasma potential profile during the current rise associated with the appearance of the fireball. These show a potential rise to occur in the region surrounding the structure, which causes the potential across the double layer to become smaller than the ionisation energy of the gas, and so halt ionisation in the object. This is avoided by increasing the disc voltage, and so enabling a stable configuration to persist.

The diameter of the objects is noted to be inversely related to pressure, but to show little dependence upon the density of the surrounding plasma. The authors formulate expressions describing both the diameter of the object, and the rise time of the current it produces, by considering the ion and electron currents across the double layer, and the property that the potential difference will be a little above the ionisation potential of the gas. These are found to describe the observed behaviour quite well.

Sanduloviciu and Lozneanu describe similar phenomena obtained in a somewhat differently-produced background plasma [103]. They additionally describe measurements of the distribution of emission that show a peak in intensity towards the edge of the object, and relate this finding to a fundamental process of self-organisation that is instrumental in causing the object to form.

Their account of this process is as follows; as electrons are drawn across the double layer potential, they acquire energies sufficient for excitation and ionisation of the background gas. The cross sections for these reactions have somewhat different dependences upon energy, with that for excitation having both a lower threshold energy, and also peaking at a relatively much-smaller energy than that for ionisation. This means that there will be a well-defined region at which electrons cause excitation but little ionisation, adjacent to and external to a region in which collisions are largely ionising. The former of these will see an effective injection of low-energy electrons (those that have suffered exciting collisions) and few ions, and so this region consists of a localised negative space charge bounding the object. The neighbouring region, in which ionisation occurs, sees injection of charges having both polarities and so is the relatively more positive region; this is made more so as electrons born here are extracted by the anode. In this manner, the effect of inelastic collisions occurring as electrons are accelerated across the double layer potential acts to accentuate the potential structure. A diagram showing the potential structure of the

object is reproduced from this work as Fig. 108. The potential drop of 15.7 V across the object illustrated corresponds to the ionisation potential of argon.

It is also noted that, should the anode voltage be increased beyond that at which the object appears, a value is reached at which the object becomes unstable. This instability is manifest by the object detaching itself from the anode and dissipating, to be replaced at the anode by a fresh formation.

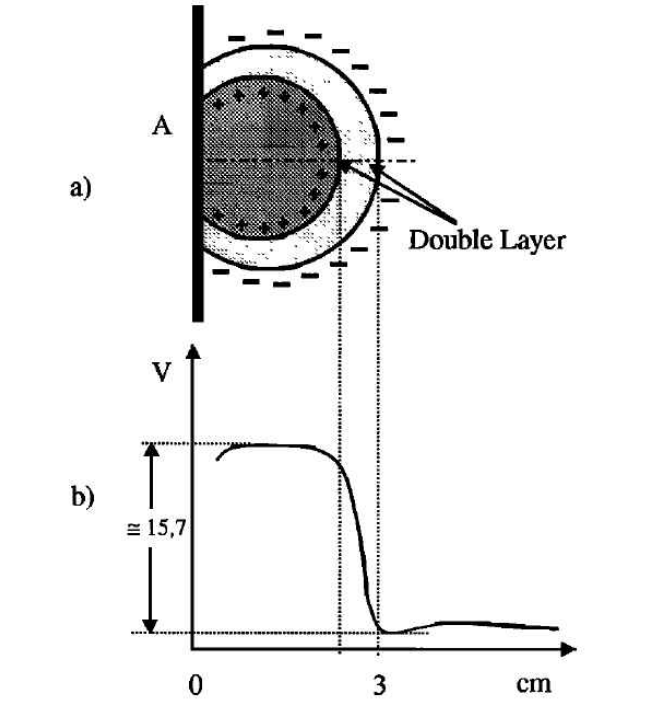

(a) Schematic representation of the internal structure of the SCC attached at the A surface.
(b) Variation of the potential measured by an emissive probe axially penetrating the double layer

Fig. 108. Diagram of anode double layer object showing internal structure and corresponding potential profile. Reproduced from [103].

Further consideration is given to this instability in a separate work by the same authors [104]. In this case, the space charge object appears attached to an auxiliary anode immersed in an argon plasma that diffuses from a region of ionisation associated with a glow discharge source. These observations are made at conditions of pressure between 120 mTorr and 160 mTorr, which are considerably greater than most of the other accounts. Objects are reported to occur consisting of one, two, or more concentric near-spherical plasma shells. The anode current-voltage relation is shown to follow a zig-zag profile, with periods of negative differential resistance following the formation of successive shells.

The instability mentioned above, that occurs with increasing levels of anode voltage, is studied for the case of an object consisting of a single shell. Probe measurements

of plasma potential made at these conditions show the regime of negative differential resistance to be associated with a double layer potential that is smaller than the ionisation potential. As anode voltage is increased the double layer potential also increases, and when this reaches the ionisation potential the structure is observed to disrupt, causing a flickering behaviour.

When capacitances are added to both the anode and to a separate electron collector that floats negative within the chamber, the flicker stabilises into coherent oscillations. These are explained in terms of the growth of the double layer potential until it reaches the ionisation energy, at which point ionisation within the structure causes the internal potential to become more positive, so that it is repelled from the anode and detaches. With the electrons produced within the positive nucleus of the object no longer extracted by the anode, the potential across the double layer is reduced until, once it is smaller than the threshold for excitation, the self-organisation mechanism ceases and the structure disrupts.

Whilst details of reported behaviour varies a little between these accounts, a broadly consistent picture emerges of the processes that cause the space charge objects to appear, sustain and disrupt, causing the observed distributions of visible emission and fluctuations in electron current.

This concludes the review of theory and observations concerned with the anode double layer objects. In the next section, the possible association between these and the spot and pea-shooter objects is explored, by considering the observed physical characteristics and spatial dependences described in Part 6.2.

6.3.2 Spot and pea-shooter objects

Experimental observations and theoretical aspects of near-spherical double layer objects were described in the previous section, from accounts found in the published literature. Although the apparatus in which these objects appear is quite different to that used for the experiments this chapter is concerned with, the objects nonetheless show some similar characteristics.

These similarities are evident in both the general appearance of the objects, and also the fluctuating behaviour observed in levels of electron current. This suggests that the processes that cause the space charge objects to appear and sustain in the two cases may be to some extent analogous, and this possible association is explored in this section.

The discussion concentrates upon two principal aspects of the occurrence of spot and pea-shooter objects. The first of these concerns the conditions at which they appear; these are characterised and compared with those at which the anode double layer objects are observed. Secondly, the physical characteristics of the objects are considered, and again compared with those of the anode double layer objects.

6.3.2.1 Conditions at which objects form

Both spots and pea-shooters consistently appear in the same respective locations within the chamber, and so some understanding of the conditions that may be expected to be prevalent in these locations may offer insight into the processes that cause the objects to appear. The differences in conditions of space charge and potential that might be expected to result from the different electrode arrangements are therefore considered in the following.

The locations at which both types of object occur are to be found along the axis of the cathode. In order to consider the likely nature of the potential distribution along the axis of the discharge, the distribution caused by the electrodes before any space charge is present is first examined.

Vacuum potential distributions along the axis of the chamber, as calculated for the electrode configurations with and without the anode grid, are shown in Fig. 109. In order to represent the negative bias, the vertical scale is arranged to have ground located at the top, and full cathode potential at the bottom.

The axial profiles calculated for the two electrode arrangements both show the vacuum potential to remain close to the cathode voltage along the axis within the cathode, and to rise to ground across the region beyond the ends of the electrodes. The distance over which much of this rise occurs is reduced somewhat by the presence of the anode grid, corresponding to a relatively greater magnitude of electric field in this case.

In order to estimate the ways in which these profiles are likely to be altered by the presence of space charge, the published accounts of potential structure in IEC operation are considered, and their relevance to the conditions described here assessed.

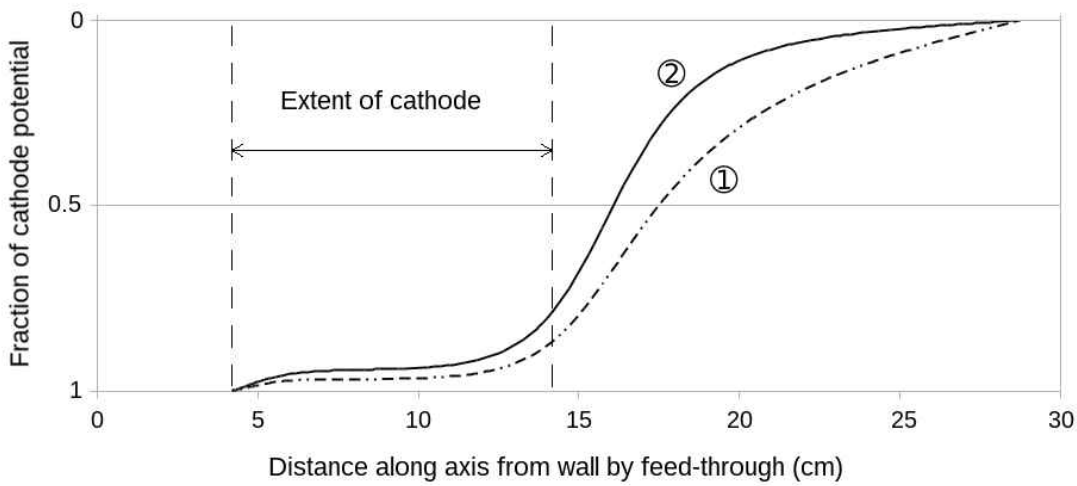

Fig. 109. Vacuum potential distribution along the axis of the electrode assembly; ① with no anode grid; ② with anode grid.

In the review of IEC literature, multiple reports were found describing the experimental measurement of an accumulation of positive space charge occurring at the centre of a spherical grid cathode. This might be expected to occur rather generally, since ions will be injected into this space, from which there is relatively little electric field to extract them, at least at vacuum conditions. The nature of the ion injection will change with pressure however, since ion energies and penetration distances into the cathode will both be determined by the collisional dynamics of ion transport. The resulting ion distribution within the cathode may therefore be expected to vary from a centrally-peaked distribution in the ballistic, low-pressure limit to one that is shifted to be closer to the cathode radius at higher pressures.

The potential distribution will also be significantly affected by high levels of ionisation occurring within the cathode, since this constitutes another input of ions into the space, and also because the electrons produced will act to modify the potential created by the ion space charge, as described above in Section 6.3.1.2. The manner in which this occurs in an IEC context is illustrated by the modelling performed by Ohnishi and co-workers [43]. This was described in Chapter 4, and is summarised in the following.

In the work described in [43], the potential structure occurring within a grid cathode is modelled for operation in both ballistic and collisional regimes. The ion influx is generated in the relatively strong electric field surrounding the cathode, and the resulting injection of positive charge through the cathode apertures is found to cause a relatively high ion density to accumulate in the interior. In the absence of any ionisation, this results in the formation of a region of significantly positive space charge, or a virtual anode, located within the centre of the cathode. The introduction of a significant degree of ionisation occurring within this region however causes equal numbers of ions and electrons to be produced, and for steady state operation these must both be transported from the region. This is shown to cause the potential to become sufficiently more negative to allow the electrons to escape via the apertures.

In the cylindrical cathode used for this study, the potential structure will be influenced by similar mechanisms, that will operate in a manner according to both the geometry of the set-up and the dynamics of ion transport associated with the operating conditions. The underlying structure will be expected to be determined by the ion distribution, with the electrons accumulating in such a manner to ensure their exit from the cathode.

At very low pressures, when ion motion is largely ballistic, the accumulation of ions within the cathode may be considered in terms of their kinetic energy; they will not be brought to a halt within the cathode at these conditions unless by a space charge potential of equal magnitude to this. At the relatively much-higher pressures relevant to this discussion however, the dynamics of ion injection are also expected to be significantly determined by the collisional path lengths. Most collisions involve either charge exchange or momentum transfer, which processes both effectively result in the collided ion losing its kinetic energy. Whilst ion energy will still have a limiting effect upon the magnitude of positive potential that may occur, this is

expected to be modified by electrons from ionisation at these pressures. The uncertainty surrounding the electric field distribution during operation of the discharge makes the estimation of ion energies subject to a correspondingly large degree of uncertainty in any case. However, the cross sections for charge exchange and momentum transfer vary relatively slowly with ion energy, and so the mean free paths for these collisions may be estimated with a better degree of confidence. These will provide some insight into processes affecting the nature of the ion influx occurring within the cathode.

In apparent contravention to the above considerations, this is done by initially estimating the electric field for relevant conditions, in order to obtain estimates for *E/N*. This is because average ion energies are quite well defined for values of *E/N*, and these may then be used to calculate mean free paths. As noted above, the values for *E/N*, and so in turn, ion energies, are subject to the possibility for considerable error. The mean free paths calculated however are relatively insensitive to this, as will be shown below.

Ion energies are estimated using the expressions given in [63] and [82]. These expressions refer to the temperature of a one-dimensional Maxwellian distribution, and are given as functions of *E/N*. It is likely that the real ion energy distributions at these conditions may vary somewhat from a Maxwellian [69], but given the degree of uncertainty concerning electric field, this is considered likely to be a lesser source of error. For the purpose of estimating *E/N*, most activity is considered to occur in the region radially surrounding the electrodes, and the strength of electric field for discharge conditions is estimated to be a nominal one-half of the vacuum value. The reasoning behind this is that the vacuum field between the electrodes constitutes most of the cathode fall, and the effect of the plasma will be likely to distribute more of the potential across a somewhat greater distance.

Ion energies are calculated for two sets of conditions which comfortably encompass those at which spots and pea-shooter objects are evident. Mean free paths are also calculated for these energies and pressures, using Eqn. (4) from Section 4.4.3:

$$\lambda_{mfp} = \frac{1}{N\sigma}$$

Where σ refers to the cross section and N is the number density of the background gas. The density was obtained from the pressure by re-arranging the ideal gas law, using Eqn. (1) from Section 3.3.1.

The cross sections used are those recommended for momentum transfer for argon in [67] and for charge exchange in helium from [86]. The results of these calculations are shown in Table 3.

As noted, the estimations of electric field strength, and therefore ion energies, are considered to be order-of-magnitude estimates at best, and are likely to be unrepresentative. These estimates are of the order 100's eV to keV at these conditions.

Electrode set-up	Cathode voltage (kV)	Helium			Argon		
		Pressure (mTorr)	Ion energy (keV)	Mean free path (cm)	Pressure (mTorr)	Ion energy (keV)	Mean free path (cm)
Anode	3	50	0.3	0.46	15	0.38	0.37
	8	30	1.84	1.07	10	1.76	0.73
No anode	3	50	0.13	0.41	15	0.18	0.33
	8	30	0.8	0.91	10	0.82	0.63

Table 3. Estimated ion temperature calculated for helium and argon at a variety of different conditions

The calculated path lengths however vary by a factor of around 2, and the difference in the path lengths calculated for the two sets of conditions may be seen to be largely a function of pressure. The distances in both cases are indicated to be smaller than 1 cm, and so whilst the radial potential fall might extend some way through the cathode apertures, these values suggest most ions will not travel further than half-way to the centre of the cathode.

From the consideration of distributions of emission made in the previous chapter, a significant degree of the ionisation occurring within the cathode is expected to be caused by the fast neutral population generated by ions travelling to the cathode. The distribution of these neutrals will be somewhat different for the discharges obtained in the apparatus with and without the anode grid, but in either case this may be broadly characterised as a radially-convergent flux. The emission distributions indicate this to pass through the cathode and continue to the wall, and so the corresponding distribution of ionisation will be expected to be peaked along the axis of the cathode, since this represents the region of greatest convergence.

The radial beams of the beam mode discharge obtained with the anode grid will cause this distribution to vary periodically along the axis, with maxima associated with the regions at which sets of beams converge. The neutrals are injected at four well-defined locations along the cathode axis, but it is noted that the radial beams associated with the two rings of apertures located closest to the midpoint of the cathode axis are notably brighter than those associated with the end rings, indicating a relatively greater degree of ionisation to occur in the more centrally-located of these regions.

This assessment suggests that charge generation by ionisation may constitute the more important process for determining the ion distribution along the axis of the cathode. A correspondingly significant degree of electron generation will therefore also be expected to occur along the axis, some of which will be transported from the cathode in the axial electron beam that is associated with the ion- and neutral-sustained discharge in either electrode arrangement.

These conditions are now briefly compared with those associated with the anode double layer objects. Conditions in which ADLOs are observed to occur are described as having similar densities of ions and electrons, as may be created by ionisation occurring within a sheath, and also in being immersed in an externally-generated plasma.

For the self-organisation mechanism described in Section 6.3.1.3 to function, which is considered important for the formation of the anode double layer objects, a well-defined gradient of electron energy is required for the spatial occurrence of excitation to be localised with respect to that of ionisation. It is noted that such a gradient might be expected to occur if thermal electrons are extracted from the border of a region of relatively high density, by a potential in excess of the ionisation energy of the surrounding gas operating across a distance that is small compared with the collisional mean free path for these electrons.

The condition of similar ambipolar charge densities may generally be found along the axis of the discharge, as indicated by the considerations made above regarding the distribution of ionisation. In the set-up without the anode, electrons are expected to be transported from the end of an axial region of relatively high charge density that extends along the axis of the cathode. This point corresponds broadly to the location at which the pea-shooter objects are observed to occur, and it is noted that such a local gradient of electron energy might conceivably occur at this location. Although the geometry is somewhat different, the behaviour observed to occur with the additionally-enclosed cathode in Chapter 4 is an example of a double layer forming at the point of electron extraction from within a grid cathode at conditions of similar pressure.

In the set-up with the anode grid, regions of locally high charge density are expected to occur at the points of beam convergence. Should any electrons be transported from these along the axis towards the open end of the cathode, then such a gradient may quite possibly occur also at the locations in which spots appear. Upon the appearance of a spot, increases are evident in levels of both axial current and anode current (Fig. 99), indicating an element of the electron current produced in the spot to be transported axially.

This assessment is necessarily somewhat conjectural, since the information available concerning both the potential structure and details of electron transport within the cathode during these discharges is very incomplete. It is however considered to be an illustration that suitable conditions for the formation of anode double layer type objects might quite conceivably exist in the locations at which the spots and pea-shooters are observed.

It is therefore considered possible for significant similarities to exist between conditions found in relevant regions within discharges described in this study and those associated with the anode double layer objects. Substantial differences clearly also exist between these different sets of circumstances however; the anode double layer objects appear attached to a physical anode, whereas the spots and pea-shooters both appear free-floating in space. If the presence of this anode is considered

intrinsically necessary for the anode double layer type of object to exist, then the spots and pea-shooters may not be expected to represent the same class of object. The relative importance of this electrode for the anode double layer object is therefore considered briefly, as follows.

In the experiments describing ADLOs, that are outlined in Section 6.3.1.3, it is the bias applied to the auxiliary anode that causes the gradient of electron energies important for the objects to form. In this respect, the anode is critically necessary for the production of these objects. The considerations above however suggest that similar conditions might be produced within the grid cathode by virtue of the charge accumulations that occur here, and so the additional electrode would not necessarily be required in these circumstances.

The effect of the anode has also been noted to assist in the maintaining of the separation in charge polarities between the regions of relatively more negative and more positive potential within an anode double layer object, by extracting thermal electrons from the ion-rich 'nucleus' of the object. This function is not considered to be required for the initial formation of such an object, since the element of self-organisation to which this is attributed is described to result from the finite range of energies at which electrons may excite, but not ionise, the background gas. As noted previously, this process may occur given a suitable distribution of electron energies, irrespective of the presence of a physical anode. The absence of the electrode does therefore not preclude the formation of such objects.

The anode is however noted to assist in the sustaining of the objects in a steady state, by extracting the electrons that result from inelastic collisions occurring within the central region of the object. Without the operation of this mechanism, the net effect of the processes causing excitation and ionisation will be to cause electrons to be transported into the central region, and ions to be transported away from this, and so causing the potential difference across the double layer to dissipate. Should ions continue to be transported away from the surrounding region however, and the object be surrounded by a plentiful supply of electrons, it might conceivably be that the object could persist, whilst becoming globally more negative.

To summarise this assessment, it is observed that conditions necessary for the formation of anode double layer objects might conceivably be found within the cathode during discharges in which spot and pea-shooter objects are observed. Insufficient information is available concerning the distributions of charge density and transport mechanics within the cathode for this to be certain, but consideration of that which is available indicates that the objects referred to as pea-shooters and spots might quite conceivably be created by the same processes of self-organisation that produce the anode double layer objects.

In the following section, some of the observed physical characteristics of the objects are considered in relation to those of the anode double layer objects, in order to evaluate whether these are consistent with the two classes of object being fundamentally similar.

6.3.2.2 Physical characteristics of objects

In the following, the physical characteristics of the spot and pea-shooter objects are considered, along with those of the anode double layer objects.

It is noted that the different sets of experimental conditions at which the spot or pea-shooter objects and the anode double layer objects were observed causes significant differences to exist between the nature of the measured parameters. This is principally because the anode double layer objects described elsewhere are generally obtained in an independently-sustained plasma, and so the currents measured at the auxiliary electrode in these cases are principally those caused directly by processes associated with the object. For the discharges described in this study, the objects constitute a relatively small part of the discharge, and measured currents are representative of all processes occurring within the chamber.

This makes the interpretation of the electrical parameters difficult. For example, the increase in levels of current associated with the appearance of the spots upon is easily identified in the current and voltage traces shown in Fig. 99, but it is not clear if this is directly caused by the object, or by a secondary effect that it has upon the wider functioning of the discharge.

Some properties of the objects are distinguishable from those of the rest of the discharge however, including the approximate size of the objects, and the AC component of the fluctuations evident in the electron currents. The observations of these characteristics are therefore considered with reference to the theoretical descriptions formulated in [100], which are as follow.

The characteristic diameters of the objects are considered first. The authors of [100] observe the diameters of anode double layer objects to be described by the effective electron mean free path for ionisation multiplied by the ionisation probability per electron transported across the double layer.

This is demonstrated by first noting that the densities of ions and electrons will be similar in a situation in which significant levels of ionisation are occurring, such as an anode sheath with a potential fall in excess of the ionisation potential. It is noted that the mechanisms by which a double layer forms from an anode sheath are imperfectly understood. Once a double layer has formed however, it is observed that should the fluxes of ions and electrons across this potential structure originate from populations of similar densities, then the magnitudes of these fluxes will be related by $I_i = I_e \times \sqrt{m_e / m_i}$, when I_e and I_i, and m_e and m_i, refer to the electron and ion currents and masses respectively. It is noted that this is expected to be the case for transport across the spherical double layer.

At steady state conditions the ionisation rate within the object is equated with the ion extraction rate across the double layer, in order to maintain an equilibrium. For the corresponding electron flux across the double layer to produce exactly this degree of ionisation, the diameter of the object is therefore required to be the fraction of the

ionisation mean free path for these electrons that corresponds to $\sqrt{m_e/m_i}$. This provides an expression for *D*, the diameter of the object:

$$D = \lambda_i \times \sqrt{m_e/m_i} \ . \qquad (6)$$

In this expression λ_i is the mean free path for ionisation, again calculated using Eqn. (4), but using cross section values for ionisation by electrons, that correspond to electron energies a little in excess of the ionisation energy for the gas.

The authors also consider a characteristic 'ionisation time', which is described by the ionisation mean free path, as evaluated above, divided by the electron velocity that will correspond to the potential fall across the double layer. This therefore describes the average time it takes for an electron to travel one mean free path, and so cause an ionisation. This may be written:

$$t_{iz} = \frac{1}{N \, \sigma_i \, v_e} \qquad (7)$$

In Eqn. (7), the term σ_i is the ionisation cross section for electrons and v_e refers to the electron velocity, which is calculated from the energy gained in acceleration across the double layer potential, Φ_{DL}, by $v_e = \sqrt{2 \times \Phi_{DL}/m_e}$.

From the expressions of Eqns. (6) and (7) it may be noted that these characterisations of the anode double layer object properties are independent of plasma conditions, other than the condition that the densities of ions and electrons are similar, and that the potential across the double layer is similar to the ionisation potential. The authors of [100] find a general order-of-magnitude agreement with the observed characteristics, when cross section values are used corresponding to those at around 2 eV above the ionisation potential. They note that discrepancies in the observed and calculated diameters of the objects will be likely due to the effect of the anode disc.

Should the objects occurring in the IEC plasma be caused by the same processes, they might also be expected to result from conditions of similar densities of ions and electrons, and to also be composed of a double layer with a potential fall similar to the ionisation potential. They should in this case be equally-well described by these expressions.

In order to test this by applying these expressions to the observed characteristics of the objects, the approximate diameters of these, and the rise time evident in the current waveforms are both assessed. This is done for the spots, since the pea-shooters show additional variation in both these respects, which will be discussed subsequently.

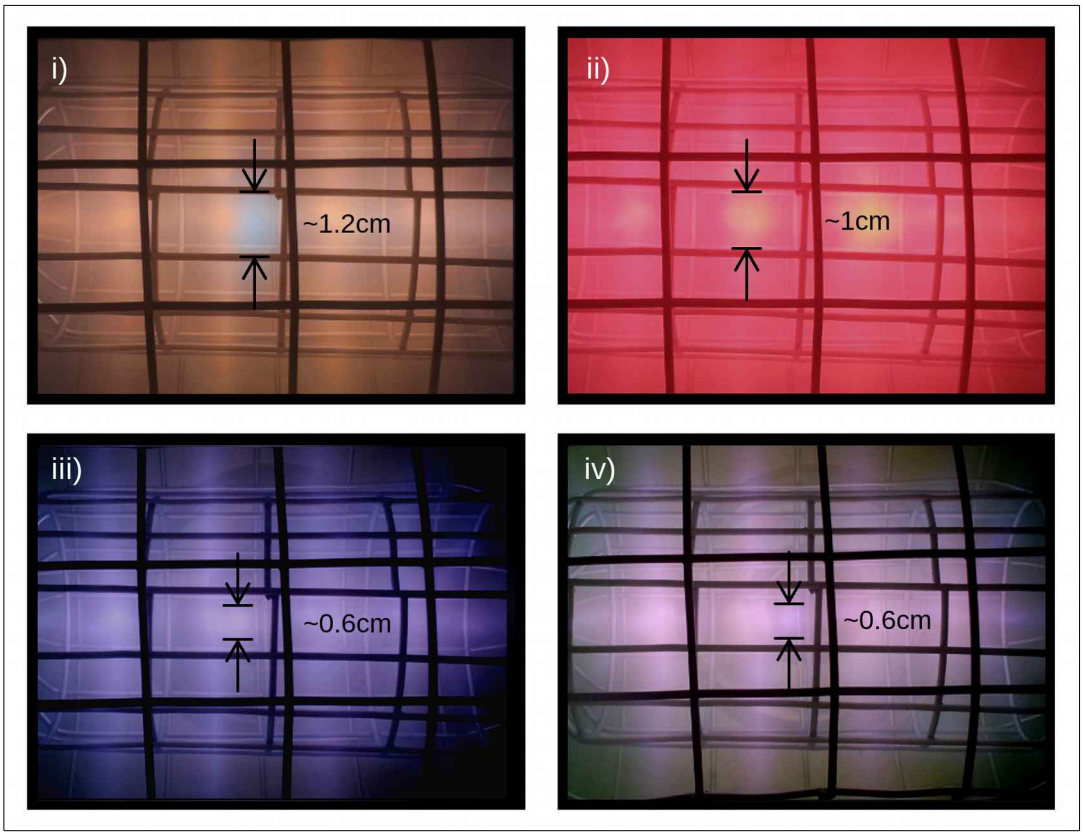

Fig. 110. Enlarged sections of photographs from Fig. 98, showing approximate diameters of spots occurring in i) helium at 41 mTorr, ii) neon at 13 mTorr, iii) argon at 7.9 mTorr and iv) krypton at 11.5 mTorr

Enlarged sections of the photographs shown previously in Fig. 98 are reproduced in Fig. 110. Using the dimensions of the electrode geometry as a guide, the approximate diameters of the spots are estimated and indicated upon the images. The resulting dimensions are noted to be quite rough estimates, both because of the method used and also because of the somewhat poorly-defined boundary of the spots.
A similar evaluation is made of the rise time of the fluctuations in axial electron current, as measured whilst spots were evident in discharges obtained in different gas species. This is done by considering the waveforms shown previously in Figs. 100 and 101, and also waveforms captured during discharges in nitrogen and neon (Fig. 111). The variation in waveforms illustrated previously in Fig. 101 are shown to have little effect upon the rise time.

In order to calculate theoretical values for these properties, the magnitudes of ionisation cross sections for each species of gas must be evaluated for energies a little in excess of the relevant ionisation potential for each case. Ionisation cross sections are taken from [110], which is the same source used in [100]. The magnitudes of these vary considerably at values close to threshold, and so the results of the calculations are somewhat sensitive to the values estimated for the potential difference across the double layer.

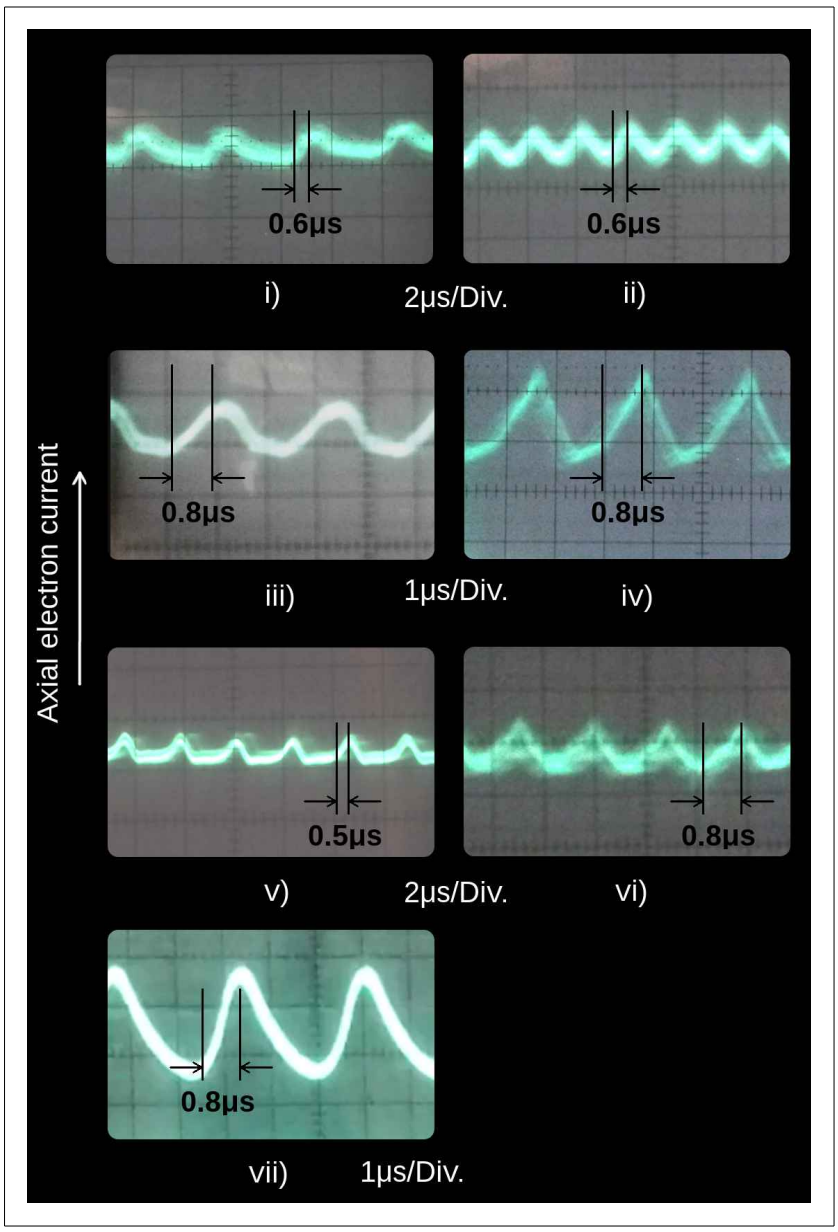

Fig. 111. Examples of waveforms in axially-collected electron current whilst spot are evident, with estimated current rise times annotated. Waveforms are reproduced from Fig. 101, showing rise time to be unaffected by: i) and ii) variation in frequency (krypton, 11.5 mTorr); iii) and iv) variation in shape (helium, 41.7 mTorr). Additional waveforms show rise times in: v) nitrogen, at 9.9 mTorr; vi) neon, at 12.6 mTorr; and vii) argon, at 8.7 mTorr

This is made additionally so for the calculations of ionisation time according to Eqn. (7), since the double layer potential determines not only the energy at which the cross section is evaluated, but also the electron velocity; an increase in energy will cause both of these factors to bring about a reduction in ionisation time.

If the condition of equal densities of ions and electrons is assumed to be met, then the free parameter for these calculations is the magnitude of the double layer potential. If

the observed characteristics are to be considered representative of anode double layer-type objects, then this should be found to be only a little above the ionisation potential for each case.

The results of calculations are listed in Table 4, showing the calculated and measured values of ionisation time and object diameter, and the amount of energy above threshold to which the cross section sizes and electron velocities correspond to. The cross sections are shown in Fig. 112. These have the values used marked upon them, which may all be observed to be towards the threshold region.

Gas species	Pressure (mTorr)	Potential above ε_{iz} (V)	Cross section ($10^{-20}m^2$)	Calculated ionisation time (μs)	Measured ionisation time (μs)	Calculated diameter (cm)	Measured diameter (cm)
Helium	41.7	2.5	0.03	0.8	0.8	2.9	1.2
Neon	12.6	7	0.085	0.9	0.8	1.5	1
Nitrogen	9.9	3.5	0.2	0.6	0.5	0.7	-
Argon	8.7	1.5	0.18	0.8	0.8	0.7	0.6
Krypton	11.5	1.2	0.18	0.6	0.6	0.4	0.6

Table 4. Results of measured and calculated dimensions and current-rise times, showing discharge parameters and values for cross sections used in calculations, evaluated at energies in excess of the ionisation potentials by the amounts also indicated.

Generally speaking, a very good degree of correspondence is found between the measured characteristics and theoretically-predicted values, when the double layer potentials are kept to within a few eV of the ionisation potentials. The characteristics observed in neon require the largest excess of potential in this respect, which is found to be around 7 V. The agreement largely extends to the observed diameters also, although the diameter predicted for helium is larger than that observed by a factor of a little greater than 2.

It is noted that cross section sizes at these energies remain smaller by an order of magnitude than the values attained at greater energies. The results of these calculations therefore suggest that the electron energies are indeed of this order.

The ionisation mean free paths at these energies are noted to be two orders of magnitude larger than the spot diameters. The bright emission localised within these objects indicates electrons to be confined around a positive space charge structure.

The spots are therefore indicated to represent structures that have similar characteristics to the anode double layer objects, in being space charge configurations consisting of a relatively-positive core, surrounded by a relatively more negative region. This structure constitutes a spherical double layer with a potential of a few volts above the ionisation potential of the background gas, so that electrons accelerated across it may cause excitation and ionisation.

It was observed that the absence of a physical anode in the vicinity of the object will be expected to result in a net influx of electrons to the object, and the dissipation of the potential difference across the double layer. The fluctuating behaviour associated with spots, and with some instances of pea-shooters, is consistent with the repeated appearance of structures that may not persist in the steady state. This is noted to be different from the flicker behaviour that was attributed to the power supply regulation.

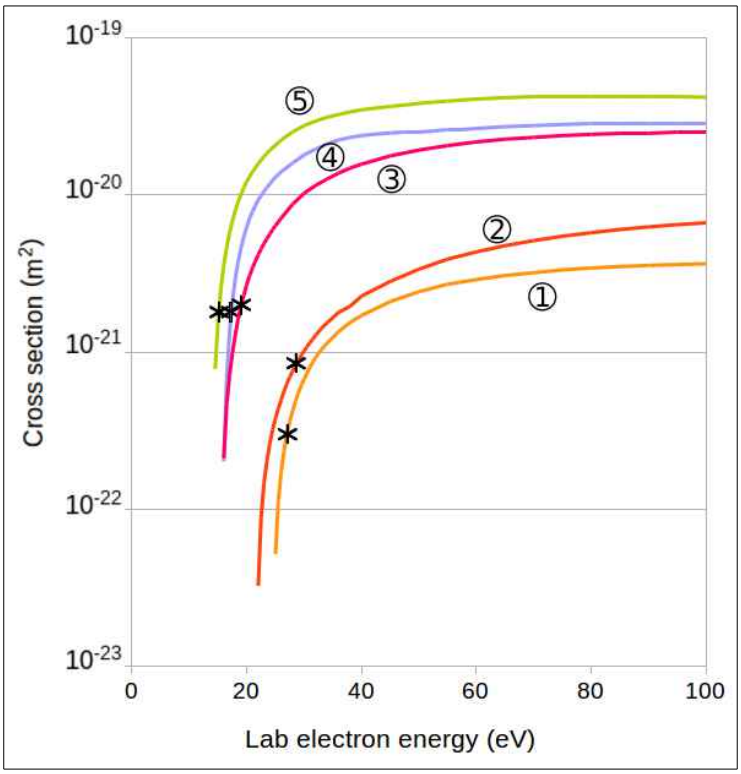

Fig. 112. Ionisation cross sections for electrons in ① helium, ② neon, ③ nitrogen, ④ argon, and ⑤ krypton. The star symbols indicate values used for the calculations, corresponding to energies a little over threshold as given in Table 4. Data are taken from [110]

This analysis has concentrated upon the observations of spots so far, and the pea-shooters will be considered briefly in the following. The analysis of the pea-shooter objects will not be made in the same detail as for spots, in part because less measurements have been made of these objects, and in part because the degree of variation they show makes interpretation more difficult.

It is noted that, once formed, the dimensions of the objects are not dissimilar to those of the spots. The current waveforms are somewhat different, and present some problems for the defining of the rise time. In Fig. 113, this is illustrated for the argon waveform shown previously in Fig. 105. The apparent rise time of 0.4 μs is indicated on the figure, but the waveform might also be interpreted as a superposition of a pulse train and a square component. The ionisation time calculated for this pressure, which was 11.2 mTorr, and using the same potential as for the spot in argon, suggests

a rise time of around 0.6 μs, which is close to that of the waveform, regardless of interpretation.

The evolution in size observed to be evident during the formation of pea-shooter objects suggests that they form in a different manner to the spots. The current waveforms are also different to those associated with spots, in that they appear more like a pulse train, although as observed above, this might be interpreted in different ways.

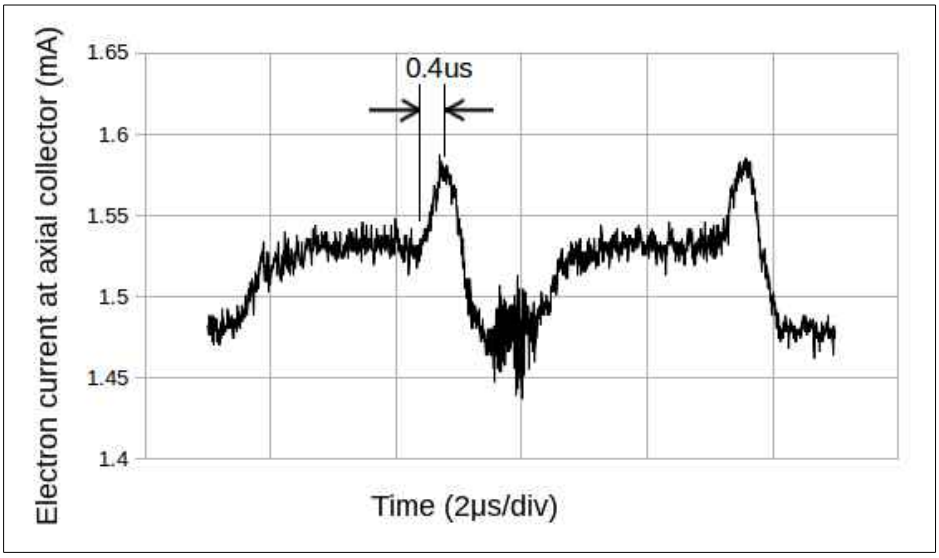

Fig. 113. Axial current waveform observed when pea-shooter was evident in argon at 11.2 mTorr, with estimated current-rise time indicated.

The behaviour in which the pea-shooters may transition from fluctuating to steady state is similar to that described in [100], and the unstable state described in that work also produced a series of current pulses. The association with the axial beam illustrated in Fig. 106, and the interpretation of the spot fluctuations, suggests that the axial beam may transport electrons from the pea-shooter sufficiently well at some conditions to maintain a steady state.

A thorough analysis is made difficult, since the axial beam is known to also be evident when the objects are not. The emission that may be attributed to the object may therefore not be definitively separated from the possible background element which may remain from the beam. Some suggestion for the axial transport of electrons from pea-shooter objects may be seen in some images in Figs. 103, 104 and 106, in which a narrower, brighter element may be observed in the axial beam when the object is evident. If electrons are transported from a stable double layer object, this might be expected to follow the same principle observed to operate for the extraction of electrons from the CC mode discharge in the enclosed cathode, in Chapter 4. This was found to occur with the ratio of areas for electron and ion extraction related by $\sqrt{m_e/m_i}$. If the pea-shooter object is characterised as having a nominal diameter of 1 cm, its surface area will be π cm^2. The corresponding diameter of a region for electron extraction, calculated according to this principle, will be

around 2 mm for helium, 1.3 mm for nitrogen and 1.2 mm for argon. The objects featured in the photographs are not exactly of this diameter, but the general relation evident between the diameters of the bright elements in the beams and the objects may be observed to be at least consistent with this.

Further work is required to better understand the behaviour of the pea-shooter objects. Despite the variation in behaviour, the similar sizes and current rise times, electron-induced emission, and occurrence at similar conditions of pressure indicate pea-shooters and spots to be quite closely-related phenomena, and they are expected to be caused by similar processes.

6.4 Conclusions

In this chapter, the appearance of spherical space charge objects was described as occurring in both the beam mode discharge and the corresponding ion- and neutral-sustained discharge obtained without the anode grid. These have been referred to as 'spots' and 'pea-shooters' respectively. The colour of emission from these objects indicates them to be sustained by the action of electrons.

These objects were noted to appear in different characteristic locations in each of these cases, and to be evident at conditions of moderate to high pressures within the beam mode range, and at conditions of moderate to high cathode current. Consideration of the conditions that may be expected to occur within the cathode during operation of the discharge indicates that the locations at which the objects form are likely to be immediately adjacent to regions of locally high densities of ions and electrons.

The spherical appearance of these objects, and the fluctuations that are often evident in the additional element of current associated with their presence, cause them to resemble phenomena described in the literature that are shown to be associated with anode double layers, and which have been referred to as 'anode double layer objects'. This type of object is most often associated with a flow of electrons to a physical anode, and has been described elsewhere to consist of a relatively more positive region of charge, surrounded by a relatively more negative region. This separation of charge is described to cause a potential fall across the spherical double layer a little in excess of the ionisation potential of the gas in which it occurs. Electrons accelerated across this potential may therefore cause excitation and ionisation, which because of the energy dependences of cross sections for these processes, will occur in well-defined spatial regions. This acts to maintain the potential difference across the double layer, and so this type of object represents a self-organising configuration.

The processes and conditions leading to the formation of these anode double layer objects have been outlined, and a comparison made with the observations made of the spot and pea-shooter objects.

At the conditions of pressure at which they are observed, both the physical size of these objects and the temporal rise time associated with the current waveforms they

produce, are found to be consistent with the characteristic behaviour reported for anode double layer objects. These similarities are indicative of the activity of electrons having energies slightly greater than the ionisation potential of the gas. Since this is a fundamental characteristic of anode double layer objects, and also since these are also described to occur at conditions of locally-high ambipolar charge densities, as are expected to be present at the locations at which the spot and pea-shooter objects appear, these similarities are considered to indicate the spot and pea-shooter objects to be caused by similar processes to those that cause the anode double layer objects to form.

The effect that the appearance of these objects has upon the overall operating characteristics of the ion- and neutral-sustained discharges is noted to be generally quite small, although the spots appearing in lighter gases may cause a substantial rise in levels of cathode current. They are therefore not considered to be as serious a cause of instability as the CC mode in the enclosed cathode, but still to constitute a somewhat unpredictable element of discharge operation.

In Chapter 4, it was found that an element of confinement is required for electrons to be significantly reactive at these pressures, and also that such a means of confinement must allow for the extraction of thermal electrons created by ionisation within the confined volume. These principles will be expected to apply generally, and so also to the objects described in this chapter. The periodic fluctuations often associated with these objects show a rise time that may be related to the ionisation time for the conditions of pressure and gas ionisation potential at which they are evident, suggesting that the issue of electron extraction may be associated with these fluctuations. The possibility that the stable states observed may involve an intrinsic electron extraction mechanism, as was found for the CC mode discharge occurring in the enclosed cathode, is interesting and worthy of further investigation.

Finally, it is noted that the cylindrical geometry used in these experiments assists in the observation of these phenomena, since this causes the spatial separation of different processes occurring along the axis of the cathode. It also helps to distinguish them from other types of plasma, such as the CC mode, that have a spatial extent determined by that of the enclosing cathode field.

To the best of the author's knowledge, no previous association has been made between anode double layer objects and space charge structures occurring in IEC operation. It seems likely that these structures will occur also in spherical geometries, and so may explain some aspects of the mode structure observed in these devices also.

Chapter 7
Space charge objects II

7.1 Introduction

The occurrence of near-spherical luminous objects within the cathode interior has been mentioned previously, and this is the second of two chapters in which their characteristics are described. In the previous chapter, space charge objects were observed to occur in both the experimental set-up with the anode grid, and also in the set-up with the anode grid removed. Some differences were evident between the formations occurring in these different circumstances, but both are considered to be sustained by the activity of a confined electron population accelerated across a localised region of relatively positive potential. This potential structure is characterised as a spherical double layer, with a potential difference a little greater than the ionisation potential of the gas in which it forms.

At certain conditions, both of these types of object may become replaced by larger entities, referred to as 'fireballs', which show a considerable range of behavioural characteristics, and appear to affect the overall state of the discharge to a much greater extent. These appear during operation at conditions of relatively high current, and at pressures similar to those at which spots appear, corresponding to moderately-high pressures in the beam mode range. Over the relatively restricted range of conditions at which they appear, these discharges constitute serious instabilities for the operation of a stable reactive source based upon the beam mode discharge, and so information concerning their dependences is of interest for the purpose of this study.

The presence of the anode grid is found to substantially affect the observed characteristics of these larger objects also, and so the distinction made previously between phenomena occurring with and without this grid is continued in this chapter. The considerable complexity of behaviour observed with these objects means that there are many characteristics to be described, and experimental results make up much of the chapter.

The structure of the chapter is as follows. In the section following this introduction, a brief account is given of the distributions of optical emission associated with these discharges, along with a description of general aspects of their occurrence. Some of the issues encountered in making observations of the objects are also outlined, and a brief account given of the experimental techniques used.

Following this, more detailed descriptions are given of behaviour observed to occur during specific experimental runs, which give an overview of some of their principal characteristics. Once these are established, further measurements are described that add further detail to this picture.

The findings are then discussed, considering the evidence these constitute for the understanding of the structure of these objects, and also how they relate to the wider understanding of IEC discharges.

7.2 Experimental observations

7.2.1 Overview of phenomena

When the discharge is operated at certain conditions, in cases both with and without the anode grid, space charge structures larger than spots and pea-shooters are observed to occur. In order to distinguish these, they will be referred to in the following as 'fireballs'. With the anode grid removed, these have been found to occur in argon, but not in helium, neon, nitrogen, or air. With the anode present, fireballs have been observed in argon, nitrogen, air and krypton. For the purpose of this study, the investigation of these objects is limited to those occurring in argon, for either electrode arrangement. Photographs of fireball objects in argon are shown in Fig. 114.

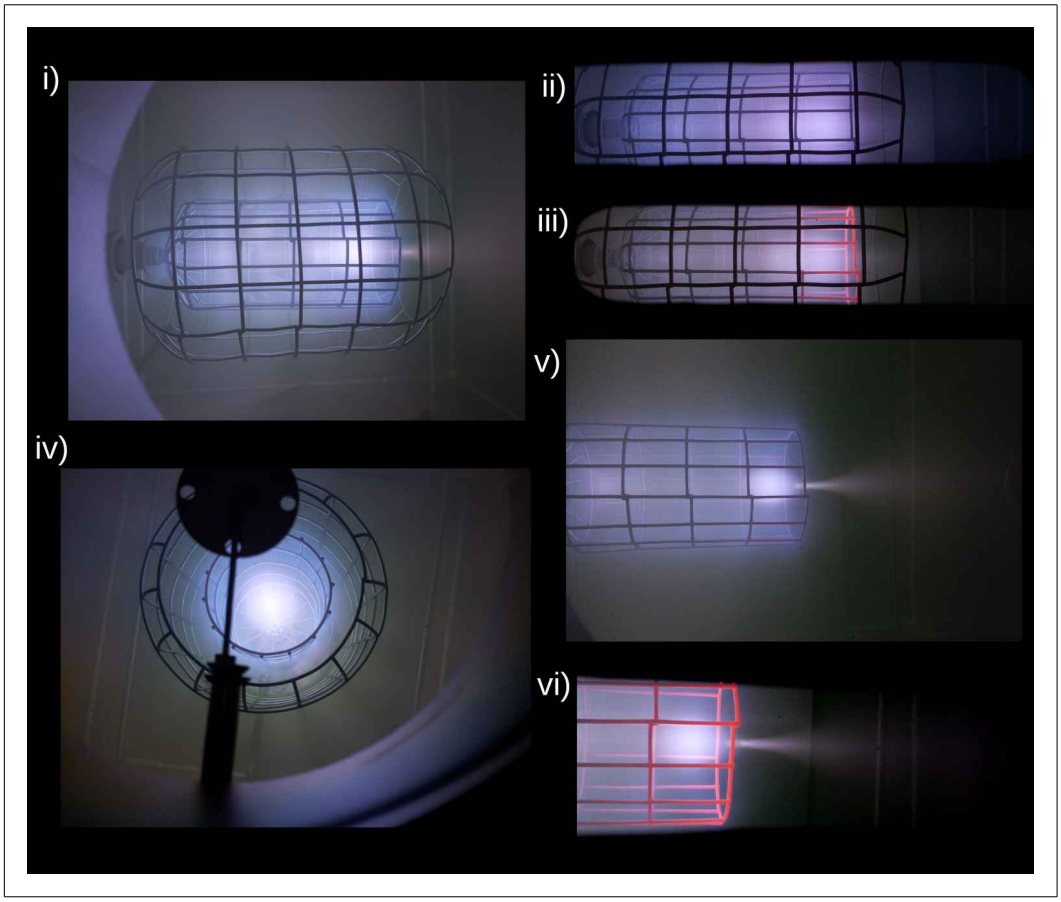

Fig. 114. Fireballs occurring in argon discharges, in i) - iv) set-up with anode grid, and v) - vi) without anode grid. i) and ii) show variation in jet; iii) and vi) show grid heating

In the case of no anode grid being present, the fireball evolves abruptly from a pea-shooter object; this change is apparent as a jump in the size of the object, and is also accompanied by a step change in voltage and levels of collected current. When running at a cathode current of 100 mA, voltages are generally in the region of around 6 kV. Characteristic regular fluctuations in electron current, as collected by the axial and radial collectors, also appear with the fireball; the frequency and waveform of these are found to vary a little with levels of current. A plume-shaped jet has been always observed to appear with the instance of the fireball that occurs without the anode grid; this is brighter than the axial pea-shooter beam that it replaces, and appears to be a characteristic feature of the fireball in this electrode arrangement. The object may appear at a fairly narrow range of pressures around 10 mTorr, and is generally found to become larger if pressure is subsequently reduced.

In the set-up with the anode grid, the fireball object appears more readily, and also shows more variation in behaviour. It appears at a similar range of pressures, and at lower values in this range may be preceded by a spot. Upon formation of these objects, cathode current generally rises instantaneously to the power supply maximum of 100 mA, and with subsequent reduction in voltage the object may persist at some conditions to currents as low as 60 mA. Typical voltages are somewhat smaller in this electrode arrangement, generally between 4 kV and 5 kV. The axial beam is generally less bright, and may vary from being as prominent as that shown in Fig. 114 i) to being hardly evident. The radial beams tend to disappear completely upon the appearance of a fireball, although an element of these may be seen to remain at the feed-through end of the cathode in Fig. 114 i). Fluctuations in electron current are also evident in this case, as collected by the anode and the axial and radial collectors. Relatively large-scale fluctuations in cathode voltage may also sometimes occur, but are not always evident.

In either electrode arrangement, running at higher levels of current causes the end of the cathode grid to become incandescent in a matter of a minute or so. A relatively high degree of sputtering is also associated with the fireball objects, with chamber viewports becoming obscured in a matter of minutes.

7.2.2 Overview of experiments

Experimental observations of the space charge objects were made under conditions of constrained available time, and equipment was at times required to be purpose-made at short notice. Ultimately, it was not possible to capture all aspects of the wide range of behaviour using all available diagnostics. Plasma conditions associated with these objects were also quite challenging, with considerable variations in discharge properties and also substantial accumulation of sputtered material on viewports occurring over relatively short timescales in these cases. These characteristics have meant that most measurements have needed to be made relatively quickly.

Measurements of electrical characteristics were recorded using the ADC arrangement as described in previous chapters. Measurements were made of cathode voltage and current, as indicated by the monitoring outputs of the power supply, and currents

collected radially and axially within the chamber. The axial and radial collectors used for this are as described previously. A diagram of the positioning of these within the chamber is reproduced as Fig. 115. The positioning of the radial collector is noted to coincide with the axial location of the row of cathode apertures closest to the open end, and so be approximately aligned radially with the location at which pea-shooter and fireball objects occur.

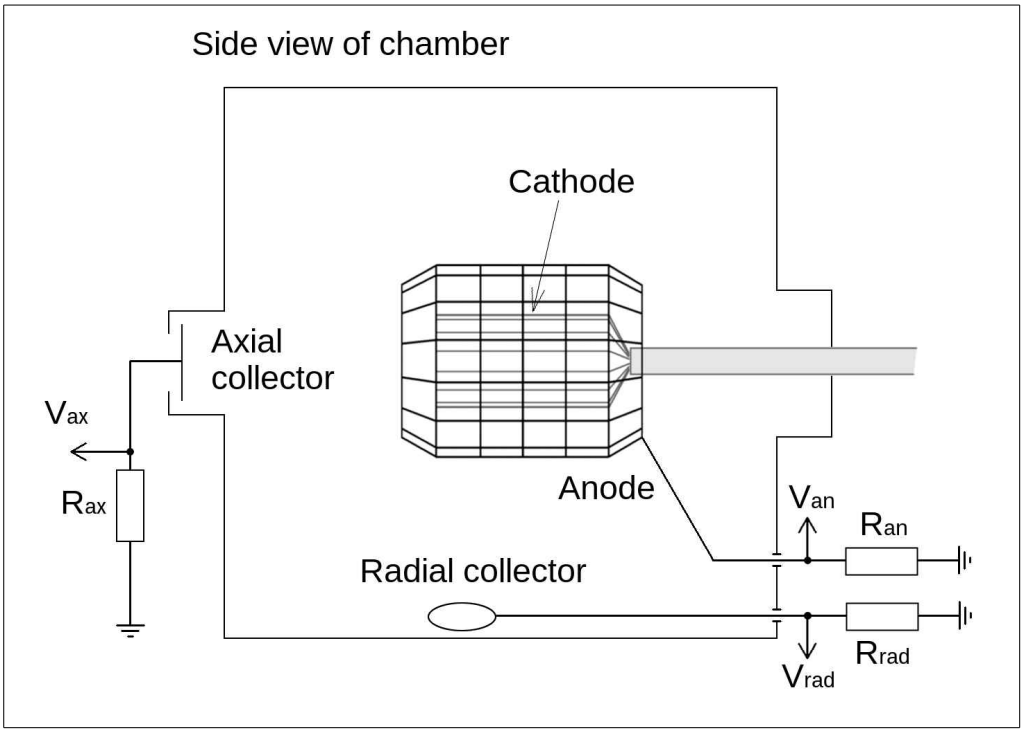

Fig. 115. Diagram showing electron current monitoring system

Shuttering was used for making some optical measurements, as this was found to increase the available time before port glasses were obscured. Spatial distributions of optical emission have been measured by photographic exposures, made using both a phone-camera and the ICCD fitted with a 35 mm lens.

The spectral composition of emission was measured using the Ocean USB spectrometer, since this enables fast captures over the entire range of wavelength sensitivity. The photo-multiplier tube was used to measure overall levels of undispersed emission over time. In order to resolve emission produced in localised regions, an optical path was set up so as to focus light produced at a point source on the axis of the discharge upon an insertion lens for an optic fibre. This meant that light emitted along a relatively small solid angle of one or two degrees subtended from the axis could be sampled. The optical pathway was mounted upon a stepper-driven translation stage, as described in Chapter 2. A seven-segment display integrated with the stage control enabled position to be monitored to a resolution of 0.1 mm. From the investigations in Chapter 3, the relative intensity of the 750.4 nm spectral line in argon dischgarges is known to be sensitive to the degree of electron activity causing excitation. The spectroscopic resolution of spatial distributions of emission was therefore made using the ICCD and a 750 nm filter.

The time-varying behaviour of the fireball discharges was monitored using both analogue and digital oscilloscopes, as described in the experimental set-up section. In addition to monitoring waveforms, the digital oscilloscopes can perform FFT analysis of signals, and also allow data capture. These captures however take a considerable length of time to be saved, during which time the display is frozen, and so the capturing of rapid evolution of time-varying behaviour may be complemented by the making of video recordings of live traces on a separate oscilloscope.

The analogue oscilloscope provides a different means of visualising the same signal, and a relative ease of adjustment, and at times this instrument may provide more information than the digital versions. Combinations of the two types of oscilloscope have been found useful in this work.

7.3 Results of measurements

In this part of the chapter, measurements made of the fireball discharges are presented. These are initially described with accounts of specific experimental runs that show characteristic behaviour, making reference to the current-voltage structure. Optical characteristics are then described, and as far as possible related to the behaviour outlined in the first section. Much of the material is devoted to the behaviour observed with the anode grid, since this is more varied.

7.3.1 Electrical measurements and visual appearance

In this section, experimental observations are described of the current-voltage behaviour of the fireballs, and how this corresponds to the visual appearance of these discharges, with distributions of emission described in each case. The first of these describes an instance of a fireball discharge occurring in the apparatus with no anode grid. The behaviour of fireballs occurring with the anode grid is then illustrated, using sets of measurements made during two separate runs, since the behaviour is more complex. The time-varying behaviour seen with the fireballs occurring in the set-up with the anode grid is also quite varied, and so these measurements are described subsequently in a separate section.

7.3.1.1 Experimental run 'No-anode FB#1'

The fireball object that appears without the anode grid often evolves from a pea-shooter type. When this occurs, the object is observed to suddenly become larger, and discontinuities are evident in measured electrical parameters. Dynamic current-voltage traces from an experimental run in which this behaviour occurs are shown in Fig. 116. During this run, electrical data were sampled at a frequency of around 44 Hz, and the ICCD camera recorded a series of images of the discharge; corresponding images are shown in Fig. 117. This run will be referred to as 'No-anode FB#1'.

The progression of the run is as follows: cathode voltage is initially increased until the object appears, at the point marked 'A', and then is then left for a while to stabilise. During this period the pressure rises and then falls again; this behaviour is commonly seen in discharges in this apparatus, and is possibly due to effects of desorption. In the case at hand, the chamber surfaces had recently been exposed to ambient pressure, and the effect is quite large. Cathode voltage may be seen to fall and then rise noticeably during this time.

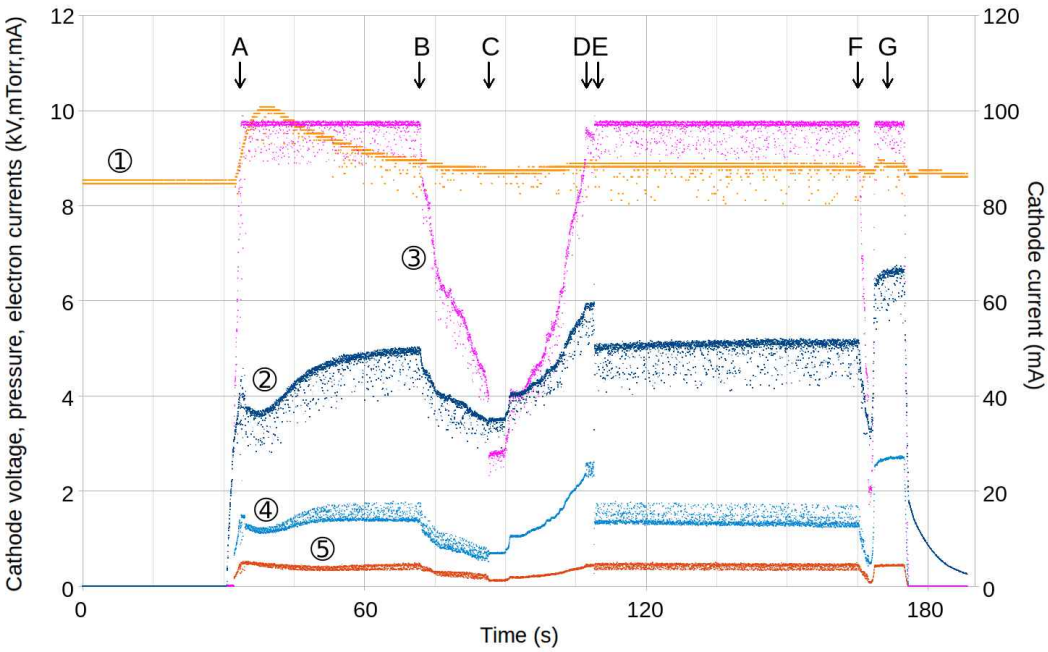

Fig. 116. Dynamic current-voltage traces recorded during a fireball discharge in the set-up without the anode grid; run No-anode FB#1. Key to traces: ① pressure; ② cathode voltage; ③ cathode current; ④ axial collector current; ⑤ radial collector current.

During this period, fluctuations in the currents to axial and radial collectors also grow in amplitude. After around 40 seconds, at the point marked 'B', the cathode voltage is reduced manually. This is continued until the point marked 'C', at which point the object disappears completely. When this happens, current falls from around 40 mA to a little over 25 mA, and fluctuations cease. Voltage is then increased again, and a pea-shooter appears almost immediately. This object remains evident until cathode current almost reaches the power supply limit. At the point marked 'D', the electron currents become time-varying again and the increase in voltage is halted; the pea-shooter also becomes larger at this point. After a few seconds, at 'E' the pea-shooter becomes a fireball; this evolution is accompanied by an instantaneous reduction in voltage of over 10 % and cathode current returns to 100 mA. No further adjustments are made for almost a minute, during which time voltage levels rise slightly. Finally, the voltage is ramped down again, at 'F', until the fireball disappears, and then quickly increased. A pea-shooter re-appears but does not evolve into a fireball ('G'), and voltage is ramped down again to finish the run.

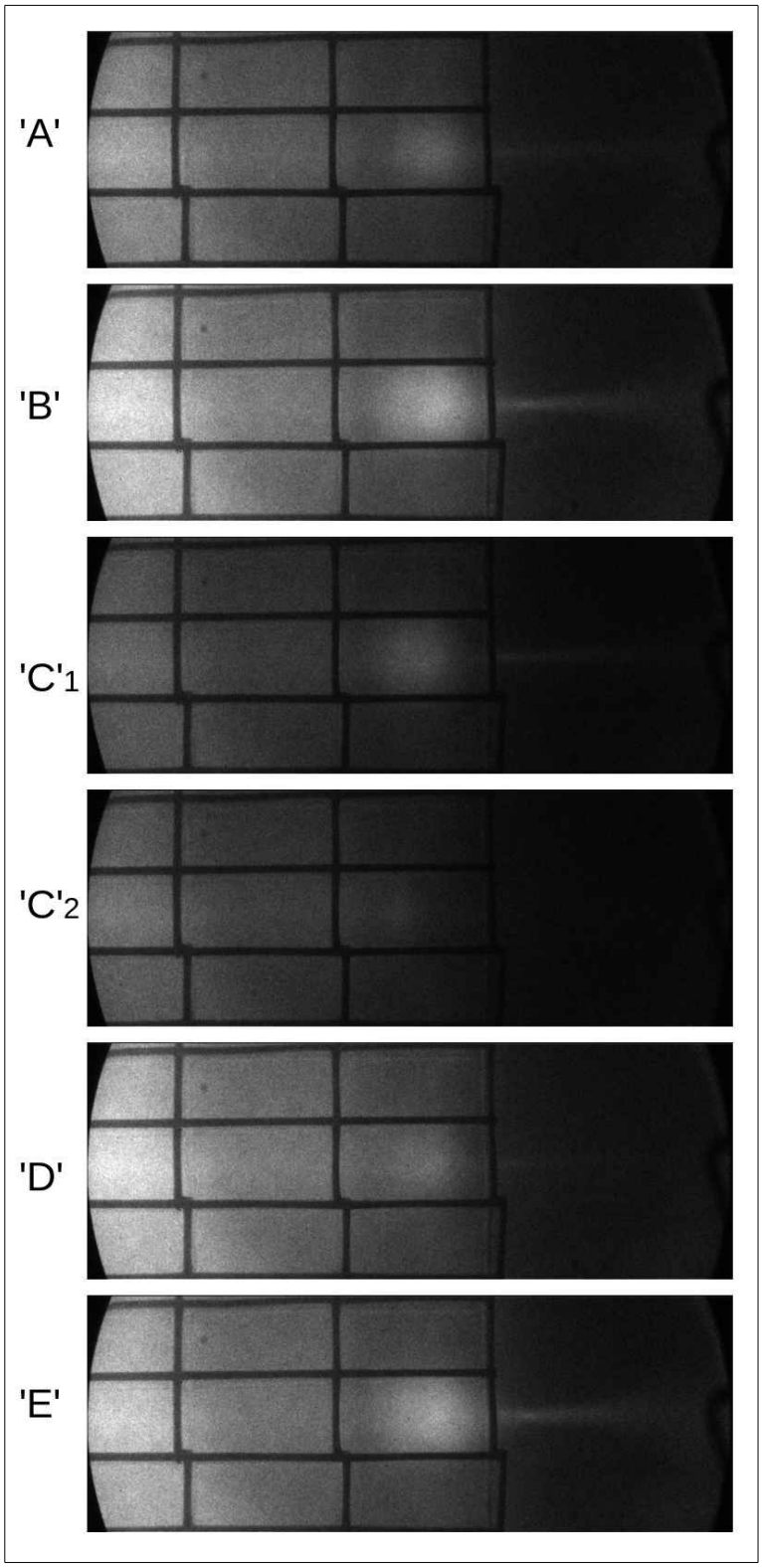

Fig. 117. Images recorded during the fireball discharge run No-anode FB#1. The frames marked 'A' to 'E' correspond to the points marked in Figs. 114 and 116; 'C'$_1$ and 'C'$_2$ show the discharge just before extinction, and just after the appearance of the pea-shooter respectively. 'D' shows the pea-shooter after it has become larger, and when the electron currents have become time-varying.

Images of the discharge during this run are shown in Fig. 117, at conditions corresponding to points 'A' to 'E' as indicated in Fig. 116. In comparing the images in Fig. 117, it may be observed that the intensity of emission from the fireball just before extinction (image marked 'C'$_1$) is similar to that of the pea-shooter just before transitioning to the fireball state (image marked 'D'). The intensity of emission from within the rest of the cathode in these images is very different however, which reflects the conditions of different cathode current at which the images were recorded.

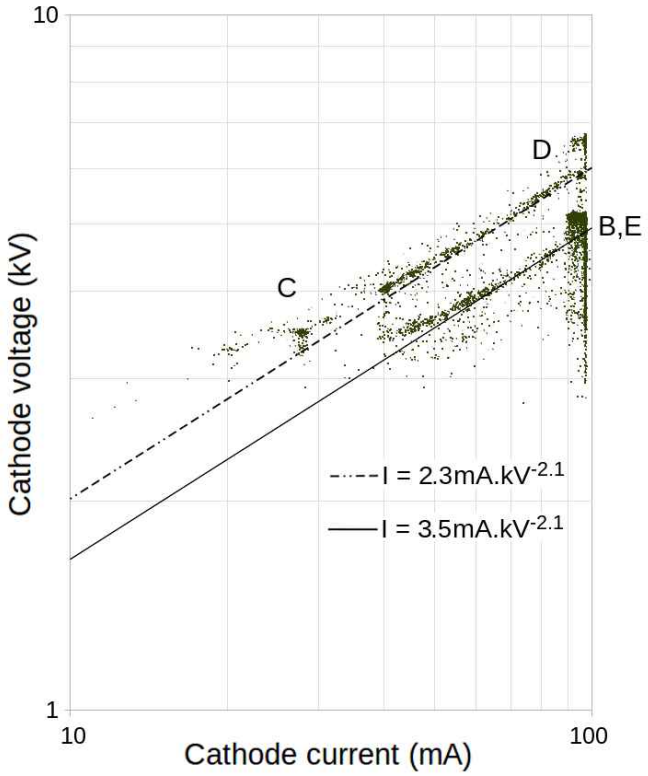

Fig. 118. Cathode voltage-current relation during the fireball discharge run No-anode FB#1. Points marked 'B'-'E' correspond to those in Fig. 116.

When values of cathode voltage and current from this discharge are plotted against each other, the same relation is found to hold for both the ramp-down between points 'B' and 'C', when the fireball is apparent, and the subsequent ramping up between 'C' and 'D' when only the pea-shooter is evident (Fig. 118). The perveance of the discharge is found to be increased by around half when the fireball is present. This term is used here (and subsequently) to describe the coefficient for a given characteristic current-voltage relation, whether or not this appears to show the three-halves power relation associated with a current limited by the Child-Langmuir Law.

An axial jet is evident at all states of the fireball discharge, and the intensity of this is observed to vary approximately with that of the fireball (Fig. 117). The axial beam that is generally visible in the beam mode or ion/neutral discharge, both with and

without the pea-shooter objects, is observed to generally have relatively little spread; this jet however shows a degree of fluting that becomes larger with increasing distance from the fireball. The jet is also much brighter than the axial beam, and the distribution of emission shows some internal structure at the end closest to the fireball, shown in detail in Fig. 119.

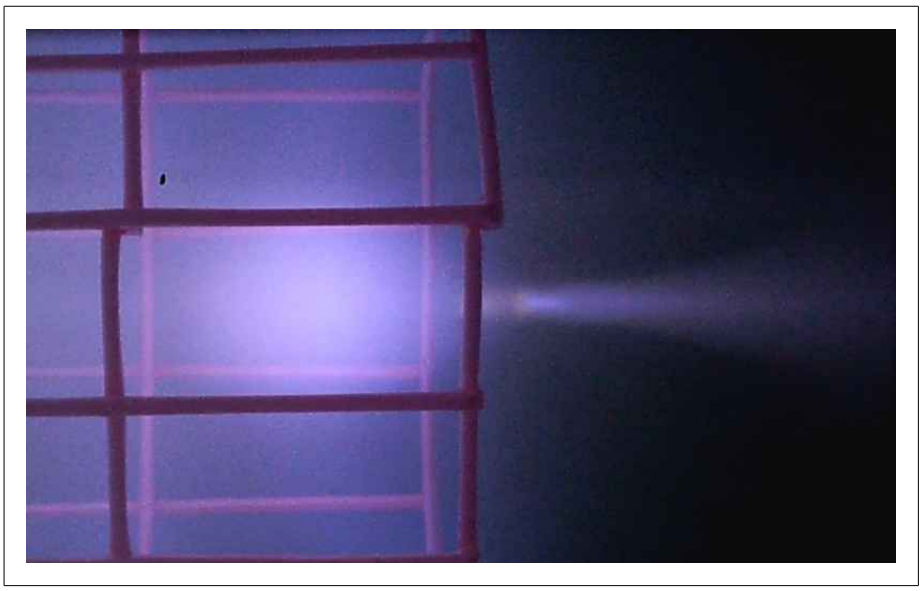

Fig. 119. Photograph of fireball discharge in the set-up without the anode grid, showing detail of the axial jet formation

During the experimental run described above, fluctuations in electron currents to the axial and radial collectors were monitored by oscilloscope. The traces were recorded by video, which lets the waveforms be associated with the different states of the discharge described above. Stills from the video recording that correspond to the points 'A' - 'E' are shown in Fig. 120. Additional frames show the evolution of the waveform in the settling period between 'A' and 'B' and the voltage ramp-down between 'B' and 'C'. The frame shown for 'C' is the last frame showing the waveform trace as the fireball extinguishes.

Oscilloscope settings were not changed between these frames, and so the scale is consistent for all of the waveforms shown in Fig. 120. The timebase in each is 5 μs per division. The signal is monitored at the resistance between the axial collector and ground, which was around 400 Ω; the electron current to the collector causes a negative voltage to develop across the resistance. As representation of magnitude of current, the trace is therefore inverted, and notches in these waveforms correspond to spikes in current.

Over the 40 seconds or so between 'A' and 'B', a regular spike in the current waveform can be seen to develop in size, which is accompanied by a fall in frequency from around 160 kHz to around 100 kHz. The evolution of conditions across this period includes a rise in voltage; when voltage is subsequently reduced, between 'B' and 'C', the change in waveform is partially reversed. The waveform appearing at 'D' is uncharacteristic for a pea-shooter, and has not been previously

observed. At 'E' the waveform is similar to that at 'B'. With the exception of the anomalous waveform at 'D', these waveforms are consistently observed for the fireballs in this set-up. In some cases, the waveform evolves a little further still from that seen here at points 'B' and 'E', to become largely composed of a train of regular pulses, superposed upon a DC current.

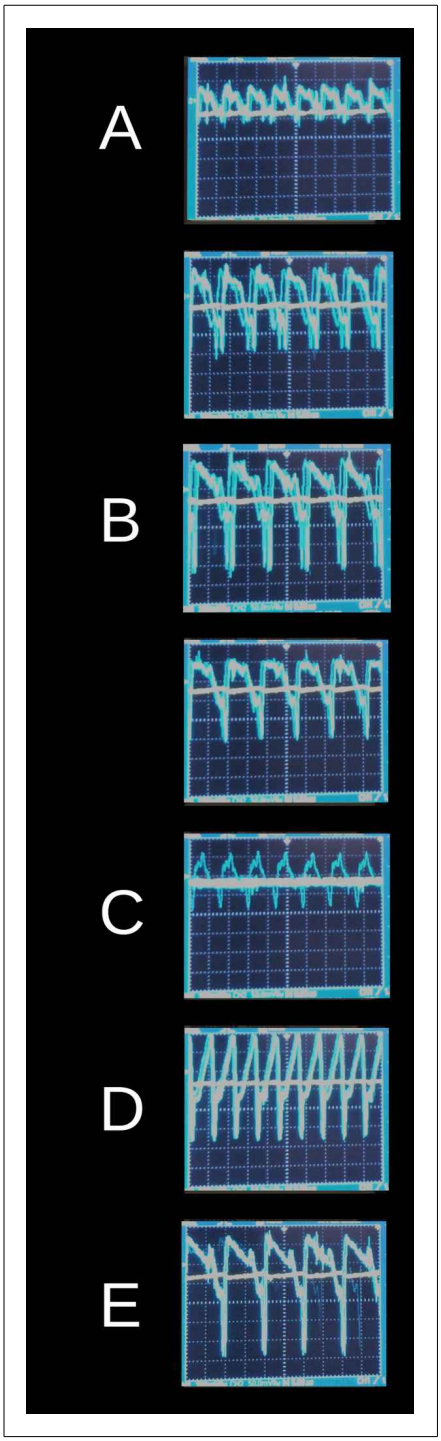

Fig. 120. Waveforms of the fluctuations in electron current incident upon the axial collector during the fireball discharge run No-anode FB#1. The frames marked 'A' to 'E' correspond to the points referred to in Figs. 114-116.

The fluctuations in axial current are also accompanied by fluctuations in the electron current incident upon the radial collector. These occur with the same periodicity, but have a different waveform. The relation between the corresponding fluctuations is largely reciprocal, although further differences are also evident between them. Examples captured with the digital oscilloscope are shown in Fig. 121, for two sets of conditions in a similar discharge. These conditions correspond to those at points 'B' or 'E', and to just before the fireball extinguishes at point 'C'.

Cathode voltage shows little corresponding variation during these fluctuations (Fig. 122). Some variation in cathode voltage is evident at 100 Hz, which is not apparent in Fig. 122. At double the line frequency these are associated with the power supply. The fluctuations occur on a timescale that is similar to the switching frequency of the power supply, which is between 70 kHz and 80 kHz, and the effect of this can be observed on all traces in Figs. 121 and 122 as bursts of noise spaced by periods of around 13 μs. Should there be any significant variation in cathode current associated with the fluctuations, the power supply would be unable to respond on this timescale, and any current fluctuations would be evident as variation in voltage dropped across the 3.9 kΩ cathode ballast resistor. The variation in cathode voltage shown in Fig. 121 is smaller than 5 V, which therefore corresponds to a variation in current of around 1 mA; this is of the order of 1 % of the current flowing through the ballast.

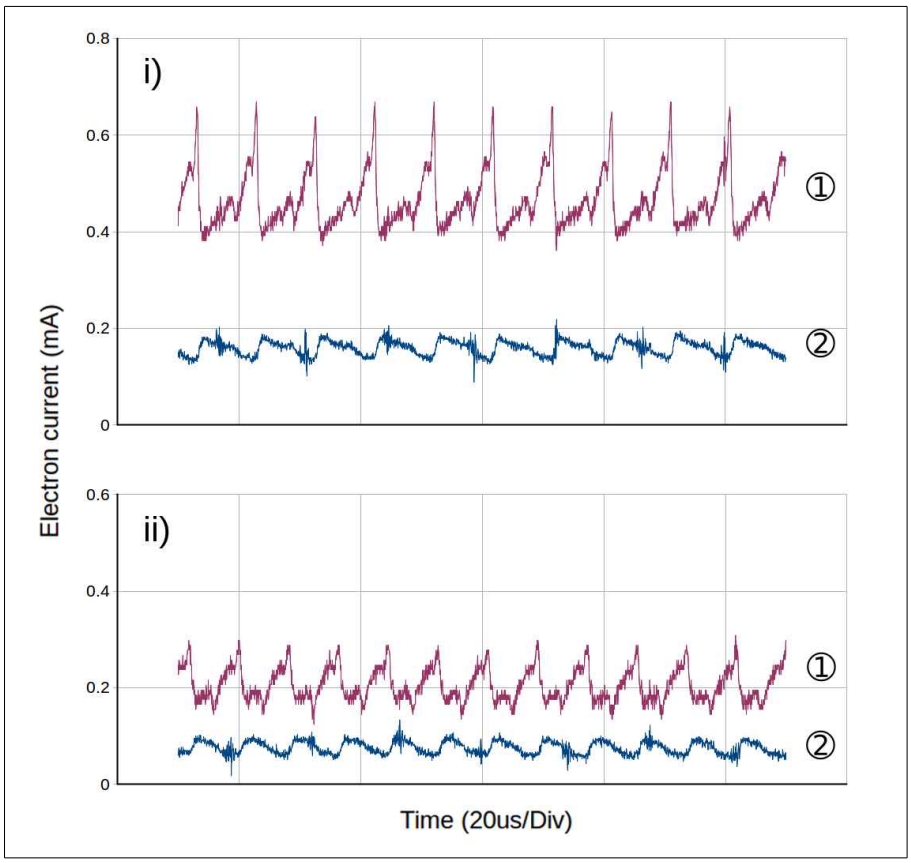

Fig. 121. Waveforms of fluctuations in electron currents incident upon ① axial and ② radial collectors, during a fireball discharge in the electrode arrangement with no anode grid, in argon at 9 mTorr. Discharge current-voltage conditions were i) 5.5 kV, 100 mA; ii) 3.6 kV, 45 mA.

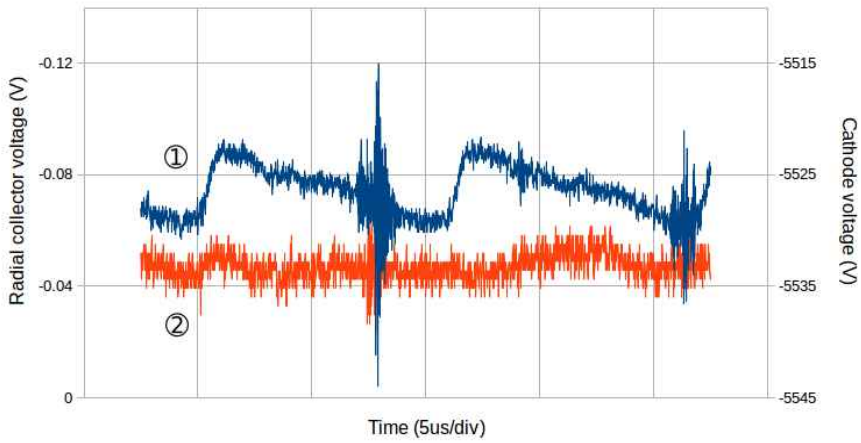

Fig. 122. Oscilloscope traces of ①, radial collector voltage; and ②, cathode voltage, during fireball discharge without anode grid. Cathode current was close to 100 mA.

The power spectra of the fluctuations in electron currents show many harmonics, which become more closely spaced, and greater in number, at conditions of greater voltage and current (Fig. 123).

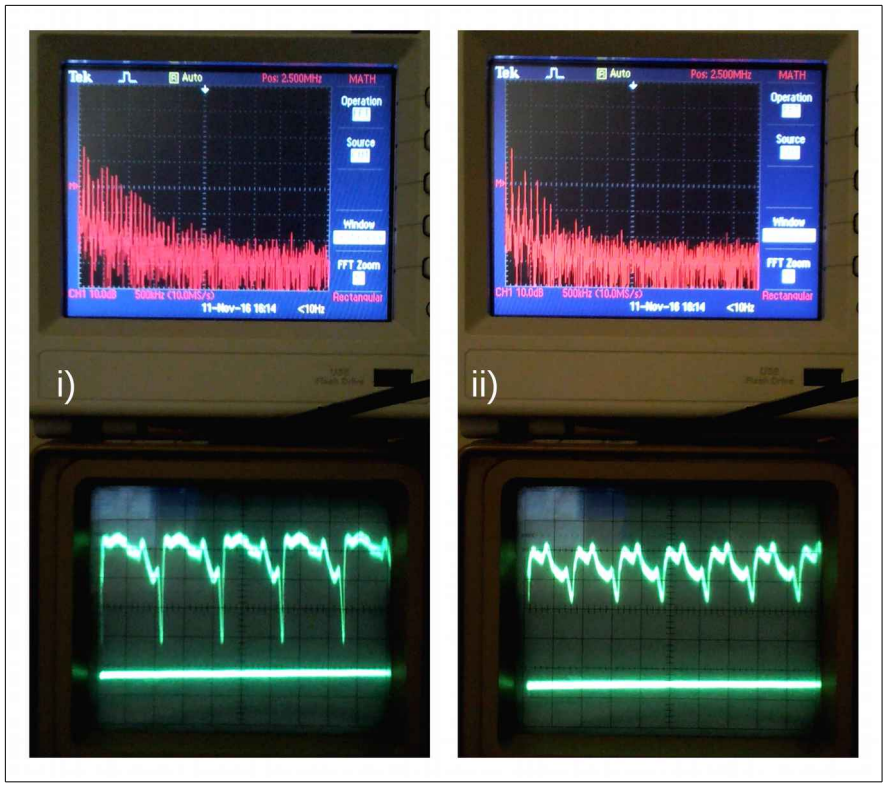

Fig. 123. Power spectra of the fluctuations in electron current to the axial collector during a fireball discharge without the anode grid, with oscilloscope traces showing the corresponding waveforms. The oscilloscope scale for the power spectra is 500 kHz/div.; that for the waveforms is 5 μs/div. Conditions for i) and ii) are approximately as those for the waveforms depicted in Fig. 120 i) and ii) respectively

7.3.1.2 Experimental run 'Anode FB#1'

The fireball discharges occurring in either electrode set-up consist of a region of relatively intense emission that is located in the open end of the cathode. In the case with the anode grid, the bright region extends further back into the cathode, and the boundary of the bright region appears less well-defined. Other visible differences concern the jet formation; this may be clearly evident, or hardly discernible. When the jet is in evidence, it appears less bright and more divergent, and the structure illustrated in Fig. 119 is less well-defined.

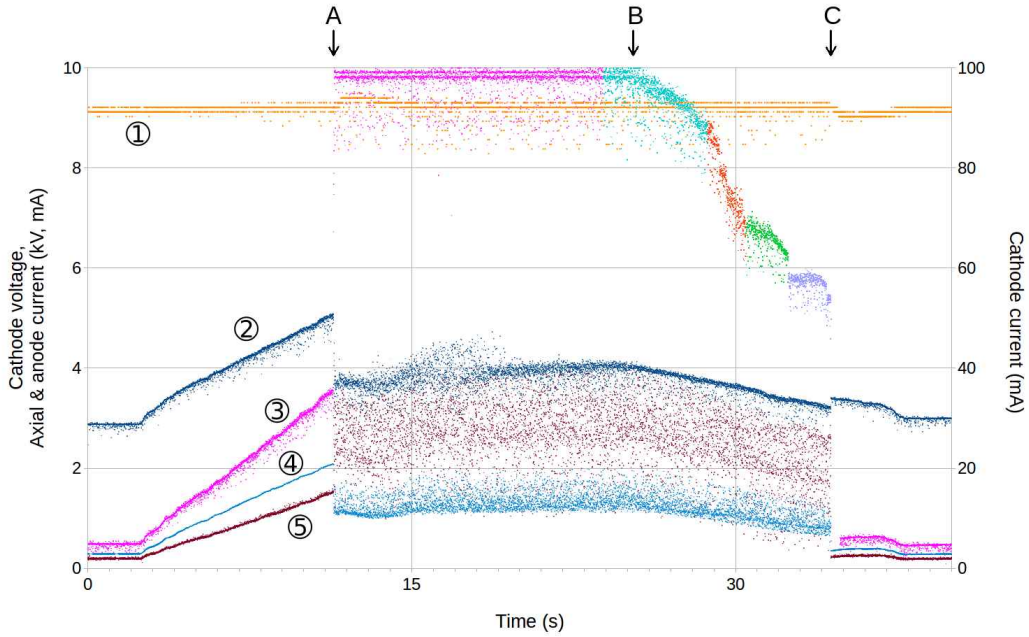

Fig. 124. Current and voltage traces recorded during a fireball discharge in the set-up with the anode grid; run Anode FB#1. Key to traces: ① pressure; ② cathode voltage; ③ cathode current; ④ axial collector current; ⑤ anode current.

Dynamic current-voltage traces recorded during a fireball discharge are shown in Fig. 124. In this experimental run, the pressure was a little greater than 9 mTorr and electrical parameters were sampled at around 250 Hz. This run will be referred to as 'Anode FB#1'.

Levels of voltage are increased until the point marked as 'A', at which the fireball ignites. At this point, cathode current jumps from 35 mA to 100 mA, and voltage falls by around 20 %, to 4 kV. The electron current to the axial collector becomes smaller, and anode current increases, so that the respective magnitudes of these become reversed in order. The fluctuations which appear in these currents are evident as a considerable degree of scatter in the traces. A rise and fall in pressure ensues, followed by a period of a few seconds in which voltage levels also fluctuate. After about 15 seconds, when the discharge has stabilised, voltage is gradually reduced; the point at which this begins is marked 'B'. This is continued for around 10 seconds, until the fireball extinguishes at point 'C'. When this occurs, cathode current falls by an order of magnitude, from around 50 mA to around 5 mA.

When cathode current is plotted against voltage (Fig. 125), the current-voltage behaviour for this run is found to show some similarity to that of NoAn FB#1 (Fig. 118). In that case, the fireball current-voltage relation was found to be the same as that of the discharge with the pea-shooter object, but with the perveance increased by around 50 %. In this case, the relation is found to be the same as that of the ramping period prior to ignition, but with the perveance increased four-fold. This is demonstrated on the log-log plot in Fig. 125, with fit lines having the same gradient.

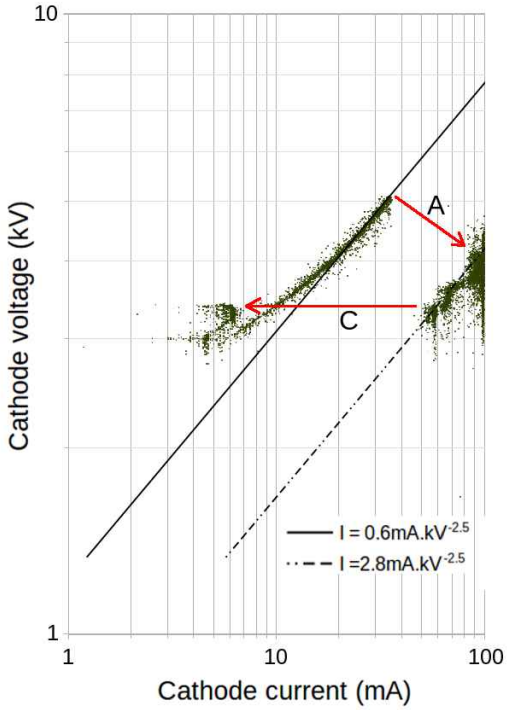

Fig. 125. Cathode voltage-current relation during fireball discharge run Anode FB#1. The discontinuities upon ignition and extinction of the fireball, marked 'A' and 'C' in Fig. 124, are indicated by arrows and labelled as such.

In the period between the points marked 'B' and 'C' in Fig. 124, during which time the cathode voltage level was reduced, cathode current can be seen to fall in an irregular fashion. This section of the trace is divided into four contiguous sections, and data points corresponding to these are colour-coded in the figure. When this data is plotted in Figs. 126 to 128, the same colours are used, so that the regions may be identified.

The current-voltage relation for the period between the points marked 'B' and 'C' is found to follow a stair-step profile (Fig. 126). Whilst the overall trend is similar to that of the low-perveance state prior to the appearance of the fireball, the 'local' perveance along the fireball current-voltage curve is observed to vary, as current alternately follows different voltage-dependences. The less severe of these is approximately linear with voltage; this relation may be identified for two separate

ranges, each of a few hundred volts. Points corresponding to these ranges are coloured green and blue, and the dependence demonstrated with linear trend lines. For the range coloured purple, the current appears to show little voltage-dependence at all; the extent of this range is insufficient however for the relation to be clear. Between these the current rise shows a more severe voltage-dependence, and discontinuities in the data show that this partly occurs in jumps.

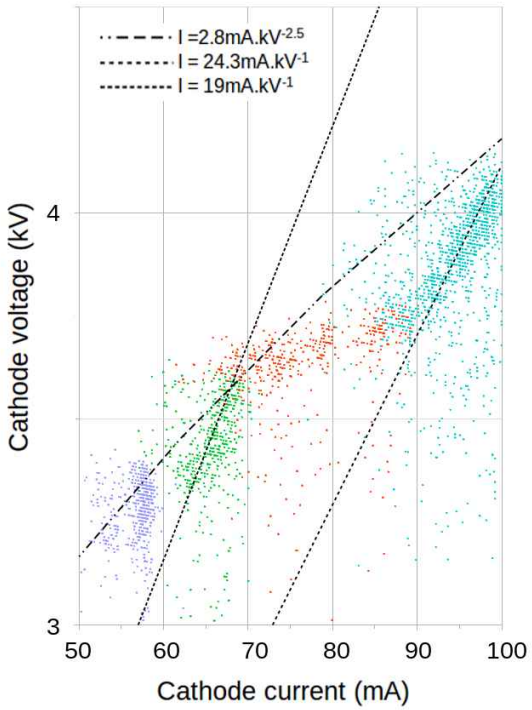

Fig. 126. Cathode voltage-current relation during fireball discharge run Anode FB#1, showing stepwise profile to be evident for the period between points marked 'B' and 'C' in Fig. 124. The differently-coloured regions correspond to those marked as such on Fig. 124

A video recording was made of the discharge during this experimental run, which enables the evolution of the visual appearance of the discharge to be correlated with the evolution in current-voltage. When still images corresponding to the points of inflection in the current-voltage relation are examined, a pattern is discernible concerning the degree of jet activity. The variation is quite subtle, but the relative brightness of the jet is consistently found to be greater at points where the local perveance along the current-voltage curve is smallest, and vice versa.

This apparent relation is examined further by considering the levels of current incident upon the axial collector during this part of the run. These are subject to a considerable degree of fluctuation, as may be seen from the traces in Fig. 124, and so values are averaged over 15 data-points (corresponding to a period of around 56 ms). The resulting time-averaged axial current levels are found to constitute a variable fraction of the corresponding levels of cathode current, and the relative magnitude of this fraction to follow the evolution in jet activity (Fig. 128).

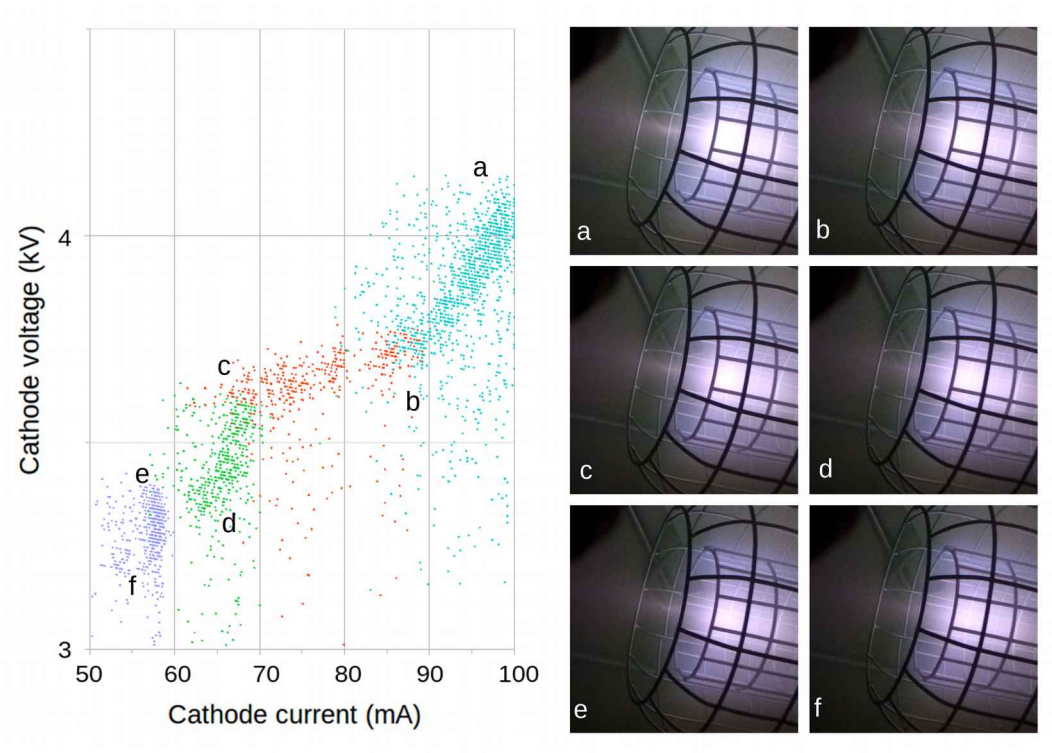

Fig. 127. Cathode voltage-current relation from fireball discharge run Anode FB#1, with points of inflection labelled, shown alongside still images from a video recording made of the same discharge, at times corresponding to the labelled points.

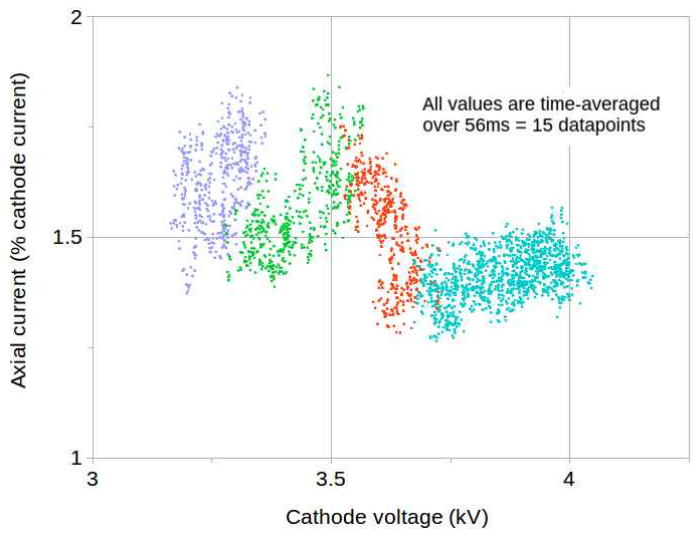

Fig. 128. Time-averaged axial current levels from fireball discharge run Anode FB#1 expressed as a percentage of the corresponding levels of cathode current, and plotted against corresponding values of cathode voltage, for the period between points marked 'B' and 'C' in Fig. 124. The differently-coloured regions correspond to those marked as such on Figs. 124, 126 and 127

The results of this experimental run have indicated that the fireball discharge in the electrode arrangement with the anode grid shows a regular variation in the current-voltage relation, and that this variation may be correlated with a corresponding variation in both collected levels of axial current and levels of visible emission associated with the axial jet.

7.3.1.3 Experimental run 'Anode FB#2'

A separate run made subsequently at a lower pressure shows further variation, which appears to be related and yet distinct from the behaviour described above. This run, which will be referred to as 'Anode FB#2', is described in the following. The same apparatus and equipment were used, with pressure reduced to be a little less than 8 mTorr. This constitutes a reduction of around 15 % in pressure from that of the run described previously, but conditions were otherwise similar. A video recording was again made of the discharge during this experiment and data was recorded at the same rate. The measurements made of electrical characteristics are plotted in Fig. 129.

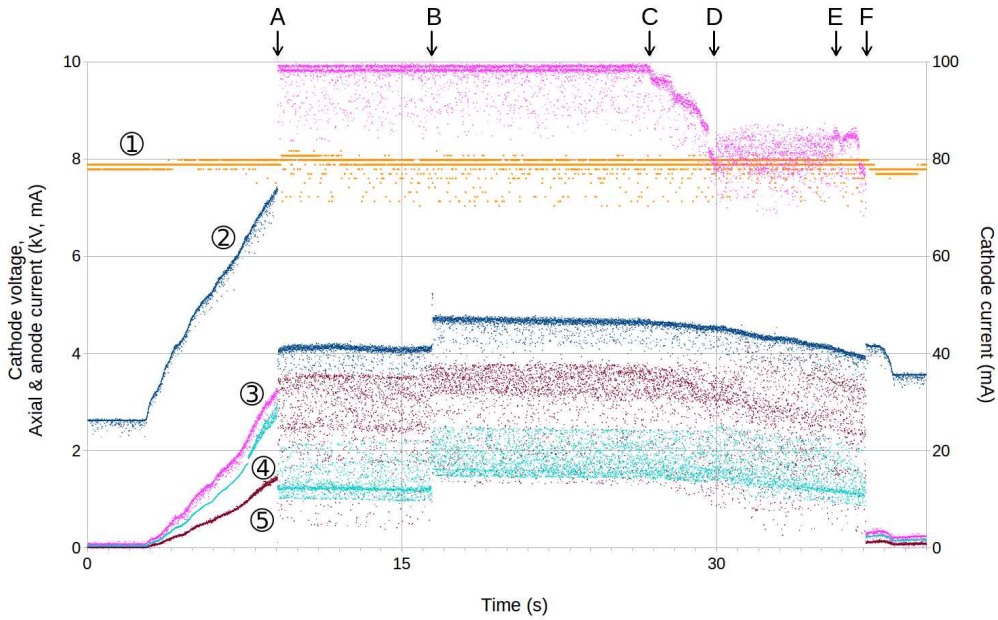

Fig. 129. I-V traces recorded during a fireball discharge in the set-up with the anode grid; run Anode FB#2. Key to traces: ① pressure; ② cathode voltage; ③ cathode current; ④ axial collector current; ⑤ anode current.

As for the previous run, voltage was increased until the fireball formed, and then left for conditions to stabilise. The point of ignition is indicated on Fig. 129 as 'A', and at this point the cathode current again jumps to 100 mA. After about 8 seconds the discharge spontaneously changes state, at the point marked 'B'. This is evident as a step change in the traces for cathode voltage, and the currents collected by the anode

and the axial collector, whilst the level of cathode current remains consistent. At point 'C' the voltage starts to be reduced, and this is continued until the fireball disappears, which occurs at the point marked 'F'. During this time the cathode current initially falls irregularly and then, at 'D', begins to fluctuate around a consistent magnitude of around 80 mA. After a further few seconds, at the point marked 'E', the current then stabilises briefly before the fireball extinguishes.

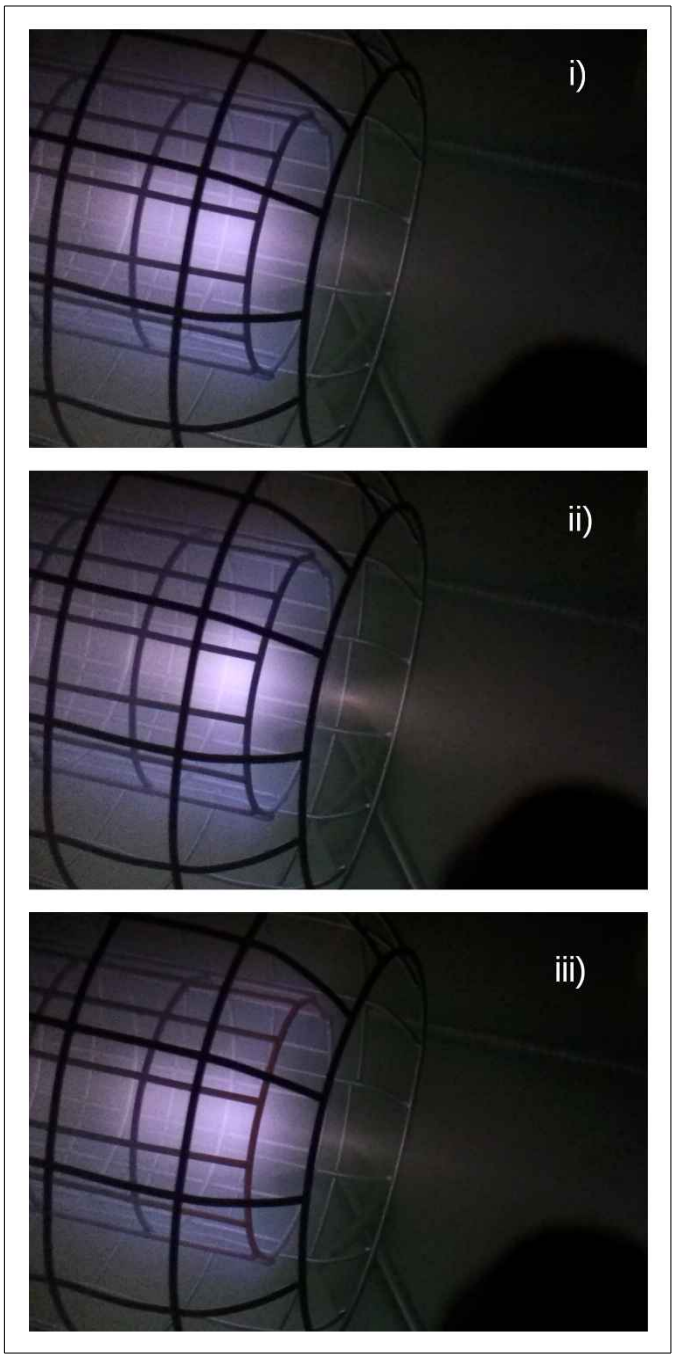

Fig. 130. Still images from the video recording made during fireball discharge run Anode FB#2, showing the appearance of the discharge i) just before, and ii) just after the change occurring at the point marked as 'B', and iii) just after the point marked 'E', on Fig. 129

The video recording showed the change occurring at point 'B' to be associated with a significant change in the appearance of the discharge (Fig. 130). When the fireball first forms, the bright region of emission extends from the open end of the cathode back into the second row of apertures, and the distribution of emission is quite even. There is little visible emission in the axial area outside the cathode end. Prior to point 'B' this distribution remains largely unaltered, but subsequently the distribution within the bright region is peaked around the axial location within the first row of apertures, causing the fireball to appear more spherical. A much brighter axial jet is also evident. The magnitude of this change is observed to be considerably greater than that of the changes occurring in the previous run, as illustrated in Fig. 127. After this change, the distribution of emission remains similar for the following period, with a reduction in intensity observed to accompany the reduction in current levels after point 'C'. At point 'D', when the cathode current starts to fluctuate, the distribution of emission starts a progressive shift back to become more similar to that seen originally, and at point 'E' this evolution makes a small step change, in which the relatively-brighter line within the axial jet disappears.

The range of cathode current at which this instance of the fireball is in evidence is considerably smaller than that previously described for experiment Anode FB#1. This makes it hard to discern the trend in the current-voltage relation from this experiment alone, and the data are considered in relation to those of the previous run.

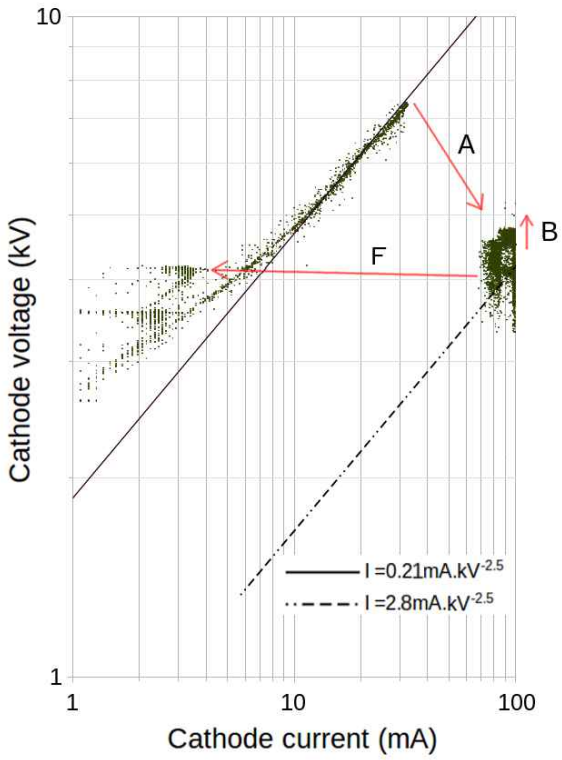

Fig. 131. Current-voltage curve from fireball discharge run Anode FB#2. The discontinuities that occur at points 'A', 'B' and 'F' on Fig. 129 are labelled as such

The current-voltage curve is shown in Fig. 131, with the principal discontinuities evident at points 'A', 'B' and 'F' in Fig. 129 labelled as such. The relation shown in the ramp-up before the fireball ignites is the same as that observed previously, with a smaller perveance; this is to be expected, from the general voltage-pressure dependence described for the beam mode in previous chapters.

Upon ignition of the fireball, and the corresponding jump in cathode current, the voltage is found to fall to a similar level to that seen in the previous run. This observation suggests the degree of current associated with the fireball to be relatively insensitive to pressure; certainly far less so that that associated with the beam mode discharge that it evolves from.

Although there is little range of cathode current evident in this case, the fireball current-voltage relation is also expected to be the same as that seen previously; in both of the fireball discharges described so far, both with and without the anode grid, the current-voltage relation has been found to remain the same as that of the discharge prior to its appearance. This is considered to be significant, and will be discussed later in the chapter; at this point, it is merely noted that for this to be so for discharges as different as the beam mode and fireball discharges, it is overwhelmingly likely to also hold between different instances of a fireball discharge. If this inference is correct, then the perveance to which the discharge transitions upon this instance of fireball ignition is very close to that seen in the previous case. This is demonstrated in Fig. 131 with a broken line indicating the same fireball perveance fit line as that shown in Fig. 125. The jump in perveance implied for this case is correspondingly much larger, being over an order of magnitude.

According to these considerations, the step change in voltage at point 'B' would appear to represent an evolution that is both related, and yet different in nature, to that which occurs step-wise in the previous case. An association with visible changes in the axial jet is evident in either case, but the magnitude of change in both the jet and the perveance are considerably greater in this instance. If the two current-voltage relations are compared, the differences in behaviour are quite apparent (Fig. 132).

In both cases, the fireball initially occurs with a similar appearance and at similar conditions of voltage and current, despite the difference in pressure. (The voltage is in fact slightly lower in the first instance, but then rises a little between points 'A' and 'B' as marked on Fig. 124 to become very similar to that of the start of the second run). As noted previously, the current-voltage curve for the first case generally follows the relation seen prior to ignition, with a relatively small variation in perveance causing it to meander from a consistent line. Assuming the current-voltage relation for the second discharge to also follow that of the beam mode, the curve for this run starts at a similar perveance, but then jumps to one with a quite different value. It then shows little variation from this line before transitioning back to the ignition perveance, via the region of fluctuating cathode current between the points marked 'D' and 'E' on Fig. 129.

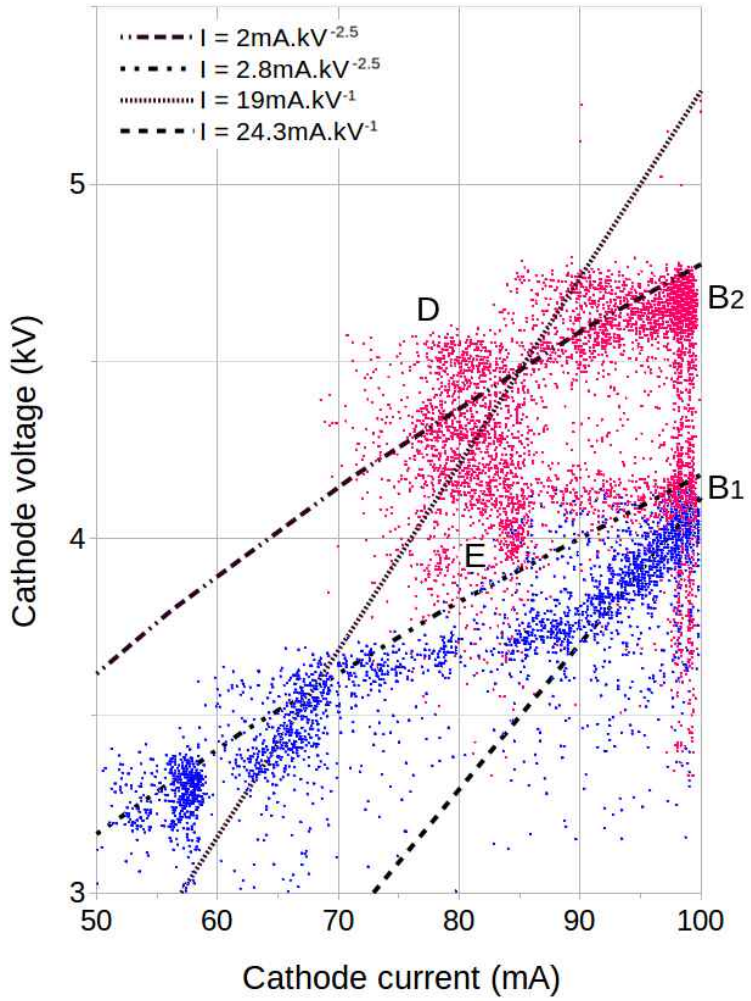

Fig. 132. Comparison of fireball current-voltage curves from runs Anode FB#1 (coloured blue) and Anode FB#2 (pink). The points marked 'B_1' and 'B_2' correspond respectively to points just before, and just after, point 'B' in Anode FB#2, as indicated on Fig. 129. Points marked 'D' and 'E' correspond to the points marked as such on the same figure.

These different patterns of operation have been described at some length, since they are found to occur consistently for fireball discharges with the anode grid. In the following descriptions of different aspects of the discharges occurring in this apparatus, they will be referred to as the low- and high-perveance fireball modes.

7.3.1.4 Time-varying currents with anode grid

The fireball discharge that occurs in the set-up with the anode grid shows a variety of periodic time-varying behaviour, which may be regular or irregular in nature. This is initially shown for the waveforms in current incident at the anode and at the axial collector, in Figs. 133 to 136, and then with waveforms evident in the voltages developed across the anode resistance and at the cathode, in Figs. 137 to 143.

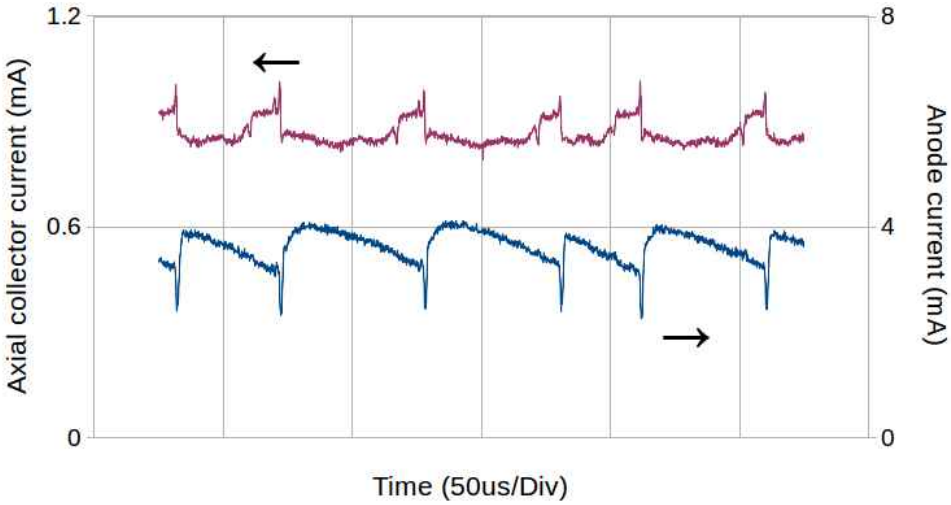

Fig. 133. Examples of the waveforms corresponding to fluctuations in anode and axial currents when these are irregular, during a fireball discharge with anode grid.

Fig. 133 shows examples of the waveforms corresponding to fluctuations in anode and axial currents when these are irregular. Figs. 134 and 135 show examples of the waveforms corresponding to fluctuations in anode and axial currents when these are regular, occurring with frequencies of around 23 kHz, and around 30.5 kHz, respectively.

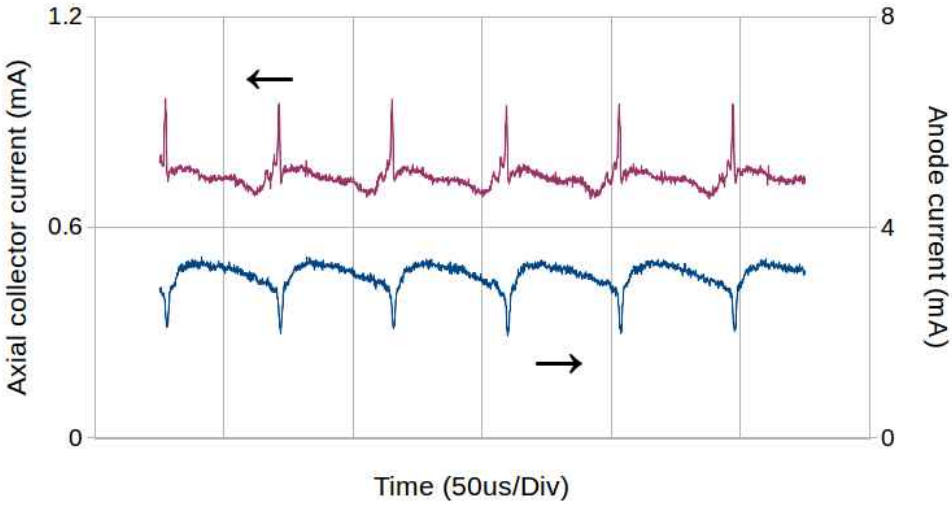

Fig. 134. Examples of the waveforms corresponding to fluctuations in anode and axial currents when these are regular, occurring with a frequency of around 23 kHz, during a fireball discharge with anode grid.

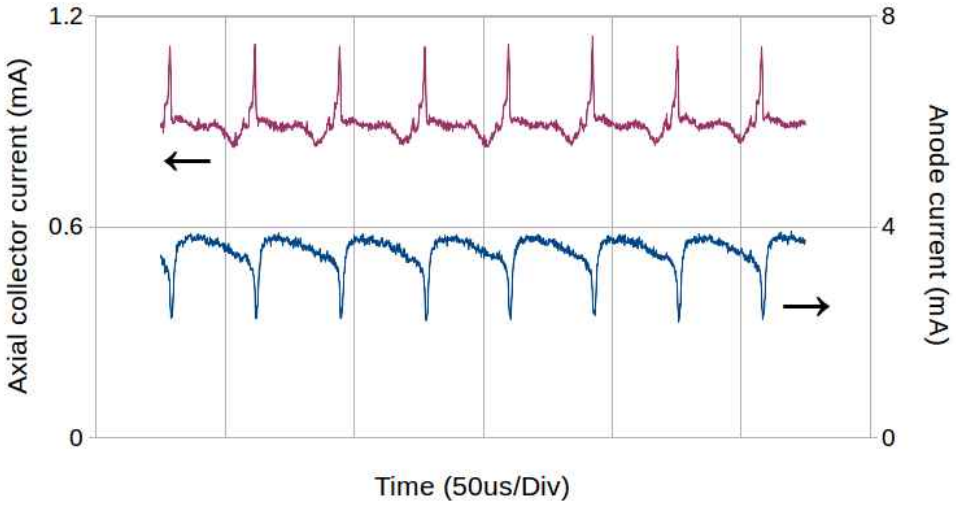

Fig. 135. Examples of the waveforms corresponding to fluctuations in anode and axial currents when these are regular, occurring with a frequency of around 30.5 kHz, during a fireball discharge with anode grid.

The fluctuations in anode and axial current illustrated in Figs. 133 to 135 show a reciprocal element is evident in the relation between these fluctuations, regardless of the degree of regularity. This may be observed to affect the general shape of the waveforms apparent during irregular fluctuations (Fig. 133), which are observed to be quite similar in general form to those appearing during the fireball discharge in the set-up with no anode grid (Fig. 121), although with a notch apparent in the anode waveform that corresponds with the spike in axial current observed in either set-up. These spikes in axial current are noted to be considerably narrower during the regular fluctuations (Fig. 135 and Fig. 136), and the waveforms in anode and axial current that are evident in these cases are observed to be more similar to each other. In these waveforms the reciprocal element is associated largely with the periodic spikes in axial current that are associated with notches in the anode current waveform.

Fig. 136 shows the relation between these spikes and notches at a higher resolution, and from this it may observed that the spike in axial current precedes the notch in anode current.

Fluctuation is also observed to occur in cathode voltage. This is subject to variation from both the voltage dropped across the ballast resistor, and the current regulation mechanism of the power supply. The time constant for the supply regulation is rated as 20 ms on the data sheet, and so is slow compared with both the supply switching frequency and the frequencies of fireball fluctuations, which are both of the order 10's kHz.

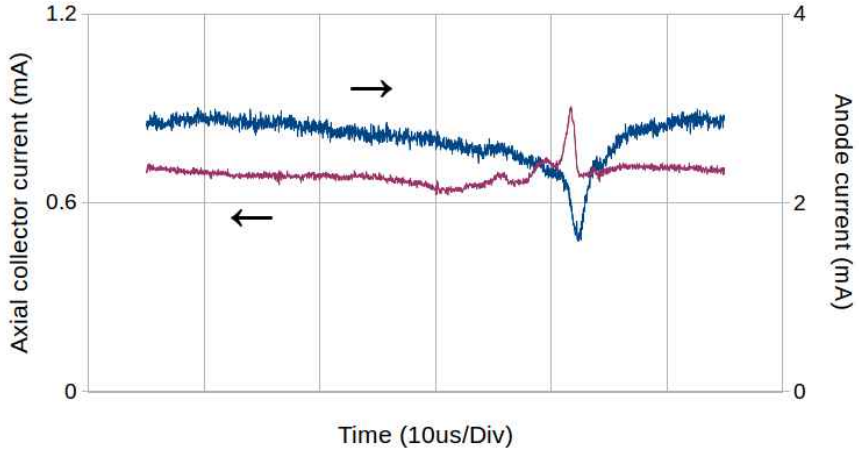

Fig. 136. Examples of the waveforms corresponding to regular fluctuations in anode and axial currents, showing the timing relation between the spike in axial current and the notch in anode current, during a fireball discharge with anode grid.

Examples showing the voltage behaviour of the cathode during instances of irregular electron current fluctuations are shown in Figs. 137 to 140, and that accompanying regular fluctuations in Figs. 141 to 143. In most of these figures, the AC component of fluctuations in cathode voltage is shown, and in Fig. 140 and Fig. 141, two captures are shown in which the cathode voltage is DC-coupled. The scales for cathode and anode voltages have opposite polarity in these figures. This is so that the anode voltage waveform corresponds to magnitude of anode current in the upward direction in the figure. Cathode voltage is plotted the other way up, since fluctuations in current over short timescales will be apparent as the change in voltage dropped across the ballast resistor. This means that the magnitude of both currents are represented vertically in the figures.

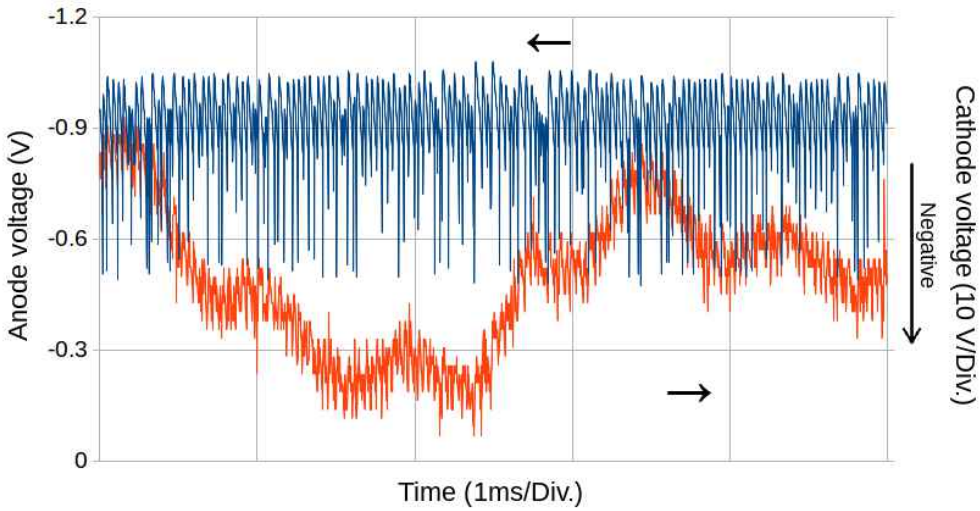

Fig. 137. Examples of the waveforms corresponding to fluctuations in anode and cathode voltage when these are irregular, during a fireball discharge with anode grid.

Fig. 137 shows examples of the waveforms of cathode and anode voltages on a millisecond scale, during a regime of irregular current fluctuations, when levels of cathode current are stable as monitored from the power supply. Anode voltage consists of a train of irregularly-spaced notches occurring on a timescale of 10's μs, corresponding to the notches in the irregular anode current waveform shown in Fig. 133. Cathode voltage is seen to be varying in a complex way, that appears to have components operating on at least three different timescales. A high-frequency component is evident, of similar order to that of the anode voltage fluctuations, and also a component that varies over several milliseconds. This appears to have a further frequency component occurring on a timescale shorter by a factor of three or four.

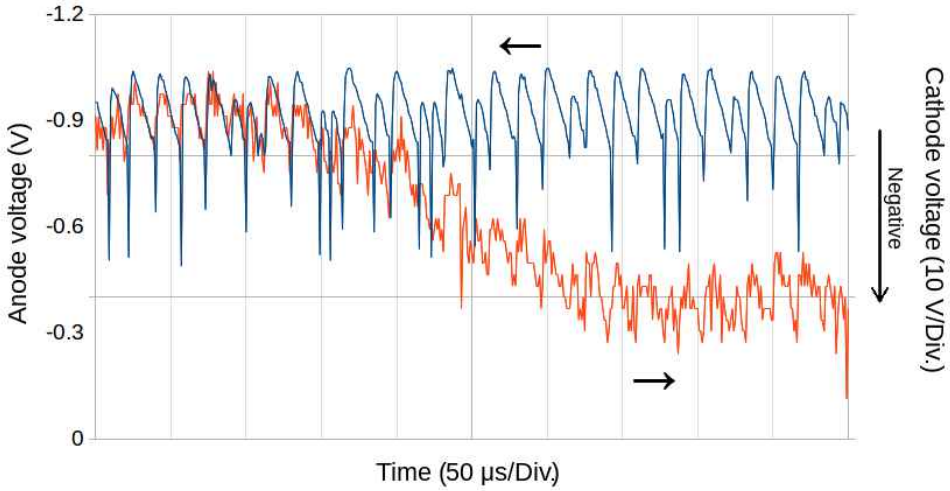

Fig. 138. Zoom of the waveforms shown in Fig. 137, corresponding to fluctuations in anode and cathode voltage when these are irregular, during a fireball discharge with anode grid.

Fig. 138 shows a zoom of part of the same data. The periodicity of the higher-frequency component of the cathode voltage waveform can be seen to be associated with that of the anode voltage.

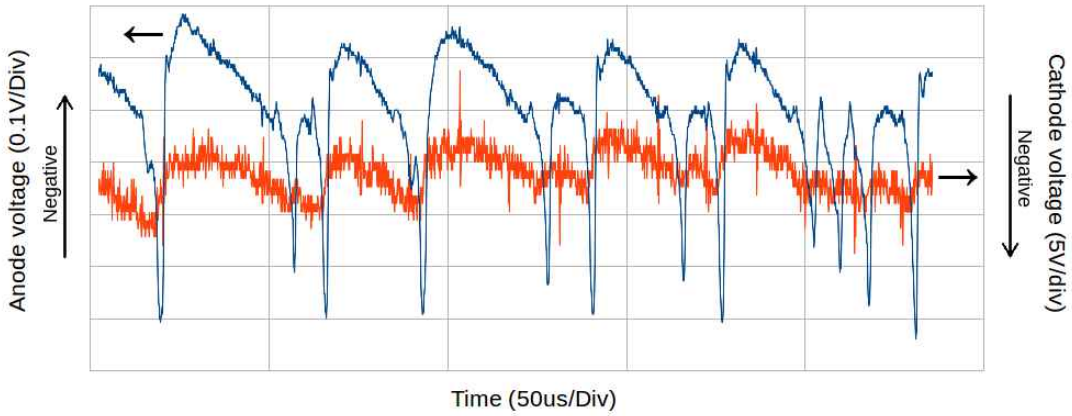

Fig. 139. Examples of the waveforms corresponding to fluctuations in anode and cathode voltage when these are irregular, during a fireball discharge with anode grid.

Further examples of the waveforms corresponding to irregular fluctuations in anode and cathode voltages are shown at a finer resolution in Fig. 139, and at a finer resolution still, and also DC-coupled, in Fig. 140. The cathode voltage waveforms shown in these figures do not show the variation over longer timescales, but remain subject to these also.

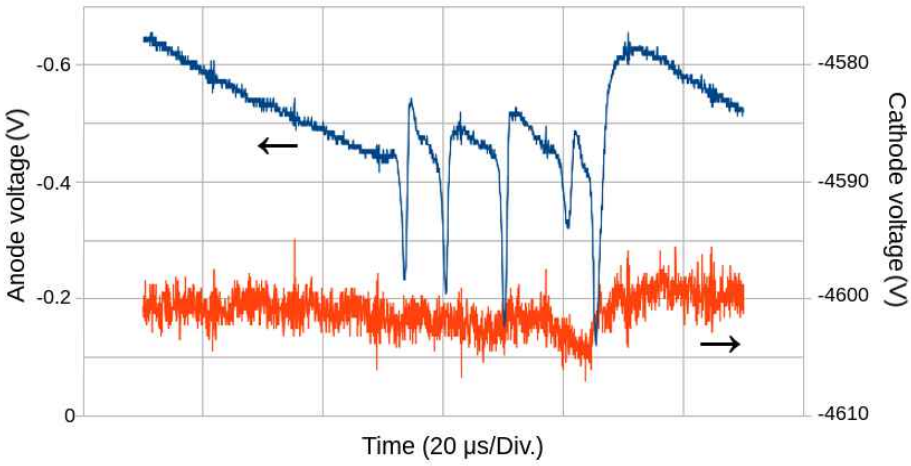

Fig. 140. Examples of the waveforms corresponding to fluctuations in anode and cathode voltage when these are irregular, during a fireball discharge with anode grid.

The nature of these waveforms during conditions at which the fluctuations are regular are shown in Figs. 141 to 143. These figures show regular fluctuations occurring at three different frequencies. In Fig. 134 and Fig. 135, the regular anode waveform is shown in more detail than previously, and can be seen to represent a repeated reduction in current ending with a deep notch. When the fluctuations become regular, the overall levels of cathode voltage become very consistent, and the cathode voltage waveforms shown in Figs. 141 to 143 are representative of the cathode voltage over longer timescales at these conditions.

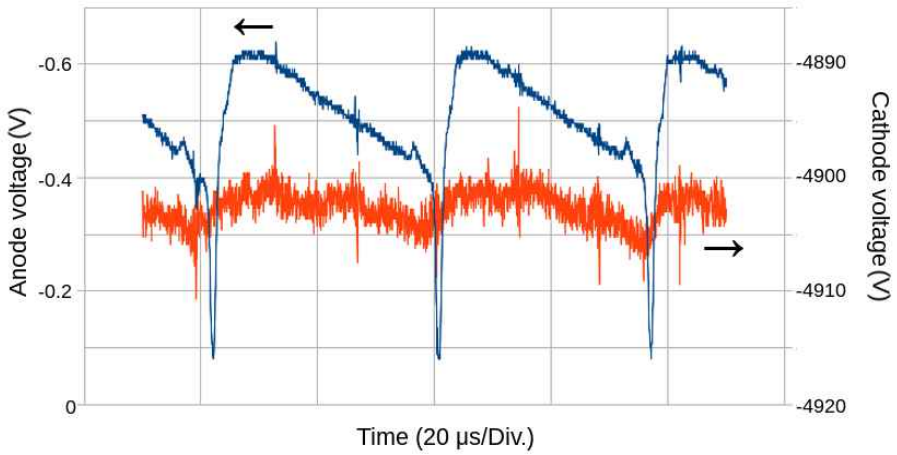

Fig. 141. DC waveforms during regular fluctuations in anode current and cathode current, occurring with a frequency of around 27 kHz, during a fireball discharge with anode grid.

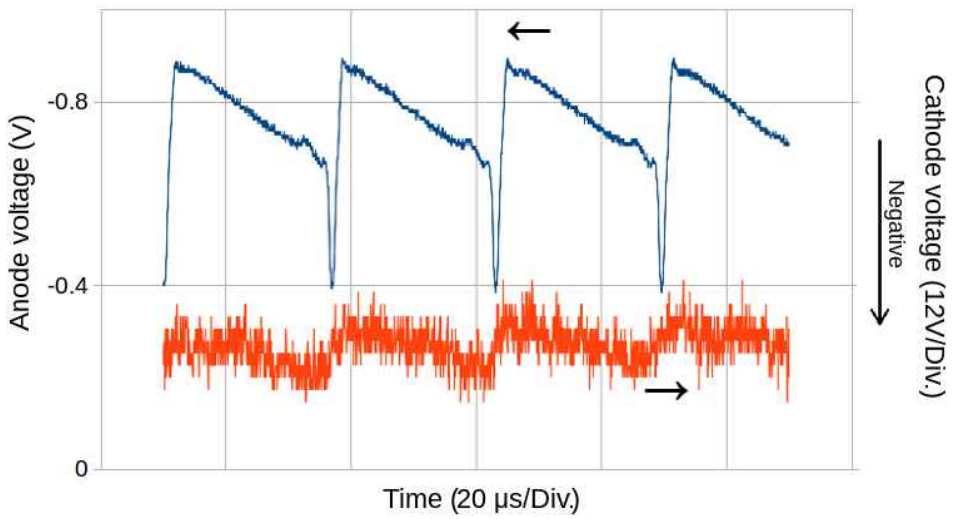

Fig. 142. Examples of the waveforms of regular fluctuations in anode current and cathode current, occurring with a frequency of around 38 kHz, during a fireball discharge with anode grid.

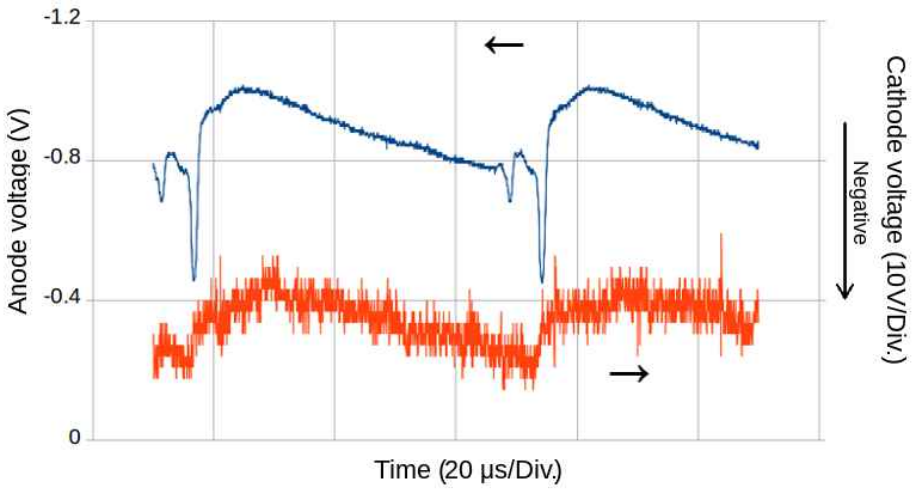

Fig. 143. Examples of the waveforms of regular fluctuations in anode current and cathode current, occurring with a frequency of around 17.5 kHz, during a fireball discharge with anode grid.

Some different periodic waveforms are also consistently observed that appear as a 'hybrid' of two different frequencies of regular operation. Two examples of these, occurring in anode and axial collector voltages, are shown in Fig. 144. The waveforms were captured in video recordings of oscilloscope traces made during experimental runs. The traces are inverted, so that the magnitude of current is represented vertically, as for the waveforms shown previously. An element of this behaviour may also be observed in the waveforms shown in Fig. 143.

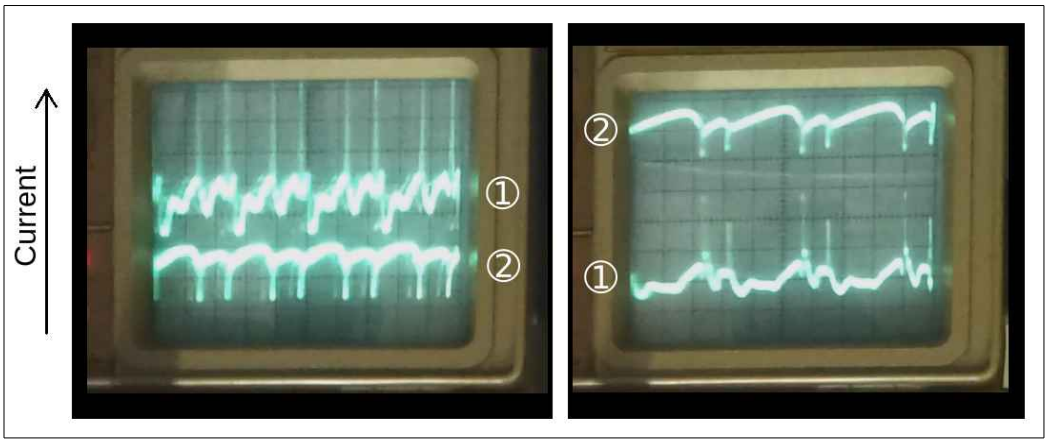

Fig. 144. Examples of waveforms occurring with 'hybrid' frequencies, during a fireball discharge with anode grid, as evident at ① axial collector; ② anode

Some insight may be offered into this by the dynamic behaviour observed during the establishing of the discharge, captured in a video recording of oscilloscope traces. A progression of stills are shown in Fig. 145, in which the (uninverted) anode waveform may be observed to evolve from a series of closely-spaced notches. These notches are spaced by around 5 μs, which is of a similar order to the spacing of the additional notches evident in the waveforms shown in Figs. 139, 140 and 143.

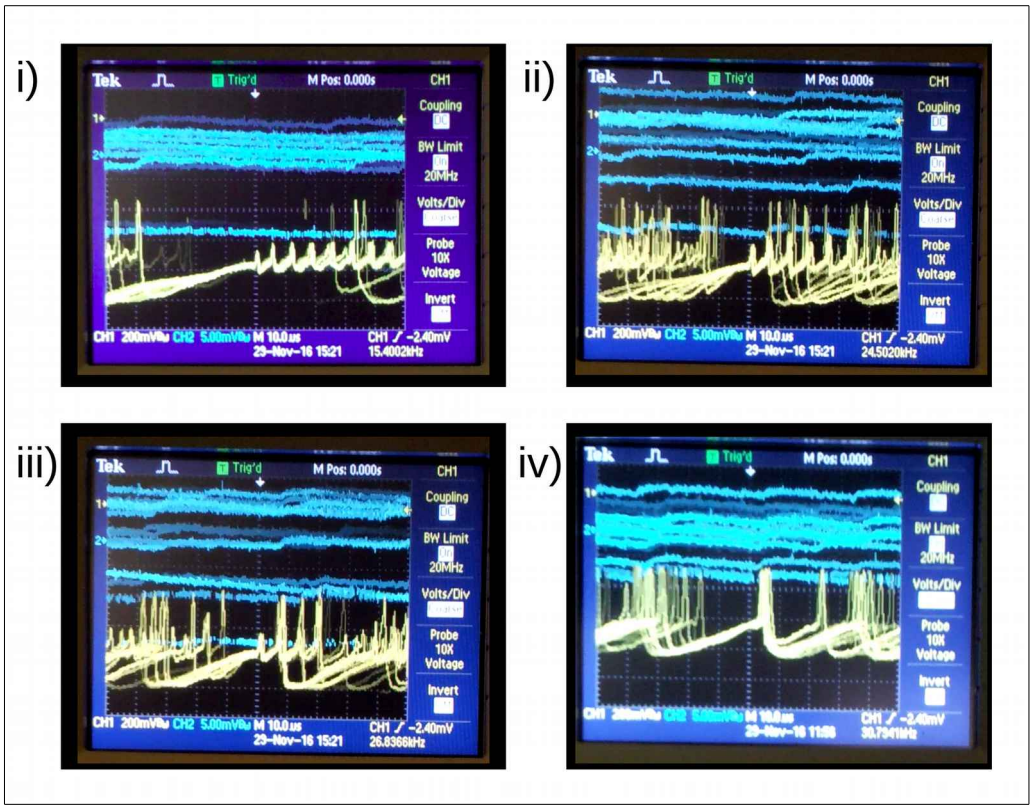

Fig. 145 Oscilloscope screen displays showing the waveform evident at the anode, as captured by video recording during the establishing of a fireball discharge with the anode grid. These frames are numbered consecutively. The traces are not inverted in these images.

The power spectrum associated with these fluctuations may show many harmonics. Examples measured at the anode and axial collector are shown in Fig. 146.

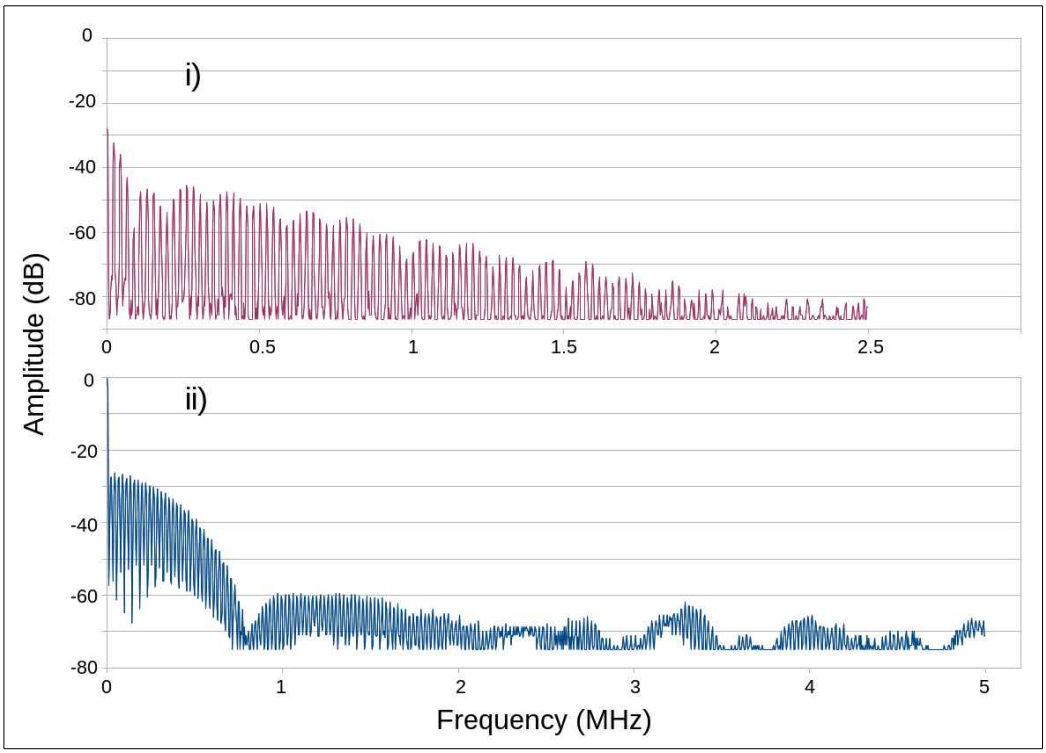

Fig. 146. Examples of power spectrum associated with fluctuations measured at i) axial collector and ii) anode. These were recorded at different times

Before moving on, brief further comments are made concerning this time-varying behaviour, regarding how it presents during operation, and how it relates to conditions of voltage and current.

The behaviour of the fluctuations at the anode in these figures is quite characteristic of fireball operation generally. The cathode voltage may vary much more significantly at times, as is evident in the dynamic current-voltage plot shown in Fig. 124. This has been observed to occur at frequencies associated with the mains frequency, and might represent some interaction with electrical characteristics of the power supply. This behaviour is not investigated further for the purpose of this account.

During operation at consistent conditions of pressure, conditions at which fluctuations are regular are found to occur at different conditions of voltage and current. Three or four different regular states may be found by varying the voltage, with differing frequencies and waveforms such as those illustrated above. The discharge is also found to be able to spontaneously change from one frequency to another, when conditions are evolving over the minute or so after the appearance of the fireball. The relation between the occurrence of these and the general current-voltage progression will be illustrated below in Section 7.3.2.2.

The waveforms with most different frequencies, shown in Fig. 142 and Fig. 143, were captured within the same run, at broadly similar conditions. The fluctuations occurring over the longest timescales are often observed to be evident during the initial evolution of conditions following the establishment of the discharge. Operation in the low-perveance state, as described for the run 'AnodeFB#2' above, is generally observed to be associated with fluctuations occurring on a shorter timescale.

7.3.2 Optical characteristics

In this section, optical characteristics of the fireball discharges are described. Measurements are presented of the spatial distributions of spectrally-filtered emission, and these are related to the electrical characteristics described previously. The relation overall levels of emission generated within the fireball and the electrical behaviour are also investigated. Finally, measurements are described that provide some information regarding the time-dependence of emission, and how this relates to the electrical fluctuations described above.

7.3.2.1 Spectrally-resolved distributions

The spectral content of light was monitored using the Ocean USB spectrometer, and this was found to show little variation with conditions of current and voltage. Little spectral variation was evident from light emitted from different regions of the fireballs either, except for some variation that was found to affect the relative intensity of the argon spectral line at 750.4 nm. The relative intensity of this line was found to be specifically associated with electron activity in the analysis of emission performed in Chapter 3, and so this element of variation is useful to quantify. Images were therefore taken using the Andor camera and a 750 nm filter, and the results of these are presented below. The results obtained using the spectrometer are not included here, since they show less information than the images.

The procedure for making these measurements was as follows. Filtered and non-filtered images were taken of the discharge using the filter apparatus described in Chapter 2. Pairs of these images were then used to assess the distribution of light at 750.4 nm relative to the unfiltered levels. The pairs show conditions separated by a second or two, so are not representative of behaviour changing over short timescales.

This was done using the Processing application, which was also used for analysis of photographs of emission distributions in previous chapters. The program written for this purpose reads pixel values from each image, and calculates the fraction of the unfiltered intensity that is represented by the filtered signal. These are stored in an array, which is then used as a mask to create false-colour images that represent the relative variation in intensity at 750.4 nm across the field of view. The mask array contains outlying values due to variation in signal recorded by individual pixels, and so a range of interest is selected that best represents the general variation evident.

Levels of overall brightness and saturation are set using the unfiltered signal. These settings are kept consistent between all of the images presented.

The results are shown for the fireball in the set-up with the anode in Fig. 147, and in the set-up without the anode in Fig. 148. Camera settings were not the same for these sets of conditions, so direct comparison of these results is not made. The key to the colours used is included to demonstrate the relative significance of these; the actual values are somewhat arbitrary, since these are a function of the filter transmission and other factors such as equipment response etc. The principal point is that blue represents the greatest relative degree of electron activity, and red the least.

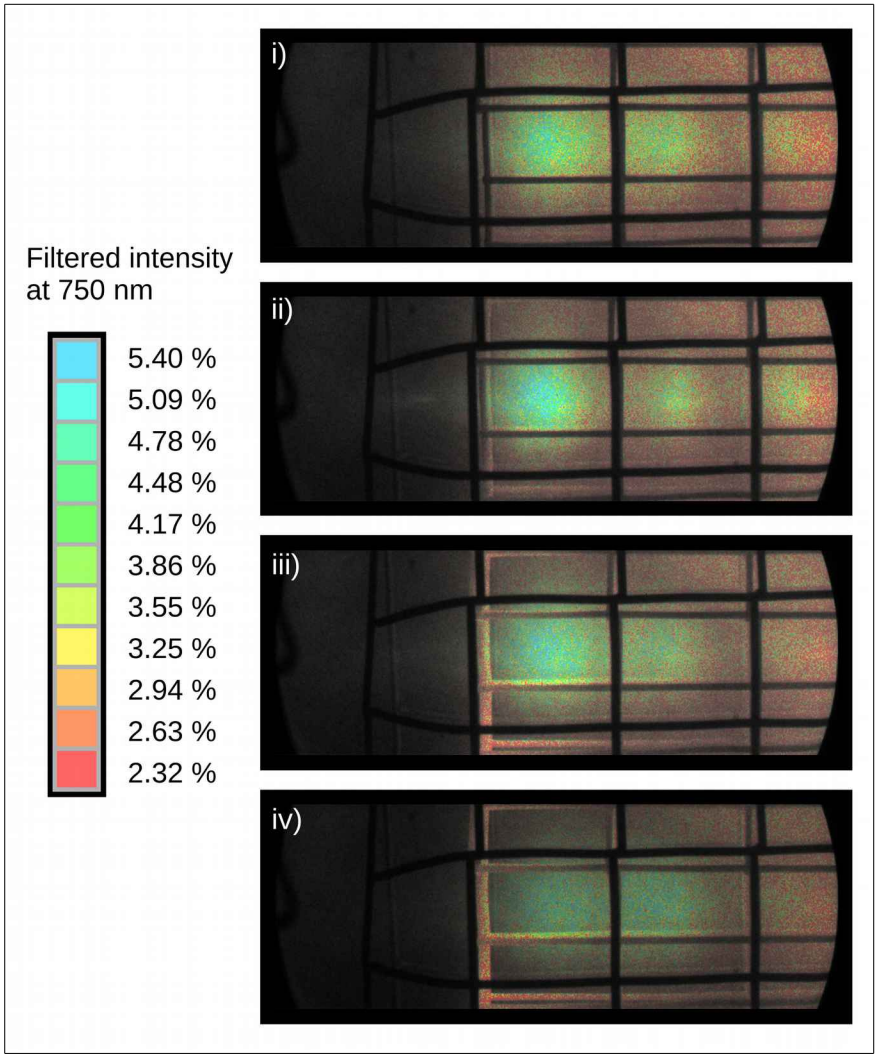

Fig. 147. Images of fireball discharge with anode grid, with false colour indicating relative intensity of 750.4 nm light

The images of the object obtained with the anode present correspond to different points in the experimental run, and are selected to also demonstrate the variation in form that is evident. These correspond to conditions as follow: i) shortly after the establishing of the discharge, at around 4 kV and 100 mA; ii) when the discharge is in the low-perveance state, showing a more spherical appearance and increased axial

jet evident, at around 4.7 kV and 100 mA. These images both represent the discharge in the first minute of operation, before conditions settle. The subsequent frames show the discharge iii) after returning to the high-perveance state, at 4.3 kV and 100 mA and iv) when current has been reduced to around 80 mA, at a voltage of a little under 4 kV. At all of these conditions the fireball may be seen to be associated with a relatively-greater degree of electron activity, as compared with the surrounding activity in the wider discharge.

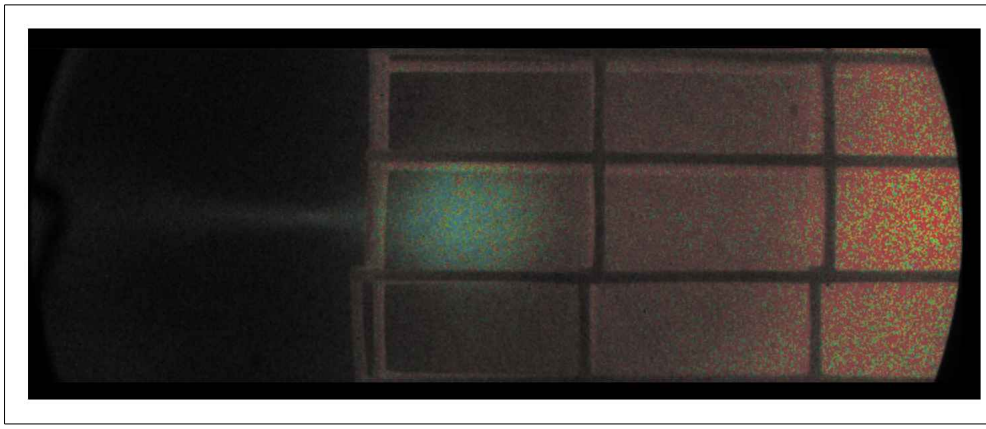

Fig. 148. Image of the fireball discharge with no anode grid. This image is as shown for point 'B' in Fig. 117. The key to the colours is the same as for Fig. 147

This is also observed to be the case for the fireball obtained without the anode grid, as shown in Fig. 148. This image is created using the same unfiltered image used to illustrate the fireball at point 'B' in the run described as 'No Anode FB#1', in Fig. 117.

The variation in the distribution of emission that was associated with the low-perveance state in the description of the run 'Anode FB#2' is shown to be associated with separate regions of activity occurring within the rings of cathode apertures further back from the open end. This is in contrast to the other images in Fig. 147, that represent the discharge in the high-perveance state, in which the distribution of emission indicates a more integral object. This may be observed to be particularly the case for the image representing the distribution of emission at conditions of lower cathode current [Fig. 147 iv)].

7.3.2.2 Optical emission, current-voltage and fluctuations

Observations were also made of the intensity of optical emission, by continuous monitoring of levels using the photo-multiplier tube whilst the discharge was operated at a range of conditions of voltage and current. This was done using the optical set-up described in Chapter 2, which allowed for the collection of light from very localised regions of the discharge. Emission was sampled from a relatively small region located on the axis of the discharge, aligned with the centre of the terminal row of cathode apertures. This location is marked '1' on Fig. 149. Light levels from the same location were also monitored during an experimental run with the anode in place.

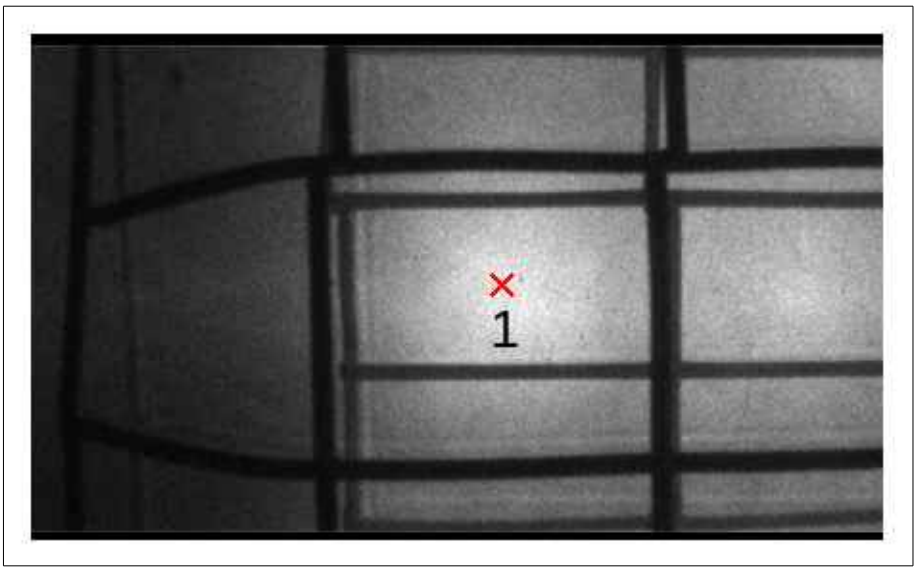

Fig. 149. Showing location from which light was sampled for the results shown in Figs. 150 to 152

These results are presented as part of an investigation into how the intensity of light emitted from the fireball relates to the levels of current and voltage. They are therefore plotted on the same axes, scaled to enable comparison. Different voltage scalings are also shown, to enable the respective relations to be perceived. These are plotted against time, since this aids the discerning of the effects of evolving conditions. For the case of the fireball in the set-up with the anode, this investigation also concerns any relation between the fluctuating behaviour and the levels of emission and current in the discharge, and so oscilloscope traces were monitored throughout the experimental run. Stills from a video made of these are included on the plot, which is shown as Fig. 150. These waveforms generally correspond to points at which thy have recently changed, although some of these changes are minor. They are therefore chiefly representative of the waveform evident in the time subsequent to that indicated on the plot.

The behaviour seen in the current-voltage plots such as Fig. 126, in which the relation alternatively followed voltage and then jumped back to the previous trend line, may be observed in Fig. 150 also. Levels of emission are observed to follow a quite consistent scaling with voltage raised to the power 1.875 or thereabouts, and do not follow the levels of cathode current where these deviate from a consistent trend with voltage. The reason for choosing this rather precise index value is that cathode current has been shown to more generally follow a dependence upon voltage raised to the power 2.5 (e.g. Fig. 125). As well as fitting the emission scaling well, the value of 1.875 lets it also be observed that emission scales with this overall trend of cathode current, raised to the power 0.75.

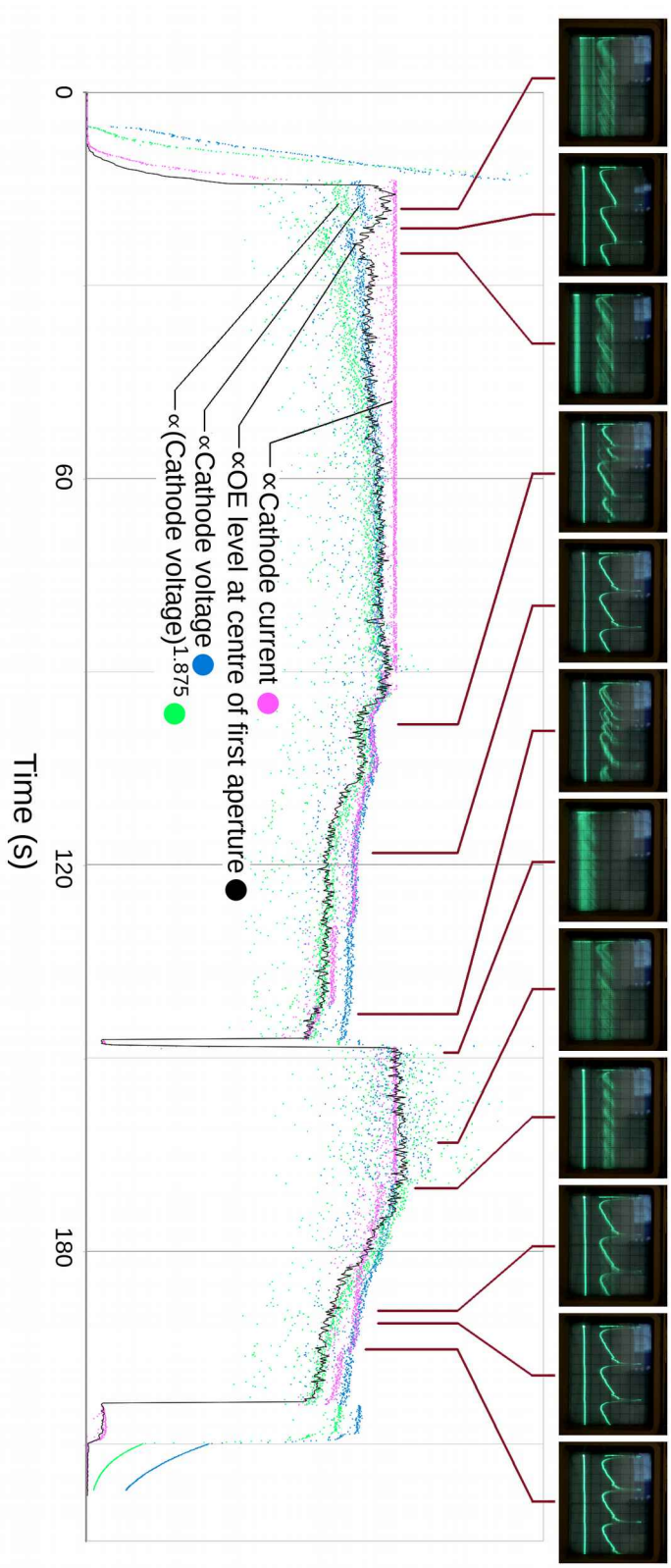

Fig. 150. Comparison of scaling of cathode current and intensity of optical emission with cathode voltage, from a fireball discharge in the set-up with the anode grid. Emission is sampled from a well-localised region at the location marked '1' on Fig. 149

The oscilloscope traces show that the regular fluctuations may also be associated with the current-voltage behaviour. Specifically, they are found to be associated with the periods in which current appears to scale with voltage.

Results are also presented for an experimental run without the anode grid, in which emission was again sampled at the location marked '1'. These are shown in Fig. 151. The same scalings, as indicated by the colour coding, are shown for traces corresponding to operation at two different pressures, which were i) 10 mTorr and ii) 8 mTorr. In both of these cases, levels of optical emission are found to also scale as cathode current raised to the power 0.75. The scaling of axial current was also investigated, and this is shown to scale more aggressively with voltage than cathode current does. It was observed previously that levels of collected axial current are treated with caution, since any change in the spread of the beam will affect the results. These are still considered significant however, since the more severe scaling seen in this case would indicate that either levels of current in the beam increase at a greater rate than cathode current does, or the beam becomes more focussed at greater levels of voltage and current.

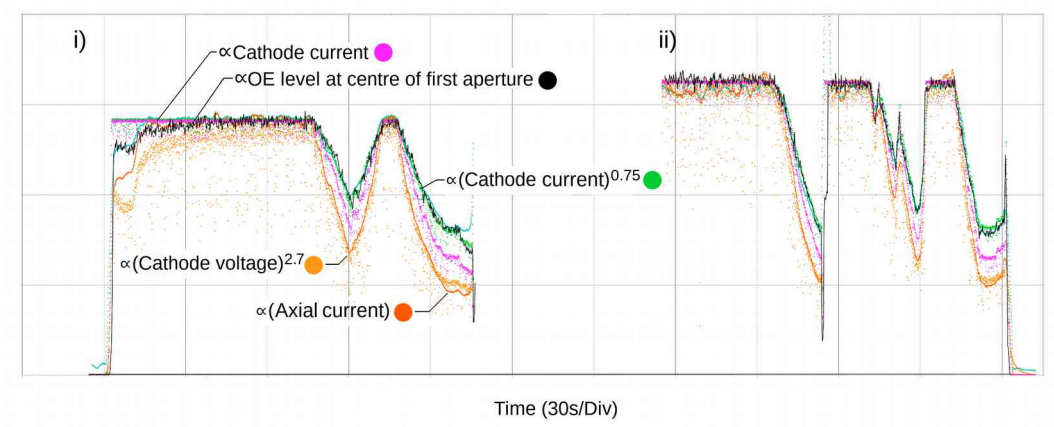

Fig. 151. Comparison between scaling of cathode current and intensity of optical emission with cathode voltage, also showing voltage-scaling of axial current, from a fireball discharge in the set-up with no anode. Emission is sampled from a well-localised region at the location marked '1' on Fig. 149

The scaling behaviour of the currents incident at the anode and axial collector in the discharge with the anode are also investigated, and these are shown in Fig. 152. Because of the large-amplitude fluctuations in these currents, the data-points have been averaged over a moving window of around one second. The results of this show considerable fluctuation in the average, but this is treated with caution, since these represent a periodic under-sampling of a substantially periodic signal, and therefore may be subject to interference. These fluctuations make it hard to be definitive about the results, and it is not really possible to say whether axial current scales with emission, or with the 2.5-power scaling that is characteristic for cathode current with voltage, when the fireball is not present. It seems quite clear however, that anode current follows the profile of cathode current, including the deviations from a consistent relation with voltage, and that axial current does not.

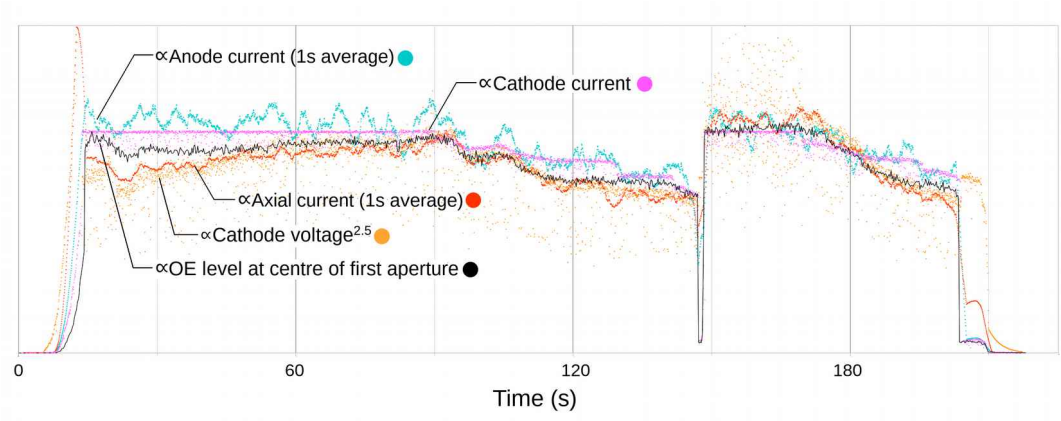

Fig. 152. Comparison of scaling of cathode current and intensity of optical emission with cathode voltage, also showing voltage-scaling of anode current and axial current, from the same fireball discharge in the set-up with the anode grid as shown in Fig. 150. Emission is sampled from a well-localised region at the location marked '1' on Fig. 149

7.3.2.3 Time-varying optical emission

When the discharge was operating in a stable state, showing regular fluctuations, the same optics set-up described for the previous experiment was used with a photodiode, to collect light from specific locations along the axis of the discharge. The output of the diode could be viewed on an oscilloscope, triggered from the anode current waveform. Levels of emission were found to fluctuate also, and so the fluctuations in current are indicated to be associated with a periodic evolution of the fireball object.

The optical arrangement was mounted on the motorised translation stage described in Chapter 2, and so could be made to move parallel with the side of the chamber, whilst continuously sampling light from along the axis of the discharge.

This was done, whilst a video recording was made of oscilloscope traces showing both the emission signal and the anode current waveform. Stills from this were subsequently analysed, corresponding to spatial locations separated by a few millimetres, so that a spatio-temporal profile of the emission could be re-constructed.

Fig. 153. shows two examples of frames used for this. The procedure used was to superpose a grid upon the still, which could be adjusted to match the timing of the anode current waveform where necessary. Points were then read off from the image using a program for extracting data from plots. The discharge flickered a couple of times during this process, but generally remained stable for the duration of the scan.

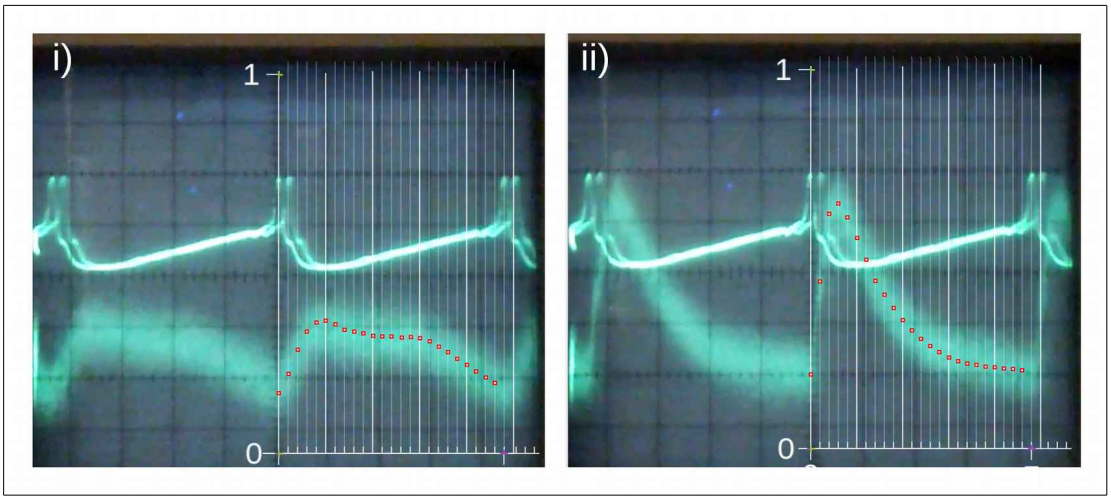

Fig. 153. Stills from the video recording made of oscilloscope traces corresponding to the optical signal from different locations along the discharge axis and the anode voltage waveform, during a fireball discharge in the arrangement with the anode grid. The anode waveform is the upper trace in this images, and the optical signal is the lower trace. These frames are broadly representative of the optical waveform in i) the end row of apertures and ii) the second row of apertures. Oscilloscope timebase is 10 μs per division

The results of the analysis are shown in Fig. 154 as three-dimensional projections, and the individual profiles are shown overlaid in Fig. 155. The period of these fluctuations was around 45 μs, and the profiles obtained are spaced by increments of a little less than 2 μs. The gaps evident in the results shown in Fig. 154 and Fig. 155 correspond to the locations of the end ring of the cathode, and the second ring.

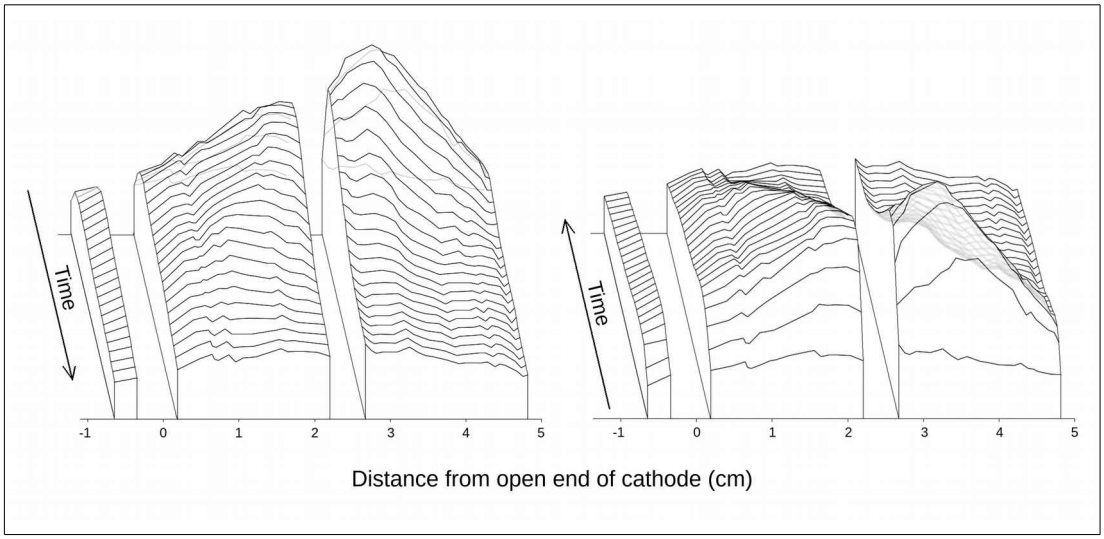

Fig. 154. 3D plots showing the spatio-temporal profile of the fluctuations in emission along the axis during regular fluctuations in a discharge with anode grid. The arrows indicate the direction of time; increments are a little less than 2 μs, and the total period is around 45 μs.

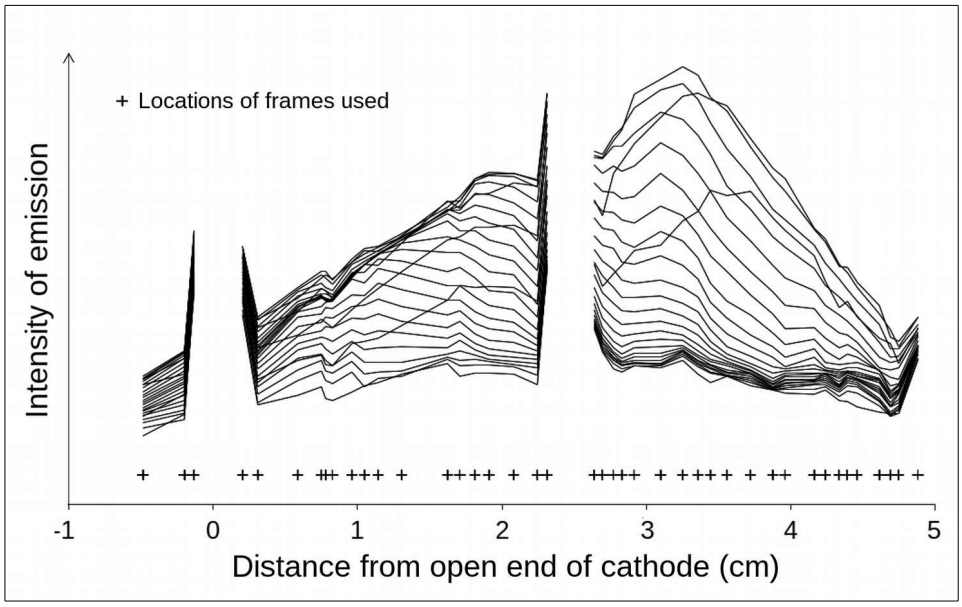

Fig. 155. Overlay of spatial profiles of the fluctuations in emission along the axis corresponding to increments in time of a little less than 2 μs, during one period of regular fluctuations in a discharge with anode grid.

The results show an initially very rapid rise in intensity to occur within the second ring of apertures, which then progresses forwards the open end of the cathode, with its amplitude decreasing as it moves.

Errors leading to an offset in the data points extracted from a still, or a momentary variation in levels of emission will cause variation in the results associated with the spatial location associated with that particular still. This is expected to be the cause of some of the smaller structural details evident in the profiles, but not for the larger structure evident at a displacement of around 3 cm on Fig. 155. This structure is observed to remain quite consistently located at this position, indicating there to be static structure in the emission profile, as well as dynamic.

7.3.3 Anomalous time-varying behaviour with anode grid

Some anomalous behaviour has been observed to occur for the object in the set-up with the anode grid, when operating in the 'hybrid' mode of fluctuation. As described in Section 7.3.1.4, this mode consists of fluctuations having two different, but consistent periods, that occur in an alternating cycle. The pattern is sufficiently regular for an alternating waveform to be viewed on an oscilloscope, as was shown in Fig. 144. At times, this progression may become less stable, with occasional repetitions of a single period causing the two halves of the pattern to abruptly switch in order on the oscilloscope screen. When two waveforms are monitored simultaneously, this behaviour is generally found to affect both similarly. On one or two occasions however, the fluctuations in anode current have been observed to become de-coupled with the fluctuations in axial current or emission levels.

An example of this de-coupling of the waveforms of anode current and optical emission is shown in the images of Fig. 156, which are stills taken from the same second of original video footage. Emission levels shown in in these images are sampled from an axial location close to the centre of the second row of cathode apertures. These results also show the intensity of emission to be initially greater for the longer period, as compared with the shorter.

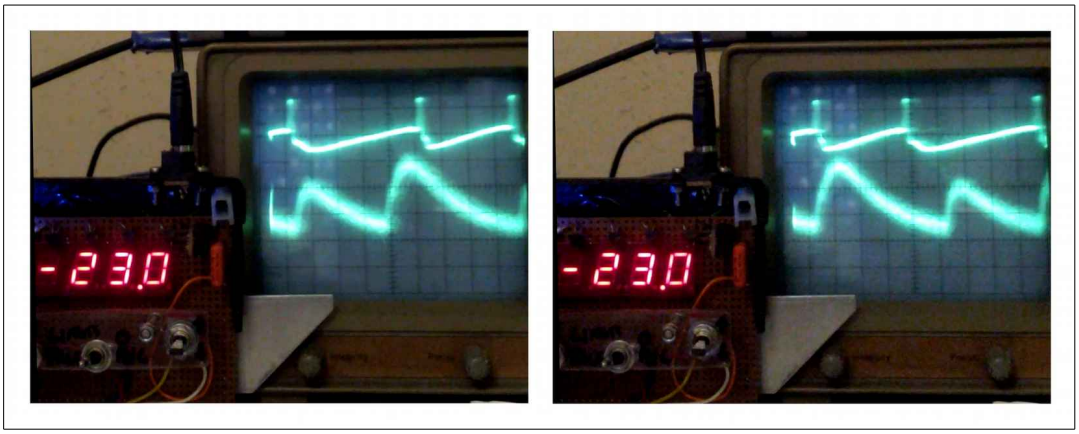

Fig. 156. Instance of anode current de-coupling from emission waveform. The upper trace shows anode voltage (the trace is not inverted, making magnitude of current downwards), and the lower trace represents intensity of optical emission.

An example of the phenomenon affecting the waveforms of the anode and axial currents is shown in Fig. 157, indicating the generally-apparent reciprocity between the spikes and notches in the anode and axial waveforms to represent a rather loosely-coupled relation. No measurements were made of the simultaneous time-variation of all three waveforms of emission, anode current and axial current during this behaviour, but it seems likely that the waveforms of emission and axial current will remain phase-locked, whilst the anode fluctuations de-couple.

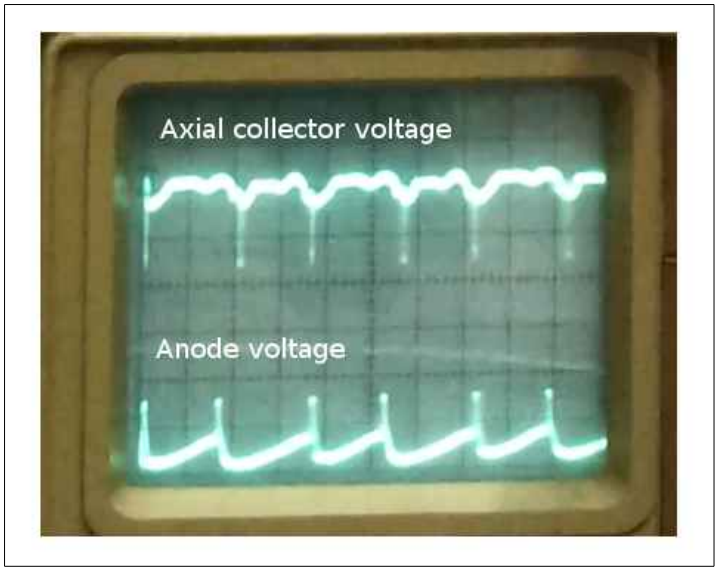

Fig. 157. Instance of anode current de-coupling from axial current. Traces are not inverted

7.3.4 Summary of experimental findings

Fireball discharges are observed to occur at pressures of around 10 mTorr in argon, over a range spanning a few mTorr. They appear as brightly luminous quasi-spherical or oblate objects, that are located within the open end of the cathode. Characteristic differences are evident in the observed behaviour of objects occurring with and without the anode grid being present, with more variation generally evident in the case of the fireball occurring with the anode grid. The principal characteristics are summarised below.

7.3.4.1 Optical emission distributions

Without anode:

The fireball object appears located within the end row of cathode apertures, and is always accompanied by a relatively-bright axial jet formation. Whilst still quite beam-like in appearance, this shows a degree of spread that is not evident for the pea-shooter beam. Spectral analysis of the light emitted from these objects indicates processes of excitation occurring within them to be primarily caused by the activity of electrons.

With anode:

The fireball occurring with the anode grid present is larger in appearance, with a less well-defined boundary. The region of bright emission extends further into the cathode, and the object is accompanied by a jet formation that is both less bright, and subject to more variation, than for the case described to occur with no anode grid. Spectral analysis of emission indicates excitation within these objects to also be caused largely by electrons.

7.3.4.2 Current-voltage behaviour

Without anode:

Upon formation, cathode current generally jumps to the power supply limit of 100 mA, at voltages between 5 kV and 6 kV. The object will persist to conditions of lower cathode current, of around 30 mA. The current-voltage relation of the fireball discharge is found to be similar to that of the discharge in which only a pea-shooter object is evident, except with the effective perveance increased by a factor of around one half.

With anode:

The current-voltage behaviour shows a significant discontinuity upon ignition. As was the case without the anode, the fireball current-voltage relation remains unchanged, but is shifted to an increased effective perveance. Observation of this is made more difficult in the case with the anode, since the range does not extend to such low cathode currents; the object has been observed to persist to currents below

60 mA, but in a well-conditioned chamber this may only be 80 mA or even 90 mA. It is also made complicated by the behaviour of the discharge in the fireball state, in which the current-voltage curve follows a characteristic stepwise profile. This occurs as cathode current repeatedly follows a quite linear dependence upon a relatively small range of cathode voltages, before transitioning back to the previous fireball perveance relation. The discharge has also observed to transition to a different perveance altogether, where a similar behaviour is then apparent. These variations and transitions in current-voltage behaviour are observed to be associated with both the degree of emission visible in the axial jet formation, and also the nature of the fluctuations in electron currents collected axially and radially.

7.3.4.3 Optical emission scaling

Levels of optical emission are found to scale similarly with cathode current for fireballs occurring both with and without the presence of the anode grid, despite the specific cathode current-voltage relation being different in each case. This indicates a generally-close association between fireball activity and ion current to the cathode. In both cases, metered cathode current scales more aggressively with voltage than levels of emission do, suggesting the secondary electron component of cathode current grows consistently with voltage. This might represent a quite consistent scaling of the secondary electron coefficient with an average collected ion energy, that itself scales quite consistently with voltage.

For the fireball with no anode present, the axial current is found to scale more closely with a consistent voltage, and anode current is found to follow the stepwise behaviour shown by the cathode current.

7.3.4.4 Time-varying behaviour

Without anode:

Characteristic, phase-locked fluctuations in electron current to the axial and radial collectors are always observed to accompany fireball discharges without the anode grid. These show similar amplitudes of between 25 % and 30 %, but have different waveforms, which suggest a degree of reciprocity between the two currents. The fluctuations in electron current are not accompanied by fluctuations in ion current to the cathode, occurring on a corresponding time-scale, of any significant magnitude. As conditions of cathode voltage and current vary, the nature of the fluctuations evolves; this is characterised by a reduction in frequency, and an increase in amplitude of a narrow spike in axial current, occurring as levels of voltage and current increase. This narrow spike causes many harmonics to be evident in the power spectrum. Lower frequencies in the range associated with the fireball fluctuations are around 80 kHz, which is several times slower than those that may occur with pea-shooter objects.

With anode:

The fireball discharge that occurs in the set-up with the anode grid shows a variety of time-varying behaviour, with fluctuations of a relatively large magnitude evident in the voltages developed across the anode and axial collector resistances. These fluctuations in electron current show some similarities to those associated with the discharge in the set-up without the anode, in there being a reciprocal element to the relation apparent between the waveforms in axial and radial current. In the case with the anode grid however, these fluctuations alternate between being irregularly- and regularly-spaced, which behaviour is associated with the step-wise evolution occurring along the current-voltage progression. When these fluctuations do become regular, this may occur at a range of different frequencies. In these regimes, cathode current shows a very much smaller degree of fluctuation, of the order 1 %.

During operation in which the current fluctuations are regular, the intensity of optical emission from within the fireball has been found to fluctuate also. Spatial resolution of the time-varying emission signal indicates that the fluctuating behaviour corresponds to a translation of the object along the axis of the cathode, towards the open end.

For these objects, instances have been observed in which anode current fluctuations may become de-coupled with those in axial current, or in intensity of optical emission.

7.4 Discussion

In the previous part of this chapter, instances of 'fireball' objects have been described to occur in both the electrode arrangement with the anode grid, and in a somewhat different form, the arrangement with the anode removed. It seems likely that these objects may be related to some spherical IEC discharge modes described previously in Section 1.4.2, such as the 'halo' mode referred to in [19]. This mode is described to be accompanied by a jet formation, and to occur when one aperture of the spherical grid cathode is enlarged. This element of asymmetry appears to be also required for the formation of fireball objects in the cylindrical set-up described here, since they have only been observed during operation with the open-ended cathode. It is also noted in [19] that the jet may disappear with the addition of an extra grid. Whilst details of this are not provided, the characteristic again agrees with the observations made here. The halo mode is noted to provide an enhanced fusion rate over other modes, and the authors believe the object to have a radial double well potential profile. In the following, the observations of fireball objects are analysed to infer information about their potential structure. The object occurring without the anode is discussed first.

7.4.1 Fireballs occurring without anode grid

These objects show a clear resemblance to those also occurring in the set-up without the anode, that were referred to in the previous chapter as 'pea-shooter' objects.

Factors linking the two include the spectroscopic evidence for both being sustained by the activity of electrons, and also the way in which a fireball may be observed to develop from a pea-shooter.

The evolution from pea-shooter to fireball is associated with a jump in both the size of the object and the level of current produced. The axial beam associated with the pea-shooter evolves to become a jet, the end of which is observed to penetrate some way into the fireball. This may be seen in the photograph shown previously in Fig. 114, with the detail reproduced as Fig. 158.

Fig. 158. Detail of photograph from Fig. 114, showing jet feature associated with the fireball occurring in the set-up with no anode, in argon at 8 mTorr.

The separate photograph of the jet formation that was shown as Fig. 119 [reproduced as Fig. 159 ii)], was taken at different exposure settings, and details of structure within the jet are discernible. There is a clear resemblance between these structural elements and those visible within the electron extraction formation that was described to accompany the beam mode discharge, during operation with the additionally-enclosed cathode, in Chapter 4 (see Fig. 57). Images of these are reproduced together for comparison in Fig. 159, with the analogous regions of the structures indicated.

The fireball jet formation [Fig.159 ii)] appears to be similar to the electron extraction beam formation observed with the enclosed cathode [Fig. 159 i)], but with an additional element attached to the end within the cathode. Comparison with the more-exposed image in Fig. 158 shows this to be the section of the jet that protrudes into the outer region of the fireball. This suggests the fireball to consist of two envelopes, each having regions of locally-positive potential from which low-energy

electrons are extracted via the two terminal elements of the jet, implying the overall potential structure of the object to be relatively more positive within the core region.

This interpretation is largely consistent with the account of the formation of multiple double layer objects in [102], in which the appearance of a second charge-generating plasma shell is described to cause a jump in both physical dimension and levels of collected current, and to be accompanied by complex, non-linear fluctuations in electron current. These similarities suggest the fireballs may be described in terms of an outer plasma shell surrounding an anode double layer object.

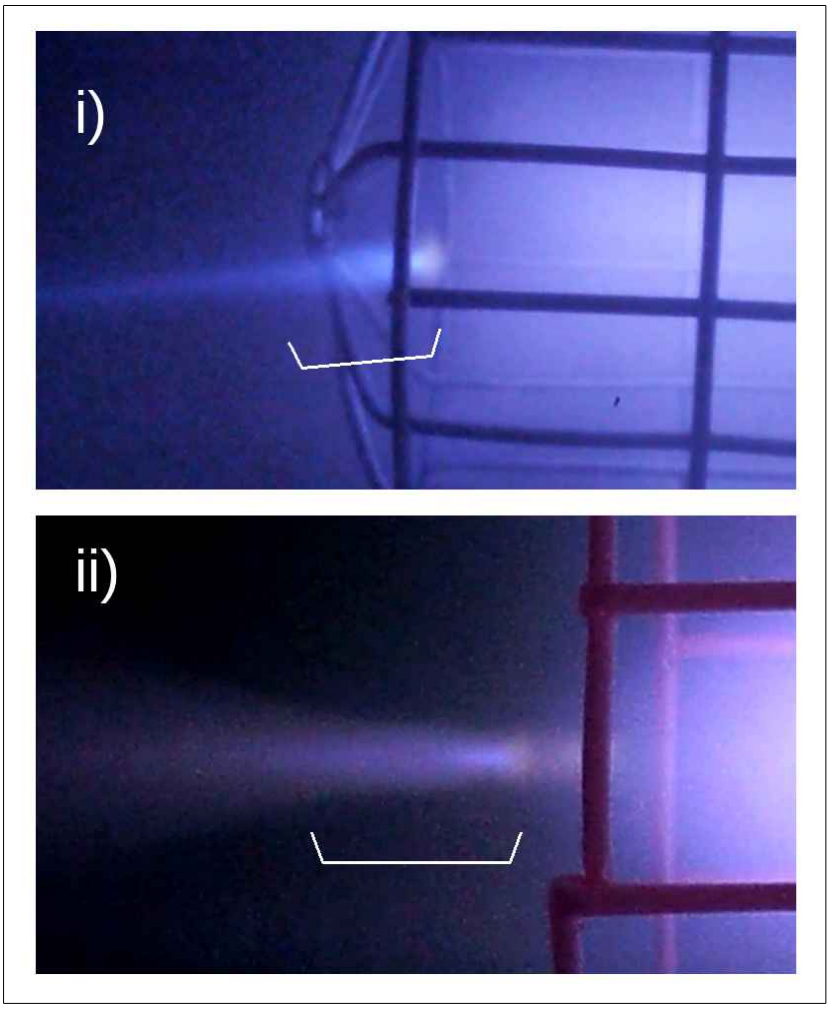

Fig. 159. Comparison of i) electron beam feature observed during operation in enclosed cathode, in argon at 7 mTorr; and ii) jet feature associated with fireball in set-up with no anode, in argon at 8 mTorr. Analogous regions indicated by brackets.

7.4.2 Fireballs occurring with anode grid

The fireball objects occurring within either electrode arrangement show similarities in terms of the general location in which they form, the high levels of electron-impact excitation and some aspects of the more regular fluctuating behaviour. The

objects occurring when the anode grid is present however show considerable additional complexity in their behaviour. Some of this may be attributed to the variation in form evident at different conditions, as was shown in the false-colour images in Fig. 147. The state shown as Fig. 147 ii) is shown to involve relatively-high levels of electron activity occurring in several distinct locations, and there is an increased element of axial jet evident for this case. This shows a similarity with the low-perveance state occurring in the run described as 'Anode FB#2'. The other distributions shown in this figure however indicate a more cohesive object, particularly the state shown as Fig. 147 iv). The additional jet activity, more spherical form and shorter timescale of fluctuations make this low-perveance state more similar to the fireball occurring without the anode, and so in the interest of brevity, the discussion will therefore concentrate upon the high-perveance state. Particular consideration is given to the behaviour of the fireball at conditions when regular fluctuations are evident, and unless specifically stated, the mention of fluctuations in the following will refer to those occurring regularly.

7.4.2.1 Source of cathode ion current

Since the appearance of a fireball is associated with a considerable increase in current, the fluctuations in emission might be expected to cause corresponding fluctuations in cathode current. This is not always found to be the case however, since during the regular fluctuations cathode voltage is found to vary by only 5 volts or so, corresponding to fluctuations in current across the ballast resistor of between 1 and 2 mA. This suggests either that ion current is drawn from a reservoir of charge, or that the levels of current produced in the fireball are negligible, and those produced elsewhere show little association with the fluctuations. This seems unlikely, and so the steady levels of cathode voltage are considered to indicate a region of ion accumulation between the fireball and the cathode, that will be referred to in the following as Φ_i.

There is evidence that some accumulation of charge occurs at larger radius also. When the fireball occurs in the electrode arrangement with the anode grid, the characteristic radial beams are observed to largely disappear. According to previous analysis of the beam formation mechanism in Chapter 5, this is suggestive of an accumulation of space charge occurring in the region beyond the anode radius, but sufficiently close to prevent the beam formation mechanism from functioning. Such an accumulation of charge could not shield the cathode from the fireball fluctuations however, and so does not constitute an alternative unique source for ion current.

7.4.2.2 Axial and radial processes

Little axial beam is evident for the fireball occurring in the regular state, suggesting a significant electron current to flow radially in this case. This is consistent with the existence of a region of relatively positive potential surrounding the object. The variation in axial jet activity that accompanies the steps in the current-voltage behaviour (Fig. 127) suggests this potential to vary in a step-wise manner also, which

is consistent with steps in levels of cathode current, if this flows from the same region.

The different scaling with voltage shown by levels of emission and the various currents shows a distinction may be made between axial and radial activity. The axial current-voltage relation was found to remain quite consistent, as was that for the levels of fireball emission, but cathode current and anode current are found to both follow the stepwise behaviour. This suggests anode current to be associated with the same potential structure as the cathode current, and that ionisation associated with this structure scales differently with that occurring in the core region.

Axial current is considered to be associated with the core region of the fireball, and although the spikes in axial current appear to be closely associated with the notches in the anode current waveform, the observations of the anode current profile becoming de-coupled from those of the optical emission and the axial current waveforms (Fig. 155 to Fig. 157) indicates that whilst anode current may be generally coupled to the core activity, it does not directly flow from this.

7.4.2.3 Radial currents and potential structure

The anode and cathode currents are considered further in the following. If these currents are supposed to flow from the same region, then the largely DC cathode current waveform suggests the potential of this will not vary much. The significantly-varying waveform evident in anode current might reflect such a relatively small variation in the potential of the source region, if either i) this potential is close to that of the anode, or ii) there were a potential barrier for electrons between the anode and the source. The strong emission, considerable increase in cathode current and considerable cathode heating associated with the fireball indicate it to cause significant levels of ionisation. The relatively small degree of axial jet emission suggest relatively little electron current to flow axially, making radial electron current correspondingly quite large. Anode current will be expected to constitute some of this radial flow. The deep notches in the waveform are therefore considered unlikely to be caused by a fluctuating source potential close to the anode.

What seems more likely is that anode current is representative of the interception of an outwardly-radial electron current, which will consist of a component from the secondary electron current, a component from ionisation occurring within the cathode, and a component from ionisation occurring within the space between the anode and cathode. Radial electron current originating from ionisation within the cathode was discussed previously in Chapter 4, in which it was observed that the potential within the apertures must not be more negative than that of the source region except by a value within the range of electron temperature for current to be able to flow. The aperture potential is referred to in the following as Φ_{ap}. Should this be quite close to cut-off, the radial current from within the cathode might be significantly affected by relatively small fluctuations in either the source potential or the aperture potential. This configuration is illustrated in Fig. 160.

Should this be causing the notches in anode current, then the components due to secondary electron current and ionisation occurring external to the cathode radius will not be affected, which is consistent with the notches not representing complete cut-off. Consideration of the anode current waveforms shown in Fig. 133 to Fig. 143 indicates that the notches generally occur as anode current levels fall to a consistent value, which agrees with this interpretation.

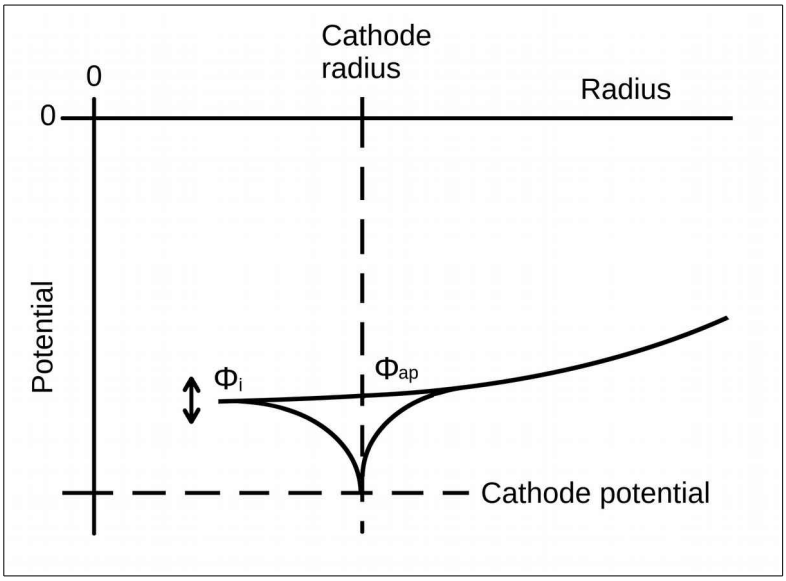

Fig. 160. Radial potential configuration in which radial ion current and radial electron current both flow from the region marked Φ_i. The arrows indicate the fluctuation in Φ_i that might cause electron current to be cut off by the potential barrier represented by the aperture potential, Φ_{ap}.

The waveforms in anode and axial current evident during regular fluctuations (Figs. 134 and 135) show these to follow similar profiles, except for the spikes and notches, and that these profiles generally involve a small rise in current followed by a longer decline. Since cathode current is virtually DC at these conditions, consideration of the charge balance within the cathode suggests that over the course of one period, the electron outflow becomes smaller, whilst ion current remains consistent. This would seem to represent the overall charge population becoming relatively more electron-rich over the cycle.

Consideration of the waveforms in anode and cathode current in Figs. 141 to 143 indicates the general shape of these to also be quite similar, although of very different relative magnitudes. This observation is not consistent with these currents flowing from the same region, since having opposite charge, ions and electrons would be expected to be affected oppositely by a fluctuation in potential.

This suggests anode current to flow from a separate region to that called Φ_i, and which will be called Φ_e. The potential configuration implied by this is illustrated in Fig. 161. This configuration allows electron current to flow from Φ_e, if Φ_i were to become more positive than Φ_{ap}. Radial electron current would be cut off in this configuration if Φ_e were to become more positive than Φ_{ap}.

According to this interpretation, the stability of cathode current levels will be affected by the stability in the value of Φ_i, and the steps in cathode current will represent a step change in Φ_i. The fluctuations in anode current represent an evolution in Φ_e, with the notches in the waveform caused as Φ_e becomes more positive than Φ_{ap}. The fireball fluctuations occur at smaller radius than this structure, which may account for the de-coupling between the axial and anode currents.

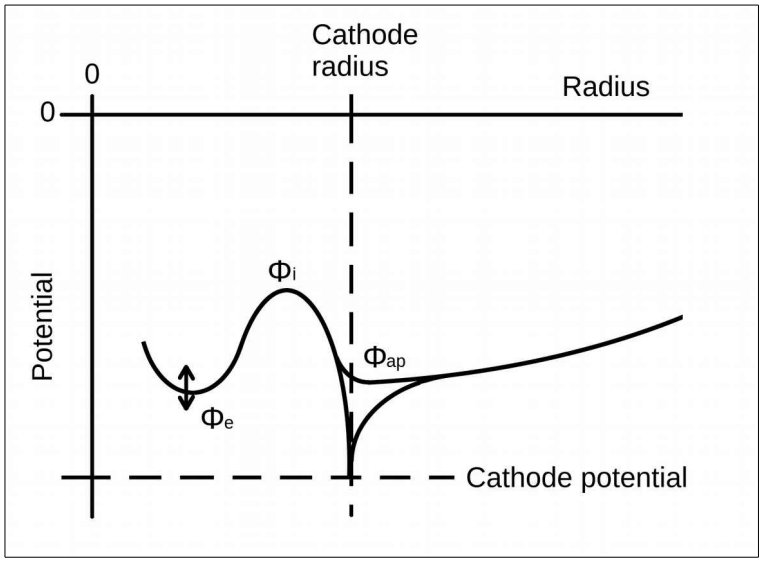

Fig. 161. Radial potential configuration in which radial ion current and radial electron current flow from separate regions marked Φ_i and Φ_e. The arrows indicate the fluctuation in Φ_e that might cause electron current to be cut off by the potential barrier represented by the aperture potential, Φ_{ap}.

This describes the behaviour evident in the radial currents from within the cathode. The fluctuations in axial current and emission will be associated with the fireball dynamics, which according to these considerations will operate within the enclosing potential structure illustrated in Fig. 161.

7.4.2.4 Core dynamics

The monitoring of the time-varying behaviour of levels of optical emission shows that this is associated with the transport of the object along the axis of the cathode towards the open end. This is similar to the behaviour described in [103] and [104], in which an anode double layer object detaches from the anode it has formed upon, and which behaviour is explained for those circumstances in terms of the repulsive electrostatic force between the object and the anode. Whilst there is no physical anode in the vicinity of these fireballs, this might still be imagined to occur if the potential further within the cathode were sufficiently positive. This might conceivably be the case for the region in the half of the cathode closest to the feed-through, and from which electrons are extracted by means of the fireball.

In the considerations of anode double layer objects made in the previous chapter, it was theorised that for such an object to persist in free space, with no beam or plume

structure extracting electrons from within its core, the entire structure would need to become more negative, without this substantially affecting the removal of ions from its surrounds. For this to be able to occur for any length of time, the object would need to be surrounded by a plentiful supply of electrons, and to exist in a potential environment that allows for it to become more negative. It therefore seems possible that the presence of a surrounding region such as that called Φ_e might allow this to occur. The functional role played by the fireball could then be characterised in terms of the extraction of electrons from the region of positive potential within the cathode, followed by the transport of these along the cathode axis whilst the potential in the core region they surround becomes more negative. This would be consistent with the general reduction in anode current seen throughout most of the period of fluctuation, as the potential difference between the fireball and Φ_e becoming smaller may cause Φ_e to become more positive.

These theories offer possible explanations for some of the observed behaviour, in particular the distinction that is evident between the characteristic behaviour of radial and axial currents. The de-coupling of anode current with both axial current and emission on the short timescales illustrated in Fig. 156 and Fig. 157 might be seen as analogous to the time-averaged de-coupling that is observed between the stepwise behaviour of radial currents and the consistent voltage-relations of axial current and emission in these discharges. It therefore seems that the axial ADLO activity in the case observed with the anode grid must occur within a separate potential structure, from which radial currents are sourced. Should the region from which radial ion current flows to the cathode be more positive than that within its apertures, then a more negative region, termed Φ_e, is required to facilitate radial electron extraction, making the structure resemble that of a 'double' potential well. The depth of such a well would be similar to the potential difference between Φ_i and Φ_{ap}.

7.4.3 Summary

In the case of the discharge obtained without the anode grid, the fireball is observed to evolve from a pea-shooter, and with the anode in place, the fireball may be preceded by the appearance of a spot. It seems likely that the processes that sustain the anode double layer objects also operate in either instance, and also that the fireball objects have a multiple double layer potential structure.

In the case of the discharge obtained with the anode grid in place, a sub-mode structure is observed in which the discharge appears to make repeated transitions between two perveances along the current-voltage progression, interspersed by discontinuities in current. A corresponding evolution in the intensity of axial emission suggests this to represent a periodic evolution in potential structure. A regime in which current fluctuations become regular is associated with each of these cycles. During such periods of regular fluctuation, the bright electron-induced emission at the core of the fireball, that is assumed to be a form of ADLO, is observed to be transported along the axis towards the cathode open end. As this occurs, this object sustains for periods that may be in excess of 50 μs, during which time the electron processes sustaining it will be expected to cause it to become more

negative. The de-coupling of axial and radial processes suggests that this dynamic may occur because the object is immersed in a region of negative potential within a surrounding radial potential structure. Consideration of the time-varying nature of the various collected currents in the chamber suggests the overall structure might be described as a complex ADLO residing within a double potential well profile. This interpretation is consistent with the generally low levels of axial emission observed.

The potential structure of the fireball occurring without the anode grid is also apparently complex, and the relatively more significant axial jet suggests the potential within the core region of these objects to be relatively more positive.

7.5 Conclusions

Observations were made of large space charge objects occurring within the cathode during operation at conditions of relatively high current. These 'fireball' objects show some similarities to the anode double layer objects described in the previous chapter, and it is expected that they rely upon similar processes to some extent for their sustenance.

These objects are found to form in the apparatus both with and without the anode grid. These types of object clearly share some similarities, and both show evidence for a complex internal structure. They also show quite different behaviour, which may correspond to different potential configurations.

The fireball objects are found to affect the operating characteristics of the discharge significantly. The degree of current generation associated with these objects is considerable, and it is likely that a significant element of this is associated with the bright electron-induced emission observed. This would be undesirable for the operation of a reactive source in which the degree of ion- and neutral-induced process were to be maximised, and so for the purposes of this research, they are likely to constitute an instability. At attainable experimental conditions, they have been observed in the relatively more massive species of gas, and by analogy to the smaller objects described as 'spots' in Chapter 6, this is expected to reflect the observed characteristic that relatively smaller currents are associated with space charge objects in more massive species. The operation of a reactive plasma source in complex molecular species might be expected to produce quite massive ions, and so it seems likely that such discharges may be susceptible to the occurrence of these objects.

The indirect evidence for double well formation suggests that these objects might be investigated further for fusion applications. Modelling by Ohnishi et al. [50] of collisional IEC plasmas found that strongly-fluctuating complex potential structures were projected to cause a fusion rate that scaled as current-squared or greater, which can be attributed to the enhanced ion densities and confinement that may occur within a virtual cathode, as outlined in Section 1.4.2. Whilst it seems unlikely that these discharges could produce net power gain, a significantly increased fusion rate could open up further non-power applications, as discussed in e.g. [19].

Further work is required however, to confirm the identification of the structure and to determine any scope for such applications. The dependence of double well depth upon operating conditions might possibly be investigated by measuring the energy spectrum of emitted fast neutrals, since an energetic ion population within a double potential well would be expected to create a flux of these. Regarding the processes operating to cause and sustain these objects, a more complete understanding would be beneficial of both the dependence upon the asymmetrical nature of the cylindrical electrode arrangement, and the importance of the element of axial transport for the potential structure.

Chapter 8
Novel electrode arrangements

8.1 Introduction

In Chapters 3 and 5 it was found that the operation of the discharge apparatus, at conditions of relatively low pressure and high voltage, resulted in the formation of radial beams of ions and neutrals that pass through the apertures of both electrodes, and this mode of operation was called the beam mode.

These beams bear some resemblance to an IEC mode described elsewhere as 'star mode' [20], [21], [42]. Upon investigation of the effect of the anode grid, it was found that if the cathode grid is axially rotated relative to this, so as to cause the apertures of the electrodes to become misaligned with each other, the positioning of the beams follows that of the anode apertures, rather than those of the cathode (see Chapter 5). The beams are therefore demonstrated to be associated with the relative positioning of the apertures of the anode grid, and not with those of the cathode. In this respect, the beam mode is distinguished from the star mode, which is shown to be caused by processes associated with the apertures of the cathode in the works referenced above.

Referring to plots of the vacuum potential distribution, this was understood in terms of the field distortion caused by the anode apertures; the effective 'bulging' of equipotential contours through the anode grid apertures acts as an array of electrostatic lenses, which serve to focus incoming ions through the apertures, and so form beams.

Consideration of this effect leads to the realisation that the mechanics of beam formation are indicated to be essentially independent of the form of the cathode. This, in turn, suggests that the same principle might be employed to form beams in a range of different geometries, and using cathodes having a variety of different structural forms.

In this chapter, the results of the experimental testing of this principle are described. This was done for two quite different electrode arrangements, one of which has elements of spherical symmetry, and one that is implemented in a planar geometry.

The structure of this chapter is as follows: in Section 8.2 the form of these electrode arrangements is described, and the results of their brief testing in the same vacuum system used for the rest of the experiments. This is separated into two sections, each of which describes one of these arrangements. In Section 8.3 the results are discussed, with reference to the plasmas obtained and the possible advantages afforded by these approaches for different applications.

8.2 Experimental findings

8.2.1 'Spherical' abstraction

8.2.1.1 Apparatus

In order to test the principle that a beam mode type plasma might be obtained using a cathode constructed quite differently from a grid, a set of electrodes was constructed using the following form:

The cathode is composed of eight steel balls, held so that their locations correspond to the corners of a cube. This can be thought of as an abstraction from a spherical grid electrode, in which the vertices of this are retained, and in which each cathode element is required to have its own dedicated electrical connection. These are routed in to the elements of the cathode along radial lines, and shielded by conical steel shrouds, which are held at ground potential and so constitute elements of the anode.

A photograph of the prototype is shown in Fig. 162 with a sketch indicating the anode and cathode elements, and the form of field topology expected to result from this arrangement. The lensing potential surfaces occur in this case between the conical shrouds. In the practical implementation, these shrouds are supported using six steel bowls, the shape of which may enhance the curvature of the field contours at larger radius.

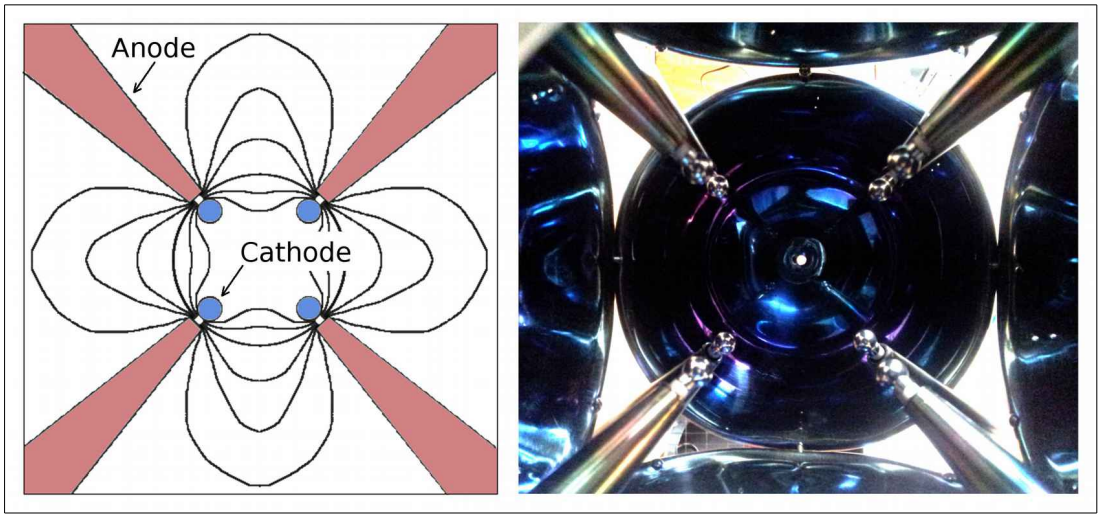

Fig. 162. Implementation of alternative electrode configuration, with sketch of field contours

A diagram of the configuration is shown in Fig. 163, with the position of a diagonal plane indicated. The form of the vacuum potential distribution calculated for this plane is shown in Fig. 164. Focussing potential surfaces may be observed to be created between the feed-through shrouds.

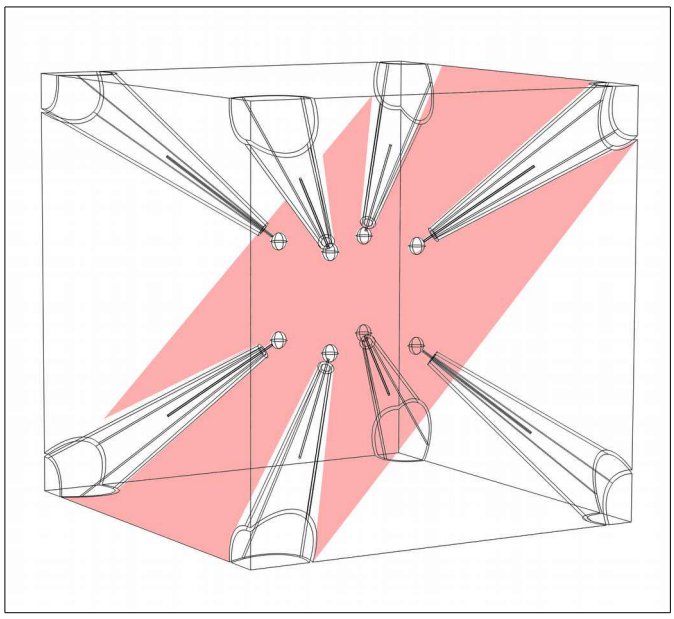

Fig. 163. Diagram of electrode arrangement showing plane corresponding to the potential distribution depicted in Fig. 164.

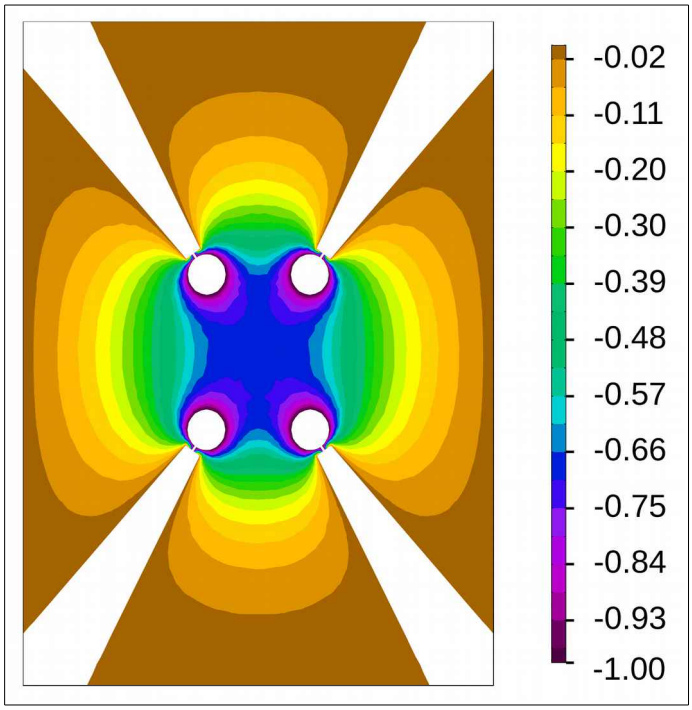

Fig. 164. Vacuum potential distribution calculated for a plane corresponding to that shown in Fig. 163.

The nature of the focussing surfaces may be appreciated from an iso-surface plot representing the potential surface corresponding to 4 % of the cathode potential, as shown in Fig. 165. The conical projections in this plot correspond to field within the feed-through shrouds, and should be disregarded.

Fig. 165. Iso-surface plot representing the 4 % contour of the potential distribution surrounding the electrodes described in Figs. 162 to 164 in 3 dimensions.

It should be noted that this is a relatively simple, yet somewhat extreme implementation, employing a minimum of anode/cathode elements. It would of course be possible to implement the principle in a variety of forms, such as other spherical geometries having more electrode elements, or in a cylindrical geometry more similar to that of the wire grid electrodes described in previous chapters.

8.2.1.2 Results

The electrodes were operated in helium and argon, at a range of pressures. The construction of these was constrained by the requirement to be a drop-in component, requiring no modification to the vacuum chamber. The use of stainless steel bowls was an efficient means of accomplishing this, but during operation these were found to quickly become hot, causing the gas temperature to rise significantly. This in turn causes the pressure to vary, and so it was difficult to maintain stable conditions over any length of time.

The results therefore do not constitute a thorough characterisation of the plasmas that may be obtained using this particular form of electrodes. These are presented in the following photographs of emission distributions observed at different conditions.

Fig. 166 shows a plasma obtained using the novel arrangement, in helium, at a pressure of 22 mTorr and cathode voltage of around 10 kV. Some bright emission may be observed close to the cathode elements, but the majority of emission is observed to be located within the centre of the space bounded by these, and also to extend into the regions between the electrode shrouds.

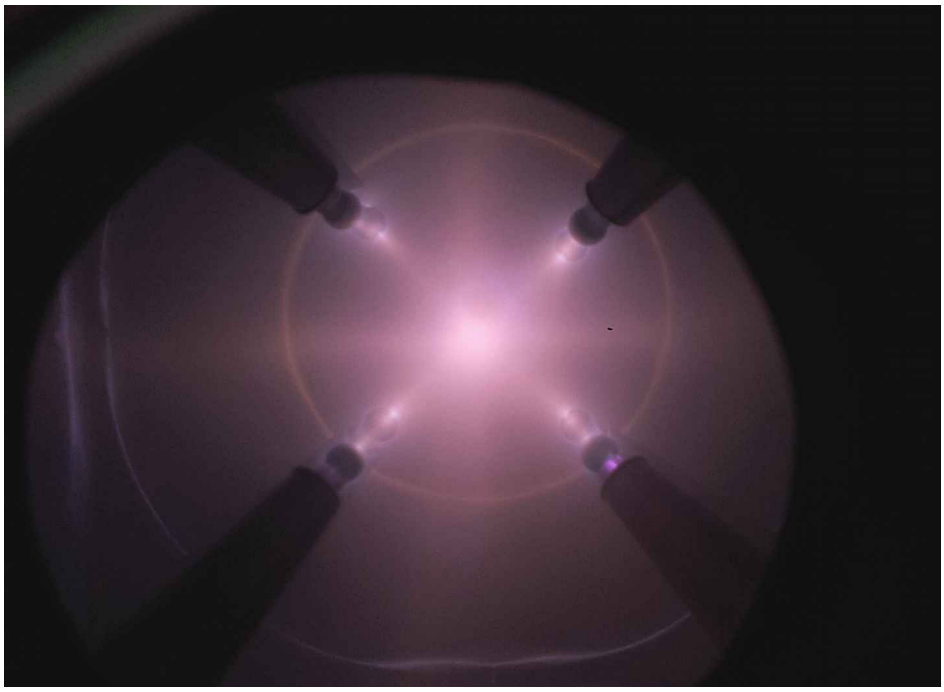

Fig. 166. Plasma produced in 'spherical' electrode arrangement, in helium at a pressure of 22 mTorr. The cathode voltage was around 10 kV. The circle is not plasma emission, but rather reflected light from the anode surface in the background.

Fig. 167 shows various plasmas obtained at conditions of somewhat greater pressure, in helium and in argon. Fig. 167 i) shows a plasma object obtained in argon at a pressure between 12 mTorr and 15 mTorr, that is not identified to closely resemble any formation found in the cylindrical arrangement described in previous chapters. It may resemble the 'halo' mode from [19] without a jet, or the 'central spot' mode described in the same reference with an additional envelope, but it is not possible to be definitive. Fig. 167 ii) shows a plasma that resembles a pea-shooter type object in helium, at a pressure of 47 mTorr. Fluctuations in electron current to the anode were found to be associated with this object. Fig. 167 iii) shows another object resembling a pea-shooter, obtained in argon at a pressure of between 12 mTorr and 15 mTorr.

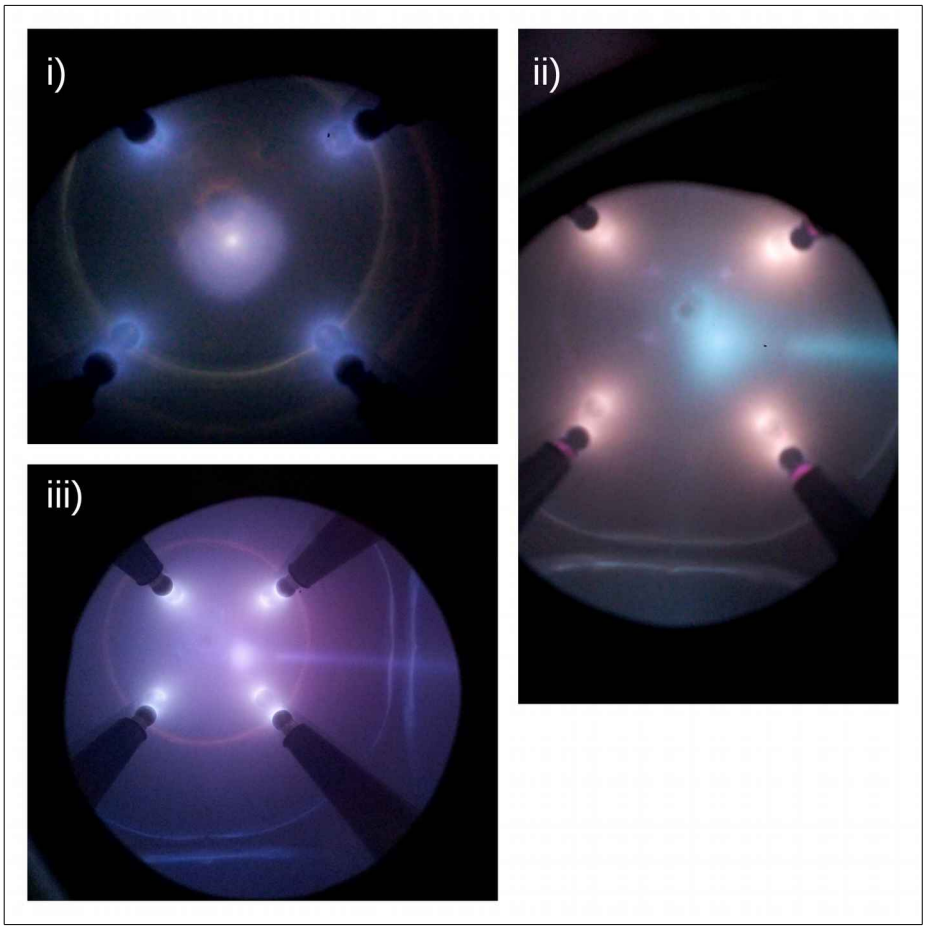

Fig. 167. Various space charge objects occurring in the 'spherical' electrode arrangement. i) unidentified object, occurring in argon between 12 mTorr and 15 mTorr; ii) pea-shooter type object in helium, at 47 mTorr; iii) pea-shooter type object occurring in argon between 12 mTorr and 15 mTorr

8.2.2 Planar abstraction

8.2.2.1 Apparatus

These electrodes were created to test the principle that a beam mode type plasma may be obtained in a planar geometry. They consist of three planar grids which are constructed using square mesh of around 0.5 cm pitch. These are held parallel to each other, with an approximately even spacing of between 2 cm and 3 cm between them, and so that the apertures of all three grids are aligned with each other.

The centrally-positioned grid is the cathode, and the outer two grids are grounded anode elements (Fig. 168). The arrangement may be thought of as being essentially similar to the cylindrical arrangement described in previous chapters, except in being abstracted to a planar geometry, and also having the cathode interior space removed.

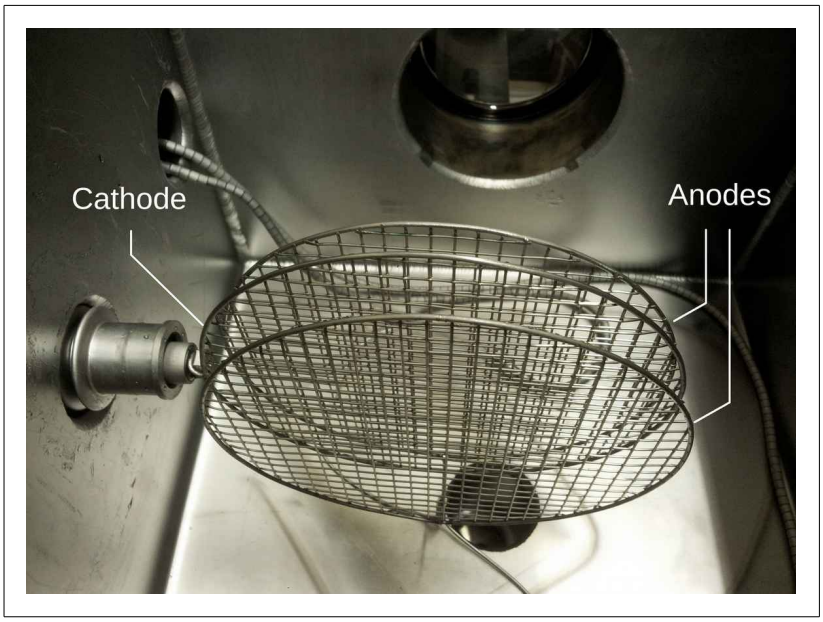

Fig. 168. Abstraction of electrode arrangement using three planar grids, with a central cathode flanked by two grounded anode grids.

8.2.2.2 Results

Time constraints only allowed for brief testing of this arrangement. This was performed in helium, at a pressure of 40 mTorr. A photograph of the plasma obtained is shown in Fig. 169, at conditions of of around 4 kV cathode voltage and 8 mA cathode current.

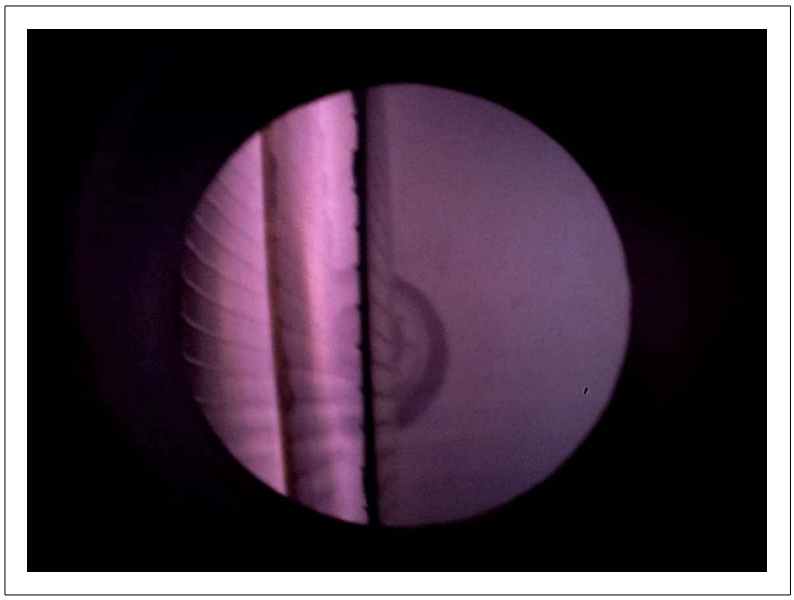

Fig. 169. Photograph showing plasma obtained using planar electrode arrangement in helium, at a pressure of 40 mTorr. The cathode voltage was 4 kV and the cathode current was 8 mA.

Relatively strong emission is observed in the space between the grids, taking the form of beam-lets that are spatially associated with the apertures, passing through these normal to the plane of the electrodes. More diffuse emission is observed from locations external to the anode grids, the distribution of which is also observed to consist of small beam-like elements associated with the apertures. This pattern is noted to be significantly similar to that observed for the cylindrical grids, as described in Chapter 5.

8.3 Discussion

The results of these tests constitute findings that are differently instructive in each case. These are outlined below, considering each arrangement separately.

'Spherical' arrangement

From the analysis of visible emission from plasmas in the cylindrical electrode arrangement, as described in Chapter 3, the colour of emission evident in the helium plasma pictured in Fig. 166 shows it to be produced by the effect of energetic ionic and neutral species. The spatial distribution of this emission indicates an element of beam formation to be occurring, showing an association with the focussing potential surfaces created by the electrode configuration in the vacuum potential distributions shown in Figs. 164 and 165..

This is considered to demonstrate that the principle by which the ion beams are formed, using focussing surfaces created by an external anode, may be extended to significantly different geometries. This implementation may be considered quite extreme, in that relatively few beams are created by surfaces of large physical area. The principle might be applied in a wide range of geometries and degrees of symmetry, which could result in somewhat different operating characteristics.

Planar arrangement

The colour of the emission from the helium plasma shown occurring in this electrode arrangement (Fig. 169) shows this to be produced by the activity of energetic ions and neutrals also. The characteristics of bright emission occurring in the region of strong electric field and diffuse emission extending far beyond the location of the anode are observed similarly to those of the beam mode described in Chapter 5. These are expected to also correspond to the activity of ions in the region between the electrodes, focussed into beams by the anode apertures and accelerated in the strong electric field. These will produce fast neutrals in charge exchange and momentum transfer collisions during this transport, which then propagate through the electrode apertures and beyond, causing emission and ionisation in the surrounding area.

Both of these approaches are found to be successful in creating plasmas sustained by the activity of energetic ions and neutrals, showing the anode-focussing principle to be a potentially very useful means of engineering different types of plasma in this high *E/N* regime.

Note on possible applications

The implementation demonstrated using the spherically-abstracted arrangement might be useful for any application requiring a degree of convergence, or conditions featuring a degree of spherical symmetry. The access afforded to individual cathode elements might be expected to also allow for additional cooling, should operation at conditions of high current be favourable. Such a regime of operation could only be achieved in devices with wire grids if operated in a pulsed manner, since the cylindrical cathode grid is observed to become incandescent after a minute or two during high current operation, as described in the previous chapter.

IEC technology is currently used for some non-power fusion applications, such as neutron generation [111]. The possible applications become progressively greater with increased yields (Fig. 170), and so the accessing of a higher-power regime of operation might be favourable for this. If a device can provide a sufficient flux of MeV protons by fusing D-^{3}He to be an effective on-site source for production of medical isotopes, then this would open up a new range of applications. Some details of this are given in [19], noting the requirement for relatively high yields.

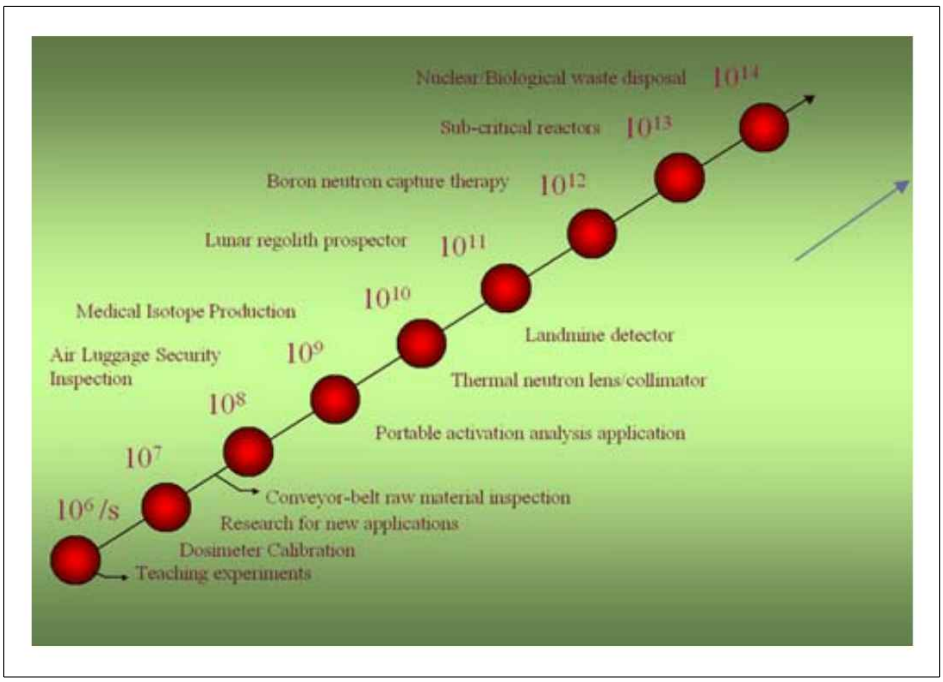

Fig. 170. Non-power fusion applications for neutrons; values indicate flux in n.s^{-1}. Reproduced from [28]

The planar arrangement features well-defined regions in the inter-electrode space in which conditions of *E/N* are relatively high and ions are energetic. This causes an outwardly-directed flux of fast neutrals having energies that correspond to those of the ions in the inter-electrode space. These are observed to be formed into beams, but the degree of spread and small size of the apertures employed in this implementation are expected to cause this to become more isotropically distributed with increasing

distance from the electrodes. This electrode assembly therefore operates as a bi-directional neutral beam source. The implementation tested was a simple, planar form; the principle however could be applied to curved surfaces also, to engineer fluxes of neutrals having different directional components.

The lack of any interior cathode space means that little of the 'electrostatically-trapped electron' effect described in Chapter 4 will be expected to occur in this arrangement. This makes it unlikely to be subject to instabilities caused by electrons confined within the cathode, such as the CC mode, or the ADLOs and fireballs. This might make it favourable for operation as a plasma source, in terms of both stability of operation and consistency of plasma properties.

8.4 Conclusions

Experimental observations of a cylindrical TCD reported in Chapter 3 showed that a plasma having ions and neutrals as principally reactive species may be created using an electrode arrangement featuring a grounded anode grid surrounding the powered cathode grid. The grid construction of the anode was also found to create focussing potential surfaces, which result in the effective formation of inwardly-directed ion beams. This understanding of the mechanics of beam formation has enabled the abstraction of these electrodes into two substantially different forms, which are found to also produce beams in a manner broadly similar to those seen in the cylindrical set-up.

These forms consist of a planar arrangement of grid electrodes, which features no interior cathode space, and an abstraction of the cathode form into individually-supported segments instead of a grid construction.

The planar implementation may be favourable for the field of applications that this research is directed towards, since this would appear to offer a stable configuration for the production of plasmas having energetic populations of ions and neutrals. Much more work is required however to characterise the plasma produced in this arrangement at a wider range of conditions to show this to be definitively the case. The apparatus would also appear to be potentially suited to applications requiring a controllable and directional flux of neutrals.

Possible applications envisaged for the segmented cathode abstraction might be those requiring high-power operation, because of the enhanced facility for cooling that this configuration may offer. These could include non-power fusion applications, should the design be found to be capable of exceeding yields achieved by conventional IEC-based sources. Further work is required to ascertain the degree of any utility in this approach.

Chapter 9
Conclusions

A Transparent Cathode Discharge has been studied in a device consisting of a central, powered cathode grid, surrounded by a grounded anode grid. Plasmas have been obtained in several different species of gas, and across a range of operating pressures. In all cases, the discharge has been self-sustained, relying upon the DC potential applied to the electrodes and collisional processes occurring in the volume to maintain populations of charged and reactive particles.

The aim of the research was to identify operating regimes in which ions and neutrals are reactive species, since ion-driven reactions may be expected to create a different plasma chemistry to conventional electron-driven sources, and thereby open up a different range of process plasma source applications.

The visual appearance of the optical emission from the discharge, and the ranges of voltage required to produce and sustain a discharge across the range of pressure conditions have been observed to show a distinctive mode structure. At pressures below a Torr, this consists of two modes, which are characterised as a 'cathode-confined' discharge occurring at higher pressures within this range, and a 'beam' mode obtained at lower pressures, of units to tens mTorr. These names reflect the different visual appearance of the plasma, since this appears to be largely contained within the interior of the cathode at higher pressures, and evolves into a series of radial beams at low pressure. The former of these modes operates at quite moderate voltages, of the order of hundreds of volts, whereas the beam mode may operate at tens of kilovolts at conditions of sufficiently low pressure.

The conditions of *E/N* at which the beam mode is evident were found to be consistent with those at which heavy particles may be expected to become reactive. Analysis of optical emission from the two modes showed excitation processes occurring in the higher-pressure, cathode-confined mode to be caused by electrons, and those occurring in the beam mode to be caused by ions and neutrals. The dependences on conditions for these processes are similar to others that will be instrumental in the sustaining of the discharge, such as ionisation, and so these findings indicate the two modes to represent discharges in which the significant processes are caused principally by electrons and ionic and neutral species respectively.

This is a very useful distinction to be able to make for this research, since it constitutes the identification of both the operating ranges of interest, and also the observable characteristics of the corresponding plasmas. Much previous IEC work has concentrated upon operation at lower pressures still, with the definition of the upper limit to this range being of little interest. No study has previously documented the nature of the transition from electron to ion/neutral processes in any detail. This work shows where this transition occurs in the overall mode structure, and how it is evident in discharge parameters.

The cathode-confined mode is therefore found to be an electron-driven mode. Consideration of the nature of the discharge in this mode, i.e. its confinement within a semi-transparent cathode, and its operation at the upper range of *E/N* conditions for electron-driven activity in this set-up, suggested that it may bear some resemblance to hollow-cathode type discharges, in terms of being assisted by a degree of electron confinement occurring within the cathode. Investigation of the dependence shown by this mode upon the geometrical form of the cathode has found it to be quite sensitive to the degree of enclosure surrounding the internal cathode space. By experimentally increasing the extent of this enclosure, it was shown that this results in the increased occurrence of the cathode-confined mode at conditions of lower pressure.

This is an important finding for the considerations of designing apparatus for the creation of ion- and neutral-driven plasmas, since confined electrons are an efficient means for causing ionisation, and a sufficient number of these will tend to dominate the plasma properties.

Investigation of the beam mode plasma has found the formation of the characteristic radial beams to be associated with an electrostatic focussing effect, which is caused by the apertures of the grounded anode grid. This is a significant finding, since it distinguishes this mode of operation from others described elsewhere in the IEC literature, and also offers insight into the functioning of the discharge. This is shown to involve the transport of ions across the inter-electrode space in the radial beams, causing them to attain reactive energies in the strong electric field found in this region. Collisions with background gas particles convey a significant amount of the ions' energy to these neutral particles, which then constitute a population of fast neutrals that are able to propagate irrespective of electric fields in the chamber. Being formed in beams that are directed towards the centre of the device, many of these pass through the apertures and continue to the opposite wall of the chamber, causing excitation and ionisation, and so producing the ion population that will be focussed into a counter-streaming beam. Observation of the Doppler-shifted hydrogen Balmer-alpha spectral line has provided direct evidence for fast excited hydrogen being present in discharges, although the mechanisms by which this comes about are not entirely clear.

Quasi-spherical space charge objects appearing in the cathode interior during beam mode discharges have been investigated and found to show considerable similarities to objects described elsewhere as occurring attached to a positive electrode immersed in a plasma. In the published literature these are attributed to a self-organising behaviour shown by electrons in certain conditions, and are indicated to consist of a central region of positive space charge surrounded by a spherical double layer, with a potential across this is a little in excess of the ionisation potential of the gas. Electrons confined around the positive charge are accelerated across the double layer, causing excitation and ionisation to occur in well-defined spatial locations, and so contribute to the potential difference. Analysis of the size of the observed objects, and the rise time of fluctuations that they cause in measured electron currents, finds both of these properties to be consistent with this identification. This is significant in being the first time that such objects occurring within an IEC discharge have been identified as such. This is interesting in itself, and it is also significant for advancing

the understanding of the different types of plasma that may occur within transparent cathodes.

Larger space charge objects occurring within the cathode have also been described, in some detail. These are found to also be principally electron-driven objects, and are observed to have a considerable effect upon the operating characteristics of the discharge. In desiring the creation of a stable ion- and neutral-driven plasma, these therefore constitute an instability in the same way that the cathode-confined mode does. Observed characteristics of these objects indicate them to be complex space charge configurations, although the details of their internal structure remains unclear. There are indications that some of these objects might represent double well-type structures, in which case they may be of interest for fusion applications. They occur at conditions of greater levels of cathode current than most previous experiments have been conducted at, and so are representative of behaviour occurring in a less well-known regime of operation.

The insights into the physical dependences shown by processes causing the formation of the radial ion beams, and also the electron-driven plasmas occurring within the cathode, enable the design of different configurations of electrodes that may be suitable for different particular purposes. Two such configurations have been conceived of, and limited testing has shown the principles behind them to operate as expected. One of these is designed to allow for the creation of more stable ion- and neutral-driven plasmas, that are less subject to electron-driven instabilities. This is accomplished by the removal of the element of enclosure found in cylindrical, or indeed spherical, cathodes, which comes at the expense of the degree of radial convergence that makes these geometries attractive for the creation of convergent flows. The other approach exploits the mechanism found to cause the formation of the ion beams, which has been found to operate largely independently of the form of the cathode. In this case, the grid cathode is replaced by an array of cathode elements, which are considered likely to afford the possibility of operation in a regime of significantly higher current, due to the enhanced access for cooling requirements. This arrangement is found to also successfully create an ion- and neutral-driven plasma, but retains the degree of convergence, and also has been shown to still enable the formation of space charge objects within the central space. Much further work is required to assess the utility of these arrangements.

Appendix 1
Work intended for publication

Various aspects of the work contained in this thesis are considered to be of sufficient interest for publication as journal articles, and it is intended to publish the material over the course of the next months. The exact content and ordering of these publications remains to be decided, but the areas of interest are as follow:

I. The analysis of emission structure made in Chapter 3, that leads to the identification of the regime of operation in which ions and neutrals are principally-reactive species. This material is of primary importance for the research project, and is anticipated to make up the first publication from this work.

II. The material from Chapter 4 in which the dependences upon cathode geometry are determined, that affect the degree to which the hollow cathode effect may function. This work has a clear relevance for the engineering of a stable ion- and neutral-reactive plasma source, and contributes to the overall understanding of the types of collisional IEC plasmas that may occur within transparent cathodes.

III. The demonstration of the significance of fast neutrals within the beam mode discharge, and the description of the ion beam formation mechanism, that are contained within Chapter 5. These areas inform the understanding of principal properties of the plasma of interest for this project, and demonstrate the physical dependences upon device configuration that allow the design to be modified in subsequent work.

IV. The identification of anode double layer type objects occurring within the cathode interior, that was made in Chapter 6. Since this constitutes the first time that such an identification has been made, it further contributes to the understanding of the different processes and types of plasma that may occur within IEC devices.

V. The material concerning the fireball objects in Chapter 7 is similarly instrumental for the understanding of the range of IEC plasmas that may occur, and is expected to be of sufficient interest for publication. The manner in which this may be arranged for presentation is yet to be determined.

VI. Finally, the alternative electrode arrangements may also be of interest for publication, since these demonstrate the practical application of some of the principal areas of understanding gained in Chapters 4 and 5.

Appendix 2
Notes on the analysis of photographs of optical emission.

These notes are organised in sections as follows:

I. Interpretation of 2D images

II. Interpretation of images recorded using a smartphone camera

III. Evaluation of the relation between emission and charge generation

Several different cameras were described in the chapter on experimental set-up, and the use of each of these was noted to be associated with various advantages and disadvantages.

Various considerations are made in the interpretation of images recorded of distributions of optical emission; some of these are intrinsic to the two-dimensional nature of an image, and some are additionally important for images recorded using certain types of camera.

Issues are initially considered which apply to all images recorded irrespective of the camera system used. Following this, the additional considerations that apply to the evaluation of photographs taken with the DSLR and smartphone cameras are outlined. These apply in general to both of these systems, and since the smartphone camera was used most, reference will be made specifically to this system. Finally, it is noted that much of the analysis of distributions of emission is directed towards the evaluation of spatial distributions of charge generation, and so considerations applying to the making of this analogy are also included in the last section of these notes.

A similar format is followed in each of these sections, in which the considerations are initially outlined, before strategies described that either mitigate these or qualify the interpretations made accordingly.

I. Interpretation of 2D images

In general, a photographic image represents the pattern, or distribution, of light intensity incident upon a flat surface held at a given location. The intensity of signal at a given point in the image may therefore be thought of as the integrated signal originating from all sources within a cone of acceptance projected outwards from the corresponding point on the sensing surface.

The recorded intensity is therefore representative of the three-dimensional spatial distribution of the source, that has been flattened into a two-dimensional representation according to the geometry of the optical pathway between the source and the sensor.

Depending upon the nature of the information to be extracted from the image, the effects of this flattening may be variously problematic. If the objective of the analysis is to ascertain the spatial distribution of signal independent of the integrated depth, then information about the three-dimensional distribution must be de-convolved from an image. This may be achieved using certain mathematical techniques, which generally require an element of symmetry. Alternatively, if the objective is to further integrate the recorded signal over specific regions of the depicted volume, then the relation between these and areas of the flattened image must be assessed.

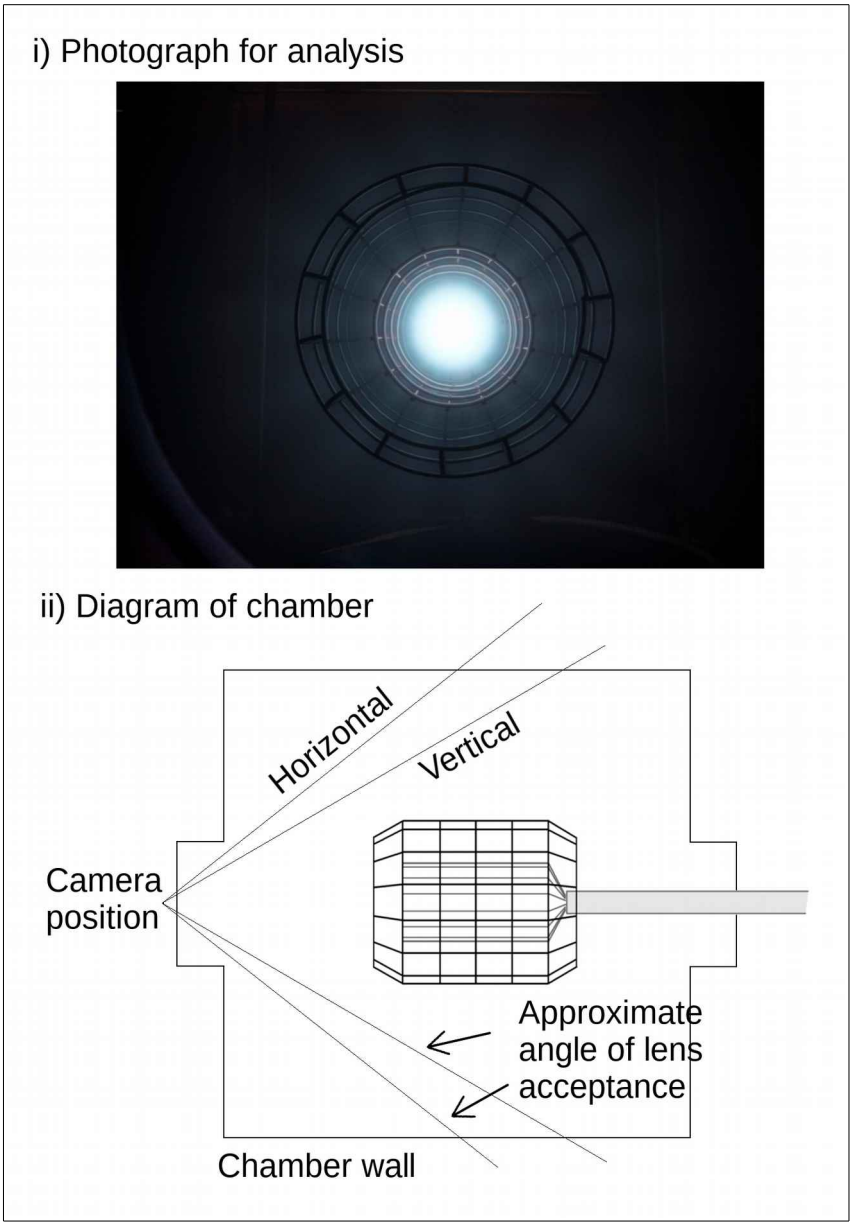

Fig. 171. Geometry associated with the capturing of an image; i) shows the image, and ii) the geometry of the camera, discharge and chamber.

The analyses of photographic images performed in this study fall into this latter category, and so consideration is made of the effects of foreshortening and perspective. These may be appreciated by sketching the geometry of the angles of acceptance involved in capturing the image, as illustrated for an example image of a CC mode discharge in Fig. 171.

As may be seen, the camera has a relatively wide-angle lens. This enables a significant portion of the chamber interior to be within the field of view, with the trade-off being a considerable degree of foreshortening due to perspective.

This simple approach provides an assessment of the extent of the chamber interior that falls within the field of view, and the degree of foreshortening associated with the flattening of the apparent distribution into that of the image.

II. Interpretation of images recorded using a smartphone camera

The ease of use of the phone camera makes it feasible to record many more images than might be recorded using more sophisticated equipment such as the ICCD camera, or even the DSLR. To be able to quantify properties of the images recorded, it is necessary to consider issues additional to those outlined above. These considerations fall into the following categories:

- Spectral sensitivity
- Exposure control
- Extraction of data
- 'Dark' signal
- On-board software manipulation

The issues relating to each of these areas are outlined below.

Spectral sensitivity

The sensor-filter-software system that makes up a phone camera is designed to approximate the response of the human eye, in its response to levels of brightness and colour. The RGB filters used to enable this type of colour discrimination may therefore be expected to cause some deviation from a flat spectral response. Since the light emitted from the discharge has a highly discrete wavelength composition, any significant spatial variation in spectral composition may therefore result in a spatially disproportionate signal.

The camera is a Samsung GT-19100 smartphone camera, with a sensor response likely to resemble the example illustrated in Fig. 172, since this is taken from a Samsung publication dating from the time at which the camera in question was a flagship product.

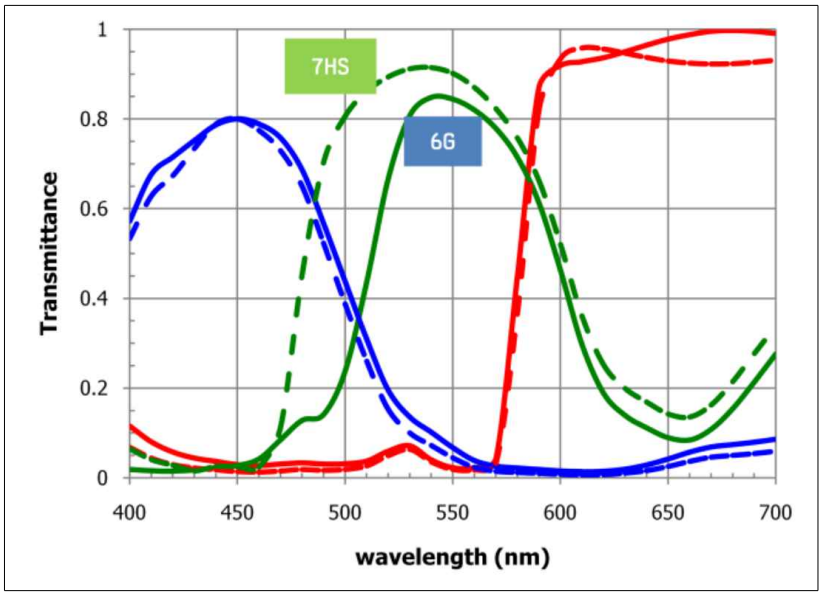

Fig. 172. Example of RGB sensor element responses, reproduced from a Samsung publication [112]

A noticeably variable colour response has been found to result when photographing emission from discharges having a significant component of the 501.6 nm helium line. This is consistent with a sensor response similar to the solid lines labelled as 6G in Fig. 172, since this wavelength can be seen to fall between the green and blue sensitivities.

The camera does display sensitivity in the NIR, which may make it superior to the DSLR in this respect, by increasing the number of spectral lines that may contribute to the recorded signal. The lack of any detailed open-access information on the camera means that further assessment of errors in this respect is not possible.

From these considerations, it may be concluded that caution must be exercised in making direct comparison between images that may contain a significantly different spectral composition. For the same reasons, care must also be taken in the comparing of regions within a distribution that have a spatially-dependent spectral composition.

Exposure control

In contrast to a DSLR, or indeed the Andor camera, the smartphone camera allows for limited control over exposure settings. Unless it is desired to specifically record images at certain settings however, this is not too much of a problem, since the exposure settings for an image are recorded as part of the file.

Extraction of data

The software that is used to control the Andor camera allows for the export of image data in various formats, and it is easy to get access to the values recorded for individual pixels. This is not the case for the DSLR or smartphone cameras, which produce image files in a jpeg format; this makes the analysis of images recorded by these means less straightforward.

A solution to this issue is provided by a program called Processing. This is a versatile, open-source coding language oriented towards the creation of visual and interactive media. Its facility for image processing makes it an ideal tool for the analysis of emission distributions in photographs.

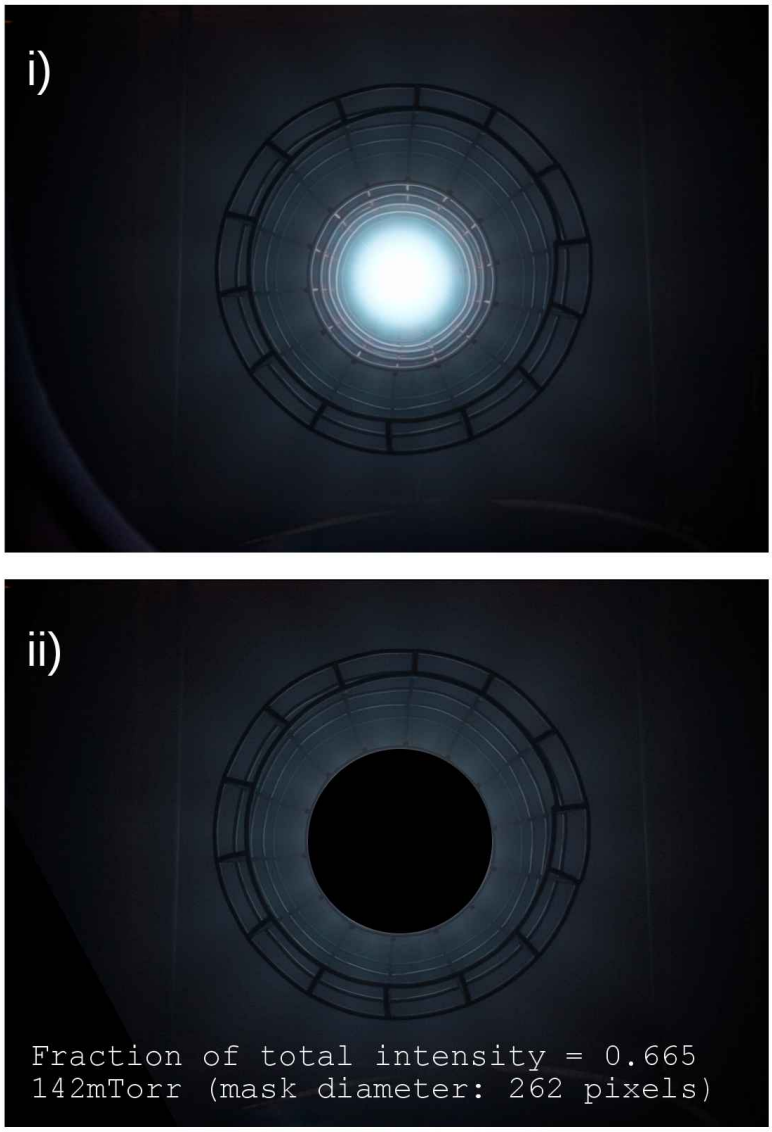

Fig. 173. Example of the output of the Processing sketch for integrating emission levels, as described in the text

In order to quantify the signal recorded in particular regions of a photograph, a simple program was created which applies the following steps:

- Image loaded; pixel values read and loaded into array
- Any areas of extraneous signal removed (e.g. obvious reflections from chamber wall)

- RGB values for each pixel read out, averaged and summed for Total Signal value
- A mask applied to area to be evaluated; these pixel values set to zero
- RGB values read, averaged and summed again for Reduced Signal value
- Reduced Signal/Total Signal calculated to evaluate contribution from unmasked area

This process provides an idea of emission levels, at wavelengths the camera is sensitive to, as integrated from the point of view of the lens. An example is shown in Fig. 173, using the same photograph as in Fig. 171.

Influence of 'dark' signal

Any signal from an electrical sensor is subject to thermal noise, and more sophisticated scientific cameras have the facility for cooling the sensor to reduce this. This is not feasible with the smartphone camera, and so the possible influence of a uniform offset to the signal was explored as follows.

The same photograph from Figs. 170 and 172 is used as a test image. The program described above was applied, using circular masks of two different diameters, with results as shown in Fig. 174 i) and ii). The smaller mask, shown in Fig. 174 i), is applied in order to output the integrated emission level from all regions outside the cathode, which was 66.5 %. The larger mask in Fig. 174 ii) was applied so as to remove most of the signal from the image, resulting in some 10 % remaining. A further step was then added into the program, which subtracted a constant value from each averaged RGB pixel value. Using the larger mask, this 'background correction' value was then varied until almost all of the signal was removed from the remaining area. The output from this is shown in Fig. 174 iv). Using the same correction factor, the program was then run again with the smaller mask, resulting in the output shown in Fig. 174 iii).

The effect of applying a correction sufficient to reduce the 10 % signal at large radius to 0.5 % is seen to affect the result for all signal outside the cathode by only 3 %. Furthermore, this is noted to be an over-correction, since the photograph shows diffuse emission extending beyond the radius of the large mask, which is not thermal noise.

It therefore seems that the background sensor noise makes only a small contribution to the signal in this photograph, which affects the result of this analysis by only a couple of percent at most, and possibly much less. This is partially because the discharge is quite bright, making the signal-to-noise ratio high. This is true of all of the images that will be analysed in this way, and so it is concluded that the sensor background noise will not be the most significant source of error in this kind of analysis.

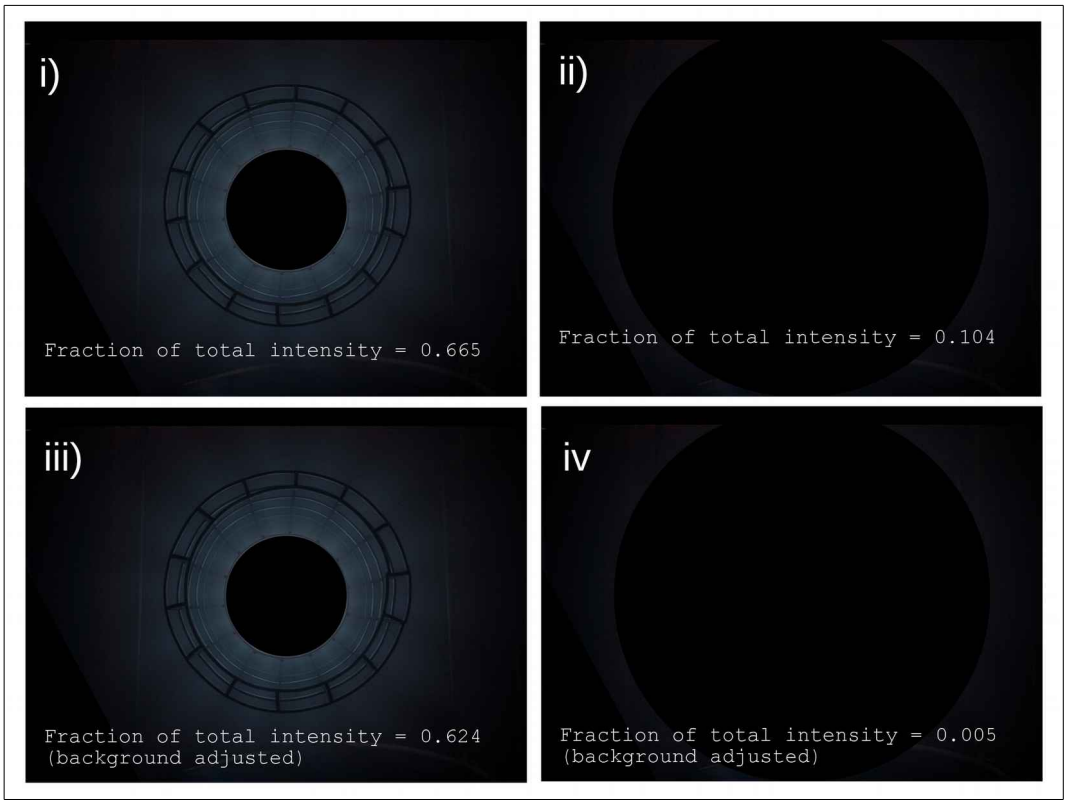

Fig. 174. Outputs from the signal integration sketch, showing the effects of applying a background correction. i) and ii) uncorrected; iii) and iv) corrected

On-board software manipulation

Finally, it is noted that the images obtained using either the DSLR or the smartphone cameras are processed before being written to accessible files. This processing affects both the values of brightness and colour, involving the interpolation of pixel values to render a smooth image.

There is little that may be done to mitigate or quantify the effects of this. It is however noted that the process is designed to produce images that appear to be faithful reproductions of the perception of the eye; meaning that the reproduction of values of brightness may be expected to remain relatively consistent, at least within an image. Colour management, on the other hand, has been observed to be extremely variable and no analysis is performed on the basis of colour.

III. Evaluation of the relation between emission and charge generation (ionisation)

For the purpose of this study, it is useful to be able to assess the distribution of charge generation occurring within the chamber volume. Much of this occurs in collisional processes that result in ionisation of the background gas, and in this respect there are parallels with processes causing excitation of this gas. This excitation in turn gives

rise to visible emission, and so it is valuable to establish the degree to which the spatial distribution of this observed quantity may be considered representative of the distribution of ionisation.

This involves consideration of the relations between both observed emission and processes of excitation, and also between processes of excitation and ionisation, as follows:

i. Relation between observed emission and processes of excitation

It is first noted that the lifetimes of most excited states are very short compared to particle velocities [113] and so emission generally occurs close to the location of excitation.

The largest cross sections for excitation are generally those to the n=2 levels [114], [87], [88], which result in emission at UV wavelengths not visible to the eye or camera, and which do not escape from the chamber.

Emission at visible wavelengths occurs following processes of direct excitation to states with n>2, with a spectral distribution determined by transition probabilities to lower-level states. At conditions of sufficiently-great gas density this emission is significantly augmented by the effects of radiation trapping, which acts to channel some of the UV radiation that also may result from relaxation from these excited states into radiation at visible wavelengths [68]. This might be expected to simply cause a general amplification of visible emission, but effects of excitation transfer at high-n levels may also cause the observed spectral distribution to vary [74].

When all of this UV emission is channelled into visible emission, the conditions are referred to as being 'optically thick'. This effect has implications for both the spectral content of emission and also the spatial distribution of emission; these are considered as follows.

Spatial distribution

To consider the effect of this upon the spatial distribution of emission; should the process operate over distances of the order of the dimensions of the volume, then this might be expected to result in visible emission being spread across such a distance, with the apparent distribution of emission in such a case reflecting this process rather than that of the initiating collisional excitation.

For the purpose of this discussion it is simply noted that distributions of emission observed at all operating conditions are significantly anisotropic. This indicates that the effects of optical opacity operate over distances considerably smaller than the chamber dimension, and so are not expected to change the spatial distribution of emission greatly from that of excitation. The spatial distributions of emission are therefore considered to be broadly representative of those of the processes of collisional excitation.

Spectral distribution

From the above considerations, the effects of optical opacity are expected to be significant at the conditions relevant to this study. These will cause the relative spectral distribution to vary somewhat with pressure, and so this may be a consideration when comparing distributions of emission corresponding to different pressures. It is observed however that the spectral content of emission varies at different conditions for other reasons also, and so this effect constitutes just one of various possible factors influencing this.

The effect of a changing spectral distribution will depend on how this relates to the spectral sensitivity of the detection equipment, as observed above. This will be determined by both the spectral profile of the detector response, and its bandwidth. Observed levels of emission in the visible range will be expected to remain broadly proportional to total levels of excitation to levels with $n>2$, since much of this excitation energy is converted to visible photons. The relation will become generally more consistent with increasing bandwidth, since this will act to average out dependences upon local conditions shown by individual spectral lines.

ii. Relation between processes of excitation and those of ionisation

As noted above, levels of visible emission will be expected to correspond broadly to those of excitation to levels with $n>2$, and yet the majority of excitation is to $n=2$. Whilst some variation is evident between cross sections for excitation to different levels, general similarities are observed in the energy ranges for these, and in conditions at which processes of excitation populate levels having $n=2$, levels with $n>2$ will also be excited.

The processes of collisional excitation and ionisation are related, since both of these result when a bound electron is given energy following a collision. Excitation may occur however at a smaller threshold energy than that required for ionisation and so, for processes caused by a flux of particles having energies sufficient to cause excitation but not ionisation, evidence for excitation will clearly not represent an accompanying degree of ionisation.

For particle energies above the threshold regime in which this will be significant, consideration of the proportionality between processes of excitation and ionisation requires an assessment of the relevant cross sections for these processes. For electron energies in excess of threshold values, the cross sections for the two processes are found to be quite proportional, and so should the electron population be sufficiently energetic, the resulting emission will be a good guide to charge generation. For ions and fast neutrals a degree of variation in this respect is found, and for these cases an assessment is made at the time of the emission analysis.

References

[1] BROWN, S.C., Basic data of plasma physics, 1966, 1967. *M.I.T. Press, Cambridge, MA.*

[2] LANGMUIR, I., 1929. The interaction of electron and positive ion space charges in cathode sheaths. *Physical Review,* **33**(6), p.954

[3] ELMORE, W.C., TUCK, J.L. and WATSON, K.M., 1959. On the Inertial Electrostatic Confinement of a Plasma. *Physics of Fluids (1958-1988),* **2**(3), pp. 239-246.

[4] LAVRENT'EV, O., OVCHARENKO, L., SAFRONOV, B., SIDORKIN, V. and NEMASHKALO, B., 1963. Jenergiya i plotnost'ionov v jelektromagnitnoj lovushke. *Ukrain Fiz,* **8**, pp. 440-445.

[5] FARNSWORTH, P.T., "Electric Discharge Device for Producing Interactions between Nuclei," U.S. Patent 3258402, June 28, 1966.

[6] FARNSWORTH, P.T., "Method and Apparatus for Producing Nuclear-Fusion Reactions," U.S. Patent 3386883, June 4, 1968.

[7] HIRSCH, R.L., 1967. Inertial Electrostatic Confinement of Ionized Fusion Gases. *Journal of Applied Physics,* **38**(11), pp. 4522-4534.

[8] BUSSARD, R.W., 1991. Some physics considerations of magnetic inertial-electrostatic confinement. A new concept for spherical converging-flow fusion. *Fusion Technology,* **19**(2), pp. 273-293.

[9] PARK, J., NEBEL, R.A., STANGE, S. and MURALI, S.K., 2005. Experimental observation of a periodically oscillating plasma sphere in a gridded inertial electrostatic confinement device. *Physical Review Letters,* **95** (1), p. 015003.

[10] DOLAN, T., 1994. Magnetic electrostatic plasma confinement. *Plasma Physics and Controlled Fusion,* **36** (10), pp. 1539.

[11] MILEY, G.H. and SVED, J., 2000. The IEC star-mode fusion neutron source for NAA—status and next-step designs. *Applied Radiation and Isotopes,* **53**(4), pp. 779-783.

[12] MILEY, G.H., MOMOTA, H., WEBBER, J., YANG, Y., THOMAS, R., TAKEYAMA, Y. and WU, L., 2005. Thruster design for IEC-based spacecraft propulsion, *American Nuclear Society Embedded Topical Meeting - 2005 Space Nuclear Conference, June 5, 2005 - June 9,* 2005 2005, American Nuclear Society, pp. 775-780.

[13] BLACKHALL, L. and KHACHAN, J., 2007. A simple electric thruster based on ion charge exchange. *Journal of Physics D: Applied Physics,* **40** (8), pp. 2491.

[14] WEIDNER, J.W., KULCINSKI, G., SANTARIUS, J., ASHLEY, R., PIEFER, G., CIPITI, B., RADEL, R. and MURALI, S.K., 2003. Production of 13 N via Inertial Electrostatic Confinement Fusion. *Fusion science and technology,* **44**(2), pp. 539-543.

[15] RIDER, T.H., 1995. General critique of inertial-electrostatic confinement fusion systems. *Physics of Plasmas,* **2**(6), pp. 1853-1853.

[16] NEVINS, W.M., 1995. Can inertial electrostatic confinement work beyond the ion-ion collisional time scale? *Physics of Plasmas,* **2**(10), pp. 3804-3804.

[17] MCGUIRE, T. and SEDWICK, R., 2005. Improved confinement in inertial electrostatic confinement for fusion space power reactors. *Journal of Propulsion and Power,* **21**(4), pp. 697-706.

[18] EVSTATIEV, E., NEBEL, R., CHACÓN, L., PARK, J. and LAPENTA, G., 2007. Space charge neutralization in inertial electrostatic confinement plasmas. *Physics of Plasmas (1994-present),* **14**(4), pp. 042701.

[19] MILEY, G.H., JAVEDANI, J., YAMAMOTO, Y., NEBEL, R., NADLER, J., GU, Y., SATSANGI, A. and HECK, p., 1994. Inertial Electrostatic Confinement Neutron/Proton Source, *Dense Z-Pinches: 3rd International Conference* 1994, AIP Publishing, pp. 675-689.

[20] MEYER, R.M., PRELAS, M.A. and LOYALKA, S.K., 2008. Experimental observations of a spherical transparent cathode glow discharge. *IEEE Transactions on Plasma Science,* **36**(4), pp. 1881-1889.

[21] MILEY, G.H., GU, Y., DEMORA, J.M., STUBBERS, R.A., HOCHBERG, T.A., NADLER, J.H. and ANDERL, R.A., 1997. Discharge characteristics of the spherical inertial electrostatic confinement (IEC) device. *IEEE Transactions on Plasma Science,* **25**(4), pp. 733-739.

[22] MEYER, R.M., SMITH, Z.M., PRELAS, M.A. and LOYALKA, S.K., 2008. Ion flow convergence in spherical inertial electrostatic confinement devices. *Physics of Plasmas,* **15**(2), p. 022105.

[23] YOUSEFI, M., DAMIDEH, V. and GHOMI, H., 2011. Low-energy electron beam extraction from spherical discharge. *IEEE Transactions on Plasma Science,* **39**(11), pp. 2554-2555.

[24] GU, Y. and MILEY, G.H., 2000. Experimental study of potential structure in a spherical IEC fusion device. *IEEE Transactions on Plasma Science,* **28**(1), pp. 331-346.

[25] MEYER, R.M., LOYALKA, S.K. and PRELAS, M.A., 2007. Double potential well regimes in collisionless spherical discharges. *IEEE Transactions on Plasma Science,* **35**(2), pp. 354-360.

[26] HIRSCH, R.L. and MEEKS, G.A., “Apparatus for Generating Fusion Reactions,” U.S. Patent 3530497, September 22, 1970.

[27] THORSON, T.A., DURST, R.D., FONCK, R.J. and WAINWRIGHT, L.p., 1997. Convergence, electrostatic potential, and density measurements in a spherically convergent ion focus. *Physics of Plasmas (1994-present)*, **4**(1), pp. 4-15.

[28] MURALI, S.K., SANTARIUS, J.F. and KULCINSKI, G.L., 2010. Study of various modes of operation of an IEC device. *Journal of Fusion Energy,* **29**(2), pp. 141-145.

[29] MURALI, S.K., SANTARIUS, J.F. and KULCINSKI, G.L., 2011. Effects of the cathode grid wires on fusion proton measurements in inertial-electrostatic confinement devices. *IEEE Transactions on Plasma Science,* **39**(2), pp. 749-755.

[30] MEYER, R.M., LOYALKA, S.K. and PRELAS, M.A., 2005. Potential well structures in spherical inertial electrostatic confinement devices. *IEEE Transactions on Plasma Science,* 33(4), pp. 1377-1394.

[31] MILEY, G.H. and MURALI, S.K., Inertial Electrostatic Confinement (IEC) Fusion, 2014. *Springer, New York, NY*

[32] SHRIER, O., KHACHAN, J., BOSI, S., FITZGERALD, M. and EVANS, N., 2006. Diverging ion motion in an inertial electrostatic confinement discharge. *Physics of Plasmas (1994-present),* **13** (1), pp. 012703.

[33] TANIUCHI, Y., MATSUMURA, Y., TAIRA, K., UTSUMI, M., CHIBA, M., SHIRAKAWA, T. and FUJII, M., 2010. Effects of Grid Cathode Structure on a Low-Input-Power Inertial Electrostatic Confinement Fusion Device. *Journal of Nuclear Science and Technology,* **47**(7), pp. 626-633.

[34] OHNISHI, M., OSAWA, H., TANAKA, R. and WAKIZAKA, N., 2005. Shape of electrodes for high performance of inertial electrostatic confinement fusion. *Journal of Nuclear Science and Technology,* **42**(4), pp. 398-405.

[35] KURT, E., 2011. A stationary multi-component cathode modeling and ion trajectories for an inertial electrostatic confinement fusion device. *International Journal of Energy Research,* **35**(2), pp. 89-95.

[36] KURT, E. and ARSLAN, S., 2012. An inertial electrostatic confinement (IEC) device modeling and the effects of different cathode structures to the fields. *Energy Conversion and Management,* **63**, pp. 55-62.

[37] DOBSON, C.C. and HRBUD, I., 2004. Electron density and two-channel neutron emission measurements in steady-state spherical inertial-electrostatically confined plasmas, with review of the one-dimensional kinetic model. *Journal of Applied Physics,* **96**(1), pp. 94-108.

[38] MURALI, S.K., SANTARIUS, J.F. and KULCINSKI, G.L., 2010. Consolidated electron emission effects in an IEC device. *Plasma Sources Science and Technology,* **19**(4), pp. 045029.

[39] EMMERT, G.A. and SANTARIUS, J.F., 2010. Atomic and molecular effects on spherically convergent ion flow. I. Single atomic species. *Physics of Plasmas,* **17** (1), p. 013502.

[40] EBRAHIMI, E.H., AMROLLAHI, R., SADIGHZADEH, A., TORABI, M., SEDAGHAT, M., SABRI, R., POURSHAHAB, B. and DAMIDEH, V., 2013. The influence of cathode voltage and discharge current on neutron production rate of inertial electrostatic confinement fusion (IR-IECF). *Journal of Fusion Energy,* **32**(1), pp. 62-65.

[41] THORSON, T., DURST, R., FONCK, R. and SONTAG, A., 1998. Fusion reactivity characterization of a spherically convergent ion focus. *Nuclear Fusion,* **38**(4), pp. 495.

[42] MURALI, S.K., SANTARIUS, J.F. and KULCINSKI, G.L., 2010. Effects of displaced grids on the fusion reactivity of an inertial electrostatic confinement device. *Journal of Fusion Energy,* **29**(3), pp. 256-260.

[43] OHNISHI, M., HOSHINO, C., MASUDA, K., YAMAMOTO, Y., TOKU, H. and YOSHIKAWA, K., 1999. Electron streaming from central core region in inertial-electrostatic confinement fusion. In *Fusion Engineering, 1999. 18th Symposium on* (pp. 213-216). IEEE.

[44] BORIS, D. and EMMERT, G., 2008. Composition of the source region plasma in inertial electrostatic confinement devices. *Physics of Plasmas (1994-present),* **15**(8), pp. 083502.

[45] EMMERT, G.A. and SANTARIUS, J.F., 2010. Atomic and molecular effects on spherically convergent ion flow. II. Multiple molecular species. *Physics of Plasmas,* **17**(1), p. 013503.

[46] BORIS, D.R., SANTARIUS, J.F. and KULCINSKI, G.L., 2009. Negative ions in inertial electrostatic confinement devices, *2009 IEEE International Conference on Plasma Science - Abstracts, ICOPS 2009, June 1, 2009 - June 5*, 2009 2009, Institute of Electrical and Electronics Engineers Inc

[47] BORIS, D., KULCINSKI, G., SANTARIUS, J., DONOVAN, D. and PIEFER, G., 2010. Measuring D (d, p) T fusion reactant energy spectra with Doppler shifted fusion products. *Journal of Applied Physics,* **107**(12), pp. 123305.

[48] MURALI, S.K., SANTARIUS, J.F. and KULCINSKI, G.L., 2009. Ion flux mapping in an inertial-electrostatic confinement device using a chordwire diagnostic. *Physics of Plasmas,* **16**(10), p. 103301.

[49] KHACHAN, J. and SAMARIAN, A., 2007. Dust diagnostics on an inertial electrostatic confinement discharge. *Physics Letters A,* **363**(4), pp. 297-301.

[50] OHNISHI, M., SATO, K., YAMAMOTO, Y. and YOSHIKAWA, K., 1997. Correlation between potential well structure and neutron production in inertial electrostatic confinement fusion. *Nuclear Fusion,* **37**(5), pp. 611.

[51] GHASEMI, M., HABIBI, M. and AMROLLAHI, R., 2013. Prediction of potential well structure formed in spherical inertial electrostatic confinement fusion devices with various parameters. *Journal of Plasma Physics,* **79**(03), pp. 295-303.

[52] TZONEV, I.V., DEMORA, J.M. and MILEY, G.H., 1995. Effect of large ion angular momentum spread and high current on inertial electrostatic confinement potential structures, Fusion Engineering, 1995. SOFE'95. Seeking a New Energy Era., 16th IEEE/NPSS Symposium 1995, IEEE, pp. 1476-1481.

[53] MOMOTA, H. and MILEY, G.H., 2001. Virtual cathode in a stationary spherical inertial electrostatic confinement. *Fusion science and technology,* **40**(1), pp. 56-65.

[54] HOCKNEY, R., 1968. Formation and stability of virtual electrodes in a cylinder. *Journal of Applied Physics,* **39**(9), pp. 4166-4170.

[55] SWANSON, D., CHERRINGTON, B.E. and VERDEYEN, J.T., 1973. Potential well structure in an inertial electrostatic plasma confinement device. *The Physics of Fluids,* **16**(11), pp. 1939-1945.

[56] MATSUURA, H., TAKAKI, T., FUNAKOSHI, K., NAKAO, Y. and KUDO, K., 2000. Ion distribution function and radial profile of neutron production rate in spherical inertial electrostatic confinement plasmas. *Nuclear Fusion,* **40**(12), pp. 1951.

[57] YOSHIKAWA, K., TAKIYAMA, K., KOYAMA, T., TARUYA, K., MASUDA, K., YAMAMOTO, Y., TOKU, T., KII, T., HASHIMOTO, H., INOUE, N. and OHNISHI, M., 2001. Measurements of strongly localized potential well profiles in an inertial electrostatic fusion neutron source. *Nuclear fusion,* **41**(6), p.717.

[58] KHACHAN, J., MOORE, D. and BOSI, S., 2003. Spatial distribution of ion energies in an inertial electrostatic confinement device. *Physics of Plasmas,* **10**(3), pp. 596-599.

[59] LAWSON, J.D., 1957. Some criteria for a power producing thermonuclear reactor. *Proceedings of the Physical Society. Section B,* **70**(1), pp. 6.

[60] GUS' KOV, S.Y. and KURILENKOV, Y.K., 2016. Neutron yield and Lawson criterion for plasma with inertial electrostatic confinement, *Journal of Physics: Conference Series* 2016, IOP Publishing, pp. 012132.

[61] OGINOV, A., KURILENKOV, Y.K., SAMOYLOV, I., SHPAKOV, K., TARAKANOV, V., OSTASHEV, V., RODIONOV, A. and KARPUKHIN, V., 2016. Recent experimental study of DD fusion in the potential well of a virtual cathode at nanosecond vacuum discharge, *Journal of Physics: Conference Series* 2016, IOP Publishing, pp. 012131.

[62] GODYAK, V., PIEJAK, R. and ALEXANDROVICH, B., 1993. Probe diagnostics of non-Maxwellian plasmas. *Journal of Applied Physics,* **73**(8), pp. 3657-3663.

[63] JELENKOVIĆ, B. and PHELPS, A., 2005. Excitation in low-current discharges and breakdown in He at low pressures and very high electric field to gas density ratios *E/N*. *Physical Review E,* **71**(1), pp. 016410.

[64] HARTMANN, p., DONKO, Z., BANO, G., SZALAI, L. and ROZSA, K., 2000. Effect of different elementary processes on the breakdown in low-pressure helium gas. *Plasma Sources Science and Technology,* **9**(2), pp. 183.

[65] HARTMANN, p. and DONKÓ, Z., 2004. Basic phenomena in low-pressure noble gas discharges: The role of heavy particle induced processes. *Acta Physica Hungarica B) Quantum Electronics,* **20**(3), pp. 193-217.

[66] KRAMIDA, A., RALCHENKO, Y., READER, J. and NIST ASD TEAM, 2015-last update, *NIST Atomic Spectra Database* (version 5.3). Available: http://physics.nist.gov/asd (retrv'd. 31/5/16)

[67] PHELPS, A.V., 1991. Cross sections and swarm coefficients for nitrogen ions and neutrals in N2 and argon ions and neutrals in Ar for energies from 0.1 eV to 10 keV. *Journal of Physical and Chemical Reference Data,* **20**(3), pp. 557-573.

[68] PHELPS, A. and JELENKOVIĆ, B., 1988. Excitation and breakdown of Ar at very high ratios of electric field to gas density. *Physical Review A,* **38**(6), pp. 2975.

[69] RAO, M., VAN BRUNT, R.J. and OLTHOFF, J.K., 1996. Resonant charge exchange and the transport of ions at high electric-field to gas-density ratios (*E/N*) in argon, neon, and helium. *Physical Review E,* **54**(5), pp. 5641.

[70] SCOTT, D. and PHELPS, A., 1991. Excitation by fast atoms at very high electric field to gas-density ratios in argon. *Physical Review A,* **43**(6), pp. 3043.

[71] HOLSTEIN, T., 1947. Imprisonment of resonance radiation in gases. *Physical Review,* **72**(12), pp. 1212.

[72] PHELPS, A., 1958. Effect of the imprisonment of resonance radiation on excitation experiments. *Physical Review,* **110**(6), pp. 1362.

[73] JOHN, R.M.S. and FOWLER, R.G., 1961. New process of excitation transfer in helium. *Physical Review,* **122**(6), pp. 1813.

[74] JOBE, J.D. and JOHN, R.M., 1972. Distribution of Excitation Transfer in Helium. *Physical Review A,* **5**(1), pp. 295.

[75] MEWE, R., 1966. Note on the singlet and triplet population in helium. *British Journal of Applied Physics,* **17**(9), pp. 1239.

[76] OKS, E., 2006. *Plasma cathode electron sources: physics, technology, applications.* John Wiley & Sons.

[77] KOLOBOV, V. and METEL, A., 2015. Glow discharges with electrostatic confinement of fast electrons. *Journal of Physics D: Applied Physics,* **48**(23), pp. 233001.

[78] HUMPHRIES, S., 2013. *Charged particle beams.* Courier Corporation.

[79] SZAPIRO, B., ROCCA, J. and PRABHURAM, T., 1988. Electron yield of glow discharge cathode materials under helium ion bombardment. *Applied Physics Letters,* **53**(5), pp. 358-360.

[80] ROUSSEL, J. and LABOIS, E., 1980. Contamination of a beam of metastable helium atoms by fast neutral atoms: Characteristics of the secondary emission of these atoms at low energy (100 eV) in interaction with the surface of a solid. *Surface Science,* **92**(2-3), pp. 561-578.

[81] HAYDEN, H.C. and UTTERBACK, N.G., 1964. Ionization of helium, neon, and nitrogen by helium atoms. *Physical Review,* **135**(6A), pp. A1575.

[82] PHELPS, A. and PETROVIC, Z.L., 1999. Cold-cathode discharges and breakdown in argon: surface and gas phase production of secondary electrons. *Plasma Sources Science and Technology,* **8**(3), pp. R21.

[83] LXCat database. Available: https://fr.lxcat.net/home/ (retrv'd. 31/10/17)

[84] WARD, G., 1968. A perforated hollow cathode electron beam gun. *Vacuum,* **18**(9), pp. 507-509.

[85] ROCCA, J., MEYER, J. and COLLINS, G., 1982. Hollow cathode electron gun for the excitation of cw lasers. *Physics Letters A,* **87**(5), pp. 237-239.

[86] IAEA Aladdin database. Available: https://www-amdis.iaea.org/ALADDIN/ (retrv'd. 31/10/17)

[87] OKASAKA, R., KONISHI, Y., SATO, Y. and FUKUDA, K., 1987. Excitation cross section in He -He collisions. I. Excitation function and potential curve crossing. *Journal of Physics B: Atomic and Molecular Physics,* **20**(15), pp. 3771.

[88] KEMPTER, V., VEITH, F. and ZEHNLE, L., 1975. Excitation processes in low-energy collisions between ground state helium atoms. *Journal of Physics B: Atomic and Molecular Physics,* **8**(7), pp. 1041.

[89] ADAMOV, M.G., OBRADOVIC, B.M., KURAICA, M.M. and KONJEVIC, N., 2003. Doppler spectroscopy of hydrogen and deuterium Balmer alpha line in an abnormal glow discharge. *IEEE Transactions on Plasma Science,* **31**(3), pp. 444-454.

[90] Ocean Optics. Available: http://oceanoptics.com/ (retrvd. 29/817)

[91] LIEBERMAN, M.A. and LICHTENBERG, A.J., 2005. *Principles of plasma discharges and materials processing.* John Wiley & Sons.

[92] MATHEWSON, A., 1976. *Ion induced desorption coefficients for titanium alloy, pure aluminium and stainless steel, (*No. CERN-ISR-VA-76-5). CM-P00064841.

[93] MCNEILL, D.H. and KIM, J., 1982. Balmer-alpha emission and hydrogen-atom energy in ion-source discharges. *Physical Review A,* **25**(4), pp. 2152.

[94] HISKES, J.R., 1961. Dissociation of molecular ions by electric and magnetic fields. *Physical Review,* **122**(4), pp. 1207.

[95] O. LEHMANN, Ann. d. Physik (Leipzig) 7, 1 (1902)

[96] MACKAY, G., 1920. Symmetrical Subdivision of Anode Glow in Helium Discharge Tubes. *Physical Review,* **15**(4), pp. 309.

[97] RUBENS, S.M. and HENDERSON, J., 1940. The characteristics and function of anode spots in glow discharges. *Physical Review,* **58**(5), pp. 446.

[98] CONDE, L. and LEON, L., 1994. Multiple double layers in a glow discharge. *Physics of Plasmas,* **1**(8), pp. 2441-2447.

[99] CONDE, L. and LEON, L., 1999. Visual observation of multiple double layers. *IEEE Transactions on Plasma Science,* **27**(1), pp. 80-81.

[100] SONG, B., D'ANGELO, N. and MERLINO, R., 1991. On anode spots, double layers and plasma contactors. *Journal of Physics D: Applied Physics,* **24**(10), pp. 1789.

[101] SCHRITTWIESER, R., AVRAM, C., BALAN, p.C., POHOATA, V., STAN, C. and SANDULOVICIU, M., 2000. New insights into the formation of nonlinear space charge structures in various plasmas. *Physica Scripta,* **2000**(T84), pp. 122.

[102] IONIŢĂ, C., DIMITRIU, D. and SCHRITTWIESER, R.W., 2004. Elementary processes at the origin of the generation and dynamics of multiple double layers in DP machine plasma. *Internatl. Journal of Mass Spectrometry,* **233**(1), pp. 343-354.

[103] SANDULOVICIU, M. and LOZNEANU, E., 2000. Ball lightning as a self organization phenomenon. *Journal of Geophysical Research: Atmospheres,* **105**(D4), pp. 4719-4727.

[104] SANDULOVICIU, M. and LOZNEANU, E., 1986. On the generation mechanism and the instability properties of anode double layers. *Plasma Physics and Controlled Fusion,* **28**(3), pp. 585.

[105] SANDULOVICIU, M., 1987. Pulsatory plasmoids formed in high frequency electric field. *Plasma physics and controlled fusion,* **29**(12), p.1687.

[106] POHOAŢĂ, V., POPA, G., SCHRITTWIESER, R., IONIŢĂ, C. and ČERČEK, M., 2003. Properties and control of anode double layer oscillations and related phenomena. *Physical Review E,* **68**(1), pp. 016405.

[107] SANDULOVICIU, M., LOZNEANU, E. and POPESCU, S., 2003. On the physical basis of pattern formation in nonlinear systems. *Chaos, Solitons & Fractals,* **17**(2), pp. 183-188.

[108] POPESCU, S., LOZNEANU, E. AND SANDULOVICIU, M., 2003. Self-organized complex space charge configurations at the origin of flicker noise. *Chaos, Solitons & Fractals,* **17**(2), pp.203-207.

[109] CHARLES, C., 2007. A review of recent laboratory double layer experiments. *Plasma Sources Science and Technology,* **16**(4), pp. R1.

[110] RAPP, D. and ENGLANDER GOLDEN, p., 1965. Total cross sections for ionization and attachment in gases by electron impact. I. Positive ionization. *The Journal of chemical physics,* **43**(5), pp. 1464-1479.

[111] Gradel. Available: www.nsd-fusion.com/ (retrv'd. 31/10/17)

[112] HWANG, S.H., 2012. Cmos image sensor: Current status and future perspectives. *Samsung Electronics*.

[113] HODGMAN, S.S., DALL, R.G., BYRON, L.J., BALDWIN, K.G.H., BUCKMAN, S.J. AND TRUSCOTT, A.G., 2009. Metastable helium: A new determination of the longest atomic excited-state lifetime. *Physical review letters,* **103**(5), p.053002.

[114] RALCHENKO, Y.V., JANEV, R., KATO, T., FURSA, D., BRAY, I. and DE HEER, F., 2000. *Cross section database for collision processes of helium atom with charged particles.1.Electron impact processes* (No. NIFS-DATA--59). National Inst. for Fusion Science.